Aus der Klinik für Kinder-Onkologie, -Hämatologie und Klinische Immunologie
der Heinrich-Heine-Universität Düsseldorf
Direktor: Prof. Dr. Arndt Borkhardt

Drug screening to identify targeted therapies in atypical teratoid/rhabdoid tumors

Dissertation

zur Erlangung des Grades eines Doktors der Medizin
der Medizinischen Fakultät der Heinrich-Heine-Universität Düsseldorf

vorgelegt von
David Pauck
2023

Als Inauguraldissertation gedruckt mit Genehmigung
der Medizinischen Fakultät der Heinrich-Heine-Universität Düsseldorf

gez.:
Dekan: Prof. Dr. med. Nikolaj Klöcker
Erstgutachter: Prof. Dr. med. Marc Remke
Zweitgutachter: Prof. Dr. med. Guido Reifenberger

Teile der im Rahmen dieser Arbeit erhobenen Daten wurden veröffentlicht:

Marquardt, V., Theruvath, J., **Pauck, D.**, Picard, D., Qin, N., Blümel, L., Maue, M., Bartl, J., Ahmadov, U., Langini, M., Meyer, F. D., Cole, A., Cruz-Cruz, J., Graef, C. M., Wolfl, M., Milde, T., Witt, O., Erdreich-Epstein, A., Leprivier, G., Kahlert, U., Stefanski, A., Stühler, K., Keir, S. T., Bigner, D. D., Hauer, J., Beez, T., Knobbe-Thomsen, C. B., Fischer, U., Felsberg, J., Hansen, F. K., Vibhakar, R., Venkatraman, S., Cheshier, S. H., Reifenberger, G., Borkhardt, A., Kurz, T., Remke, M., and Mitra, S., *Tacedinaline (CI-994), a class I HDAC inhibitor, targets intrinsic tumor growth and leptomeningeal dissemination in MYC-driven medulloblastoma while making them susceptible to anti-CD47-induced macrophage phagocytosis via NF-kB-TGM2 driven tumor inflammation.* J Immunother Cancer, 2023. **11**(1).

Nobre, L., **Pauck, D.**, Golbourn, B., Maue, M., Bouffet, E., Remke, M., and Ramaswamy, V., *Effective and safe tumor inhibition using vinblastine in medulloblastoma.* Pediatr Blood Cancer, 2019. **66**(6): p. e27694.

I. Zusammenfassung

Pädiatrische Hirntumoren stellen die häufigste Ursache der Krebs-assoziierten Mortalität in Industrieländern dar. Unter diesen Tumoren weist der atypische teratoide/rhabdoide Tumor (AT/RT) eine besonders schlechte Prognose auf und macht ca. 2,6 % aller neu diagnostizierten Hirntumoren bei Kindern aus, wobei hauptsächlich Säuglinge und Kleinkinder betroffen sind. Obwohl immense Fortschritte bei der Erforschung der zugrundeliegenden molekularen Mechanismen gemacht wurden, die zur Entstehung eines AT/RT führen, sind zielgerichtete Therapieansätze, die Schwachstellen in der Biologie des AT/RT ausnutzen, bisher nicht verfügbar. Dementsprechend umfasst das aktuelle multimodale Behandlungskonzept eine chirurgische Tumorresektion, Chemotherapie und kraniospinale Bestrahlung, was bei den jungen Patientinnen und Patienten häufig langfristige Folgeschäden hervorruft. Angesichts der Seltenheit des AT/RT stellt die Neupositionierung von etablierten Medikamenten eine geeignete Alternative zur Identifizierung neuer Behandlungsansätze dar, was die notwendigen Ressourcen und die Zeit, die zur Entwicklung eines gänzlich neuen Medikaments notwendig wären, drastisch reduzieren kann. Daher wurde im Rahmen dieses Promotionsprojektes ein Arbeitsablauf zur *in vitro*-Medikamententestung entwickelt, um Medikamente in AT/RT-Zelllinien zu untersuchen, die sich bereits in klinischer Anwendung oder in frühen oder späten Stadien der Entwicklung befinden, um zielgerichtete Therapieansätze durch Medikamenten-Neupositionierung abzuleiten. Im Zusammenhang mit der Entwicklung des Arbeitsablaufes wurde unter anderem eine Software zur effizienten Datenverarbeitung und -auswertung entwickelt. Nach mehreren Ebenen der Validierung wurden 768 Medikamente in 13 AT/RT-Zelllinien sowie 23 anderen *in vitro*-Tumormodellen, einschließlich Medulloblastom- und Glioblastom-Zelllinien, als Vergleichskohorte getestet. Die Daten zeigten eine spezifische Wirksamkeit von MEK- und MDM2-Inhibitoren sowie eines Inhibitors der ribosomalen RNA-Synthese, Pidnarulex, in AT/RT-Zelllinien. Darüber hinaus kam eine Heterogenität innerhalb der Wirkprofile zur Darstellung. Durch die Einbeziehung von RNA-Sequenzierungsdaten und DNA-Methylierungsanalysen konnte diese Heterogenität auf die molekularen Subgruppen des AT/RT zurückgeführt werden, entsprechend einer spezifischen Wirksamkeit von BCL2-, HSP90- und Notch-Inhibitoren in AT/RT-SHH-Zelllinien, wohingegen Mikrotubuli-Inhibitoren, Kinesin-Inhibitoren und der eIF4E-Inhibitor Briciclib in einem Teil der AT/RT-MYC-Zelllinien wirksam waren. Der Blut-Hirn-

Schranken-gängige Mikrotubuli-Inhibitor Patupilone wurde dementsprechend weiter auf seinen Wirkmechanismus hin untersucht, wobei mehrere Assays, einschließlich einer Lebendzell-Bildgebung-basierten Analyse, eine gesteigerte Apoptoserate durch dieses Medikament anzeigten. Zusammenfassend wurde ein klinisch orientierter Arbeitsablauf zur *in vitro*-Medikamententestung entwickelt, mit dessen Hilfe präklinische Daten zur zielgerichteten Therapie des AT/RT erhoben wurden, die als Grundlage zur Durchführung klinischer Studien dienen können, um die Therapie des AT/RT in Zukunft sicherer und effizienter zu machen.

II. Summary

Pediatric brain tumors are the most frequent cause of cancer-related death in children in industrial countries. Amongst these tumors, atypical teratoid/rhabdoid tumors (AT/RT) exhibit a particular poor prognosis and account for 2.6 % of all newly diagnosed brain tumors in children, mostly affecting toddlers and infants. Although tremendous progress was made concerning the elucidation of the underlying molecular mechanisms leading to the initiation of AT/RT, targeted therapeutic approaches that hijack AT/RT biology have not yet been identified. Thus, intensive multimodal treatment, usually consisting of surgical tumor resection, chemotherapy and craniospinal irradiation, is administered to the young patients conveying critical long-term sequelae. Given the rarity of AT/RT, drug repurposing constitutes a suitable alternative for the identification of new drugs to treat AT/RT, cutting down the time and resources required for the development of an entirely new drug. Thus, in this MD thesis project, an *in vitro* drug screening workflow was developed to investigate a clinically oriented drug library covering drugs in clinical use as well as drugs in early and late stages of development in AT/RT cell lines to unravel targeted therapeutic approaches through drug repurposing. Along with the evolution of the workflow, a software was developed to enable efficient data processing and evaluation. After multiple layers of workflow validation, 768 drugs were tested in 13 AT/RT cell lines, along with 23 other *in vitro* tumor models including medulloblastoma and glioblastoma cell lines for comparison. The data showed specific activity of MEK and MDM2 inhibitors and the ribosomal RNA synthesis inhibitor Pidnarulex across AT/RTs. Moreover, analyses indicated heterogeneity among the drug response profiles of AT/RT cell lines. Through the incorporation of RNASeq data and DNA methylation profiling these heterogenous response patterns were linked to the molecular subgroups of AT/RT, revealing specific activity of BCL2, HSP90 and Notch inhibitors in AT/RT-SHH cell lines, whereas a subset of AT/RT-MYC cell lines responded well to microtubule inhibitors, spindle kinesin protein (KSP) inhibitors and Briciclib, a specific eIF4E inhibitor. A blood-brain barrier-permeable microtubule inhibitor, namely Patupilone, thus underwent further examination of its mechanism of action, displaying induction of apoptosis in AT/RT-MYC cell lines in multiple assays, including live-cell imaging-based analyses. In summary, a clinically oriented drug screening workflow was developed to provide preclinical evidence for targeted therapy of AT/RTs, which in turn may serve as a basis to initiate clinical trials to treat AT/RTs more safely and efficiently in the future.

III. Abbreviations

Units

°C	Degrees Celsius
µg	Micrograms
µl	Microliters
µM	Micromolar
µm²	Square micrometer
d	Days
g	G-force
h	Hours
min	Minutes
ml	Milliliters
mM	Millimolar
ms	Milliseconds
ng	Nanograms
nM	Nanomolar
nm	Nanometers
p	Photons
pM	Picomolar
s	Seconds

Other abbreviations

ADA	Adenosine deaminase
ADC	Antibody drug conjugates
AKT	AKT serine/threonine kinase, also protein kinase B (PKB)
AKT, PKB	Protein kinase B
ALK	Anaplastic lymphoma kinase
ANOVA	Analysis of variance
ARK	Aurora kinase
AT/RT	Atypical teratoid/rhabdoid tumor
ATM/ATR	Ataxia telangiectasia mutated/Ataxia telangiectasia and Rad3-related protein
BCL2	B-cell lymphoma 2

BCR-ABL	Breakpoint cluster region-abelson murine leukemia viral oncogene homolog
BTK	Bruton’s tyrosine kinase inhibitors
CDK	Cyclin dependent kinase
CHEK	Checkpoint kinase
CIS	Combined inhibition score
CNS	Central nervous system
CoV(s)	Coefficient(s) of variation
CRISPR/Cas9	Clustered regularly interspaced short palindromic repeats associated protein 9
CSF1R	Colony stimulating factor 1 receptor
CTG	CellTiter-Glo
d h	Disodium hexahydrate
dhcl	Dihydrochloride
DMEM	Dulbecco's Modified Eagle Medium
DNA A/C	DNA Alkylator/Crosslinker
DNA/RNA S	DNA/RNA Synthesis
ds	Disodium
EGF	Epidermal growth factor
EGFR	Epidermal growth factor receptor
eIF	Eukaryotic initiation factor
eIF4E	Eukaryotic translation initiation factor 4E
EM	Endogenous Metabolite
ER	Estrogen Receptor
ERK	Extracellular signal-regulated kinase
EZH2	Enhancer of zeste homolog 2
FAK	Focal adhesion kinase, also protein tyrosine kinase 2 (PTK2)
fAUC	Fitted area under the curve
FBS	Fetal bovine serum
FGF	Fibroblast growth factor
FGFR	Fibroblast growth factor receptor
FLT3	fms related receptor tyrosine kinase 3
FTase	Farnesyltransferase
G9a/GLP	Euchromatic histone lysine methyltransferase 2/G9a-like protein
GSK3	Glycogen synthase kinase 3

HAT	Histone acetyltransferases
hcl	Hydrochloride
HDAC	Histone deacetylase
HMT	Histone methyltransferase
HSP90	Heat shock protein 90
HTS	High-throughput screening
IAP	Inhibitor of apoptosis
IGF-1R	Insulin-like growth factor 1 receptor
IKK	IkappaB kinase
IMDM	Iscove's Modified Dulbecco's Medium
ITS	Insulin-Transferrin-Selen
JAK	Janus kinase
JMJD	Jumonji domain
JNK	c-Jun N-terminal kinase
KIT	KIT proto-oncogene, receptor tyrosine kinase
KSP	Spindle kinesin protein
MDM2	Mouse double minute 2 homolog
MEK	Mitogen-activated protein kinase kinase
MEM	Minimum Essential Medium
MET/HGFR	MET proto-oncogene/Hepatocyte growth factor receptor
MMP	Matrix metalloproteinases
MNP 2.0	Molecular Neuropathology 2.0
ms	Mesylate
MT	Microtubule
MTOR	Mammalian target of rapamycin
MWU	Mann-Whitney U
MYC	MYC proto-oncogene
n.s.	Not significant/non-significant
NA	Nucleoside antimetabolite
NT	Non-treated
P/S	Penicillin/Streptomycin
PARP	Poly(ADP-ribose) polymerase
PBS	Phosphate buffered saline
PI	Propidium Iodide
PI3K	PI3 kinase

PIM	Pim kinase
PKA	Protein kinase a
PKC	Protein kinase c
PLK	Polo-like kinase
RAF	Rapidly accelerated fibrosarcoma
RAR/RXR	Retinoic acid receptor/retinoid X receptor
RNASeq	RNA sequencing
rRNA	Ribosomal RNA
SHH	Sonic hedgehog
SIRT	Sirtuin
STAT	Signal transducer and activator of transcription
SYK	Spleen associated tyrosine kinase
tAUC	Trapezoidal area under the curve
TP	Topoisomerase
TRK	Neurotrophic receptor tyrosine kinase
TYR	Tyrosinase
VEGFR	Vascular endothelial growth factor receptor
WNT	Wingless-type MMTV integration site family
YAP	Yes1 associated transcriptional regulator

IV. Table of contents

1. Introduction

1.1. Oncology in the era of molecular medicine

Cancer is a fatal disease characterized by increased proliferation of malignant cells and often proves to be incurable despite intensive treatment strategies. Thus, oncology research continuously aims to refine our understanding of the underlying disease mechanisms and improve patient outcomes. Mechanistically, cancer is the result of genomic alterations inferring a loss-of-function to tumor suppressors and a gain-of-function to proto-oncogenes [1, 2]. As the era of molecular medicine is evolving rapidly, the opportunities for analyzing cancer tissue developed far beyond the limits of histomorphological characterization [3-12]. A time-efficient and purposeful translation of new findings into clinically meaningful biomarkers empowers physicians to personalize cancer therapy: While markers of high risk might justify an intensified therapy with critical side effects to be applied, a good prognosis allows to de-escalate the scheme to prevent therapy-induced damage to the patient. This concept has proven to reduce the occurrence of secondary neoplasms and severe chronic health conditions in survivors of acute lymphoblastic leukemia [13]. In a similar fashion, the molecular classification of medulloblastoma facilitated risk stratification as the Wingless-type MMTV integration site family (WNT) subgroup of medulloblastoma exhibited a more favorable prognosis compared to other subgroups [14]. The strong interplay between risk stratification and therapy optimization is evident. Moreover, therapy may target cancer-specific traits as vulnerabilities in their biology to treat tumors more effectively while reducing side effects of treatment. A well-established example of targeted therapy is the invention of Trastuzumab (Herceptin) for the treatment of breast cancer: Based on the overexpression of HER2, a growth factor receptor, tumor cells can be depleted by the administration of an antibody which specifically binds to HER2 and induces tumor cell death [15, 16]. In summary, modern technologies drive our understanding of tumor biology into more refined classification and risk stratification, but also targeted treatment strategies.

1.2. Drug repurposing and high-throughput screening

Apart from the invention of tailored drugs for cancer therapy in pharmaceutical drug development, drug repurposing (also known as drug repositioning) describes the process of inventing new applications for an existing drug. This concept makes drug repurposing very attractive especially for rare diseases for which the development of

drugs is not worthwhile from a commercial perspective, which most pharmaceutical companies are forced to pursue. In addition, if a drug has already reached a far stage in development or is even approved for clinical usage, the timeline required for approval in a different disease is way shorter than inventing an entirely new drug [17-21]. The acceleration of this process can be crucial for patients suffering from progressive disease after completing primary therapeutic options, who are thus awaiting new therapies to be released. In line with the previously introduced example, the indications of Trastuzumab were advanced for the treatment of gastric cancer with HER2 overexpression by drug repurposing [22]. Moreover, drug repurposing recently gained tremendous attention in COVID-19/SARS-CoV-2 research [23].

Complementing the advantages of drug repurposing, the continuous advancement of life science technologies brings (ultra) high-throughput screening (HTS) equipment even to smaller laboratories, allowing to test hundreds of drugs by microplate-based exposure of cells to selected libraries of drugs. Thus, HTS enables scientists to perform drug repurposing studies in disease-specific models while linking drug responsiveness to biomarker research [24-27]. Taken together, the identification of drugs suitable for cancer treatment by HTS-based drug repurposing studies allows to rapidly translate therapeutic alternatives, even for rare diseases, to clinical usage offering personalized treatments for patients in a desperate situation [28].

1.3. Pediatric brain tumors

In pediatrics, brain tumors represent about 11 % of all newly diagnosed cancers worldwide depicting the second to most common pediatric cancer type after the acute leukemias. Mortality strongly varies among different regions with about 14.2 % of cancer-related deaths worldwide, 29.3 % in North America and 32.9 % in Germany. In the latter, brain tumors thus prove to be the leading cause for cancer-related deaths looking at patients between the ages of 0-19 years [29].

Clinical presentation varies depending on the age and the tumor location. Along with symptoms linked to direct displacement of CNS structures like seizures or neurological deficits and symptoms caused by an increase of intracranial pressure like headache, nausea/vomiting and papilloedema, especially younger children show more diffuse symptoms like increased irritability, lethargy, delayed achievement of developmental milestones or weight loss. In children below the age of four years, macrocephaly is also very common as the neurocranium is still flexible due to unclosed sutures and fontanelles. While symptoms of supratentorial tumors focus on seizures or focal

neurological deficits, infratentorial tumors rather cause nausea/vomiting, headache and impaired coordination and gait. Tumors in the brain stem in addition cause specific central nerve palsies, while back pain is a typical symptom of spinal tumors [30].

Magnetic resonance imaging (MRI) emerged as the key diagnostic tool in pediatric brain tumors, as it became largely available and does not burden the patient with any ionizing radiation, which is critical especially at younger ages. It is also used for measuring response to therapy and relapse during or after therapy. In most cases, primary surgery is conducted without prior biopsy so that MRI becomes the only diagnostic step to indicate surgery when patients present with clinical manifestations of a brain tumor [31-36]. During surgery, tumor tissue for subsequent histopathological classification as well as for molecular analyses is acquired, which is essential to assign a tumor type defined by the World Health Organization (WHO) classification of central nervous system tumors [37].

Cancer therapy is based on three pillars: Surgery, irradiation, and chemotherapy. Concerning the management of pediatric brain tumors apart from diffuse lesions such as histone H3 K27-altered diffuse midline glioma, the extent of surgical resection remains the primary goal in terms of the overall prognosis [38, 39]. The continuous development of neurosurgical techniques and advances in assistive technology thus aimed at maximizing the margins of resection [40, 41]. Subsequent treatment, which is particularly necessary among malignant lesions, proved to be challenging, as the developing brain in children is more sensitive to chemo- and radiotherapy as compared to the mature brain in adults [42-47]. However, to treat aggressive disease the application of multimodal therapy is inevitable and may cause therapy-induced sequelae [48-50]. In brain tumors, due to localization, these predominantly include neurological disorders, such as strokes, seizures, severe headache, hydrocephalus requiring shunting, paralysis, hearing loss, other focal neurological dysfunction, and autonomic nervous system dysfunction [51-55]. Moreover, patients suffer from neurocognitive sequelae including reduced "*overall cognitive functioning, academic achievement, attention, psychomotor and visual-spatial skill, verbal memory, and language*", especially when treated at younger ages and/or with high doses of cranial irradiation [56-61]. However, a large study investigating long-term therapy-induced effects in patients with CNS tumors showed that sequelae are not limited to the primary tumor site but may also frequently affect endocrine, cardiovascular, musculoskeletal, pulmonary, gastrointestinal and reproductive organ systems, and may even cause secondary neoplasms [62]. While alkylators and topoisomerase II inhibitors are well

established to induce secondary leukemia or myelodysplastic syndromes [63-66], more recent studies showed an increased occurrence of breast cancer after anthracycline treatment, more frequent cases of sarcoma after cyclophosphamide treatment [67] and more frequent cases of melanoma and thyroid cancer after treatment using platinum derivatives or alkylators [64]. Moreover, especially high-dose chemotherapy in conjunction with hematopoietic stem cell rescue is associated with a comparable incidence of secondary solid neoplasms than total body irradiation [68]. Radiotherapy on the other hand may cause a larger variety of secondary neoplasms, depending on the site of treatment. After irradiation of CNS tumors, studies found an increased incidence of meningiomas and gliomas [69]. In summary, cancer therapy in children requires interdisciplinary discussion along with well-deliberated treatment strategies to achieve disease control while avoiding lifelong sequelae.

1.3.1. Atypical teratoid/rhabdoid tumors (AT/RT)

1.3.1.1. Overview

AT/RT is a rare childhood CNS tumor accounting for about 2.6 % of all CNS tumors in patients below the age of 18 years. It belongs to the group of embryonal CNS tumors and represents the second most common (16.2 %) type after medulloblastoma (73.3 %). AT/RT owes its name to harboring variable histologic features, including simultaneously occurring epithelial and mesenchymal components, reminiscent of teratoma, and rhabdoid cells [70]. Notably, AT/RT primarily affects infants and toddlers with a median onset of disease at 17 months. Thus, from 66 CNS embryonal tumors diagnosed below the age of one year, AT/RTs account for 47 (71.2 %) cases [71, 72]. Another study based on data from embryonal tumors from any location report a proportion of 2.1 % for AT/RTs [73]. AT/RTs may also occur in adult patients, but there are very few cases described [74-91]. The tumors may be located throughout the CNS [92], including the spine [91, 93-95] and the trigeminal nerve [76, 90, 96]. Studies reported that 19-30 % of the patients present with disseminated disease, either intracerebral or along the spine [97-99]. The prognosis remains poor despite intensive multimodal therapy with 5-year overall survival and progression-free survival rates of 34.7 % and 30.5 %, respectively [97]. The rare survivors of AT/RT often suffer from long-term therapy-induced sequelae [100].

1.3.1.2. Tumor biology

In terms of their biological background, large-scale whole genome sequencing approaches revealed a surprisingly bland genome without recurrent aberrations other than biallelic deletions or loss-of-function mutations of the *SMARCB1* or, much rarer, *SMARCA4* genes [101-103]. Thus, immunohistochemical staining for expression of the respective proteins became the established clinical tool to diagnose AT/RTs [104-106]. Both proteins are part of the SWItch/Sucrose Non-Fermentable (SWI/SNF) complex which regulates gene expression through remodeling of nucleosomes [107, 108]. Considering the bland genome and the emerging knowledge about the SWI/SNF complex, further studies focused on the epigenetic landscape to further unravel the drivers of AT/RT. Gene expression and DNA methylation profiling showed three distinct molecular subgroups, AT/RT-TYR, AT/RT-SHH and AT/RT-MYC, which were named according to the overexpression of group-specific markers. AT/RT-TYR owes its name to the overexpression of the enzyme Tyrosinase, a key enzyme in melanin synthesis, along with other genes involved in melanogenesis such as *MITF* and *TRP2* [109]. Notably, AT/RT-TYR subgroup is overrepresented in patients below the age of one year and appears at infratentorial location more frequently. AT/RT-SHH features an overexpression of genes related to the Sonic hedgehog (SHH) cluster, especially *GLI2* and *MYCN*, as well as Notch signaling. SHH activation is a hallmark of many different cancers including basal cell carcinoma of the skin which may occur at multiple sites if the patient harbors a germline loss-of-function mutation of the SHH pathway member *PTCH1*, which is referred to as nevoid basal cell carcinoma syndrome or Gorlin syndrome [110]. AT/RT-SHH tumors tend to appear in older children and are equally distributed in the supra- and infratentorial compartments. Lastly, AT/RT-MYC expresses the *MYC* proto-oncogene, which is well known as a key driver of cancer initiation and progression [111, 112]. Tumors from AT/RT-MYC preferentially appear in the supratentorial compartment and rather affect older patients. The *SMARCB1* mutation status appears to vary among subgroups with AT/RT-TYR exhibiting primarily broad deletions including 22q monosomy, whereas "*ATRT-SHH and ATRT-MYC tumors most frequently showed no chromosome 22 copy aberrations, particularly in ATRT-SHH (48 %), focal gains (ATRT-SHH, 23 %), or focal deletions (ATRT-MYC, 79 %)*" [113]. A more recent study based on data from the European Rhabdoid Registry (EU-RHAB) validated this finding, however reporting a higher frequency of frame-shift mutations (11.5 vs. 27 %) in AT/RT-TYR tumors whereas these are rare in AT/RT-SHH and never appeared among the investigated tumors of the AT/RT-MYC subgroup [97].

Regarding the role of *SMARCB1* mutation/loss in the formation of the epigenetic alterations observed in AT/RTs, recent chromatin immunoprecipitation (ChIP) sequencing studies showed, that 80 % of the genes that usually are bound by SMARCB1 appear to be targeted by the histone methyltransferase enhancer of zeste homolog 2 (EZH2), which is part of the Polycomb repressive complex 2 (PRC2), a known counterplayer of the SWI/SNF complex. However, most of the genes do not show a trimethylation as expected in the presence of EZH2, which indicates that they remain expressed. Further analyses revealed SMARCA4-dependent residual activity of the SWI/SNF complex to be responsible for the retained gene expression by the prevention of trimethylation. Interestingly, subgroup-specific super-enhancers, previously identified through histone H3 lysine 27 acetylation ChIP sequencing, were found among the genes which were kept in the active state by SMARCA4-dependent residual activity of the SWI/SNF complex, thus leading to the hypothesis that AT/RTs are SMARCA4-dependent. This concept was finally validated through SMARCA4 knockdown, which induced growth arrest in AT/RT cell lines [114].

1.3.1.3. Therapy and prognostic factors

Until now, a standard protocol for the treatment of AT/RT is lacking. The EU-RHAB advises to perform maximum achievable surgical tumor resection, followed by chemotherapy consisting of three sequences of cycles of Doxorubicin (DOX), Ifosfamide, Carboplatin and Etoposide (ICE), and Vincristine, Cyclophosphamide and Actinomycin D (VCA), all combined with intra-ventricular application of Methotrexate. A consolidation by means of high-dose chemotherapy using a combination of Carboplatin and Thiotepa may subsequently be appended. Radiotherapy should only be considered after the age of 18 months. Under certain circumstances, such as local disease, large residual tumor volume or the availability of proton therapy, radiotherapy may be conducted earlier, but never before the age of eight months [115]. Recently, it has been reported that subgroup affiliation and age at diagnosis emerged as independent prognostic factors, stratifying AT/RT as follows:

- High-risk (Patients < 1 year of age + non-TYR subgroup)
- Intermediate risk, either
    - Patients < 1 year of age or
    - Patients > 1 year of age and non-TYR subgroup
- Standard-risk (Patients > 1 year of age + TYR subgroup)

Radiotherapy, achievement of complete remission, absence of synchronous tumors and metastases, and germline wildtype-status of the *SMARCB1* gene were found to be dependent positive prognostic factors, with *SMARCB1* germline mutations indicate a particular poor prognosis [97].

1.3.1.4. Targeted therapies in clinical trials

Multiple ongoing trials investigate the targetability of AT/RTs by means of small molecule inhibitors. In line with the reported upregulation of cyclin-dependent kinase 6 (CDK6) in AT/RTs [113, 114], a phase I trial was initiated to reveal the sensitivity of solid tumors, including malignant rhabdoid tumors, against LEE011 (also referred to as Ribociclib), a CDK4/6 inhibitor. Ribociclib achieved stable disease in a subpopulation of patients [116]. On the other hand, another phase I trial investigating therapy responses of combinatory treatment using Ribociclib and Everolimus, an mammalian target of rapamycin (MTOR) inhibitor, yielded no objective response [117]. A trial investigating Sirolimus, another MTOR inhibitor, combined with chemotherapy in pediatric CNS tumor patients is still ongoing (NCT02574728). Moreover, multiple studies reported on sensitivity of AT/RTs to Alisertib [118-120], an aurora kinase (ARK) inhibitor, which lead to the initiation of a phase II trial, which, however, did not meet the expected study criteria, while achieving partial response or stable disease in a subpopulation of patients [121]. Furthermore, due to promising results of Tazemetostat, an EZH2 inhibitor, in a phase I trial [122], a phase II trial (NCT02574728) is now ongoing. A phase 1 trial investigating Vorinostat, a histone deacetylase (HDAC) inhibitor, and Temozolomide, a DNA alkylator, for the treatment of recurrent brain or spinal cord tumors showed no response among two patients with AT/RT [123]. Another phase I trial aimed to reveal the activity of Vorinostat and Isotretinoin, an inhibitor of the retinoic acid receptor/retinoid X receptor (RAR/RXR), in pediatric embryonal brain tumor patients. However, all patients with AT/RT were excluded according to a recent report [124]. MK-0752, a gamma secretase inhibitor, was evaluated in pediatric patients with recurrent CNS tumors. No objective treatment response was observed in the single AT/RT patient included in this study. Another gamma secretase inhibitor was investigated in a phase I trial (NCT01088763) that was terminated. Moreover, a study investigated chemotherapy with additional Dasatinib, a breakpoint cluster region-abelson murine leukemia viral oncogene homolog 1 (BCR-ABL) inhibitor, (NCT00788125). The study was terminated due to a lack of treatment response. A large study at the St. Jude Children's Research Hospital investigates the activity of

multiple drugs in pediatric patients with recurrent CNS tumors, including Ribociclib, Sonidegib and Trametinib (NCT03434262). Another study investigating the activity of Panobinostat in pediatric cancer patients, including patients with AT/RT, was terminated due to drug supply issues (NCT04897880). An ongoing phase I study investigates the dual murine double minute 2/4 homolog (MDM2/MDM4) inhibitor ALRN-6924 in pediatric cancer patients with various entities (NCT03654716). This is interesting, as very recently radiosensitization through RG7388, another MDM2 inhibitor, has been reported in AT/RTs [125]. Lastly, two ongoing phase II trials investigate PD-L1 antibodies for the treatment of AT/RTs (NCT04416568 and NCT05286801).

1.4. Analysis of dose-response data in drug screening studies

There are multiple parameters to describe dose-response data with distinct underlying calculation methodology. The by far best-known parameter is the half maximal inhibitory/effective concentration (IC50/EC50) which is based on multi-parameter logistic fitting. In logistic fitting, data points representing an outcome parameter under exposure to ascending concentrations of a substance are used to interpolate a sigmoidal curve. While EC50 is used to describe kinetics in which the addition of a substance leads to an increase of the measured outcome parameter, the IC50 indicates a decrease [126]. In addition, two variants of the IC50 are distinguished. In the case that the maximum effect is defined as zero, the IC50 is called the absolute IC50, whereas in the case that the maximum effect is defined as the bottom level of each individual experiment, the IC50 is called the relative IC50 [127].

An alternative term for the absolute IC50 is called the half maximal growth-inhibitory concentration (GI50), which is predominantly used in studies measuring the viability of biological material (e.g. cell lines, primary cultures, organoids and others) after exposure to a substance [128]. However, in this thesis, for the most part, the relative IC50 is used and thus, it will not be termed GI50, although cell viability is measured.

The underlying equations to calculate dose-response curves from dose-response data usually contain four or five parameters, one of which is the IC50 corresponding to the curve's inflection point. In four-parametric logistic fitting the IC50 is complemented by the upper (Top) and lower (Bottom or E_{max}) asymptotes and the slope. While four-parametric fitting thus is limited to provide symmetrical sigmoidal curves, in five-parametric fitting a symmetry constant is added to allow fitting of asymmetrical data.

The additional degree of freedom showed superior performance under certain circumstances [129, 130].
Apart from the IC50 and other parameters derived through multi-parametric logistic fitting, the area under the curve (AUC) is a different approach for the quantification of dose-response data. It can be calculated from a fitted dose-response curve (fitted AUC or fAUC), but also from a connection line between the data points (trapezoidal AUC or tAUC). The tAUC thus works independent from fitting algorithms [131].

1.5. Aims of this thesis

As it was pointed out in the introduction, AT/RT patients have a dismal prognosis requiring intensive treatment protocols often linked to therapy-induced sequelae in the rare survivors. Thus, there is an urgent need for targeted therapeutic approaches to be developed. This thesis aimed to evolve the workflow among the in-house semi-automated drug screening devices, especially in terms of throughput and capabilities. As a part of this aim, a software should be designed to automatically process, store and arrange drug screening data. Data processing should also comprise the derandomization through definition files and the rendering of dose-response parameters. By reviewing these parameters adequate markers of activity should be chosen.

Aim 1: Design a software to automatically evaluate drug screening data and identify suitable markers of activity.

Along with continuous usage, critical evaluation of the data quality and the reliability of the workflow should be conducted. Furthermore, a clinically oriented drug library covering anti-cancer drugs in clinical use as well as late stage developed drugs in phase III trials (Clinical library) should be evaluated. Miniaturization of the plate format should enable screening of models with limited growth capacity.

Aim 2: Asses the data quality and the reliability of the drug screening workflow and introduce a clinical library as well as a miniaturized plate format.

Using the workflow, a cohort of AT/RT cell lines should undergo drug screening, along with cell lines derived from other brain tumors. The results should allow to identify drugs

with selective activity in AT/RT cell lines. As controls for toxicity, non-neoplastic cells should be screened as well.

Aim 3: Identify targeted therapeutic approaches in AT/RTs by means of drug screening through comparison to other brain tumors.

Apart from comparing AT/RT cell lines to other brain tumor cell lines, the screening data should be analyzed for heterogenous responses within AT/RT. Consequently, it should be evaluated whether heterogenous response patterns may be linked to biomarkers such as molecular subgroups using RNA sequencing (RNASeq) and 850k DNA methylation profiling.

Aim 4: Analyze heterogenous response patterns in AT/RT cell lines to reveal biomarkers of therapy response.

2. Materials and Methods

Table 1 provides an overview of the basal media used for cell culture while Table 2 lists the respective supplements. Table 3 summarizes the other reagents used for the own experiments.

2.1. Reagents

Table 1. List of cell culture basal media.

Media	Cat. No.	Manufacturer
Astrocyte Medium	1801	ScienCell Research Laboratories (Carlsbad, CA)
DMEM/F-12	11330-032	Thermo Fisher Scientific (Waltham, MA, USA)
Dulbecco's Modified Eagle Medium (DMEM)	41965-039	Thermo Fisher Scientific (Waltham, MA, USA)
Improved Minimum Essential Medium (MEM)	A10489-01	Thermo Fisher Scientific (Waltham, MA, USA)
Iscove's Modified Dulbecco's Medium (IMDM)	12440-053	Thermo Fisher Scientific (Waltham, MA, USA)
KnockOut DMEM/F-12 Basal Medium	12660-012	Thermo Fisher Scientific (Waltham, MA, USA)
MEM	10370-047	Thermo Fisher Scientific (Waltham, MA, USA)
Neurobasal-A Medium	10888-022	Thermo Fisher Scientific (Waltham, MA, USA)
NeuroCult NS-A Basal Medium (Human)	05750	STEMCELL Technologies (Vancouver, BC, Canada)
ReNcell NSC Maintenance Media	SCM005	Merck (Darmstadt, Germany)
RPMI 1640	31870-025	Thermo Fisher Scientific (Waltham, MA, USA)

Table 2. List of cell culture supplements.

Supplements	Cat. No.	Manufacturer
B-27 supplement, minus vitamin A	12587-010	Thermo Fisher Scientific (Waltham, MA, USA)
Epidermal growth factor (EGF), human	PHG0311	Thermo Fisher Scientific (Waltham, MA, USA)
Fetal bovine serum (FBS)	F9665, P30-3302	Merck (Darmstadt, Germany), PAN Biotech (Aidenbach, Germany)
Fibroblast growth factor (FGF), human	50361.5	Biomol (Hamburg, Germany)
HEPES solution	15630-080	Thermo Fisher Scientific (Waltham, MA, USA)
Insulin-Transferrin-Selen (ITS) solution	41400-045	Thermo Fisher Scientific (Waltham, MA, USA)
Leukemia inhibitory factor (LIF), human	LIF1010	Merck (Darmstadt, Germany)
L-Glutamine solution	25030-024	Thermo Fisher Scientific (Waltham, MA, USA)
MEM non-essential amino acid (NEAA) solution	11140-035	Thermo Fisher Scientific (Waltham, MA, USA)
MEM vitamin solution	11120-037	Thermo Fisher Scientific (Waltham, MA, USA)
Penicillin/streptomycin (P/S) solution	P4333	Merck (Darmstadt, Germany)
Sodium bicarbonate solution	25080-094	Thermo Fisher Scientific (Waltham, MA, USA)
Sodium pyruvate solution	11360-070	Thermo Fisher Scientific (Waltham, MA, USA)

Table 3. List of other reagents.

Reagents	Cat. No.	Manufacturer
Accutase	25-058-CI	Corning (Corning, NY, USA)
Annexin V binding buffer	556454	BD Biosciences (Franklin Lakes, NJ, USA)
CellTiter-Glo (CTG) Luminescent Cell Viability Assay	G7573	Promega (Madison, WI, USA)
Chloroform	1.02445	Merck (Darmstadt, Germany)
Dimethyl sulfoxide (DMSO)	D8418, A3672	Merck (Darmstadt, Germany), AppliChem (Darmstadt, Germany)
Ethanol	20821.330	VWR (Radnor, PA, USA)
Fluorescein isothiocyanate (FITC) Annexin V antibody	556419	BD Biosciences (Franklin Lakes, NJ, USA)
Incucyte Caspase-3/7 Green Apoptosis Reagent	4440	Sartorius (Göttingen, Germany)
Isopropanol	20842.330	VWR (Radnor, PA, USA)
Laminin, mouse	354232	Corning (Corning, NY, USA)
Maxwell RSC Cultured Cells DNA Kit	AS1620	Promega (Madison, WI, USA)
Nuclease-free water	AM9916	Thermo Fisher Scientific (Waltham, MA, USA)
Phosphate buffered saline (PBS)	D8537	Merck (Darmstadt, Germany)
Plasmocin Treatment	ant-mpt-1	InvivoGen (Toulouse, France)
Propidium iodide (PI)	P4864	Merck (Darmstadt, Germany)
QuantiFluor ONE dsDNA System	E2670	Promega (Madison, WI, USA)
Qubit RNA HS Assay-Kit	Q32852	Thermo Fisher Scientific (Waltham, MA, USA)
RNase AWAY	10666421	Thermo Fisher Scientific (Waltham, MA, USA)
TRIzol	15596018	Thermo Fisher Scientific (Waltham, MA, USA)
TruSeq RNA Library Preparation Kit v2	RS-122-2001	Illumina (San Diego, CA, USA)
Trypsin-EDTA	25200-056	Thermo Fisher Scientific (Waltham, MA, USA)
Venor GeM Advance Kit	11-7096	Minerva Biolabs (Berlin, Germany)

2.2. Materials and devices

The consumables including microplates, dispenser equipment, centrifuge tubes, pipette tips and other plastic ware are listed in Table 4. In addition, Table 5 provides an overview of the laboratory devices used for the own experiments.

Table 4. List of consumables.

Consumables	Cat. No.	Manufacturer
6-well microplates	657185, 657160, 3335	Greiner Bio-One (Kremsmünster, Austria), Corning (Corning, NY, USA)
384-well microplates	3570, 3701, 4681	Corning (Corning, NY, USA)
1536-well microplates	3727, 3893	Corning (Corning, NY, USA)
Aspiration pipettes	86.1252.011	Sarstedt (Nümbrecht, Germany)
Cell culture flasks	690195, 658195, 690175, 658175, 3289, 3290	Greiner Bio-One (Kremsmünster, Austria), Corning (Corning, NY, USA)
Cell scraper	541070, 83.3951	Greiner Bio-One (Kremsmünster, Austria), Sarstedt (Nümbrecht, Germany)
Cell strainer	542040, 542040	Greiner Bio-One (Kremsmünster, Austria)
Centrifuge/reaction tubes	188271, 227261, 0030123328, 0030123344	Greiner Bio-One (Kremsmünster, Austria), Eppendorf (Hamburg, Germany)
Cryoconservation tubes	430488	Corning (Corning, NY, USA)
Dispensehead cassette	30097370, 30097371	Tecan (Männedorf, Switzerland)
Dispensing cassette	24072670, 24073290	Thermo Fisher Scientific (Waltham, MA, USA)
Infinium MethylationEPIC BeadChip Kit	WG-317-1001	Illumina (San Diego, CA, USA)
Large centrifuge tubes	430776	Corning (Corning, NY, USA)
Parafilm	PM996	Bemis (Neenah, WI, USA)
Pipette tips	S1120-3810, S1120-1810, S1120-1840, S1120-8810, S1126-7810	Starlab (Hamburg, Germany)
Pipettes	4487, 4488, 4489	Corning (Corning, NY, USA)
Sterile filtration system	155-0045, 157-0045, 158-0045	Thermo Fisher Scientific (Waltham, MA, USA)

Table 5. List of devices.

Devices	Manufacturer
Axiovert 200 inverted microscope	Zeiss (Oberkochen, Germany)
Bioanalyzer automated electrophoresis instrument	Agilent (Santa Clara, CA, USA)
C170 incubator	Binder (Tuttlingen, Germany)
cBot automated clonal amplification system	Illumina (San Diego, CA, USA)
CytoFLEX flow cytometer	Beckman Coulter (Brea, CA, USA)
D300e digital dispenser	Tecan (Männedorf, Switzerland)
Eppendorf Reference pipette	Eppendorf (Hamburg, Germany)
Eppendorf Research pipette	Eppendorf (Hamburg, Germany)
Forma 3141 incubator	Thermo Fisher Scientific (Waltham, MA, USA)
Fresco 21 refrigerated centrifuge	Thermo Fisher Scientific (Waltham, MA, USA)
HERAfreeze ultra-low freezer	Thermo Fisher Scientific (Waltham, MA, USA)
HiSeq 2500 sequencer	Illumina (San Diego, CA, USA)
Incucyte S3 live-cell analysis system	Sartorius (Göttingen, Germany)
Maxwell RSC instrument	Promega (Madison, WI, USA)
Megafuge 3.0R centrifuge	Thermo Fisher Scientific (Waltham, MA, USA)
Milli-Q water purification system	Merck (Darmstadt, Germany)
Mr. Frosty freezing container	Thermo Fisher Scientific (Waltham, MA, USA)
Multidrop Combi reagent dispenser	Thermo Fisher Scientific (Waltham, MA, USA)
Multifuge 4KR centrifuge	Thermo Fisher Scientific (Waltham, MA, USA)
Multifuge X3R centrifuge	Thermo Fisher Scientific (Waltham, MA, USA)
PIPETBOY acu 2 pipetting controller	INTEGRA Biosciences Corp. (Hudson, NH, USA)
Quantus fluorometer	Promega (Madison, WI, USA)
Qubit fluorometer	Thermo Fisher Scientific (Waltham, MA, USA)
Safe 2020 biological safety cabinet	Thermo Fisher Scientific (Waltham, MA, USA)
Spark microplate reader	Tecan (Männedorf, Switzerland)
Vi-Cell XR cell viability analyzer	Beckman Coulter (Brea, CA, USA)

2.3. Software

Table 6 lists the various software tools used for the evaluation of *in vitro* drug screening results, data analyses, as well as preparation of text, tables and figures.

Table 6. List of software.

Software	Developer
CytExpert	Beckman Coulter (Brea, CA, USA)
D300eControl	Tecan (Männedorf, Switzerland)
D300eControl Data Merge	Tecan (Männedorf, Switzerland)
Drug screening analzyer (DSA)	Pauck, David
FILLit for Multidrop Combi	Thermo Fisher Scientific (Waltham, MA, USA)
Illustrator	Adobe (San José, CA, USA)
Incucyte S3 software	Sartorius (Göttingen, Germany)
Ingenuity Pathway Analysis (IPA)	Qiagen (Venlo, Netherlands)
Microsoft Office (Excel, Word)	Microsoft (Redmond, WA, USA)
Partek Flow & Partek Genomics Suite	Partek (Chesterfield, MO, USA)
Prism 8	Graphpad (San Diego, CA, USA)
SparkControl	Tecan (Männedorf, Switzerland)

2.4. Cell culture

Cell lines were obtained from the American Type Culture Collection (ATCC, Manassas, VA) (CHLA-01, CHLA-01R, CHLA-02, CHLA-04, DAOY, U138, U251, U87), the Children's Oncology Group (COG) Cell Line and Xenograft Repository (Texas Tech University Health Sciences Center, Lubbock, TX) (BT-12, CHLA-200, CHLA-266), the Children’s Hospital Los Angeles (Los Angeles, CA) (CHLA-05, CHLA-06), the Brain Tumor Resource Laboratory (Fred Hutchinson Cancer Research, Seattle, WA) (ATRT-310-FHTC, ATRT-311-FHTC), the Japanese Collection of Research Bioresources (JCRB) Cell Bank (National Institutes of Biomedical Innovation, Health and Nutrition, Tokyo, Japan) (AM-38, YH-13), ScienCell Research Laboratories (Carlsbad, CA) (Astrocytes-cerebellum, Astrocytes-cerebrum) Merck (Darmstadt, Germany) (mycINP) and Thermo Fisher Scientific (Waltham, MA) (NSC). VU397, ATRT13808 and JC-ATRT were kindly provided by Siddhartha Mitra, University of Colorado, Denver Anschutz Medical Campus, Aurora, CO. BT-16 was a gift from Annie Huang, Associate Chair of Research, Department of Pediatrics, SickKids and University of Toronto, Toronto, Canada. LN308 and LNT229 were kindly provided by Monika Hegi, Laboratory of Brain Tumour Biology and Genetics, University of Lausanne, Lausanne, Switzerland. D283, D425, Med8a, ONS76, UW-228-2 and UW-228-3 were kindly provided by Pablo Landgraf, Children's Clinic, University Hospital Cologne, Cologne, Germany. HD-MB03 was a gift by Till Milde, Heidelberg University Hospital, Heidelberg, Germany. MB3W1 was kindly provided by Matthias Wölfl, University

Children’s Hospital, Pediatric Oncology, Hematology and Stem Cell Transplantation, University of Würzburg, Würzburg, Germany. HHU-ATRT-01 was generated from AT/RT tumor tissue (Ethics vote study no. 2018-102-FmB). Culturing conditions for each cell line are depicted in Table 7. For the cell lines BT-12, BT-16 and CHLA-266 two different growth conditions were analyzed, one of which contained fetal bovine serum (FBS) and the other did not. Under serum-free conditions, 5 µg/ml Laminin were added to the cell suspension before subculturing/seeding. Cells were grown at 37 °C and 5 % CO_2 until confluent and then split accordingly. For adherent cell lines, prior enzymatic dissociation either using TrypLE (serum-free media) or Trypsin (FBS-supplemented media) was employed to retrieve a cell suspension. If necessary, clusters in suspension cell lines were broken up by repeated pipetting and/or incubation in Accutase. Prior to reseeding, cells were centrifuged at 300 x g and resuspended in fresh media. The cell density was measured by means of the Vi-Cell XR cell viability analyzer when required. Upon retrieval, STR profiling was conducted to exclude contamination with other commonly grown cell lines. Moreover, PCR-based mycoplasma testing using the Venor GeM Advance Kit was performed according to manufacturer's instructions to ensure absence of mycoplasma prior to prolonged cultivation. ATRT13808 required decontamination by means of the Plasmocin Treatment reagent, which was repeatedly added to the culturing media according to manufacturer's instructions. Re-testing was performed to verify the results. After negative testing, cryopreservation of cells was conducted by centrifuging cells at 300 x g and resuspending in culturing media supplemented with 10 % DMSO to generate stocks. Culturing of cells for longer than 20 passages was avoided by thawing earlier passages from stocks.

Table 7. Culturing conditions.

Cell Line	Entity	Media	Supplements	Seeding density
ATRT13808	AT/RT	DMEM/F-12 + Neurobasal-A Medium	2 % B27, 4 mM L-Glutamin, 1 % P/S, 10ng/ml LIF + EGF + FGF	3500
ATRT-310-FHTC	AT/RT	NeuroCult NS-A Basal Medium (Human)	10 % NeuroCult NS-A Proliferation Supplement (Human), 1 % P/S, 20 ng/ml EGF + FGF	5500
ATRT-311-FHTC	AT/RT	NeuroCult NS-A Basal Medium (Human)	10 % NeuroCult NS-A Proliferation Supplement (Human), 1 % P/S, 20 ng/ml EGF + FGF	7000
BT-12	AT/RT	IMDM	20 % FBS, 4mM L-Gluatmine, 1 % ITS	1750
BT-12SF	AT/RT	DMEM/F-12	2 % B27, 20 ng/ml EGF + FGF	5000
BT-16	AT/RT	IMDM	20 % FBS, 4mM L-Gluatmine, 1 % ITS	3500
BT-16SF	AT/RT	DMEM/F-12	2 % B27, 20 ng/ml EGF + FGF	5000
CHLA-02	AT/RT	DMEM/F-12	2 % B27, 20 ng/ml EGF + FGF	5000
CHLA-04	AT/RT	DMEM/F-12	2 % B27, 20 ng/ml EGF + FGF	4000
CHLA-05	AT/RT	DMEM/F-12	2 % B27, 20 ng/ml EGF + FGF	9000
CHLA-06	AT/RT	DMEM/F-12	2 % B27, 20 ng/ml EGF + FGF	6500
CHLA-266	AT/RT	IMDM	20 % FBS, 4mM L-Gluatmine, 1 % ITS	4500
CHLA-266SF	AT/RT	DMEM/F-12	2 % B27, 20 ng/ml EGF + FGF	10000
HHU-ATRT-01	AT/RT	Neurobasal-A Medium	2 % B27, 4mM L-Glutamin, 1 % P/S, 20ng/ml EGF + FGF	3500
JC-ATRT	AT/RT	DMEM/F-12 + Neurobasal-A Medium	2 % B27, 4 mM L-Glutamin, 1 % P/S, 10ng/ml LIF + EGF + FGF	7000
VU397	AT/RT	DMEM/F-12 + Neurobasal-A Medium	2 % B27, 4 mM L-Glutamin, 1 % P/S, 10ng/ml LIF + EGF + FGF	4500
AM-38	GBM	MEM	20 % FBS, 4 mM L-Glutamine	4000
CHLA-200	GBM	IMDM	20 % FBS, 4mM L-Gluatmine, 1 % ITS	1750
LN308	GBM	DMEM	10 % FBS, 1 % P/S	1750
LNT229	GBM	DMEM	10 % FBS, 1 % P/S	1000
U138	GBM	DMEM	10 % FBS, 1 % P/S	3500
U251	GBM	DMEM	10 % FBS, 1 % P/S	1250
U87	GBM	DMEM	10 % FBS, 1 % P/S	2000
YH-13	GBM	MEM	20 % FBS, 4 mM L-Glutamine	4000
CHLA-01	MB	DMEM/F-12	2 % B27, 20 ng/ml EGF + FGF	10000
CHLA-01R	MB	DMEM/F-12	2 % B27, 20 ng/ml EGF + FGF	10000
D283	MB	MEM	10 % FBS, 1 % GlutaMAX, 1 % P/S	5000
D425	MB	Improved MEM	10 % FBS, 1 % P/S	2500
DAOY	MB	DMEM	10 % FBS, 1 % P/S	1000
HD-MB03	MB	RPMI 1640	10 % FBS, 1 % NEAA	4000
MB3W1	MB	DMEM/F-12	2 % B27, 0.4 % P/S, 1 % MEM Vitamin solution, 20 ng/ml EGF + FGF	4000
Med8a	MB	DMEM	10 % FBS, 1 % P/S	2000
ONS76	MB	DMEM	10 % FBS, 1 % P/S	1000
UW-228-2	MB	DMEM	10 % FBS, 1 % P/S	750
UW-228-3	MB	DMEM	10 % FBS, 1 % P/S	1250
Human Astrocytes	Control	Astrocyte Medium	-	10000
Human Astrocytes (TAg)	Control	Astrocyte Medium	-	10000
Human Astrocytes-cerebellar	Control	Astrocyte Medium	-	10000
Human Neural Stem Cells (NSC) (H9-Derived)	Control	KnockOut DMEM/F-12	2 % StemPro Neural Supplement, 1 % GlutaMAX, 20ng/ml EGF + FGF	3500
ReNcell CX Immortalized Cell Line (mycINP)	Control	ReNcell NSC Maintenance Medium	20ng/ml EGF + FGF	1000

2.5. Seeding optimization procedure

To achieve a high assay performance, all cell lines underwent a seeding optimization procedure, which consisted of plating cells in 384-well plates in descending density by continuous dilution and reviewing confluency after 72 h of incubation at 37 °C and 5 % CO_2. The seeding density resulting in about 70-80 % confluency was chosen (cf. Table 7). As confluency is hard to estimate among cell lines growing in suspension, the CellTiter-Glo (CTG) Luminescent Cell Viability Assay was performed instead according to manufacturer's instructions. A seeding density reaching pre-plateau luminescence signal intensities after 72 h of incubation at 37 °C and 5 % CO_2 was identified that resulted in the lowest achievable coefficient of variation (CoV) between the wells.

2.6. Plate preparation

Upon receival, drug libraries (cf. 2.8) pre-dissolved in DMSO at a concentration of 10 mM were aliquoted. Using the manufacturer's datasheet, dispensing protocols were created using the D300eControl software by adding serial dilutions for all drugs distributed to an adequate number of plates. Based on pre-experiments (data not shown) performed by Viktoria Marquardt, a DMSO percentage of 0.25 % was chosen for the own screening workflow. Based on a 10 mM stock solution, a percentage of 0.25 % DMSO allowed to dispense a maximum screening concentration of 25,000 nM (i.e. 25 µM). Increasing the dispensing stocks above a concentration of 10 mM was not advised by the best practice instructions of the D300e dispenser, as this might influence the dispensing quality due to an increased viscosity of solutions with a higher molarity. The lower end of the concentration range was 5 nM as this concentration corresponded to the minimum droplet size to be dispensed using a 10 mM stock solution by the D300e. Due to a short-term decision to reduce the working volume in 1536-well plates from 5 µl to 4 µl, the 0.25 % DMSO margin was slightly exceeded to 0.3125 % in the 1536-well plate-based screenings in this thesis. Each plate held at least three non-treated (NT) wells as negative controls as well as three DMSO-treated wells for normalization. Moreover, a positive control, i.e., a dilution series of a control drug, usually Staurosporine, was added to each plate. White 384-well plates were transferred (either newly unboxed or filled with cell suspension, cf. 3.1.3) to the biological safety cabinet and labeled with library, library version, dispensing cycle, plate number and replicate. Dispensing protocols prepared earlier were loaded into D300eControl, D300e was connected to the computer and the dispensing procedure was started. D300eControl then guided the operator through the dispensing (from now

on referred to as “printing”) process by instructing to exchange dispensehead cassettes, pipet drugs or load plates. To avoid unnecessary degradation, drugs were thawed immediately before pipetting to the dispensehead cassettes. After printing the plates were sealed using Parafilm and immediately stored frozen at -80 °C (or incubated at 37 °C and 5 % CO_2 if the plates were containing cells, cf. 3.1.3).

2.7. Drug screening

After initial optimization of the seeding density (cf. 2.5) cells were cultured until reaching sufficient numbers for drug screening. Readily prepared plates were thawed for 60-120 minutes at room temperature and cells were harvested to receive a single cell suspension. After removal of any clumps by straining, the cell density was measured using the Vi-Cell XR. Then cells were diluted to the corresponding density for screening (cf. Table 7. Culturing conditions) and stored in a large centrifuge tube with conical bottom. Prior to seeding the MultiDrop Combi dispenser was equipped with a dispensing cassette and flushed using Ethanol for disinfection and primed with phosphate buffered saline (PBS) for equilibration. Next, the cell suspension was resuspended by repeated inversions. Then the tubings of the MultiDrop Combi were placed aseptically into the cell suspension and microplates were immediately filled one after the other with 30 µl (384-well plates) or 4 µl (1536-well plate) of cell suspension per well. During the dispensing process, the cell suspension was gently agitated to avoid settling of the cells. After dispensing, the MultiDrop Combi was immediately flushed using ultrapure water, Ethanol and again twice using ultrapure water. The dispensing cassette was removed and allowed to air dry. Plates were transferred to the incubator and incubated for 72 h at 37 °C and 5 % CO_2. After the incubation period, plates were equilibrated to room temperature. After equilibration, the readout was conducted by adding equal volumes of CTG to each well using the MultiDrop Combi, which was prepared and cleaned as previously described. Following at least 10 minutes of additional incubation at room temperature the luminescence signal intensities of each well were acquired at an integration time of 500 ms (384-well plates) or 250 ms (1536-well plates) using the Spark microplate reader. The raw data were stored as Excel sheets by the SparkControl software. The MultiDrop Combi was regularly cleaned in accordance with maintenance guidelines.

2.8. Drug libraries

Table 8 shows the list of drugs included in the drug libraries used for *in vitro* drug screening. The following abbreviations were used: Epigenetics Toolbox (EG), Kinase Inhibitor Toolbox (KI), Clinical Library Standard (CLS) and Clinical Library Extended (CLE).

Table 8. List of drugs included in the used drug libraries.

Drug	Class	Library	Cat. No.	Manufacturer
3-Deazaneplanocin A hydrochloride	HMT	Clinical Library Standard	HY-12186	MedChemExpress (Monmouth Junction, NJ, USA)
5-Azacytidine	Nucleoside Antimetabolite	Clinical Library Standard	HY-10586	MedChemExpress (Monmouth Junction, NJ, USA)
5-Fluorouracil	Nucleoside Antimetabolite	Clinical Library Standard	HY-90006	MedChemExpress (Monmouth Junction, NJ, USA)
6-Mercaptopurine	Nucleoside Antimetabolite	Clinical Library Standard	HY-13677	MedChemExpress (Monmouth Junction, NJ, USA)
6-Thioguanine	DNMT	Clinical Library Standard	HY-13765	MedChemExpress (Monmouth Junction, NJ, USA)
Abiraterone	Cytochrome P450	Clinical Library Standard	HY-70013	MedChemExpress (Monmouth Junction, NJ, USA)
ABT-199	BCL2	Clinical Library Standard	HY-15531	MedChemExpress (Monmouth Junction, NJ, USA)
Actinomycin D	DNA/RNA Synthesis	Clinical Library Standard	HY-17559	MedChemExpress (Monmouth Junction, NJ, USA)
Afatinib dimaleate	EGFR	Clinical Library Standard	HY-10261A	MedChemExpress (Monmouth Junction, NJ, USA)
AG-221	IDH	Clinical Library Standard	HY-18690	MedChemExpress (Monmouth Junction, NJ, USA)
AICAR	AMPK	Clinical Library Standard	HY-13417	MedChemExpress (Monmouth Junction, NJ, USA)
Alisertib	ARK	Clinical Library Standard	HY-10971	MedChemExpress (Monmouth Junction, NJ, USA)
Altretamine	DNA Alkylator/Crosslinker	Clinical Library Standard	HY-B0181	MedChemExpress (Monmouth Junction, NJ, USA)
Amonafide	Topoisomerase	Clinical Library Standard	HY-10982	MedChemExpress (Monmouth Junction, NJ, USA)
Amsacrine	Topoisomerase	Clinical Library Standard	HY-13551	MedChemExpress (Monmouth Junction, NJ, USA)
Anacetrapib	CETP	Clinical Library Standard	HY-12090	MedChemExpress (Monmouth Junction, NJ, USA)
Anastrozole	Aromatase	Clinical Library Standard	HY-14274	MedChemExpress (Monmouth Junction, NJ, USA)
ARN-509	AR	Clinical Library Standard	HY-16060	MedChemExpress (Monmouth Junction, NJ, USA)
Auranofin	Others	Clinical Library Standard	HY-B1123	MedChemExpress (Monmouth Junction, NJ, USA)
Axitinib	VEGFR	Clinical Library Standard	HY-10065	MedChemExpress (Monmouth Junction, NJ, USA)
AZD-9291	EGFR	Clinical Library Standard	HY-15772A	MedChemExpress (Monmouth Junction, NJ, USA)
Bardoxolone methyl	IKK	Clinical Library Standard	HY-13324	MedChemExpress (Monmouth Junction, NJ, USA)
Baricitinib phosphate	JAK	Clinical Library Standard	HY-15315A	MedChemExpress (Monmouth Junction, NJ, USA)
BAY 80-6946	PI3K	Clinical Library Standard	HY-15346	MedChemExpress (Monmouth Junction, NJ, USA)
Bazedoxifene acetate	ER	Clinical Library Standard	HY-A0036	MedChemExpress (Monmouth Junction, NJ, USA)
Belinostat	HDAC	Clinical Library Standard	HY-10225	MedChemExpress (Monmouth Junction, NJ, USA)
Bendamustine hydrochloride	DNA Alkylator/Crosslinker	Clinical Library Standard	HY-B0077	MedChemExpress (Monmouth Junction, NJ, USA)
Bestatin	Antibiotic	Clinical Library Standard	HY-B0134	MedChemExpress (Monmouth Junction, NJ, USA)
Bexarotene	RAR/RXR	Clinical Library Standard	HY-14171	MedChemExpress (Monmouth Junction, NJ, USA)
BIBF 1120	FGFR	Clinical Library Standard	HY-50904	MedChemExpress (Monmouth Junction, NJ, USA)
Bicalutamide	AR	Clinical Library Standard	HY-14249	MedChemExpress (Monmouth Junction, NJ, USA)
Bleomycin sulfate	DNA/RNA Synthesis	Clinical Library Standard	HY-17565	MedChemExpress (Monmouth Junction, NJ, USA)
BMN-673	PARP	Clinical Library Standard	HY-16106A	MedChemExpress (Monmouth Junction, NJ, USA)
Bortezomib	Proteasome	Clinical Library Standard	HY-10227	MedChemExpress (Monmouth Junction, NJ, USA)
Bosutinib	BCR-ABL	Clinical Library Standard	HY-10158	MedChemExpress (Monmouth Junction, NJ, USA)
Brigatinib	ALK	Clinical Library Standard	HY-12857	MedChemExpress (Monmouth Junction, NJ, USA)
Brivanib	VEGFR	Clinical Library Standard	HY-10337	MedChemExpress (Monmouth Junction, NJ, USA)
BSI-201	PARP	Clinical Library Standard	HY-12015	MedChemExpress (Monmouth Junction, NJ, USA)
Busulfan	DNA Alkylator/Crosslinker	Clinical Library Standard	HY-B0245	MedChemExpress (Monmouth Junction, NJ, USA)
BYL-719	PI3K	Clinical Library Standard	HY-15244	MedChemExpress (Monmouth Junction, NJ, USA)
Cabazitaxel	Microtubule/Tubulin	Clinical Library Standard	HY-15459	MedChemExpress (Monmouth Junction, NJ, USA)
Cabozantinib S-malate	VEGFR	Clinical Library Standard	HY-12044	MedChemExpress (Monmouth Junction, NJ, USA)
CAL-101	PI3K	Clinical Library Standard	HY-13026	MedChemExpress (Monmouth Junction, NJ, USA)
Canertinib	EGFR	Clinical Library Standard	HY-10367	MedChemExpress (Monmouth Junction, NJ, USA)
Capecitabine	Nucleoside Antimetabolite	Clinical Library Standard	HY-B0016	MedChemExpress (Monmouth Junction, NJ, USA)
Carboplatin	DNA Alkylator/Crosslinker	Clinical Library Standard	HY-17393	MedChemExpress (Monmouth Junction, NJ, USA)
Carfilzomib	Proteasome	Clinical Library Standard	HY-10455	MedChemExpress (Monmouth Junction, NJ, USA)
Carmustine	DNA Alkylator/Crosslinker	Clinical Library Standard	HY-13585	MedChemExpress (Monmouth Junction, NJ, USA)
Cediranib	PDGFR	Clinical Library Standard	HY-10205	MedChemExpress (Monmouth Junction, NJ, USA)
Celecoxib	COX	Clinical Library Standard	HY-14398	MedChemExpress (Monmouth Junction, NJ, USA)
CH5424802	ALK	Clinical Library Standard	HY-13011	MedChemExpress (Monmouth Junction, NJ, USA)
Chlorambucil	DNA Alkylator/Crosslinker	Clinical Library Standard	HY-13593	MedChemExpress (Monmouth Junction, NJ, USA)
Chlormethine hydrochloride	Others	Clinical Library Standard	HY-B1253	MedChemExpress (Monmouth Junction, NJ, USA)
CI-994	HDAC	Clinical Library Standard	HY-50934	MedChemExpress (Monmouth Junction, NJ, USA)
Cisplatin	DNA Alkylator/Crosslinker	Clinical Library Standard	HY-17394	MedChemExpress (Monmouth Junction, NJ, USA)
Cladribine	ADA	Clinical Library Standard	HY-13599	MedChemExpress (Monmouth Junction, NJ, USA)
Clofarabine	Nucleoside Antimetabolite	Clinical Library Standard	HY-A0005	MedChemExpress (Monmouth Junction, NJ, USA)
Cobimetinib	MEK	Clinical Library Standard	HY-13064	MedChemExpress (Monmouth Junction, NJ, USA)
Crizotinib	ALK	Clinical Library Standard	HY-50878	MedChemExpress (Monmouth Junction, NJ, USA)
Cytarabine	Nucleoside Antimetabolite	Clinical Library Standard	HY-13605	MedChemExpress (Monmouth Junction, NJ, USA)
Dabrafenib mesylate	RAF	Clinical Library Standard	HY-14660A	MedChemExpress (Monmouth Junction, NJ, USA)
Dacarbazine	Nucleoside Antimetabolite	Clinical Library Standard	HY-B0078	MedChemExpress (Monmouth Junction, NJ, USA)
Dacomitinib	EGFR	Clinical Library Standard	HY-13272	MedChemExpress (Monmouth Junction, NJ, USA)
Dapagliflozin	SGLT	Clinical Library Standard	HY-10450	MedChemExpress (Monmouth Junction, NJ, USA)
Dasatinib	BCR-ABL	Clinical Library Standard	HY-10181A	MedChemExpress (Monmouth Junction, NJ, USA)
Daunorubicin hydrochloride	Topoisomerase	Clinical Library Standard	HY-13062	MedChemExpress (Monmouth Junction, NJ, USA)
Decitabine	Nucleoside Antimetabolite	Clinical Library Standard	HY-A0004	MedChemExpress (Monmouth Junction, NJ, USA)
Deforolimus	MTOR	Clinical Library Standard	HY-50908	MedChemExpress (Monmouth Junction, NJ, USA)
Dinaciclib	CDK	Clinical Library Standard	HY-10492	MedChemExpress (Monmouth Junction, NJ, USA)
Docetaxel	Microtubule/Tubulin	Clinical Library Standard	HY-B0011	MedChemExpress (Monmouth Junction, NJ, USA)
Dovitinib	KIT	Clinical Library Standard	HY-50905	MedChemExpress (Monmouth Junction, NJ, USA)
Doxorubicin hydrochloride	Topoisomerase	Clinical Library Standard	HY-15142	MedChemExpress (Monmouth Junction, NJ, USA)
Elesclomol	Apoptosis	Clinical Library Standard	HY-12040	MedChemExpress (Monmouth Junction, NJ, USA)
Entinostat	HDAC	Clinical Library Standard	HY-12163	MedChemExpress (Monmouth Junction, NJ, USA)
Entrectinib	ALK	Clinical Library Standard	HY-12678	MedChemExpress (Monmouth Junction, NJ, USA)
Enzastaurin	PKC	Clinical Library Standard	HY-10342	MedChemExpress (Monmouth Junction, NJ, USA)
Epirubicin hydrochloride	Topoisomerase	Clinical Library Standard	HY-13624A	MedChemExpress (Monmouth Junction, NJ, USA)
EPZ-6438	HMT	Clinical Library Standard	HY-13803	MedChemExpress (Monmouth Junction, NJ, USA)
Eribulin mesylate	Microtubule/Tubulin	Clinical Library Standard	HY-13442A	MedChemExpress (Monmouth Junction, NJ, USA)
Erlotinib hydrochloride	EGFR	Clinical Library Standard	HY-50896	MedChemExpress (Monmouth Junction, NJ, USA)
Estramustine phosphate sodium	Microtubule/Tubulin	Clinical Library Standard	HY-13627	MedChemExpress (Monmouth Junction, NJ, USA)
Etoposide	Topoisomerase	Clinical Library Standard	HY-13629	MedChemExpress (Monmouth Junction, NJ, USA)
Everolimus	MTOR	Clinical Library Standard	HY-10218	MedChemExpress (Monmouth Junction, NJ, USA)
Floxuridine	Nucleoside Antimetabolite	Clinical Library Standard	HY-B0097	MedChemExpress (Monmouth Junction, NJ, USA)
Fludarabine phosphate	Nucleoside Antimetabolite	Clinical Library Standard	HY-B0028	MedChemExpress (Monmouth Junction, NJ, USA)

Drug	Class	Library	Cat. No.	Manufacturer
Flutamide	AR	Clinical Library Standard	HY-B0022	MedChemExpress (Monmouth Junction, NJ, USA)
Fosbretabulin disodium	Microtubule/Tubulin	Clinical Library Standard	HY-17449	MedChemExpress (Monmouth Junction, NJ, USA)
Ganetespib	HSP90	Clinical Library Standard	HY-15205	MedChemExpress (Monmouth Junction, NJ, USA)
GANT-61	Hedgehog	Clinical Library Standard	HY-13901	MedChemExpress (Monmouth Junction, NJ, USA)
Gefitinib	EGFR	Clinical Library Standard	HY-50895	MedChemExpress (Monmouth Junction, NJ, USA)
Gilteritinib	FLT3	Clinical Library Standard	HY-12432	MedChemExpress (Monmouth Junction, NJ, USA)
GSK126	HMT	Clinical Library Standard	HY-13470	MedChemExpress (Monmouth Junction, NJ, USA)
GSK343	HMT	Clinical Library Standard	HY-13500	MedChemExpress (Monmouth Junction, NJ, USA)
GSK525762A	BET	Clinical Library Standard	HY-13032	MedChemExpress (Monmouth Junction, NJ, USA)
Homoharringtonine	STAT	Clinical Library Standard	HY-14944	MedChemExpress (Monmouth Junction, NJ, USA)
Honokiol	AKT	Clinical Library Standard	HY-N0003	MedChemExpress (Monmouth Junction, NJ, USA)
Idarubicin hydrochloride	Topoisomerase	Clinical Library Standard	HY-17381	MedChemExpress (Monmouth Junction, NJ, USA)
Imatinib mesylate	BCR-ABL	Clinical Library Standard	HY-50946	MedChemExpress (Monmouth Junction, NJ, USA)
IPI-145	PI3K	Clinical Library Standard	HY-17044A	MedChemExpress (Monmouth Junction, NJ, USA)
Irinotecan	Topoisomerase	Clinical Library Standard	HY-16562	MedChemExpress (Monmouth Junction, NJ, USA)
Itraconazole	Hedgehog	Clinical Library Standard	HY-17514	MedChemExpress (Monmouth Junction, NJ, USA)
Ivosidenib	IDH	Clinical Library Standard	HY-18767	MedChemExpress (Monmouth Junction, NJ, USA)
Ixabepilone	Microtubule/Tubulin	Clinical Library Standard	HY-10222	MedChemExpress (Monmouth Junction, NJ, USA)
Lapatinib	EGFR	Clinical Library Standard	HY-50898	MedChemExpress (Monmouth Junction, NJ, USA)
LDE225	Hedgehog	Clinical Library Standard	HY-16582A	MedChemExpress (Monmouth Junction, NJ, USA)
LDK378	ALK	Clinical Library Standard	HY-15656	MedChemExpress (Monmouth Junction, NJ, USA)
LEE011	CDK	Clinical Library Standard	HY-15777	MedChemExpress (Monmouth Junction, NJ, USA)
Lenvatinib	KIT	Clinical Library Standard	HY-10981	MedChemExpress (Monmouth Junction, NJ, USA)
Letrozole	Aromatase	Clinical Library Standard	HY-14248	MedChemExpress (Monmouth Junction, NJ, USA)
LGX818	RAF	Clinical Library Standard	HY-15605	MedChemExpress (Monmouth Junction, NJ, USA)
Linifanib	CSF1R	Clinical Library Standard	HY-50751	MedChemExpress (Monmouth Junction, NJ, USA)
Linsitinib	IGF-1R	Clinical Library Standard	HY-10191	MedChemExpress (Monmouth Junction, NJ, USA)
Lomustine	DNA Alkylator/Crosslinker	Clinical Library Standard	HY-13669	MedChemExpress (Monmouth Junction, NJ, USA)
Lonafarnib	FTase	Clinical Library Standard	HY-15136	MedChemExpress (Monmouth Junction, NJ, USA)
Losmapimod	p38 MAPK	Clinical Library Standard	HY-10402	MedChemExpress (Monmouth Junction, NJ, USA)
LY2835219	CDK	Clinical Library Standard	HY-16297	MedChemExpress (Monmouth Junction, NJ, USA)
LY3009120	RAF	Clinical Library Standard	HY-12558	MedChemExpress (Monmouth Junction, NJ, USA)
Marimastat	MMP	Clinical Library Standard	HY-12169	MedChemExpress (Monmouth Junction, NJ, USA)
Masitinib	KIT	Clinical Library Standard	HY-10209	MedChemExpress (Monmouth Junction, NJ, USA)
MEK162	MEK	Clinical Library Standard	HY-15202	MedChemExpress (Monmouth Junction, NJ, USA)
Melphalan	DNA Alkylator/Crosslinker	Clinical Library Standard	HY-17575	MedChemExpress (Monmouth Junction, NJ, USA)
Methotrexate	Antifolate	Clinical Library Standard	HY-14519	MedChemExpress (Monmouth Junction, NJ, USA)
Mitomycin C	DNA Alkylator/Crosslinker	Clinical Library Standard	HY-13316	MedChemExpress (Monmouth Junction, NJ, USA)
Mitoxantrone dihydrochloride	Topoisomerase	Clinical Library Standard	HY-13502A	MedChemExpress (Monmouth Junction, NJ, USA)
MLN9708	Proteasome	Clinical Library Standard	HY-10452	MedChemExpress (Monmouth Junction, NJ, USA)
Motesanib diphosphate	KIT	Clinical Library Standard	HY-10229	MedChemExpress (Monmouth Junction, NJ, USA)
Nelarabine	Nucleoside Antimetabolite	Clinical Library Standard	HY-13701	MedChemExpress (Monmouth Junction, NJ, USA)
Neratinib	EGFR	Clinical Library Standard	HY-32721	MedChemExpress (Monmouth Junction, NJ, USA)
Nilotinib	BCR-ABL	Clinical Library Standard	HY-10159	MedChemExpress (Monmouth Junction, NJ, USA)
Obatoclax mesylate	BCL2	Clinical Library Standard	HY-10969	MedChemExpress (Monmouth Junction, NJ, USA)
Olaparib	PARP	Clinical Library Standard	HY-10162	MedChemExpress (Monmouth Junction, NJ, USA)
Oxaliplatin	DNA Alkylator/Crosslinker	Clinical Library Standard	HY-17371	MedChemExpress (Monmouth Junction, NJ, USA)
Paclitaxel	Microtubule/Tubulin	Clinical Library Standard	HY-B0015	MedChemExpress (Monmouth Junction, NJ, USA)
Pacritinib	FLT3	Clinical Library Standard	HY-16379	MedChemExpress (Monmouth Junction, NJ, USA)
Palbociclib	CDK	Clinical Library Standard	HY-50767	MedChemExpress (Monmouth Junction, NJ, USA)
Panobinostat	HDAC	Clinical Library Standard	HY-10224	MedChemExpress (Monmouth Junction, NJ, USA)
Pazopanib hydrochloride	CSF1R	Clinical Library Standard	HY-12009	MedChemExpress (Monmouth Junction, NJ, USA)
PCI-32765	BTK	Clinical Library Standard	HY-10997	MedChemExpress (Monmouth Junction, NJ, USA)
Pemetrexed	Antifolate	Clinical Library Standard	HY-13781	MedChemExpress (Monmouth Junction, NJ, USA)
Pentostatin	Adenosine Deaminase	Clinical Library Standard	HY-A0006	MedChemExpress (Monmouth Junction, NJ, USA)
Perifosine	AKT	Clinical Library Standard	HY-50909	MedChemExpress (Monmouth Junction, NJ, USA)
PF-04449913	Hedgehog	Clinical Library Standard	HY-16391	MedChemExpress (Monmouth Junction, NJ, USA)
PF-06463922	ALK	Clinical Library Standard	HY-12215	MedChemExpress (Monmouth Junction, NJ, USA)
Pipobroman	Others	Clinical Library Standard	HY-16398	MedChemExpress (Monmouth Junction, NJ, USA)
Ponatinib	BCR-ABL	Clinical Library Standard	HY-12047	MedChemExpress (Monmouth Junction, NJ, USA)
Pralatrexate	Antifolate	Clinical Library Standard	HY-10446	MedChemExpress (Monmouth Junction, NJ, USA)
Procarbazine hydrochloride	DNA Alkylator/Crosslinker	Clinical Library Standard	HY-13733	MedChemExpress (Monmouth Junction, NJ, USA)
Quizartinib	FLT3	Clinical Library Standard	HY-13001	MedChemExpress (Monmouth Junction, NJ, USA)
Regorafenib	PDGFR	Clinical Library Standard	HY-10331	MedChemExpress (Monmouth Junction, NJ, USA)
Retinoic acid	PPAR	Clinical Library Standard	HY-14649	MedChemExpress (Monmouth Junction, NJ, USA)
Rigosertib sodium	PI3K	Clinical Library Standard	HY-12037	MedChemExpress (Monmouth Junction, NJ, USA)
Romidepsin	HDAC	Clinical Library Standard	HY-15149	MedChemExpress (Monmouth Junction, NJ, USA)
Rucaparib phosphate	PARP	Clinical Library Standard	HY-10617	MedChemExpress (Monmouth Junction, NJ, USA)
Ruxolitinib phosphate	JAK	Clinical Library Standard	HY-50858	MedChemExpress (Monmouth Junction, NJ, USA)
Selumetinib	MEK	Clinical Library Standard	HY-50706	MedChemExpress (Monmouth Junction, NJ, USA)
Semagacestat	Notch	Clinical Library Standard	HY-10009	MedChemExpress (Monmouth Junction, NJ, USA)
SNS-314 mesylate	ARK	Clinical Library Standard	HY-12003	MedChemExpress (Monmouth Junction, NJ, USA)
Sorafenib tosylate	FLT3	Clinical Library Standard	HY-10201A	MedChemExpress (Monmouth Junction, NJ, USA)
Streptozocin	DNA Alkylator/Crosslinker	Clinical Library Standard	HY-13753	MedChemExpress (Monmouth Junction, NJ, USA)
Sunitinib	PDGFR	Clinical Library Standard	HY-10255	MedChemExpress (Monmouth Junction, NJ, USA)
TAK-632	ARK	Clinical Library Standard	HY-15767	MedChemExpress (Monmouth Junction, NJ, USA)
TAK-715	p38 MAPK	Clinical Library Standard	HY-10456	MedChemExpress (Monmouth Junction, NJ, USA)
Tamoxifen	ER	Clinical Library Standard	HY-13757A	MedChemExpress (Monmouth Junction, NJ, USA)
Tariquidar	P-glycoprotein	Clinical Library Standard	HY-10550	MedChemExpress (Monmouth Junction, NJ, USA)
Tasquinimod	HDAC	Clinical Library Standard	HY-10528	MedChemExpress (Monmouth Junction, NJ, USA)
Temozolomide	DNA Alkylator/Crosslinker	Clinical Library Standard	HY-17364	MedChemExpress (Monmouth Junction, NJ, USA)
Temsirolimus	MTOR	Clinical Library Standard	HY-50910	MedChemExpress (Monmouth Junction, NJ, USA)
Teniposide	Topoisomerase	Clinical Library Standard	HY-13761	MedChemExpress (Monmouth Junction, NJ, USA)
TG-101348	JAK	Clinical Library Standard	HY-10409	MedChemExpress (Monmouth Junction, NJ, USA)
Thalidomide	E3 Ligase	Clinical Library Standard	HY-14658	MedChemExpress (Monmouth Junction, NJ, USA)
Thio-TEPA	DNA Alkylator/Crosslinker	Clinical Library Standard	HY-17574	MedChemExpress (Monmouth Junction, NJ, USA)
Tipifarnib	FTase	Clinical Library Standard	HY-10502A	MedChemExpress (Monmouth Junction, NJ, USA)
Tipiracil hydrochloride	Nucleoside Antimetabolite	Clinical Library Standard	HY-A0063	MedChemExpress (Monmouth Junction, NJ, USA)
Tivantinib	MET/HGFR	Clinical Library Standard	HY-50686	MedChemExpress (Monmouth Junction, NJ, USA)
Tivozanib	VEGFR	Clinical Library Standard	HY-10977	MedChemExpress (Monmouth Junction, NJ, USA)
Topotecan hydrochloride	Topoisomerase	Clinical Library Standard	HY-13768A	MedChemExpress (Monmouth Junction, NJ, USA)
Trametinib	MEK	Clinical Library Standard	HY-10999	MedChemExpress (Monmouth Junction, NJ, USA)
Trifluorothymidine	Nucleoside Antimetabolite	Clinical Library Standard	HY-A0061	MedChemExpress (Monmouth Junction, NJ, USA)
TSU-68	FGFR	Clinical Library Standard	HY-10517	MedChemExpress (Monmouth Junction, NJ, USA)
Tubastatin A hydrochloride	HDAC	Clinical Library Standard	HY-13271	MedChemExpress (Monmouth Junction, NJ, USA)
Uramustine	DNA Alkylator/Crosslinker	Clinical Library Standard	HY-13544	MedChemExpress (Monmouth Junction, NJ, USA)
Valproic acid	HDAC	Clinical Library Standard	HY-10585A	MedChemExpress (Monmouth Junction, NJ, USA)
Valrubicin	PKC	Clinical Library Standard	HY-13772	MedChemExpress (Monmouth Junction, NJ, USA)
Vandetanib	VEGFR	Clinical Library Standard	HY-10260	MedChemExpress (Monmouth Junction, NJ, USA)
Vatalanib dihydrochloride	VEGFR	Clinical Library Standard	HY-12018	MedChemExpress (Monmouth Junction, NJ, USA)
Veliparib	PARP	Clinical Library Standard	HY-10130	MedChemExpress (Monmouth Junction, NJ, USA)
Vemurafenib	RAF	Clinical Library Standard	HY-12057	MedChemExpress (Monmouth Junction, NJ, USA)
Vinblastine sulfate	Microtubule/Tubulin	Clinical Library Standard	HY-13780	MedChemExpress (Monmouth Junction, NJ, USA)
Vincristine sulfate	Microtubule/Tubulin	Clinical Library Standard	HY-N0488	MedChemExpress (Monmouth Junction, NJ, USA)

Drug	Class	Library	Cat. No.	Manufacturer
Vinflunine tartrate	Microtubule/Tubulin	Clinical Library Standard	HY-B0628A	MedChemExpress (Monmouth Junction, NJ, USA)
Vismodegib	Hedgehog	Clinical Library Standard	HY-10440	MedChemExpress (Monmouth Junction, NJ, USA)
Volasertib	PLK	Clinical Library Standard	HY-12137	MedChemExpress (Monmouth Junction, NJ, USA)
Vorinostat	HDAC	Clinical Library Standard	HY-10221	MedChemExpress (Monmouth Junction, NJ, USA)
WP1066	JAK	Clinical Library Standard	HY-15312	MedChemExpress (Monmouth Junction, NJ, USA)
Zibotentan	ET	Clinical Library Standard	HY-10088	MedChemExpress (Monmouth Junction, NJ, USA)
Zoledronic acid monohydrate	Others	Clinical Library Standard	HY-13777A	MedChemExpress (Monmouth Junction, NJ, USA)
Zosuquidar trihydrochloride	P-glycoprotein	Clinical Library Standard	HY-50671	MedChemExpress (Monmouth Junction, NJ, USA)
(-)-Epigallocatechin gallate	Endogenous Metabolite	Clinical Library Extended	HY-13653	MedChemExpress (Monmouth Junction, NJ, USA)
(-)-p-Bromotetramisole oxalate	Phosphatase	Clinical Library Extended	HY-19695	MedChemExpress (Monmouth Junction, NJ, USA)
(R,S)-Ivosidenib	IDH	Clinical Library Extended	HY-18767A	MedChemExpress (Monmouth Junction, NJ, USA)
(S)-10-Hydroxycamptothecin	Topoisomerase	Clinical Library Extended	HY-N0095	MedChemExpress (Monmouth Junction, NJ, USA)
(S)-MCPG	Receptor Antagonist	Clinical Library Extended	HY-100406	MedChemExpress (Monmouth Junction, NJ, USA)
17-AAG	HSP90	Clinical Library Extended	HY-10211	MedChemExpress (Monmouth Junction, NJ, USA)
2-Methoxyestradiol	Microtubule/Tubulin	Clinical Library Extended	HY-12033	MedChemExpress (Monmouth Junction, NJ, USA)
3,3'-Diindolylmethane	AR	Clinical Library Extended	HY-15758	MedChemExpress (Monmouth Junction, NJ, USA)
4SC-202 tosylate	HDAC	Clinical Library Extended	HY-16012	MedChemExpress (Monmouth Junction, NJ, USA)
Abarelix	GNRH Receptor	Clinical Library Extended	HY-13534	MedChemExpress (Monmouth Junction, NJ, USA)
ABC294640	Others	Clinical Library Extended	HY-16015	MedChemExpress (Monmouth Junction, NJ, USA)
ABT-737	BCL2	Clinical Library Extended	HY-50907	MedChemExpress (Monmouth Junction, NJ, USA)
ABT-751	Microtubule/Tubulin	Clinical Library Extended	HY-13270	MedChemExpress (Monmouth Junction, NJ, USA)
ACY-1215	HDAC	Clinical Library Extended	HY-16026	MedChemExpress (Monmouth Junction, NJ, USA)
Adarotene	Apoptosis	Clinical Library Extended	HY-14808	MedChemExpress (Monmouth Junction, NJ, USA)
AEE788	EGFR	Clinical Library Extended	HY-10045	MedChemExpress (Monmouth Junction, NJ, USA)
Afuresertib	AKT	Clinical Library Extended	HY-15727	MedChemExpress (Monmouth Junction, NJ, USA)
AG-490	EGFR	Clinical Library Extended	HY-12000	MedChemExpress (Monmouth Junction, NJ, USA)
AGI-5198	IDH	Clinical Library Extended	HY-18082	MedChemExpress (Monmouth Junction, NJ, USA)
Alendronate sodium hydrate	Others	Clinical Library Extended	HY-11101	MedChemExpress (Monmouth Junction, NJ, USA)
Alprenolol hydrochloride	5-HT Receptor	Clinical Library Extended	HY-B1517A	MedChemExpress (Monmouth Junction, NJ, USA)
Alvespimycin hydrochloride	HSP90	Clinical Library Extended	HY-12024	MedChemExpress (Monmouth Junction, NJ, USA)
AMG-208	MET/HGFR	Clinical Library Extended	HY-12035	MedChemExpress (Monmouth Junction, NJ, USA)
AMG-232	MDM2	Clinical Library Extended	HY-12296	MedChemExpress (Monmouth Junction, NJ, USA)
AMG-319	PI3K	Clinical Library Extended	HY-12948	MedChemExpress (Monmouth Junction, NJ, USA)
AMG-337	MET/HGFR	Clinical Library Extended	HY-18696	MedChemExpress (Monmouth Junction, NJ, USA)
AMG-900	ARK	Clinical Library Extended	HY-13253	MedChemExpress (Monmouth Junction, NJ, USA)
AMG-925	CDK	Clinical Library Extended	HY-15889	MedChemExpress (Monmouth Junction, NJ, USA)
Amifostine	Others	Clinical Library Extended	HY-B0639	MedChemExpress (Monmouth Junction, NJ, USA)
Amiselimod hydrochloride	Receptor Antagonist	Clinical Library Extended	HY-16734A	MedChemExpress (Monmouth Junction, NJ, USA)
Amisulpride	Receptor Antagonist	Clinical Library Extended	HY-14545	MedChemExpress (Monmouth Junction, NJ, USA)
Amuvatinib	KIT	Clinical Library Extended	HY-10206	MedChemExpress (Monmouth Junction, NJ, USA)
Amygdalin	Endogenous Metabolite	Clinical Library Extended	HY-N0190	MedChemExpress (Monmouth Junction, NJ, USA)
Anamorelin	GHSR	Clinical Library Extended	HY-14734	MedChemExpress (Monmouth Junction, NJ, USA)
Ancitabine hydrochloride	Nucleoside Antimetabolite	Clinical Library Extended	HY-N0093	MedChemExpress (Monmouth Junction, NJ, USA)
Andrographolide	NF-κB	Clinical Library Extended	HY-N0191	MedChemExpress (Monmouth Junction, NJ, USA)
Anethole	Others	Clinical Library Extended	HY-B0900	MedChemExpress (Monmouth Junction, NJ, USA)
Apocynin	Apoptosis	Clinical Library Extended	HY-N0088	MedChemExpress (Monmouth Junction, NJ, USA)
Aprepitant	Others	Clinical Library Extended	HY-10052	MedChemExpress (Monmouth Junction, NJ, USA)
APTO-253	MYC	Clinical Library Extended	HY-16291	MedChemExpress (Monmouth Junction, NJ, USA)
ARQ-092	AKT	Clinical Library Extended	HY-19719	MedChemExpress (Monmouth Junction, NJ, USA)
ARRY-520	KSP	Clinical Library Extended	HY-15187A	MedChemExpress (Monmouth Junction, NJ, USA)
Artesunate	STAT	Clinical Library Extended	S-S2265	Selleck Chemicals (Houston, TX, USA)
AS703026	MEK	Clinical Library Extended	HY-12042	MedChemExpress (Monmouth Junction, NJ, USA)
ASC-J9	AR	Clinical Library Extended	HY-15194	MedChemExpress (Monmouth Junction, NJ, USA)
ASP3026	ALK	Clinical Library Extended	HY-13326	MedChemExpress (Monmouth Junction, NJ, USA)
AT13148	AKT	Clinical Library Extended	HY-16071	MedChemExpress (Monmouth Junction, NJ, USA)
AT13387	HSP90	Clinical Library Extended	HY-14463	MedChemExpress (Monmouth Junction, NJ, USA)
AT7519	CDK	Clinical Library Extended	HY-50940	MedChemExpress (Monmouth Junction, NJ, USA)
AT9283	ARK	Clinical Library Extended	HY-50514	MedChemExpress (Monmouth Junction, NJ, USA)
Atrasentan hydrochloride	ET	Clinical Library Extended	HY-15403A	MedChemExpress (Monmouth Junction, NJ, USA)
Auristatin PE	Microtubule/Tubulin	Clinical Library Extended	HY-14672	MedChemExpress (Monmouth Junction, NJ, USA)
Aurora A inhibitor I	ARK	Clinical Library Extended	HY-70061	MedChemExpress (Monmouth Junction, NJ, USA)
AV-412	EGFR	Clinical Library Extended	HY-10346A	MedChemExpress (Monmouth Junction, NJ, USA)
AVL-292	BTK	Clinical Library Extended	HY-18012	MedChemExpress (Monmouth Junction, NJ, USA)
AVN-944	DNA/RNA Synthesis	Clinical Library Extended	HY-13560	MedChemExpress (Monmouth Junction, NJ, USA)
AXL1717	IGF-1R	Clinical Library Extended	HY-15494	MedChemExpress (Monmouth Junction, NJ, USA)
AZ505 ditrifluoroacetate	HMT	Clinical Library Extended	HY-15226A	MedChemExpress (Monmouth Junction, NJ, USA)
AZ5104	EGFR	Clinical Library Extended	HY-B0793	MedChemExpress (Monmouth Junction, NJ, USA)
AZ6102	PARP	Clinical Library Extended	HY-12975	MedChemExpress (Monmouth Junction, NJ, USA)
AZD-1152-HQPA	ARK	Clinical Library Extended	HY-10126	MedChemExpress (Monmouth Junction, NJ, USA)
AZD-1208	PIM	Clinical Library Extended	HY-15604	MedChemExpress (Monmouth Junction, NJ, USA)
AZD-1480	JAK	Clinical Library Extended	HY-10193	MedChemExpress (Monmouth Junction, NJ, USA)
AZD-2014	MTOR	Clinical Library Extended	HY-15247	MedChemExpress (Monmouth Junction, NJ, USA)
AZD-2461	PARP	Clinical Library Extended	HY-13536	MedChemExpress (Monmouth Junction, NJ, USA)
AZD-3514	AR	Clinical Library Extended	HY-16079	MedChemExpress (Monmouth Junction, NJ, USA)
AZD-3759	EGFR	Clinical Library Extended	HY-18750	MedChemExpress (Monmouth Junction, NJ, USA)
AZD-3839	Others	Clinical Library Extended	HY-13438	MedChemExpress (Monmouth Junction, NJ, USA)
AZD-3965	Others	Clinical Library Extended	HY-12750	MedChemExpress (Monmouth Junction, NJ, USA)
AZD-4547	FGFR	Clinical Library Extended	HY-13330	MedChemExpress (Monmouth Junction, NJ, USA)
AZD-5363	AKT	Clinical Library Extended	HY-15431	MedChemExpress (Monmouth Junction, NJ, USA)
AZD-5438	CDK	Clinical Library Extended	HY-10012	MedChemExpress (Monmouth Junction, NJ, USA)
AZD-6482	PI3K	Clinical Library Extended	HY-10344	MedChemExpress (Monmouth Junction, NJ, USA)
AZD-6738	ATM/ATR	Clinical Library Extended	HY-19323	MedChemExpress (Monmouth Junction, NJ, USA)
AZD-7762	CHEK	Clinical Library Extended	HY-10992	MedChemExpress (Monmouth Junction, NJ, USA)
AZD-8055	MTOR	Clinical Library Extended	HY-10422	MedChemExpress (Monmouth Junction, NJ, USA)
AZD-8186	PI3K	Clinical Library Extended	HY-12330	MedChemExpress (Monmouth Junction, NJ, USA)
AZD-8330	MEK	Clinical Library Extended	HY-12058	MedChemExpress (Monmouth Junction, NJ, USA)
Bafetinib	BCR-ABL	Clinical Library Extended	HY-50868	MedChemExpress (Monmouth Junction, NJ, USA)
Bakuchiol	p38 MAPK	Clinical Library Extended	HY-N0235	MedChemExpress (Monmouth Junction, NJ, USA)
Berberine	Topoisomerase	Clinical Library Extended	HY-17577	MedChemExpress (Monmouth Junction, NJ, USA)
Bergapten	Cytochrome P450	Clinical Library Extended	HY-N0370	MedChemExpress (Monmouth Junction, NJ, USA)
Betahistine dihydrochloride	Receptor Antagonist	Clinical Library Extended	HY-B0524A	MedChemExpress (Monmouth Junction, NJ, USA)
BEZ235	MTOR	Clinical Library Extended	HY-50673	MedChemExpress (Monmouth Junction, NJ, USA)
BI-2536	PLK	Clinical Library Extended	HY-50698	MedChemExpress (Monmouth Junction, NJ, USA)
BI-78D3	JNK	Clinical Library Extended	HY-10366	MedChemExpress (Monmouth Junction, NJ, USA)
BI-847325	ARK	Clinical Library Extended	HY-18955	MedChemExpress (Monmouth Junction, NJ, USA)
BIBR 1532	TERT	Clinical Library Extended	HY-17353	MedChemExpress (Monmouth Junction, NJ, USA)
BIBX 1382	EGFR	Clinical Library Extended	HY-10322	MedChemExpress (Monmouth Junction, NJ, USA)
BIIB021	HSP90	Clinical Library Extended	HY-10212	MedChemExpress (Monmouth Junction, NJ, USA)
Bioymifi	TNF	Clinical Library Extended	HY-18377	MedChemExpress (Monmouth Junction, NJ, USA)
Birinapant	IAP	Clinical Library Extended	HY-16591	MedChemExpress (Monmouth Junction, NJ, USA)
Bithionol	Others	Clinical Library Extended	HY-17592	MedChemExpress (Monmouth Junction, NJ, USA)
BKT140	CXCR	Clinical Library Extended	HY-P0171	MedChemExpress (Monmouth Junction, NJ, USA)
BLU-554	FGFR	Clinical Library Extended	HY-100492	MedChemExpress (Monmouth Junction, NJ, USA)
BMS-214662	FTase	Clinical Library Extended	HY-16111	MedChemExpress (Monmouth Junction, NJ, USA)

Drug	Class	Library	Cat. No.	Manufacturer
BMS-599626 hydrochloride	EGFR	Clinical Library Extended	HY-12010	MedChemExpress (Monmouth Junction, NJ, USA)
BMS-690514	EGFR	Clinical Library Extended	HY-10333	MedChemExpress (Monmouth Junction, NJ, USA)
BMS-708163	Notch	Clinical Library Extended	HY-50845	MedChemExpress (Monmouth Junction, NJ, USA)
BMS-754807	IGF-1R	Clinical Library Extended	HY-10200	MedChemExpress (Monmouth Junction, NJ, USA)
BMS-777607	MET/HGFR	Clinical Library Extended	HY-12076	MedChemExpress (Monmouth Junction, NJ, USA)
BMS-794833	MET/HGFR	Clinical Library Extended	HY-10497	MedChemExpress (Monmouth Junction, NJ, USA)
BMS-833923	Hedgehog	Clinical Library Extended	HY-13809	MedChemExpress (Monmouth Junction, NJ, USA)
BMS-911543	JAK	Clinical Library Extended	HY-15270	MedChemExpress (Monmouth Junction, NJ, USA)
Briciclib	eIF	Clinical Library Extended	HY-16366	MedChemExpress (Monmouth Junction, NJ, USA)
Buserelin acetate	GNRH Receptor	Clinical Library Extended	HY-13581A	MedChemExpress (Monmouth Junction, NJ, USA)
Calcitonin	Others	Clinical Library Extended	HY-P0090	MedChemExpress (Monmouth Junction, NJ, USA)
Calcitriol	VDR	Clinical Library Extended	HY-10002	MedChemExpress (Monmouth Junction, NJ, USA)
Capsaicin	Others	Clinical Library Extended	HY-10448	MedChemExpress (Monmouth Junction, NJ, USA)
Captopril	Others	Clinical Library Extended	HY-B0368	MedChemExpress (Monmouth Junction, NJ, USA)
Carmofur	Nucleoside Antimetabolite	Clinical Library Extended	HY-B0182	MedChemExpress (Monmouth Junction, NJ, USA)
Catechin	Endogenous Metabolite	Clinical Library Extended	HY-N0898	MedChemExpress (Monmouth Junction, NJ, USA)
CB-5083	Others	Clinical Library Extended	HY-12861	MedChemExpress (Monmouth Junction, NJ, USA)
CB-839	Others	Clinical Library Extended	HY-12248	MedChemExpress (Monmouth Junction, NJ, USA)
CC-401 hydrochloride	JNK	Clinical Library Extended	HY-13022	MedChemExpress (Monmouth Junction, NJ, USA)
Cecropin B	Cytochrome P450	Clinical Library Extended	HY-P0092	MedChemExpress (Monmouth Junction, NJ, USA)
CEP-32496	RAF	Clinical Library Extended	HY-15200	MedChemExpress (Monmouth Junction, NJ, USA)
CEP-37440	ALK	Clinical Library Extended	HY-15841	MedChemExpress (Monmouth Junction, NJ, USA)
Cerdulatinib	JAK	Clinical Library Extended	HY-15999	MedChemExpress (Monmouth Junction, NJ, USA)
Cevipabulin	Microtubule/Tubulin	Clinical Library Extended	HY-14949	MedChemExpress (Monmouth Junction, NJ, USA)
CH5132799	PI3K	Clinical Library Extended	HY-15466	MedChemExpress (Monmouth Junction, NJ, USA)
CH5183284	FGFR	Clinical Library Extended	HY-19957	MedChemExpress (Monmouth Junction, NJ, USA)
Chidamide	HDAC	Clinical Library Extended	HY-13592	MedChemExpress (Monmouth Junction, NJ, USA)
CI-1040	MEK	Clinical Library Extended	HY-50295	MedChemExpress (Monmouth Junction, NJ, USA)
Ciclosporin A	Others	Clinical Library Extended	HY-B0579	MedChemExpress (Monmouth Junction, NJ, USA)
Cilengitide	Integrin	Clinical Library Extended	HY-16141	MedChemExpress (Monmouth Junction, NJ, USA)
Ciliobrevin D	Dynein	Clinical Library Extended	250401	Merck (Darmstadt, Germany)
Cinobufotalin	Endogenous Metabolite	Clinical Library Extended	HY-N0880	MedChemExpress (Monmouth Junction, NJ, USA)
Citarinostat	HDAC	Clinical Library Extended	HY-15994	MedChemExpress (Monmouth Junction, NJ, USA)
CO-1686	EGFR	Clinical Library Extended	HY-15729	MedChemExpress (Monmouth Junction, NJ, USA)
Cortisone	GR	Clinical Library Extended	HY-17461	MedChemExpress (Monmouth Junction, NJ, USA)
CPI-613	Apoptosis	Clinical Library Extended	HY-15453	MedChemExpress (Monmouth Junction, NJ, USA)
Crenolanib	FLT3	Clinical Library Extended	HY-13223	MedChemExpress (Monmouth Junction, NJ, USA)
CTS-1027	MMP	Clinical Library Extended	HY-10398	MedChemExpress (Monmouth Junction, NJ, USA)
CUDC-101	EGFR	Clinical Library Extended	HY-10223	MedChemExpress (Monmouth Junction, NJ, USA)
CUDC-427	IAP	Clinical Library Extended	HY-15835	MedChemExpress (Monmouth Junction, NJ, USA)
CUDC-907	HDAC	Clinical Library Extended	HY-13522	MedChemExpress (Monmouth Junction, NJ, USA)
Curcumin	HAT	Clinical Library Extended	HY-N0005	MedChemExpress (Monmouth Junction, NJ, USA)
Curcumol	Apoptosis	Clinical Library Extended	HY-N0104	MedChemExpress (Monmouth Junction, NJ, USA)
CX-4945	Others	Clinical Library Extended	HY-50855	MedChemExpress (Monmouth Junction, NJ, USA)
CX-5461	DNA/RNA Synthesis	Clinical Library Extended	HY-13323	MedChemExpress (Monmouth Junction, NJ, USA)
CYC-116	ARK	Clinical Library Extended	HY-10558	MedChemExpress (Monmouth Junction, NJ, USA)
Cyclic somatostatin	Others	Clinical Library Extended	HY-P0084	MedChemExpress (Monmouth Junction, NJ, USA)
CYT387	JAK	Clinical Library Extended	HY-10961	MedChemExpress (Monmouth Junction, NJ, USA)
D-3263 hydrochloride	Others	Clinical Library Extended	HY-16162A	MedChemExpress (Monmouth Junction, NJ, USA)
Dalcetrapib	CETP	Clinical Library Extended	HY-14950	MedChemExpress (Monmouth Junction, NJ, USA)
Danusertib	ARK	Clinical Library Extended	HY-10179	MedChemExpress (Monmouth Junction, NJ, USA)
DCC-2036	BCR-ABL	Clinical Library Extended	HY-13024	MedChemExpress (Monmouth Junction, NJ, USA)
DCC-2618	KIT	Clinical Library Extended	HY-15240	MedChemExpress (Monmouth Junction, NJ, USA)
Debio 0932	HSP90	Clinical Library Extended	HY-13469	MedChemExpress (Monmouth Junction, NJ, USA)
Defactinib	FAK	Clinical Library Extended	HY-12289	MedChemExpress (Monmouth Junction, NJ, USA)
Delamanid	Antibiotic	Clinical Library Extended	HY-10846	MedChemExpress (Monmouth Junction, NJ, USA)
Delanzomib	Proteasome	Clinical Library Extended	HY-10454	MedChemExpress (Monmouth Junction, NJ, USA)
Dihydroartemisinin	NF-κB	Clinical Library Extended	HY-N0176	MedChemExpress (Monmouth Junction, NJ, USA)
Dimethylenastron	KSP	Clinical Library Extended	HY-19944	MedChemExpress (Monmouth Junction, NJ, USA)
Disulfiram	Others	Clinical Library Extended	HY-B0240	MedChemExpress (Monmouth Junction, NJ, USA)
DMXAA	Others	Clinical Library Extended	HY-10964	MedChemExpress (Monmouth Junction, NJ, USA)
Dofequidar fumarate	P-glycoprotein	Clinical Library Extended	HY-17013A	MedChemExpress (Monmouth Junction, NJ, USA)
Doxifluridine	Nucleoside Antimetabolite	Clinical Library Extended	HY-B0021	MedChemExpress (Monmouth Junction, NJ, USA)
Dutasteride	5-Alpha Reductase	Clinical Library Extended	HY-13613	MedChemExpress (Monmouth Junction, NJ, USA)
E-3810	FGFR	Clinical Library Extended	HY-15391	MedChemExpress (Monmouth Junction, NJ, USA)
E-7050	MET/HGFR	Clinical Library Extended	HY-13068	MedChemExpress (Monmouth Junction, NJ, USA)
E-7449	PARP	Clinical Library Extended	HY-12418	MedChemExpress (Monmouth Junction, NJ, USA)
E-7820	Integrin	Clinical Library Extended	HY-14571	MedChemExpress (Monmouth Junction, NJ, USA)
Efaproxiral	Others	Clinical Library Extended	HY-13619	MedChemExpress (Monmouth Junction, NJ, USA)
Ellipticine hydrochloride	Topoisomerase	Clinical Library Extended	HY-15753A	MedChemExpress (Monmouth Junction, NJ, USA)
Embelin	IAP	Clinical Library Extended	HY-17473	MedChemExpress (Monmouth Junction, NJ, USA)
EMD-1214063	MET/HGFR	Clinical Library Extended	HY-14721	MedChemExpress (Monmouth Junction, NJ, USA)
Empagliflozin	SGLT	Clinical Library Extended	HY-15409	MedChemExpress (Monmouth Junction, NJ, USA)
Endoxifen (E-isomer)	ER	Clinical Library Extended	HY-18719D	MedChemExpress (Monmouth Junction, NJ, USA)
ENMD-2076	ARK	Clinical Library Extended	HY-10987A	MedChemExpress (Monmouth Junction, NJ, USA)
Ensartinib	ALK	Clinical Library Extended	HY-16590	MedChemExpress (Monmouth Junction, NJ, USA)
Patupilone	Microtubule/Tubulin	Clinical Library Extended	HY-17029	MedChemExpress (Monmouth Junction, NJ, USA)
EPZ-5676	HMT	Clinical Library Extended	HY-15593	MedChemExpress (Monmouth Junction, NJ, USA)
Equol	ER	Clinical Library Extended	HY-100583A	MedChemExpress (Monmouth Junction, NJ, USA)
Evodiamine	Endogenous Metabolite	Clinical Library Extended	HY-N0114	MedChemExpress (Monmouth Junction, NJ, USA)
EW-7197	TGFb	Clinical Library Extended	HY-19928	MedChemExpress (Monmouth Junction, NJ, USA)
Exatecan mesylate	Topoisomerase	Clinical Library Extended	HY-13631A	MedChemExpress (Monmouth Junction, NJ, USA)
Exemestane	Aromatase	Clinical Library Extended	HY-13632	MedChemExpress (Monmouth Junction, NJ, USA)
Exherin	Others	Clinical Library Extended	HY-13541	MedChemExpress (Monmouth Junction, NJ, USA)
Ezatiostat	Others	Clinical Library Extended	HY-13634A	MedChemExpress (Monmouth Junction, NJ, USA)
Fasudil hydrochloride	Calcium Channel	Clinical Library Extended	HY-10341	MedChemExpress (Monmouth Junction, NJ, USA)
Fenretinide	RAR/RXR	Clinical Library Extended	HY-15373	MedChemExpress (Monmouth Junction, NJ, USA)
FG-4592	HIF-PH	Clinical Library Extended	HY-13426	MedChemExpress (Monmouth Junction, NJ, USA)
Finasteride	5-Alpha Reductase	Clinical Library Extended	HY-13635	MedChemExpress (Monmouth Junction, NJ, USA)
FK866	Others	Clinical Library Extended	HY-50876	MedChemExpress (Monmouth Junction, NJ, USA)
Flavopiridol hydrochloride	CDK	Clinical Library Extended	HY-10006	MedChemExpress (Monmouth Junction, NJ, USA)
Flumatinib	BCR-ABL	Clinical Library Extended	HY-13904	MedChemExpress (Monmouth Junction, NJ, USA)
Foretinib	MET/HGFR	Clinical Library Extended	HY-10338	MedChemExpress (Monmouth Junction, NJ, USA)
Formestane	Aromatase	Clinical Library Extended	HY-B0697	MedChemExpress (Monmouth Junction, NJ, USA)
Forodesine hydrochloride	Nucleoside Antimetabolite	Clinical Library Extended	HY-16209	MedChemExpress (Monmouth Junction, NJ, USA)
GANT-58	Hedgehog	Clinical Library Extended	HY-13282	MedChemExpress (Monmouth Junction, NJ, USA)
GDC-0032	PI3K	Clinical Library Extended	HY-13898	MedChemExpress (Monmouth Junction, NJ, USA)
GDC-0068	AKT	Clinical Library Extended	HY-15186	MedChemExpress (Monmouth Junction, NJ, USA)
GDC-0068 dihydrochloride	AKT	Clinical Library Extended	HY-15186A	MedChemExpress (Monmouth Junction, NJ, USA)
GDC-0152	IAP	Clinical Library Extended	HY-13638	MedChemExpress (Monmouth Junction, NJ, USA)
GDC-0349	MTOR	Clinical Library Extended	HY-15248	MedChemExpress (Monmouth Junction, NJ, USA)
GDC-0623	MEK	Clinical Library Extended	HY-15610	MedChemExpress (Monmouth Junction, NJ, USA)
GDC-0941	PI3K	Clinical Library Extended	HY-50094	MedChemExpress (Monmouth Junction, NJ, USA)
GDC-0980	MTOR	Clinical Library Extended	HY-13246	MedChemExpress (Monmouth Junction, NJ, USA)

Drug	Class	Library	Cat. No.	Manufacturer
GDC-0994	ERK	Clinical Library Extended	HY-15947	MedChemExpress (Monmouth Junction, NJ, USA)
Gemcitabine	Nucleoside Antimetabolite	Clinical Library Extended	HY-17026	MedChemExpress (Monmouth Junction, NJ, USA)
Genistein	Endogenous Metabolite	Clinical Library Extended	HY-14596	MedChemExpress (Monmouth Junction, NJ, USA)
Genz-644282	Topoisomerase	Clinical Library Extended	HY-16228	MedChemExpress (Monmouth Junction, NJ, USA)
Gimeracil	Others	Clinical Library Extended	HY-17469	MedChemExpress (Monmouth Junction, NJ, USA)
GLPG0634	JAK	Clinical Library Extended	HY-18300	MedChemExpress (Monmouth Junction, NJ, USA)
Gossypol acetic acid	BCL2	Clinical Library Extended	HY-17510	MedChemExpress (Monmouth Junction, NJ, USA)
GS-9973	SYK	Clinical Library Extended	HY-15968	MedChemExpress (Monmouth Junction, NJ, USA)
GSK1059615	MTOR	Clinical Library Extended	HY-12036	MedChemExpress (Monmouth Junction, NJ, USA)
GSK1070916	ARK	Clinical Library Extended	HY-70044	MedChemExpress (Monmouth Junction, NJ, USA)
GSK2110183	AKT	Clinical Library Extended	HY-15727	MedChemExpress (Monmouth Junction, NJ, USA)
GSK2126458	MTOR	Clinical Library Extended	HY-10297	MedChemExpress (Monmouth Junction, NJ, USA)
GSK2141795	AKT	Clinical Library Extended	HY-15965	MedChemExpress (Monmouth Junction, NJ, USA)
GSK2636771	PI3K	Clinical Library Extended	HY-15245	MedChemExpress (Monmouth Junction, NJ, USA)
GSK2879552	LSD1	Clinical Library Extended	HY-18632	MedChemExpress (Monmouth Junction, NJ, USA)
GSK461364	PLK	Clinical Library Extended	HY-50877	MedChemExpress (Monmouth Junction, NJ, USA)
GSK690693	AKT	Clinical Library Extended	HY-10249	MedChemExpress (Monmouth Junction, NJ, USA)
GSK923295	KSP	Clinical Library Extended	HY-10299	MedChemExpress (Monmouth Junction, NJ, USA)
Hesperidin	Endogenous Metabolite	Clinical Library Extended	HY-15337	MedChemExpress (Monmouth Junction, NJ, USA)
Hexaminolevulinate hydrochloride	Others	Clinical Library Extended	HY-16045	MedChemExpress (Monmouth Junction, NJ, USA)
Hydroxyfasudil	ROCK	Clinical Library Extended	HY-13911	MedChemExpress (Monmouth Junction, NJ, USA)
Icaritin	Endogenous Metabolite	Clinical Library Extended	HY-N0678	MedChemExpress (Monmouth Junction, NJ, USA)
Icotinib hydrochloride	EGFR	Clinical Library Extended	HY-15164	MedChemExpress (Monmouth Junction, NJ, USA)
Imisopasem manganese	Others	Clinical Library Extended	HY-13336	MedChemExpress (Monmouth Junction, NJ, USA)
INCB024360	Others	Clinical Library Extended	HY-15689	MedChemExpress (Monmouth Junction, NJ, USA)
INCB28060	MET/HGFR	Clinical Library Extended	HY-13404	MedChemExpress (Monmouth Junction, NJ, USA)
Ingenol mebutate	PKC	Clinical Library Extended	HY-B0719	MedChemExpress (Monmouth Junction, NJ, USA)
INK 128	MTOR	Clinical Library Extended	HY-13328	MedChemExpress (Monmouth Junction, NJ, USA)
INNO-206	ADC Cytotoxin	Clinical Library Extended	HY-16261	MedChemExpress (Monmouth Junction, NJ, USA)
INO-1001	PARP	Clinical Library Extended	HY-12022	MedChemExpress (Monmouth Junction, NJ, USA)
Inolitazone dihydrochloride	PPAR	Clinical Library Extended	HY-14792B	MedChemExpress (Monmouth Junction, NJ, USA)
Irbinitinib	EGFR	Clinical Library Extended	HY-16069	MedChemExpress (Monmouth Junction, NJ, USA)
Isoliquiritigenin	Endogenous Metabolite	Clinical Library Extended	HY-N0102	MedChemExpress (Monmouth Junction, NJ, USA)
Isotretinoin	RAR/RXR	Clinical Library Extended	HY-15127	MedChemExpress (Monmouth Junction, NJ, USA)
Ispinesib	KSP	Clinical Library Extended	HY-50759	MedChemExpress (Monmouth Junction, NJ, USA)
Jervine	Hedgehog	Clinical Library Extended	HY-N0836	MedChemExpress (Monmouth Junction, NJ, USA)
JK184	Hedgehog	Clinical Library Extended	HY-13307	MedChemExpress (Monmouth Junction, NJ, USA)
JNJ-38877605	MET/HGFR	Clinical Library Extended	HY-50683	MedChemExpress (Monmouth Junction, NJ, USA)
K-115 hydrochloride	ROCK	Clinical Library Extended	HY-15685	MedChemExpress (Monmouth Junction, NJ, USA)
Kevetrin hydrochloride	MDM2	Clinical Library Extended	HY-16271	MedChemExpress (Monmouth Junction, NJ, USA)
KU-57788	CRISPR/Cas9	Clinical Library Extended	HY-11006	MedChemExpress (Monmouth Junction, NJ, USA)
KW-2449	ARK	Clinical Library Extended	HY-10339	MedChemExpress (Monmouth Junction, NJ, USA)
KX2-391 mesylate	Microtubule/Tubulin	Clinical Library Extended	HY-10340B	MedChemExpress (Monmouth Junction, NJ, USA)
LB-100	Phosphatase	Clinical Library Extended	HY-18597	MedChemExpress (Monmouth Junction, NJ, USA)
LCL161	IAP	Clinical Library Extended	HY-15518	MedChemExpress (Monmouth Junction, NJ, USA)
Lexibulin	Microtubule/Tubulin	Clinical Library Extended	HY-10498	MedChemExpress (Monmouth Junction, NJ, USA)
LGK974	WNT	Clinical Library Extended	HY-17545	MedChemExpress (Monmouth Junction, NJ, USA)
Licochalcone A	Endogenous Metabolite	Clinical Library Extended	HY-N0372	MedChemExpress (Monmouth Junction, NJ, USA)
Lurbinectedin	DNA/RNA Synthesis	Clinical Library Extended	HY-16293	MedChemExpress (Monmouth Junction, NJ, USA)
Luteolin	Endogenous Metabolite	Clinical Library Extended	HY-N0162	MedChemExpress (Monmouth Junction, NJ, USA)
LY2090314	GSK3	Clinical Library Extended	HY-16294	MedChemExpress (Monmouth Junction, NJ, USA)
LY2157299	TGFb	Clinical Library Extended	HY-13226	MedChemExpress (Monmouth Junction, NJ, USA)
LY2228820 dimesylate	p38 MAPK	Clinical Library Extended	HY-13241	MedChemExpress (Monmouth Junction, NJ, USA)
LY2510924	CXCR	Clinical Library Extended	HY-12488	MedChemExpress (Monmouth Junction, NJ, USA)
LY2584702	S6K	Clinical Library Extended	HY-12493	MedChemExpress (Monmouth Junction, NJ, USA)
LY2603618	CHEK	Clinical Library Extended	HY-14720	MedChemExpress (Monmouth Junction, NJ, USA)
LY2606368 dihydrochloride	CHEK	Clinical Library Extended	HY-18174A	MedChemExpress (Monmouth Junction, NJ, USA)
LY2784544	FGFR	Clinical Library Extended	HY-13034	MedChemExpress (Monmouth Junction, NJ, USA)
LY2801653	MET/HGFR	Clinical Library Extended	HY-15514A	MedChemExpress (Monmouth Junction, NJ, USA)
LY2874455	FGFR	Clinical Library Extended	HY-13304	MedChemExpress (Monmouth Junction, NJ, USA)
LY2940680	Hedgehog	Clinical Library Extended	HY-13242	MedChemExpress (Monmouth Junction, NJ, USA)
LY3023414	MTOR	Clinical Library Extended	HY-12513	MedChemExpress (Monmouth Junction, NJ, USA)
LY3039478	Notch	Clinical Library Extended	HY-12449	MedChemExpress (Monmouth Junction, NJ, USA)
Malotilate	Others	Clinical Library Extended	HY-A0060	MedChemExpress (Monmouth Junction, NJ, USA)
Mc-Val-Cit-PABC-PNP	Others	Clinical Library Extended	HY-20336	MedChemExpress (Monmouth Junction, NJ, USA)
MI-773	MDM2	Clinical Library Extended	HY-17493	MedChemExpress (Monmouth Junction, NJ, USA)
Mibefradil dihydrochloride	Calcium Channel	Clinical Library Extended	HY-15553A	MedChemExpress (Monmouth Junction, NJ, USA)
Miriplatin	DNA Alkylator/Crosslinker	Clinical Library Extended	HY-16325A	MedChemExpress (Monmouth Junction, NJ, USA)
Mitotane	Apoptosis	Clinical Library Extended	HY-13690	MedChemExpress (Monmouth Junction, NJ, USA)
MK-0752	Notch	Clinical Library Extended	HY-10974	MedChemExpress (Monmouth Junction, NJ, USA)
MK-1775	WEE1	Clinical Library Extended	HY-10993	MedChemExpress (Monmouth Junction, NJ, USA)
MK-2206 dihydrochloride	AKT	Clinical Library Extended	HY-10358	MedChemExpress (Monmouth Junction, NJ, USA)
MK-2461	MET/HGFR	Clinical Library Extended	HY-50703	MedChemExpress (Monmouth Junction, NJ, USA)
MK-4827 tosylate	PARP	Clinical Library Extended	HY-10619B	MedChemExpress (Monmouth Junction, NJ, USA)
MK-5108	ARK	Clinical Library Extended	HY-13252	MedChemExpress (Monmouth Junction, NJ, USA)
MLN1117	PI3K	Clinical Library Extended	HY-12285	MedChemExpress (Monmouth Junction, NJ, USA)
MLN2480	RAF	Clinical Library Extended	HY-15246	MedChemExpress (Monmouth Junction, NJ, USA)
MLN4924 hydrochloride	NAE	Clinical Library Extended	HY-10484	MedChemExpress (Monmouth Junction, NJ, USA)
MLN8054	ARK	Clinical Library Extended	HY-10180	MedChemExpress (Monmouth Junction, NJ, USA)
Mocetinostat	HDAC	Clinical Library Extended	HY-12164	MedChemExpress (Monmouth Junction, NJ, USA)
Motolimod	TLR	Clinical Library Extended	HY-13773	MedChemExpress (Monmouth Junction, NJ, USA)
Mozavaptan	Receptor Antagonist	Clinical Library Extended	HY-18346	MedChemExpress (Monmouth Junction, NJ, USA)
MSX-122	CXCR	Clinical Library Extended	HY-13696	MedChemExpress (Monmouth Junction, NJ, USA)
Mubritinib	EGFR	Clinical Library Extended	HY-13501	MedChemExpress (Monmouth Junction, NJ, USA)
Napabucasin	STAT	Clinical Library Extended	HY-13919	MedChemExpress (Monmouth Junction, NJ, USA)
Naringenin	PPAR	Clinical Library Extended	HY-N0100	MedChemExpress (Monmouth Junction, NJ, USA)
Navitoclax	BCL2	Clinical Library Extended	HY-10087	MedChemExpress (Monmouth Junction, NJ, USA)
Nedaplatin	DNA/RNA Synthesis	Clinical Library Extended	HY-13700	MedChemExpress (Monmouth Junction, NJ, USA)
Nelotanserin	5-HT Receptor	Clinical Library Extended	HY-10559	MedChemExpress (Monmouth Junction, NJ, USA)
NMS-1286937	PLK	Clinical Library Extended	HY-15828	MedChemExpress (Monmouth Junction, NJ, USA)
Nocodazole	BCR-ABL	Clinical Library Extended	HY-13520	MedChemExpress (Monmouth Junction, NJ, USA)
Noscapine	Endogenous Metabolite	Clinical Library Extended	HY-13716	MedChemExpress (Monmouth Junction, NJ, USA)
NVP-AUY922	HSP90	Clinical Library Extended	HY-10215	MedChemExpress (Monmouth Junction, NJ, USA)
NVP-BKM120	PI3K	Clinical Library Extended	HY-70063	MedChemExpress (Monmouth Junction, NJ, USA)
ODM-201	AR	Clinical Library Extended	HY-16985	MedChemExpress (Monmouth Junction, NJ, USA)
Oleanolic acid	Endogenous Metabolite	Clinical Library Extended	HY-N0156	MedChemExpress (Monmouth Junction, NJ, USA)
Oltipraz	HIF-PH	Clinical Library Extended	HY-12519	MedChemExpress (Monmouth Junction, NJ, USA)
Ombrabulin hydrochloride	Microtubule/Tubulin	Clinical Library Extended	HY-18256	MedChemExpress (Monmouth Junction, NJ, USA)
ONO-4059 hydrochloride	BTK	Clinical Library Extended	HY-15771A	MedChemExpress (Monmouth Junction, NJ, USA)
Oprozomib	Proteasome	Clinical Library Extended	HY-12113	MedChemExpress (Monmouth Junction, NJ, USA)
Orteronel	Others	Clinical Library Extended	HY-10505	MedChemExpress (Monmouth Junction, NJ, USA)
OSI-027	MTOR	Clinical Library Extended	HY-10423	MedChemExpress (Monmouth Junction, NJ, USA)
OSI-930	CSF1R	Clinical Library Extended	HY-10204	MedChemExpress (Monmouth Junction, NJ, USA)
Osilodrostat	Receptor Antagonist	Clinical Library Extended	HY-16276	MedChemExpress (Monmouth Junction, NJ, USA)

Drug	Class	Library	Cat. No.	Manufacturer
Ospemifene	ER	Clinical Library Extended	HY-B0723	MedChemExpress (Monmouth Junction, NJ, USA)
Ostarine	AR	Clinical Library Extended	HY-13273	MedChemExpress (Monmouth Junction, NJ, USA)
OTX-015	BET	Clinical Library Extended	HY-15743	MedChemExpress (Monmouth Junction, NJ, USA)
PAC-1	Caspase	Clinical Library Extended	HY-13523	MedChemExpress (Monmouth Junction, NJ, USA)
Palomid 529	MTOR	Clinical Library Extended	HY-14581	MedChemExpress (Monmouth Junction, NJ, USA)
Parthenolide	NF-κB	Clinical Library Extended	HY-N0141	MedChemExpress (Monmouth Junction, NJ, USA)
PCI-24781	HDAC	Clinical Library Extended	HY-10990	MedChemExpress (Monmouth Junction, NJ, USA)
PCI-34051	HDAC	Clinical Library Extended	HY-15224	MedChemExpress (Monmouth Junction, NJ, USA)
PD0325901	MEK	Clinical Library Extended	HY-10254	MedChemExpress (Monmouth Junction, NJ, USA)
PD98059	MEK	Clinical Library Extended	HY-12028	MedChemExpress (Monmouth Junction, NJ, USA)
Pelitinib	EGFR	Clinical Library Extended	HY-32718	MedChemExpress (Monmouth Junction, NJ, USA)
Pexidartinib	CSF1R	Clinical Library Extended	HY-16749	MedChemExpress (Monmouth Junction, NJ, USA)
PF-03814735	ARK	Clinical Library Extended	HY-14574	MedChemExpress (Monmouth Junction, NJ, USA)
PF-04217903 methanesulfonate	MET/HGFR	Clinical Library Extended	HY-12017A	MedChemExpress (Monmouth Junction, NJ, USA)
PF-04691502	MTOR	Clinical Library Extended	HY-15177	MedChemExpress (Monmouth Junction, NJ, USA)
PFK-158	Others	Clinical Library Extended	HY-12203	MedChemExpress (Monmouth Junction, NJ, USA)
PH-797804	p38 MAPK	Clinical Library Extended	HY-10403	MedChemExpress (Monmouth Junction, NJ, USA)
PHA-665752	MET/HGFR	Clinical Library Extended	HY-11107	MedChemExpress (Monmouth Junction, NJ, USA)
PHA-793887	CDK	Clinical Library Extended	HY-11001	MedChemExpress (Monmouth Junction, NJ, USA)
PHA-848125	CDK	Clinical Library Extended	HY-10424	MedChemExpress (Monmouth Junction, NJ, USA)
Phenformin hydrochloride	AMPK	Clinical Library Extended	HY-16397A	MedChemExpress (Monmouth Junction, NJ, USA)
Pixantrone dimaleate	Topoisomerase	Clinical Library Extended	HY-13727A	MedChemExpress (Monmouth Junction, NJ, USA)
PKC412	PKC	Clinical Library Extended	HY-10230	MedChemExpress (Monmouth Junction, NJ, USA)
Plinabulin	Microtubule/Tubulin	Clinical Library Extended	HY-14444	MedChemExpress (Monmouth Junction, NJ, USA)
PND-1186	FAK	Clinical Library Extended	HY-13917	MedChemExpress (Monmouth Junction, NJ, USA)
Poziotinib	EGFR	Clinical Library Extended	HY-15730	MedChemExpress (Monmouth Junction, NJ, USA)
PQR620	MTOR	Clinical Library Extended	HY-100026	MedChemExpress (Monmouth Junction, NJ, USA)
Pracinostat	HDAC	Clinical Library Extended	HY-13322	MedChemExpress (Monmouth Junction, NJ, USA)
Pranlukast hemihydrate	Receptor Antagonist	Clinical Library Extended	HY-B0290A	MedChemExpress (Monmouth Junction, NJ, USA)
Prinaberel	ER	Clinical Library Extended	HY-14933	MedChemExpress (Monmouth Junction, NJ, USA)
Psoralen	Endogenous Metabolite	Clinical Library Extended	HY-N0053	MedChemExpress (Monmouth Junction, NJ, USA)
Psoralidin	COX	Clinical Library Extended	HY-N0232	MedChemExpress (Monmouth Junction, NJ, USA)
PX-12	Others	Clinical Library Extended	HY-13734	MedChemExpress (Monmouth Junction, NJ, USA)
PX-478 dihydrochloride	HIF-PH	Clinical Library Extended	HY-10231	MedChemExpress (Monmouth Junction, NJ, USA)
Quercetin	Endogenous Metabolite	Clinical Library Extended	HY-18085	MedChemExpress (Monmouth Junction, NJ, USA)
Quinacrine dihydrochloride	Others	Clinical Library Extended	HY-13735A	MedChemExpress (Monmouth Junction, NJ, USA)
Quisinostat	HDAC	Clinical Library Extended	HY-15433	MedChemExpress (Monmouth Junction, NJ, USA)
R428	AXL	Clinical Library Extended	HY-15150	MedChemExpress (Monmouth Junction, NJ, USA)
R788 disodium hexahydrate	SYK	Clinical Library Extended	HY-13038B	MedChemExpress (Monmouth Junction, NJ, USA)
Raltitrexed	Nucleoside Antimetabolite	Clinical Library Extended	HY-10821	MedChemExpress (Monmouth Junction, NJ, USA)
Rapamycin	MTOR	Clinical Library Extended	HY-10219	MedChemExpress (Monmouth Junction, NJ, USA)
Refametinib	MEK	Clinical Library Extended	HY-14691	MedChemExpress (Monmouth Junction, NJ, USA)
Resminostat hydrochloride	HDAC	Clinical Library Extended	HY-14718A	MedChemExpress (Monmouth Junction, NJ, USA)
RG108	DNMT	Clinical Library Extended	HY-13642	MedChemExpress (Monmouth Junction, NJ, USA)
RG7112	MDM2	Clinical Library Extended	HY-10959	MedChemExpress (Monmouth Junction, NJ, USA)
RG7388	MDM2	Clinical Library Extended	HY-15676	MedChemExpress (Monmouth Junction, NJ, USA)
RGB-286638	CDK	Clinical Library Extended	HY-15504A	MedChemExpress (Monmouth Junction, NJ, USA)
RGFP966	HDAC	Clinical Library Extended	HY-13909	MedChemExpress (Monmouth Junction, NJ, USA)
Ritonavir	Others	Clinical Library Extended	HY-90001	MedChemExpress (Monmouth Junction, NJ, USA)
Ro 4929097	Notch	Clinical Library Extended	HY-11102	MedChemExpress (Monmouth Junction, NJ, USA)
Ro 4987655	MEK	Clinical Library Extended	HY-14719	MedChemExpress (Monmouth Junction, NJ, USA)
Ro 5126766	MEK	Clinical Library Extended	HY-18652	MedChemExpress (Monmouth Junction, NJ, USA)
Roscovitine	CDK	Clinical Library Extended	HY-30237	MedChemExpress (Monmouth Junction, NJ, USA)
Ruboxistaurin hydrochloride	PKC	Clinical Library Extended	HY-10195B	MedChemExpress (Monmouth Junction, NJ, USA)
RVX-208	BET	Clinical Library Extended	HY-16652	MedChemExpress (Monmouth Junction, NJ, USA)
RX-3117	Nucleoside Antimetabolite	Clinical Library Extended	HY-15228	MedChemExpress (Monmouth Junction, NJ, USA)
Salinomycin	WNT	Clinical Library Extended	HY-15597	MedChemExpress (Monmouth Junction, NJ, USA)
Salirasib	RAS	Clinical Library Extended	HY-14754	MedChemExpress (Monmouth Junction, NJ, USA)
SAR245409	MTOR	Clinical Library Extended	HY-15900	MedChemExpress (Monmouth Junction, NJ, USA)
Saracatinib	SRC	Clinical Library Extended	HY-10234	MedChemExpress (Monmouth Junction, NJ, USA)
Satraplatin	DNA Alkylator/Crosslinker	Clinical Library Extended	HY-17576	MedChemExpress (Monmouth Junction, NJ, USA)
Savolitinib	MET/HGFR	Clinical Library Extended	HY-15959	MedChemExpress (Monmouth Junction, NJ, USA)
SB 1317	CDK	Clinical Library Extended	HY-15166	MedChemExpress (Monmouth Junction, NJ, USA)
SB 743921 hydrochloride	KSP	Clinical Library Extended	HY-12069	MedChemExpress (Monmouth Junction, NJ, USA)
SCIO-469	p38 MAPK	Clinical Library Extended	HY-10406	MedChemExpress (Monmouth Junction, NJ, USA)
Seocalcitol	VDR	Clinical Library Extended	HY-32341	MedChemExpress (Monmouth Junction, NJ, USA)
Serdemetan	MDM2	Clinical Library Extended	HY-12025	MedChemExpress (Monmouth Junction, NJ, USA)
Sertraline	Others	Clinical Library Extended	HY-B0176A	MedChemExpress (Monmouth Junction, NJ, USA)
SGC-CBP30	HAT	Clinical Library Extended	HY-15826	MedChemExpress (Monmouth Junction, NJ, USA)
SGI-1027	DNMT	Clinical Library Extended	HY-13962	MedChemExpress (Monmouth Junction, NJ, USA)
SGI-1776	PIM	Clinical Library Extended	HY-13287	MedChemExpress (Monmouth Junction, NJ, USA)
SGX-523	MET/HGFR	Clinical Library Extended	HY-12019	MedChemExpress (Monmouth Junction, NJ, USA)
Silibinin	Endogenous Metabolite	Clinical Library Extended	HY-13748	MedChemExpress (Monmouth Junction, NJ, USA)
SJG-136	DNA Alkylator/Crosslinker	Clinical Library Extended	HY-14573	MedChemExpress (Monmouth Junction, NJ, USA)
SN-38	ADC Cytotoxin	Clinical Library Extended	HY-13704	MedChemExpress (Monmouth Junction, NJ, USA)
SNS-032	CDK	Clinical Library Extended	HY-10008	MedChemExpress (Monmouth Junction, NJ, USA)
Sotrastaurin	PKC	Clinical Library Extended	HY-10343	MedChemExpress (Monmouth Junction, NJ, USA)
SSR128129E sodium	FGFR	Clinical Library Extended	HY-15599	MedChemExpress (Monmouth Junction, NJ, USA)
Stibogluconate sodium	Phosphatase	Clinical Library Extended	HY-100595	MedChemExpress (Monmouth Junction, NJ, USA)
SU 5416	VEGFR	Clinical Library Extended	HY-10374	MedChemExpress (Monmouth Junction, NJ, USA)
Sulfatinib	FGFR	Clinical Library Extended	HY-12297	MedChemExpress (Monmouth Junction, NJ, USA)
TAK-285	EGFR	Clinical Library Extended	HY-15196	MedChemExpress (Monmouth Junction, NJ, USA)
TAK-593	PDGFR	Clinical Library Extended	HY-15506	MedChemExpress (Monmouth Junction, NJ, USA)
TAK-733	MEK	Clinical Library Extended	HY-13449	MedChemExpress (Monmouth Junction, NJ, USA)
TAK-901	ARK	Clinical Library Extended	HY-12201	MedChemExpress (Monmouth Junction, NJ, USA)
TAK-960	PLK	Clinical Library Extended	HY-15160	MedChemExpress (Monmouth Junction, NJ, USA)
Talabostat mesylate	Others	Clinical Library Extended	HY-13233A	MedChemExpress (Monmouth Junction, NJ, USA)
Tamibarotene	RAR/RXR	Clinical Library Extended	HY-14652	MedChemExpress (Monmouth Junction, NJ, USA)
Tandutinib	KIT	Clinical Library Extended	HY-10202	MedChemExpress (Monmouth Junction, NJ, USA)
TAS-102	Nucleoside Antimetabolite	Clinical Library Extended	HY-16478	MedChemExpress (Monmouth Junction, NJ, USA)
Tauroursodeoxycholate sodium	Caspase	Clinical Library Extended	HY-19696A	MedChemExpress (Monmouth Junction, NJ, USA)
Telatinib	KIT	Clinical Library Extended	HY-10527	MedChemExpress (Monmouth Junction, NJ, USA)
TG100-115	PI3K	Clinical Library Extended	HY-10111	MedChemExpress (Monmouth Junction, NJ, USA)
TG100-801	FGFR	Clinical Library Extended	HY-10186	MedChemExpress (Monmouth Junction, NJ, USA)
TGR-1202	PI3K	Clinical Library Extended	HY-12279	MedChemExpress (Monmouth Junction, NJ, USA)
TH-302	DNA Alkylator/Crosslinker	Clinical Library Extended	HY-10535	MedChemExpress (Monmouth Junction, NJ, USA)
Thioridazine hydrochloride	5-HT Receptor	Clinical Library Extended	HY-B0965	MedChemExpress (Monmouth Junction, NJ, USA)
TIC10	TNF	Clinical Library Extended	HY-15615A	MedChemExpress (Monmouth Junction, NJ, USA)
TIC10 isomer	Others	Clinical Library Extended	HY-15615	MedChemExpress (Monmouth Junction, NJ, USA)
Tirapazamine	Others	Clinical Library Extended	HY-13767	MedChemExpress (Monmouth Junction, NJ, USA)
Toceranib phosphate	KIT	Clinical Library Extended	HY-10330A	MedChemExpress (Monmouth Junction, NJ, USA)
Tofacitinib citrate	JAK	Clinical Library Extended	HY-40354A	MedChemExpress (Monmouth Junction, NJ, USA)
TOK-001	Cytochrome P450	Clinical Library Extended	HY-70006	MedChemExpress (Monmouth Junction, NJ, USA)
Toremifene citrate	ER	Clinical Library Extended	HY-B0005	MedChemExpress (Monmouth Junction, NJ, USA)

Drug	Class	Library	Cat. No.	Manufacturer
Tozasertib	ARK	Clinical Library Extended	HY-10161	MedChemExpress (Monmouth Junction, NJ, USA)
Tramiprosate	Others	Clinical Library Extended	HY-14602	MedChemExpress (Monmouth Junction, NJ, USA)
Treosulfan	DNA Alkylator/Crosslinker	Clinical Library Extended	HY-16503	MedChemExpress (Monmouth Junction, NJ, USA)
Triapine	DNA/RNA Synthesis	Clinical Library Extended	HY-10082	MedChemExpress (Monmouth Junction, NJ, USA)
Trichostatin A	HDAC	Clinical Library Extended	HY-15144	MedChemExpress (Monmouth Junction, NJ, USA)
Triciribine	AKT	Clinical Library Extended	HY-15457	MedChemExpress (Monmouth Junction, NJ, USA)
Triptorelin	GNRH Receptor	Clinical Library Extended	HY-12551	MedChemExpress (Monmouth Junction, NJ, USA)
Troglitazone	PPAR	Clinical Library Extended	HY-50935	MedChemExpress (Monmouth Junction, NJ, USA)
Turofexorate isopropyl	Others	Clinical Library Extended	HY-50911	MedChemExpress (Monmouth Junction, NJ, USA)
Ursolic acid	Endogenous Metabolite	Clinical Library Extended	HY-N0140	MedChemExpress (Monmouth Junction, NJ, USA)
VAL-083	DNA Alkylator/Crosslinker	Clinical Library Extended	HY-16513	MedChemExpress (Monmouth Junction, NJ, USA)
Valspodar	P-glycoprotein	Clinical Library Extended	HY-17384	MedChemExpress (Monmouth Junction, NJ, USA)
VcMMAE	ADC Cytotoxin	Clinical Library Extended	HY-15575	MedChemExpress (Monmouth Junction, NJ, USA)
VE-822	ATM/ATR	Clinical Library Extended	HY-13902	MedChemExpress (Monmouth Junction, NJ, USA)
Verteporfin	YAP	Clinical Library Extended	HY-B0146	MedChemExpress (Monmouth Junction, NJ, USA)
VLX1570	Others	Clinical Library Extended	HY-12471	MedChemExpress (Monmouth Junction, NJ, USA)
Voreloxin hydrochloride	Topoisomerase	Clinical Library Extended	HY-16518	MedChemExpress (Monmouth Junction, NJ, USA)
VRT752271	ERK	Clinical Library Extended	HY-15816	MedChemExpress (Monmouth Junction, NJ, USA)
VS-5584	MTOR	Clinical Library Extended	HY-16585	MedChemExpress (Monmouth Junction, NJ, USA)
VT-464	Others	Clinical Library Extended	HY-15996A	MedChemExpress (Monmouth Junction, NJ, USA)
VX-661	Others	Clinical Library Extended	HY-15448	MedChemExpress (Monmouth Junction, NJ, USA)
Xanthohumol	Endogenous Metabolite	Clinical Library Extended	HY-N1067	MedChemExpress (Monmouth Junction, NJ, USA)
XL019	JAK	Clinical Library Extended	HY-13775	MedChemExpress (Monmouth Junction, NJ, USA)
XL147	PI3K	Clinical Library Extended	HY-16526	MedChemExpress (Monmouth Junction, NJ, USA)
XL228	ARK	Clinical Library Extended	HY-15749	MedChemExpress (Monmouth Junction, NJ, USA)
YM-155 bromide	IAP	Clinical Library Extended	HY-10194	MedChemExpress (Monmouth Junction, NJ, USA)
ZSTK474	PI3K	Clinical Library Extended	HY-50847	MedChemExpress (Monmouth Junction, NJ, USA)
(-)-Terreic acid	BTK	Kinase Inhibitor Toolbox	1405	Tocris (Minneapolis, MN, USA)
1,2,3,4,5,6-Hexabromocyclohexane	JAK	Kinase Inhibitor Toolbox	2291	Tocris (Minneapolis, MN, USA)
10-DEBC hydrochloride	AKT	Kinase Inhibitor Toolbox	2558	Tocris (Minneapolis, MN, USA)
1-Naphthyl PP1	SRC	Kinase Inhibitor Toolbox	3063	Tocris (Minneapolis, MN, USA)
Aminopurvalanol A	CDK	Kinase Inhibitor Toolbox	2072	Tocris (Minneapolis, MN, USA)
API-2	AKT	Kinase Inhibitor Toolbox	2151	Tocris (Minneapolis, MN, USA)
Arctigenin	MEK	Kinase Inhibitor Toolbox	1777	Tocris (Minneapolis, MN, USA)
Arcyriaflavin A	CDK	Kinase Inhibitor Toolbox	2457	Tocris (Minneapolis, MN, USA)
BIBX 1382 dihydrochloride	EGFR	Kinase Inhibitor Toolbox	2416	Tocris (Minneapolis, MN, USA)
BIO	GSK3	Kinase Inhibitor Toolbox	3194	Tocris (Minneapolis, MN, USA)
CGK 733	ATM/ATR	Kinase Inhibitor Toolbox	2639	Tocris (Minneapolis, MN, USA)
CGP 53353	PKC	Kinase Inhibitor Toolbox	2442	Tocris (Minneapolis, MN, USA)
CGP 57380	Others	Kinase Inhibitor Toolbox	2731	Tocris (Minneapolis, MN, USA)
Compound 401	DNA-PK	Kinase Inhibitor Toolbox	3271	Tocris (Minneapolis, MN, USA)
D 4476	Others	Kinase Inhibitor Toolbox	2902	Tocris (Minneapolis, MN, USA)
EO 1428	p38 MAPK	Kinase Inhibitor Toolbox	2908	Tocris (Minneapolis, MN, USA)
ER 27319 maleate	SYK	Kinase Inhibitor Toolbox	2471	Tocris (Minneapolis, MN, USA)
FPA 124	AKT	Kinase Inhibitor Toolbox	2926	Tocris (Minneapolis, MN, USA)
GF 109203X	PKC	Kinase Inhibitor Toolbox	741	Tocris (Minneapolis, MN, USA)
GSK650394	Others	Kinase Inhibitor Toolbox	3572	Tocris (Minneapolis, MN, USA)
GW 441756	TRK	Kinase Inhibitor Toolbox	2238	Tocris (Minneapolis, MN, USA)
GW 5074	RAF	Kinase Inhibitor Toolbox	1381	Tocris (Minneapolis, MN, USA)
GW 583340 dihydrochloride	EGFR	Kinase Inhibitor Toolbox	2239	Tocris (Minneapolis, MN, USA)
GW 843682X	PLK	Kinase Inhibitor Toolbox	2977	Tocris (Minneapolis, MN, USA)
H 89 dihydrochloride	PKA	Kinase Inhibitor Toolbox	2910	Tocris (Minneapolis, MN, USA)
HA 1100 hydrochloride	ROCK	Kinase Inhibitor Toolbox	2415	Tocris (Minneapolis, MN, USA)
IKK 16	IKK	Kinase Inhibitor Toolbox	2539	Tocris (Minneapolis, MN, USA)
IMD 0354	IKK	Kinase Inhibitor Toolbox	2611	Tocris (Minneapolis, MN, USA)
Iressa	EGFR	Kinase Inhibitor Toolbox	3000	Tocris (Minneapolis, MN, USA)
Ki 8751	VEGFR	Kinase Inhibitor Toolbox	2542	Tocris (Minneapolis, MN, USA)
LFM-A13	BTK	Kinase Inhibitor Toolbox	1300	Tocris (Minneapolis, MN, USA)
LY294002 hydrochloride	PI3K	Kinase Inhibitor Toolbox	1130	Tocris (Minneapolis, MN, USA)
LY364947	TGFb	Kinase Inhibitor Toolbox	2718	Tocris (Minneapolis, MN, USA)
ML 9 hydrochloride	Others	Kinase Inhibitor Toolbox	431	Tocris (Minneapolis, MN, USA)
NH 125	Others	Kinase Inhibitor Toolbox	3439	Tocris (Minneapolis, MN, USA)
NSC 693868	CDK	Kinase Inhibitor Toolbox	1937	Tocris (Minneapolis, MN, USA)
NU 7026	DNA-PK	Kinase Inhibitor Toolbox	2828	Tocris (Minneapolis, MN, USA)
Olomoucine	CDK	Kinase Inhibitor Toolbox	1284	Tocris (Minneapolis, MN, USA)
PD198306	MEK	Kinase Inhibitor Toolbox	2605	Tocris (Minneapolis, MN, USA)
PD407824	CHEK	Kinase Inhibitor Toolbox	2694	Tocris (Minneapolis, MN, USA)
PI 828	PI3K	Kinase Inhibitor Toolbox	2814	Tocris (Minneapolis, MN, USA)
PP 1	SRC	Kinase Inhibitor Toolbox	1397	Tocris (Minneapolis, MN, USA)
PP 2	SRC	Kinase Inhibitor Toolbox	1407	Tocris (Minneapolis, MN, USA)
PQ 401	IGF-1R	Kinase Inhibitor Toolbox	2768	Tocris (Minneapolis, MN, USA)
Purvalanol A	CDK	Kinase Inhibitor Toolbox	1580	Tocris (Minneapolis, MN, USA)
Purvalanol B	CDK	Kinase Inhibitor Toolbox	1581	Tocris (Minneapolis, MN, USA)
Ro 08-2750	TRK	Kinase Inhibitor Toolbox	2272	Tocris (Minneapolis, MN, USA)
Ro 31-8220 mesylate	PKC	Kinase Inhibitor Toolbox	2002	Tocris (Minneapolis, MN, USA)
Ryuvidine	CDK	Kinase Inhibitor Toolbox	2609	Tocris (Minneapolis, MN, USA)
SB 202190	p38 MAPK	Kinase Inhibitor Toolbox	1264	Tocris (Minneapolis, MN, USA)
SB 203580 hydrochloride	p38 MAPK	Kinase Inhibitor Toolbox	1402	Tocris (Minneapolis, MN, USA)
SB 216763	GSK3	Kinase Inhibitor Toolbox	1616	Tocris (Minneapolis, MN, USA)
SB 218078	CHEK	Kinase Inhibitor Toolbox	2560	Tocris (Minneapolis, MN, USA)
SB 239063	p38 MAPK	Kinase Inhibitor Toolbox	1962	Tocris (Minneapolis, MN, USA)
SB 415286	GSK3	Kinase Inhibitor Toolbox	1617	Tocris (Minneapolis, MN, USA)
SB 431542	TGFb	Kinase Inhibitor Toolbox	1614	Tocris (Minneapolis, MN, USA)
SC 514	IKK	Kinase Inhibitor Toolbox	3318	Tocris (Minneapolis, MN, USA)
SD 208	TGFb	Kinase Inhibitor Toolbox	3269	Tocris (Minneapolis, MN, USA)
SL 327	MEK	Kinase Inhibitor Toolbox	1969	Tocris (Minneapolis, MN, USA)
SP 600125	JNK	Kinase Inhibitor Toolbox	1496	Tocris (Minneapolis, MN, USA)
SU 4312	VEGFR	Kinase Inhibitor Toolbox	1459	Tocris (Minneapolis, MN, USA)
TBB	Others	Kinase Inhibitor Toolbox	2275	Tocris (Minneapolis, MN, USA)
TCS 359	FLT3	Kinase Inhibitor Toolbox	2591	Tocris (Minneapolis, MN, USA)
TPCA-1	IKK	Kinase Inhibitor Toolbox	2559	Tocris (Minneapolis, MN, USA)
U0126	MEK	Kinase Inhibitor Toolbox	1144	Tocris (Minneapolis, MN, USA)
Y-27632 dihydrochloride	ROCK	Kinase Inhibitor Toolbox	1254	Tocris (Minneapolis, MN, USA)
ZM 306416 hydrochloride	VEGFR	Kinase Inhibitor Toolbox	2499	Tocris (Minneapolis, MN, USA)
ZM 323881 hydrochloride	VEGFR	Kinase Inhibitor Toolbox	2475	Tocris (Minneapolis, MN, USA)
ZM 336372	RAF	Kinase Inhibitor Toolbox	1321	Tocris (Minneapolis, MN, USA)
ZM 39923 hydrochloride	JAK	Kinase Inhibitor Toolbox	1367	Tocris (Minneapolis, MN, USA)
ZM 447439	ARK	Kinase Inhibitor Toolbox	2458	Tocris (Minneapolis, MN, USA)
ZM 449829	JAK	Kinase Inhibitor Toolbox	1366	Tocris (Minneapolis, MN, USA)
(+)-JQ1	BET	Epigenetics Toolbox	4499	Tocris (Minneapolis, MN, USA)
3-Aminobenzamide	PARP	Epigenetics Toolbox	788	Tocris (Minneapolis, MN, USA)
A 366	G9a/GLP	Epigenetics Toolbox	5163	Tocris (Minneapolis, MN, USA)
AK 7	SIRT	Epigenetics Toolbox	4754	Tocris (Minneapolis, MN, USA)
BIX 01294	G9a/GLP	Epigenetics Toolbox	3364	Tocris (Minneapolis, MN, USA)

Drug	Class	Library	Cat. No.	Manufacturer
Bromosporine	BET	Epigenetics Toolbox	4758	Tocris (Minneapolis, MN, USA)
C 646	HAT	Epigenetics Toolbox	4200	Tocris (Minneapolis, MN, USA)
Daminozide	Others	Epigenetics Toolbox	4684	Tocris (Minneapolis, MN, USA)
EGCG	DNMT	Epigenetics Toolbox	4524	Tocris (Minneapolis, MN, USA)
EX 527	SIRT	Epigenetics Toolbox	2780	Tocris (Minneapolis, MN, USA)
Fisetin	DNMT	Epigenetics Toolbox	5016	Tocris (Minneapolis, MN, USA)
Forskolin	Others	Epigenetics Toolbox	1099	Tocris (Minneapolis, MN, USA)
GSKJ1	JMJD	Epigenetics Toolbox	4593	Tocris (Minneapolis, MN, USA)
GSKJ2	Others	Epigenetics Toolbox	4688	Tocris (Minneapolis, MN, USA)
GSKJ4	JMJD	Epigenetics Toolbox	4594	Tocris (Minneapolis, MN, USA)
GSKJ5	Others	Epigenetics Toolbox	4689	Tocris (Minneapolis, MN, USA)
I-BET 151 hydrochloride	BET	Epigenetics Toolbox	4650	Tocris (Minneapolis, MN, USA)
I-CBP 112	BET	Epigenetics Toolbox	4891	Tocris (Minneapolis, MN, USA)
IOX 1	JMJD	Epigenetics Toolbox	4464	Tocris (Minneapolis, MN, USA)
IOX 2	HIF-PH	Epigenetics Toolbox	4451	Tocris (Minneapolis, MN, USA)
JIB 04	JMJD	Epigenetics Toolbox	4972	Tocris (Minneapolis, MN, USA)
Kaempferol	Endogenous Metabolite	Epigenetics Toolbox	3603	Tocris (Minneapolis, MN, USA)
KD 5170	HDAC	Epigenetics Toolbox	4001	Tocris (Minneapolis, MN, USA)
KU-55933	ATM/ATR	Epigenetics Toolbox	3544	Tocris (Minneapolis, MN, USA)
KU-60019	ATM/ATR	Epigenetics Toolbox	4176	Tocris (Minneapolis, MN, USA)
L002	HAT	Epigenetics Toolbox	5045	Tocris (Minneapolis, MN, USA)
LMK 235	HDAC	Epigenetics Toolbox	4830	Tocris (Minneapolis, MN, USA)
Lomeguatrib	DNMT	Epigenetics Toolbox	4359	Tocris (Minneapolis, MN, USA)
LY303511	BET	Epigenetics Toolbox	2418	Tocris (Minneapolis, MN, USA)
M 344	HDAC	Epigenetics Toolbox	2771	Tocris (Minneapolis, MN, USA)
MC 1568	HDAC	Epigenetics Toolbox	4077	Tocris (Minneapolis, MN, USA)
MS 436	BET	Epigenetics Toolbox	5173	Tocris (Minneapolis, MN, USA)
NSC 3852	HDAC	Epigenetics Toolbox	2521	Tocris (Minneapolis, MN, USA)
P 22077	Others	Epigenetics Toolbox	4485	Tocris (Minneapolis, MN, USA)
PFI 1	BET	Epigenetics Toolbox	4445	Tocris (Minneapolis, MN, USA)
PFI 3	SMARCA4	Epigenetics Toolbox	5072	Tocris (Minneapolis, MN, USA)
PJ 34 hydrochloride	PARP	Epigenetics Toolbox	3255	Tocris (Minneapolis, MN, USA)
PRT 4165	E3 Ligase	Epigenetics Toolbox	5047	Tocris (Minneapolis, MN, USA)
Pyroxamide	HDAC	Epigenetics Toolbox	4403	Tocris (Minneapolis, MN, USA)
Resveratrol	SIRT	Epigenetics Toolbox	1418	Tocris (Minneapolis, MN, USA)
RN 1 dihydrochloride	LSD1	Epigenetics Toolbox	4977	Tocris (Minneapolis, MN, USA)
SAHA	HDAC	Epigenetics Toolbox	4652	Tocris (Minneapolis, MN, USA)
Salermide	SIRT	Epigenetics Toolbox	4127	Tocris (Minneapolis, MN, USA)
SB 747651A dihydrochloride	MSK1	Epigenetics Toolbox	4630	Tocris (Minneapolis, MN, USA)
SBHA	HDAC	Epigenetics Toolbox	3810	Tocris (Minneapolis, MN, USA)
Scriptaid	HDAC	Epigenetics Toolbox	2421	Tocris (Minneapolis, MN, USA)
SGC 0946	HMT	Epigenetics Toolbox	4541	Tocris (Minneapolis, MN, USA)
Sirtinol	SIRT	Epigenetics Toolbox	3521	Tocris (Minneapolis, MN, USA)
Sodium 4-phenylbutyrate	HDAC	Epigenetics Toolbox	2682	Tocris (Minneapolis, MN, USA)
Splitomicin	SIRT	Epigenetics Toolbox	1542	Tocris (Minneapolis, MN, USA)
TC-E 5003	HMT	Epigenetics Toolbox	5099	Tocris (Minneapolis, MN, USA)
TC-H 106	HDAC	Epigenetics Toolbox	4270	Tocris (Minneapolis, MN, USA)
TCS HDAC6 20b	HDAC	Epigenetics Toolbox	4805	Tocris (Minneapolis, MN, USA)
Tenovin-1	SIRT	Epigenetics Toolbox	3365	Tocris (Minneapolis, MN, USA)
Tranylcypromine hydrochloride	LSD1	Epigenetics Toolbox	3852	Tocris (Minneapolis, MN, USA)
Triptolide	DNA/RNA Synthesis	Epigenetics Toolbox	3253	Tocris (Minneapolis, MN, USA)
UNC 0224	G9a/GLP	Epigenetics Toolbox	3861	Tocris (Minneapolis, MN, USA)
UNC 0638	G9a/GLP	Epigenetics Toolbox	4343	Tocris (Minneapolis, MN, USA)
UNC 0642	G9a/GLP	Epigenetics Toolbox	5132	Tocris (Minneapolis, MN, USA)
UNC 0646	G9a/GLP	Epigenetics Toolbox	4342	Tocris (Minneapolis, MN, USA)
UNC 1215	L3MBTL	Epigenetics Toolbox	4666	Tocris (Minneapolis, MN, USA)
UNC 926 hydrochloride	L3MBTL	Epigenetics Toolbox	4516	Tocris (Minneapolis, MN, USA)
Zebularine	DNMT	Epigenetics Toolbox	2293	Tocris (Minneapolis, MN, USA)

2.9. Data processing and storage

Processing raw plate reader luminescence data derived from the drug screening workflow required several steps to retrieve readable results in the form of dose-response data. Within this process, various software was involved: Excel, Prism and Drug Screening Analyzer (DSA). The latter was custom-made for this project, programmed in Microsoft Visual Basic. It allowed to process, manage and archive drug screening data and ran the required transformations:

- Creation of config files from D300eControl printing report files as definitions for derandomization
- Extraction of raw data from Excel sheets created by SparkControl storing the data as single-plate files
- Derandomization of single-plate files to receive single-drug files
- Importation of single-drug files into Prism to run the calculation of dose-response data using the Prism script interface

- Collection of descriptive statistics of choice in Excel sheets to allow further calculations and comparison
- Generation of multi-cell line files to automatically render overlapped dose-response curves using the Prism script interface visualizing data from multiple cell lines in one graph, either as individual curves or grouped curves

In the following chapters, the steps summarized above were explained in more detail.

2.9.1. Creation of config files from printing report files

Whenever a printing cycle was launched, D300e printed drugs according to the protocol file (.tdd file) which had been created using D300eControl. D300eControl controlled the printing process and wrote a report file (.xml file) which comprised information about plates, wells, drugs, concentrations and the dispensing process with precise time stamps. All screening plates were printed in randomized fashion, i.e., the data had to be derandomized prior to evaluation. As derandomization using the included D300eControl Data Merge software required lots of manual steps it was unsuitable for larger studies. Therefore, an automated solution for the derandomization procedure had to be implemented. As neither the protocol nor the report file offered a summary sheet depicting the non-random wells and their random counterparts at a glance, a transformation function was developed to process the report files into easy-to-use text files, named config files, with condensed derandomization instructions. DSA used three sheets from the report file to generate these config files:

- The “Plates” sheet which contained the exact plate count and the plate formats stored within the protocol. DSA could process 384- and 1536-well plates in an arbitrary order.
- The “Fluids” sheet which obtained the number of drugs and their respective names. DSA copied the names used in D300eControl.
- The “Tabular” sheet. DSA went through each line and column to retrieve the random coordinates of each concentration of each drug on each plate. Thereby, it ordered the coordinates in ascending order according to the concentrations and matched the DMSO wells to the respective drugs. The checkbox “DMSO priming well” allowed to compensate for 0.75 % DMSO wells required to prime the printer on 1536-well plates.

The transformation resulted in tab-delimited config files of four different types, exemplarily depicted in Figure 1. Each file listed the drugs in order of appearance in

the protocol file in the first column. The following columns contained the concentrations in ascending order (dilution files), the corresponding random locations in ascending order according to the concentrations (measure files), the control fluid's (usually DMSO) random locations (control files), and the non-treated well's random locations (nontreated files), the latter two in the order of appearance in the report file. All locations were stored as coordinates consisting of the row number, followed by the column number separated by a comma.

Dilution file:

Panobinostat	4.32	13.33	40	122	354	1025	2973	8621	25000
Marimastat	4.32	13.33	40	122	354	1025	2973	8621	25000
Linsitinib	4.32	13.33	40	122	354	1025	2973	8621	25000

Measure file:

Panobinostat	13,22	13,12	12,6	9,16	6,3	10,7	7,6	12,15	9,10
Marimastat	3,6	3,4	3,7	7,7	4,4	13,20	10,5	14,13	13,21
Linsitinib	12,3	12,13	11,17	8,21	9,6	11,6	10,19	5,17	8,11

Control file:

Panobinostat	4,11	7,15	11,11
Marimastat	4,11	7,15	11,11
Linsitinib	4,11	7,15	11,11

Non-treated file:

Panobinostat	13,3	10,8	7,19
Marimastat	13,3	10,8	7,19
Linsitinib	13,3	10,8	7,19

Figure 1. Config files generated by DSA. While the dilution file contains the inhibitor concentrations in ascending order, the measure file shows the corresponding random locations. The control file obtains the random locations of control wells used for normalization. Non-treated wells can be identified using the non-treated file.

2.9.2. Extraction of single-plate files from plate reader output files

To ease the handling of the output data from SparkControl (Excel sheets/.xlsx files) a transformation function was implemented to derive single-plate files. Each single-plate file mirrored a plate from the plate reader output file. DSA could handle 384- and 1536-well plates stored either as a single sheet with plates appearing in the course of the sheet or stored as individual sheets for each plate. It assumed that the latter format was used whenever there was more than one sheet in the plate reader output file. Before writing a plate, the plate format was detected by moving along column one until

the word “Plate” appeared. DSA then expected the plate format as a number in the fifth column of the same row (i.e., where SparkControl had usually stored the plate format). The plate order was derived from their appearance in the plate reader output file and adopted for the naming of the single-plate files. Notably, sheet names were ignored. In case multiple plates were stored in one sheet, DSA expected a marker (“<>”) in the top left corner of each plate to indicate the beginning of a plate. An exemplary plate reader output file as well as the corresponding single-plate file are depicted in Figure 2 and Figure 3.

Method name: HHUCL_CellTiter-Glo																							
Application: SparkControl			1.1																				
Date:			2016-04-01																				
Time:			16:06																				
User			VMED\Pauck																				
Plate			[COS384fw] - Corning 384 Flat White [COS384fw]																				
List of actions in this measurement script:																							
Plate																							
	Luminescence						CHLA-266_HHUCL_V1_C1_R8																	
Plate layout																							
Name			COS384fw																				
Mode	Luminescence																						
Name	CHLA-266_HHUCL_V1_C1_R8																						
Attenuation			None																				
Settle time			0	ms																			
Integration time			500	ms																			
Output			Counts / s																				
Part of Plate			C3-N22																				
Start Time			2016-04-01 16:02:31																				
Temperature			28.85	°C																			

<>	1	2	3	4	5	6	7	8	9	10	11	12	13	14	15	16	17	18	19	20	21	22	23	24
A																								
B																								
C			886857	1307749	314308	1413281	1379837	1181098	1358678	1423177	1373468	1442348	1387262	1513875	1103560	12566	1362928	26152	1297663	915352	1425529	1489728		
D			1029122	1540455	664186	1466802	63881	1527784	1488120	1564673	1501601	1499305	1467857	1551227	1533068	1537940	1524577	1544539	27993	1391628	1414832	1514091		
E			75326	1193823	855327	1220753	44013	533094	1250701	64775	1022252	1328986	212294	1335375	1250065	1128176	1038930	1311865	691163	1332007	1119884	794872		
F			129718	1479319	683733	916180	1435948	1321194	560718	1411606	1418225	1014301	1436290	1433831	1341227	1188393	1533146	1375114	1491956	1373791	1422317	1643435		
G			1438075	828741	1193171	61287	1406898	1204798	1499425	837728	62781	1308464	65957	1392072	1315748	1192545	1181118	1322408	1542563	1324810	1297642	930566		
H			1514568	1437476	513073	1498074	1609914	1490560	1535533	1321169	806863	1518236	1516389	816458	1497380	1496929	255082	1504170	1413552	1407600	1351102	1313009		
I			1093011	1038286	1507107	1319289	760906	1376863	926715	31274	390196	49053	1161145	902614	469611	190020	1437829	1470299	772350	893131	281355	702154		
J			1359657	1496382	1503497	1466863	65800	1568160	1442908	1355316	1397853	1319837	913511	1372105	1222832	97437	67202	1348848	1102289	840560	1298961	1438696		
K			259056	1483884	850515	1345789	1493696	1441035	327425	1481164	1419221	1492351	1423263	1497415	78940	954310	1451384	1405856	1120939	1033794	1303669	1505257		
L			1402402	1461604	13272	452613	65532	1410451	1375058	771855	1469719	1402849	1407623	632571	34086	1408658	16151	1380671	1314491	1481313	1374094	1361261		
M			1433796	1351650	1364984	207930	1419124	176367	1354169	714175	1370538	944607	1344064	979926	1250931	1405419	1368985	1352806	56879	1327013	1065033	1226361		
N			1247795	1501570	1486617	371567	1375345	1439941	1333237	1491202	1485429	1232210	1479013	1450531	1445227	1345205	833787	10159	1470781	25135	1405618	1429313		
O																								
P																								
End Time				2016-04-01 16:04:50																				

Figure 2. Excel sheet from SparkControl (CHLA-266_HHUCL_V1_C1_R8.xlsx).

```
886857  1307749  314308  1413281  1379837  1181098  1358678  1423177  1373468  1442348  1387262  1513875  1103560  12566  1362928  26152  1297663  915352  1425529  1489728
1029122  1540455  664186  1466802  63881  1527784  1488120  1564673  1501601  1499305  1467857  1551227  1533068  1537940  1524577  1544539  27993  1391628  1414832  1514091
75326  1193823  855327  1220753  44013  533094  1250701  64775  1022252  1328986  212294  1335375  1250065  1128176  1038930  1311865  691163  1332007  1119884  794872
129718  1479319  683733  916180  1435948  1321194  560718  1411606  1418225  1014301  1436290  1433831  1341227  1188393  1533146  1375114  1491956  1373791  1422317  1643435
1438075  828741  1193171  61287  1406898  1204798  1499425  837728  62781  1308464  65957  1392072  1315748  1192545  1181118  1322408  1542563  1324810  1297642  930566
1514568  1437476  513073  1498074  1609914  1490560  1535533  1321169  806863  1518236  1516389  816458  1497380  1496929  255082  1504170  1413552  1407600  1351102  1313009
1093011  1038286  1507107  1319289  760906  1376863  926715  31274  390196  49053  1161145  902614  469611  190020  1437829  1470299  772350  893131  281355  702154
1359657  1496382  1503497  1466863  65800  1568160  1442908  1355316  1397853  1319837  913511  1372105  1222832  97437  67202  1348848  1102289  840560  1298961  1438696
259056  1483884  850515  1345789  1493696  1441035  327425  1481164  1419221  1492351  1423263  1497415  78940  954310  1451384  1405856  1120939  1033794  1303669  1505257
1402402  1461604  13272  452613  65532  1410451  1375058  771855  1469719  1402849  1407623  632571  34086  1408658  16151  1380671  1314491  1481313  1374094  1361261
1433796  1351650  1364984  207930  1419124  176367  1354169  714175  1370538  944607  1344064  979926  1250931  1405419  1368985  1352806  56879  1327013  1065033  1226361
1247795  1501570  1486617  371567  1375345  1439941  1333237  1491202  1485429  1232210  1479013  1450531  1445227  1345205  833787  10159  1470781  25135  1405618  1429313
```

Figure 3. Example of a single-plate file (CHLA-266_HHUCL_V1_C1_R8_plate6.txt).

2.9.3. Generation of single-drug files through derandomization

To finally derive easy-to-use files for batch processing, the raw drug screening data stored as single-plate files was transformed into single-drug files using the derandomization instructions from the config files. Single-drug files contained the name of the drug with the unit of its concentration in brackets depicted in column one of the top row and the type of the output data and its unit in brackets stored in the second column of the top row. The following rows showed the concentrations in ascending

order and the respective output data. An example is depicted in Figure 4. Single-drug files could be imported into any program, e.g. Prism.

Concentration [nM]	Luminescence [Counts/s]
1	1412190
4.32	1226361
13.33	944607
40	452613
122	190020
354	129718
1025	65800
2973	61287
8621	34086
25000	31274

Figure 4. Example of a single-drug file (CHLA-266_HHUCL_V1_C1_R8_plate6_Panobinostat.txt).

2.9.4. Data rendering using Prism

To generate dose-response curves and calculate parameters of drug activity, DSA created a Prism script-file and executed it. The script opened a customizable template Prism file (.pzf file), imported data from a single-drug file, rendered the data and saved three types of output files:

- A Prism file based on the template containing the data from the single-drug file, along with all rendered data
- A text file (.txt) obtaining the most important descriptive parameters of the dose-response curve (result file, exemplarily depicted in Figure 5)
- An image file (.png) with the dose-response curve (exemplarily depicted in Figure 5)

The Prism script was automatically repeated until all single-drug files had been processed.

IC50	Bottom
21.04	Bottom = 2.215
CI of IC50	Top
18.64 to 23.75	Top = 100
LogIC50	S
1.323	0.6426
CI of LogIC50	tAUC
1.270 to 1.376	144.8
HillSlope	fAUC
-1.431	144.1
R square	
0.9982	

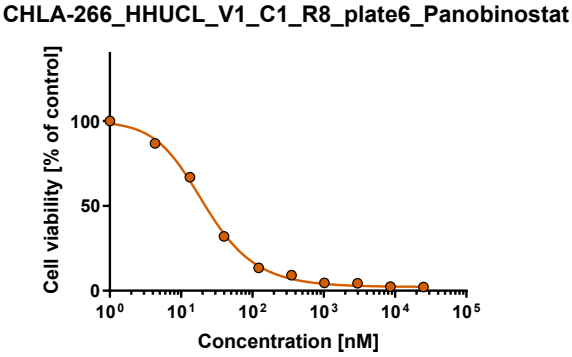

Figure 5. Example of a result file (CHLA-266_HHUCL_V1_C1_R8_plate6_Panobinostat_results.txt) and the corresponding dose-response curve (CHLA-266_HHUCL_V1_C1_R8_plate6_Panobinostat_results.png).

2.9.5. Summary of activity parameters

To compare drug screening results from different cell lines, DSA could summarize datasets in one Excel file while each sheet comprised data of one of the following parameters: IC50, Bottom, Rsquare, fAUC and tAUC. While the first column of each sheet listed the drugs, the first row assigned the cell lines. Drugs appearing multiple times (e.g. when a drug was covered in more than one library) were stored in the corresponding "_Duplicates" sheets. To monitor the activity of control drugs on each plate, DSA allowed to define drugs as controls using the "Control drugs" textbox which were consequently stored separately in the corresponding "_Control" sheets. Additionally, the analysis could be limited to a subset of drugs by writing the desired drugs to the "Only analyze the following drugs" textbox, divided by ";".

2.9.6. Overlap of multiple dose-response datasets

Comparing drug screening data by overlapping dose-response curves enabled an in-depth review of the different responses in two or more cell lines. Thus, DSA allowed to join single-drug files to multi-cell line files so that a graph with multiple curves could be rendered to either compare individual cell lines ("Single Curves" function) or groups of cell lines summarized as one curve ("Grouped" function). Examples of both modes are depicted in Figure 6.

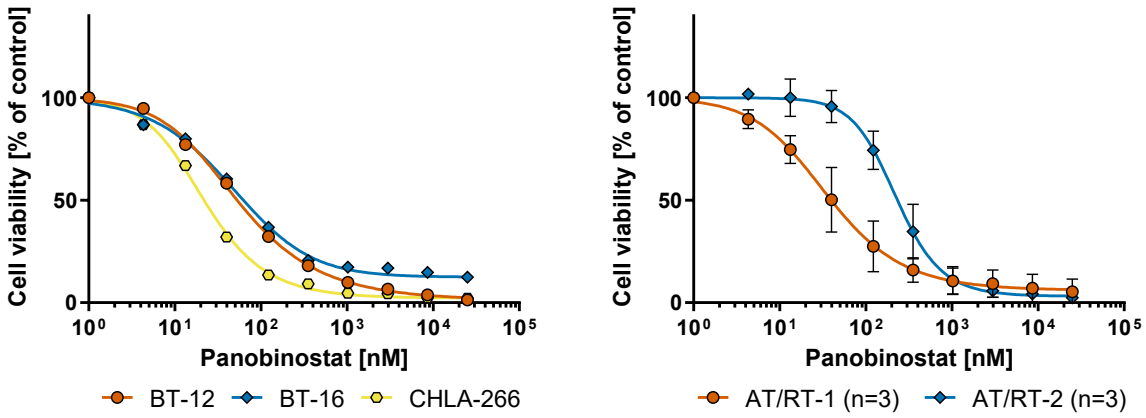

Figure 6. Dose-response curves of multiple AT/RT cell lines treated using Panobinostat either shown as three individual curves (“Single Curves” function, left) or curves derived from grouping three cell lines each (“Grouped” function, right).

2.9.7. Graphical user interface

The graphical user interface of DSA (Figure 7) shows two main boxes: The “Working Box” on the left and the “Database Box” on the right. To import new data, drag and drop a plate reader output file to the “Working Box” and hit the “AutoImport” button. DSA then automatically generates single-plate and single-drug files as well as rendered data through Prism. The data is saved to DSA’s library and then appears as an element in the “Database Box” adopting the name of the plate reader output file. To perform additional analyses, elements can be chosen from the “Database Box” and moved to the “Working Box” by drag and drop. By clicking on the buttons “Integrate”, “Single Curves” or “Grouped”, a procedure can be executed on the elements within the “Working Box”.

Moreover, DSA allows to configure unit (nM [default] and µM), the fitting algorithm in prism (four-parametric and five-parametric fitting), the “zero" value for rendering, and the path to GraphPad Prism (tested with Version 8). The zero value is required because algorithms for dose-response calculations work in logarithmic scale and thus, “0” cannot be used, as there is no log(0). As a replacement, 1 nM is used, which corresponds to 0 on log-scale and maps about one distribution step apart from the lowest concentration used in the own drug screening workflow (5 nM). The settings are stored in a small text file (“settings.ini”), once DSA is closed.

Additional tools which simplify working with DSA are grouping and queue features. Grouping allows to save a collection of datasets (dragged from the “Database Box” and dropped to the “Working Box”) as a group by hitting the “Define Group” button next to the “Grouping Box”. DSA requests a name for the group and then lists the group as

an element in the “Grouping Box”. Using the “Add to WB” button, the datasets behind the selected group are added to the “Working Box” again. The queue feature enables to create queue files, which contain a specific task. A queued task can be created in the same fashion as one would usually start a procedure. With the “Queue mode” checkbox checked, DSA creates a queue file, instead of starting the procedure. When the desired queue files have been created, the queue may be executed by hitting the “Start Queue” button.

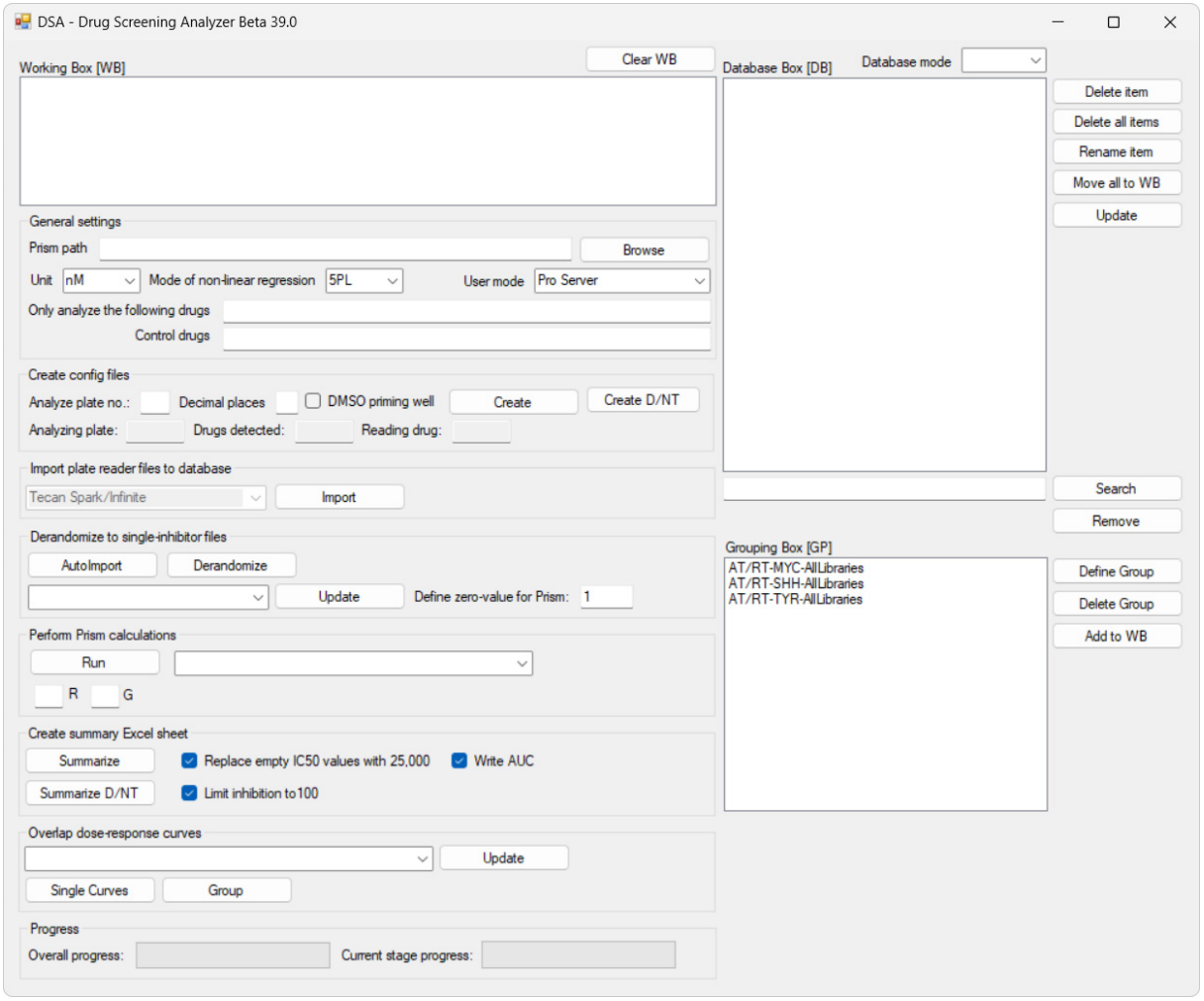

Figure 7. Graphical user interface of Drug screening analyzer (DSA).

2.10. Pellet preparation

Cell pellets were necessary to process follow-up analyses after drug screening and thus, pellets were stored after each drug screen. The procedure differed depending on the growth pattern of the cells and the intended use (DNA, RNA or protein isolation). For adherent cells, the cell layer was washed twice with PBS and cells were then harvested using a scraper (protein pellet) or using TrypLE/Trypsin (DNA pellet). After collecting the cells in 10 ml of PBS, the resulting cell suspension was centrifuged at

300 x g for 5 minutes. The supernatant was discarded, so that the pellet could be dissolved in 1 ml of PBS again to finally transfer the resulting cell suspension to a 1.5 ml reaction tube. The tube was centrifuged once more at 300 x g for 5 minutes. After discarding the supernatant again, the dry pellet was stored at -80 °C. For RNA pellets, cells were lysed within the flask by adding 1-2 ml of TRIzol reagent. The flask was repeatedly tilted until the solution turned homogenous. The cell lysates were transferred to a 1.5 ml reaction tube and stored at -80 °C. For cells growing in suspension, the cell suspension was collected in a centrifuge tube and washed twice with PBS by centrifuging at 300 x g for 5 minutes. As explained before, the pellet was transferred to a 1.5 ml reaction tube and stored dry at -80 °C. For protein pellets, all steps were conducted with ice-cold PBS and vessels on ice as well as using pre-cooled centrifuges at 4 °C. For semi-adherent cell lines, both methods were combined to collect and pool both, suspension and adherent fractions.

2.11. DNA methylation profiling

Cell pellets for DNA isolation were generated as explained above (cf. 2.10). The pellets were thawed and DNA was isolated using the Maxwell RSC Cultured Cells DNA Kit according to manufacturer's instructions. DNA concentration was then measured using the QuantiFluor ONE dsDNA System in a Quantus fluorometer according to manufacturer's instructions. DNA methylation profiling was conducted by LIFE & BRAIN GmbH (Bonn, Germany) using the Infinium MethylationEPIC BeadChip Kit. The data were analyzed using the platform Molecular Neuropathology 2.0 by means of the Brain Tumor Classifier (v12.5) (https://www.molecularneuropathology.org) [132].

2.12. RNA sequencing

Cell pellets for RNA isolation were generated as explained above (cf. 2.10). The lysed pellets stored in TRIzol were thawed on ice and the RNA isolation was conducted according to manufacturer's instructions. The RNA quality was assessed through Bioanalyzer RNA Analysis. To receive barcoded libraries, 100 ng of total RNA per sample were processed using the TruSeq RNA Library Preparation Kit v2. RNA concentration quantification was conducted using Qubit RNA HS Assay-Kit and a Qubit fluorometer according to manufacturer's instructions. Library quality was assessed through Bioanalyzer High Sensitivity DNA Analysis. Clonal amplification was conducted using 7.5 pM denatured libraries by means of a cBot, "*followed by deep sequencing on a HiSeq 2500* [sequencer] *(Illumina) for 101 cycles, with an additional*

seven cycles for index reading. [The resulting] *Fastq files were imported into Partek Flow. Quality analysis and quality control were performed on all reads to assess the read quality and to determine the amount of trimming required (both ends: 13 bases 5´ and 1 base 3´). Trimmed reads were aligned against the hg38 genome using the STAR v2.4.1d aligner, and unmapped reads were then aligned using Bowtie 2 - 2.2.5. After combining the aligned reads, gene expression was quantified using the ENSEMBL (release 84) database by the Partek Expectation-Maximization algorithm, and the data were normalized by RPKM. Partek Flow defaults were used in all analyses.*" [133].

2.13. Time course of caspase activation

For time course experiments cells were seeded to white (luminescent readout) 384-well plates at the density used in drug screening (cf. Table 7). One plate was prepared for each time point. The plates were incubated at 37 °C and 5 % CO_2 for 24 h to allow the cells to adhere/rest. After incubation the actual experiment was started by printing dilution series of the intended drugs on each plate using specific printing protocols by means of the D300e. The incubation at 37 °C and 5 % CO_2 was continued. After 3 h, 6 h, 12 h, 18 h, 24 h, 36 h, 48 h and 72 h, one plate for each time point was removed from the incubator and equilibrated to room temperature. CTG and Caspase-Glo reagents were added to the respective wells at equal volumes as the cell suspension and after additional 10 minutes of incubation at room temperature the readout was conducted using the Spark.

2.14. Apoptosis assay using Annexin V-/propidium iodide-costaining

For Annexin V-based evaluation of apoptosis, cells were seeded to 6-well plates and incubated at 37 °C and 5 % CO_2 for 24 h to allow the cells to adhere/rest. Then the drugs were added to the wells at a single concentration. Control wells were treated with the corresponding amount of DMSO. After 30 h of additional incubation at 37 °C and 5 % CO_2, cells were harvested on ice, counted, and an amount of 100,000 cells was co-stained with Fluorescein isothiocyanate (FITC) Annexin V antibodies and propidium iodide (PI). Right after staining, cells were measured in PC7 and PE channels by means of the CytoFlex cytometer. Single cells were selected by front- vs. side-scatter plot. Gating was then applied to derive four fractions:

- PI-negative, Annexin V-negative = viable cells
- PI-negative, Annexin V-positive = early apoptotic cells
- PI-positive, Annexin V-positive = late apoptotic cells
- PI-positive, Annexin V-negative = dead cells

2.15. Live-cell imaging-based apoptosis assay

To perform live-cell imaging-based evaluation of drug activity, cells were seeded to black 384-well plates with clear bottom at the density used in drug screening (cf. Table 7). Before seeding, the Incucyte Caspase-3/7 Green Apoptosis Reagent was added to the cell suspension at a concentration of 0.1 %. Cells were incubated at 37 °C and 5 % CO_2 for 24 h to rest/adhere. After incubation, drugs were printed to the plates by specific printing protocols using the D300e, including DMSO controls and sparing wells for non-treated controls. After dispensing, the plates were mounted to the Incucyte S3, which was placed into an incubator to provide an incubation atmosphere of 37 °C and 5 % CO_2 during the experiment. The measurement was initiated using a 10x objective with a measurement interval of 1 h to collect phase contrast and green fluorescence images using excitation wavelengths from 441 to 481 nm and emission wavelengths from 503 to 544 nm. After completion, cell line-specific traits were configured in the Incucyte S3 software to analyze the images and obtain the total integrated fluorescence signal intensity [Green calibrated units x µm²/image] and confluency [%] of each image.

3. Results

3.1. Development of the drug screening workflow

3.1.1. Review of constraint configurations and fitting models

As variations of the curve fitting algorithm or the adjustment of its constraints may alter results, the impact of different configurations was analyzed. For each drug, a sigmoidal curve was calculated. The viability of the control is 100 % by definition and consequently the top level was constrained to 100 % for all further calculations. Constraining the bottom level was more complicated: First of all, the minimum viability is zero %, i.e., the constraint should exclude the interpolation of negative bottom levels. Thus, the easiest way of constraining the bottom level was to set it to a value between zero and 100 %. This open setup promotes the occurrence of outlier overestimation (Figure 8) and is unable to detect activators which reach a bottom level above 100 %. Although the latter situation is rare, other publications have shown that it may be of great importance to detect (paradoxical) activators like BRAF inhibitors in *KIAA1549-BRAF* fusion-positive pilocytic astrocytoma [134]. To circumvent this problem, the bottom level was constrained to a value between zero and the lowest viability measured. This setup proved to also encourage the overestimation of outliers (Figure 8).

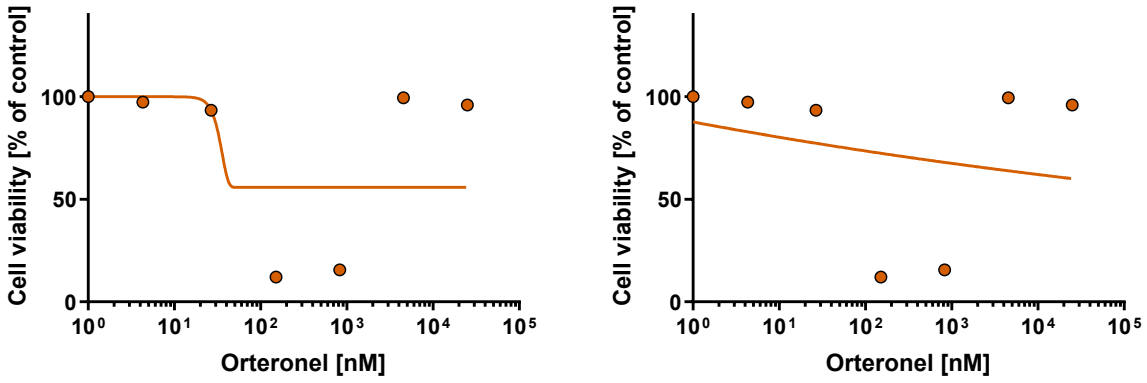

Figure 8. Dose-response curves from treating YH-13 cells with Orteronel. The bottom level was either constrained to a value between zero and 100 % (left) or between zero and the lowest viability measured (right). Both configurations overestimate outliers.

A more engineered approach is to extract the viability of the well containing the highest concentration, as one would expect the highest concentration of a drug to be most active. However, if the inhibition at a concentration of 25,000 nM is above zero, it is difficult to say if additional drug may further reduce the viability or if a plateau has been

reached above zero. In case that the algorithm was allowed to freely fit the dose-response curve between zero and the viability measured in the well containing the highest concentration, an increased occurrence of overestimated bottom levels was observed (Figure 9). Thus, finally and even more restrictive, the bottom level was constrained to the viability measured in the well containing the highest concentration, which resulted in a robust fit in most scenarios (Figure 9).

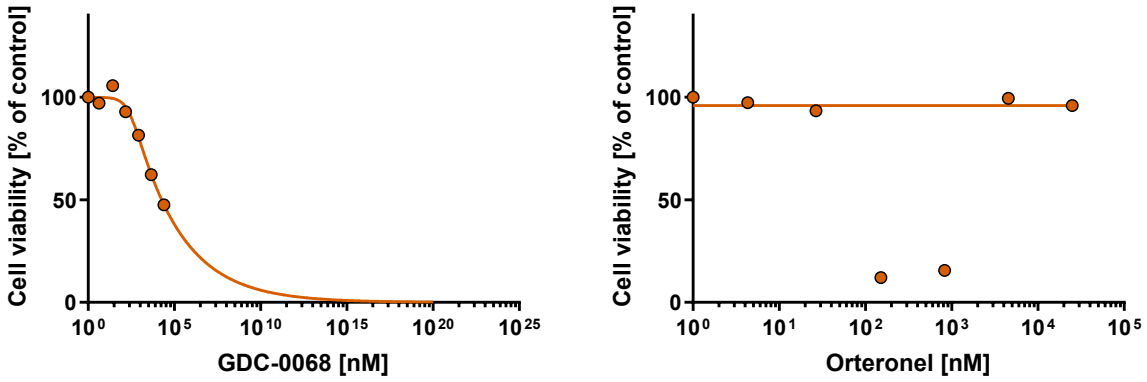

Figure 9. Dose-response curve of GDC-0068 in CHLA-04 cells with the bottom level constrained to a viability between zero and the viability measured in the well containing the highest concentration (left). An infinitely large bottom level is estimated from the data, along with a very high IC50 value. Dose-response curve of Orteronel in YH-13 cells (cf. Figure 8) with the bottom level constrained to the viability measured in the well containing the highest concentration (right). This configuration successfully ignored the two outliers avoiding the inclusion of a false-positive result.

As a last parameter constraining the IC50 was evaluated for additional refinement of our data analysis. As described above, constraining the bottom level fixed the calculation of asymptotes at infinitely small or large concentrations and, thus, also prevented the estimation of unrealistically small or large IC50 values in most cases. However, there was a relevant number of cases for which unrealistically small or large IC50 values remained to be calculated, especially in curves with a flat slope. After an in-depth review of these cases, it was concluded that this happens if the curve disrespects going straight through the constrained bottom level, but rather estimates to reach it at infinitely small or large concentrations (Figure 10). To circumvent this problem, the IC50 was finally constrained to a value between zero and the largest concentration within the screen, i.e. usually 25,000 nM. This adjustment simplified to work with the data, because there was no need to handle infinitely small or large values.

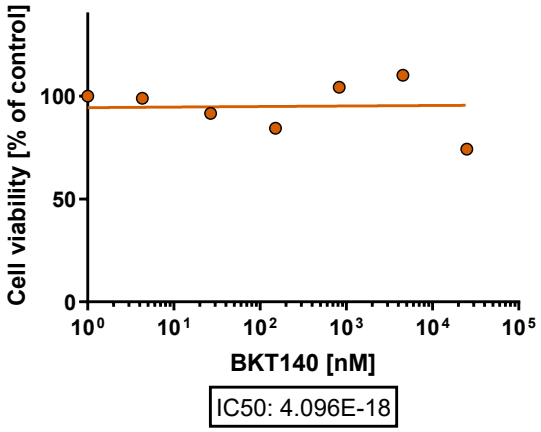

Figure 10. Dose-response curve of BKT140 in VU397 cells using a non-constrained (relative) IC50. The algorithm fits the IC50 to an infinitely small value.

After defining adequate constraints, the most suitable fitting model was selected by comparing the performance of four and five-parametric logistic regression models in the own data. In general, both models provided a robust fit and only minor differences were detected. Cases of non-converged curves were slightly more frequent using five-parametric fitting (3.14 %) than using four-parametric fitting (2.23 %). The deviation of fAUC and tAUC data remained low in both models with a mean absolute deviation of 0.018 and 0.017 using five-parametric and four-parametric fitting, respectively. Thus, both models were suitable for the evaluation of the own data.
In summary, if not stated otherwise, in this thesis it was decided to use a five-parametric logistic fitting model for all further analyses using the following constraints:

- The top level was constrained to 100 %.
- The bottom level was constrained to the viability derived from the well containing the highest concentration.
- The IC50 was constrained between zero and the highest concentration.

3.1.2. Identification of markers of activity

Considering the IC50 to evaluate dose-response data raises the question to use the relative or the absolute IC50. On the one hand, as the absolute IC50 is constrained to a viability of 50 %, it simplifies the comparison of different datasets. On the other hand, the absolute IC50 is not suitable for situations, in which the bottom level of the experiment is above zero. In this scenario it is either unable to derive an IC50 value (if the bottom level is above 50 % viability) or it overestimates the effect (if the bottom level is between zero and 50 %, Figure 11). As this situation frequently occurred in the

own data, it was decided to use the relative IC50, which is consequently just termed as IC50 anywhere else in this thesis.

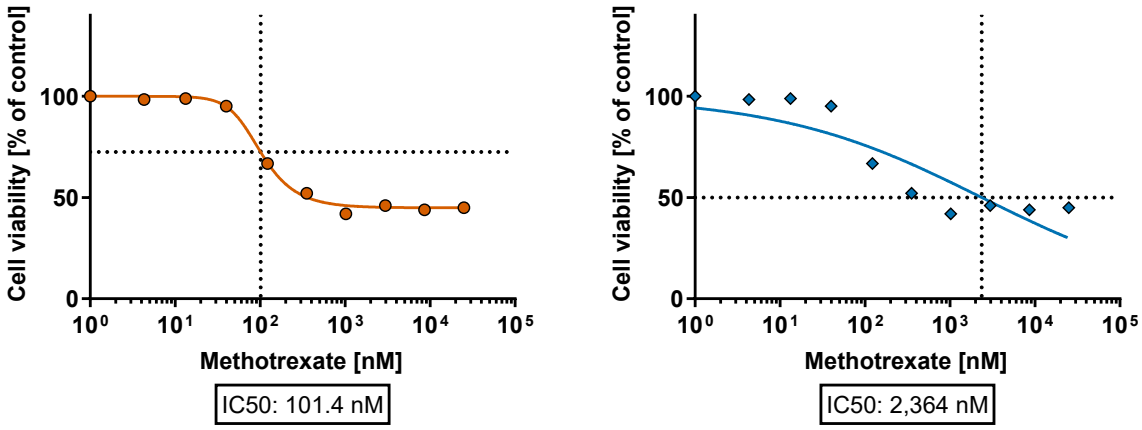

Figure 11. Dose-response curves of CHLA-04 cells treated with Methotrexate highlighting the calculation of either the relative IC50 (left) or the absolute IC50 (right). The absolute IC50 overestimated the total effect of Methotrexate.

Reviewing the suitability of the relative IC50 for large-scale dose-response data analyses showed that it often performed inferior in estimating the total effect compared to the bottom level. Figure 12 shows the activity of Paclitaxel in LN18, LNT229 and U87 cells. While the IC50 does hardly display any difference between the three cell lines, the bottom level indicates a differential response. Thus, in this experiment, the IC50 was unable to characterize the total effect of the drug, as the bottom levels were not identical in each cell line.

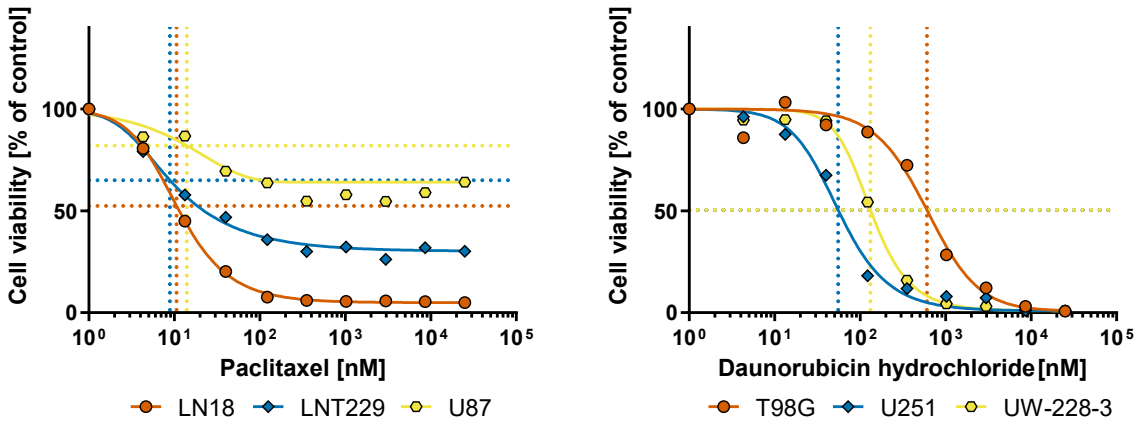

Paclitaxel

Cell line	IC50 [nM]	Inhibition [%]	CIS	fAUC
LN18	11	95.08	0.73	0.72
LNT229	9	69.82	0.55	0.53
U87	14	35.9	0.27	0.27

Daunorubicin hydrochloride

Cell line	IC50 [nM]	Inhibition [%]	CIS	fAUC
T98G	605	99.23	0.37	0.37
U251	55	99.13	0.60	0.59
UW-228-3	132	99.14	0.51	0.50

Figure 12. Dose-response curves and descriptive parameters of T98G, U251 and UW-228-3 cells treated with Daunorubicin hydrochloride and LN18, LNT229 and U87 cells treated with Paclitaxel. Either the IC50 or the inhibition was unable to convincingly characterize the drug activity.

The insufficient suitability of the IC50 as a quantitative measure for dose-response data has been reported [131, 135]. To circumvent this problem, the fAUC was calculated which precisely characterized the drug activity in either setting (Figure 12). Depending on whether the experimental parameters were equalized, additional steps during calculation were required, as the concentration range of the experiment defines the start and end points of the integral. When two datasets with different concentration ranges were analyzed, the interpolation of unknowns is necessary to cover the whole range of both experiments (Figure 13). Alternatively, the integration range must be limited to specific intervals around the inflection point, which is hard to automate.

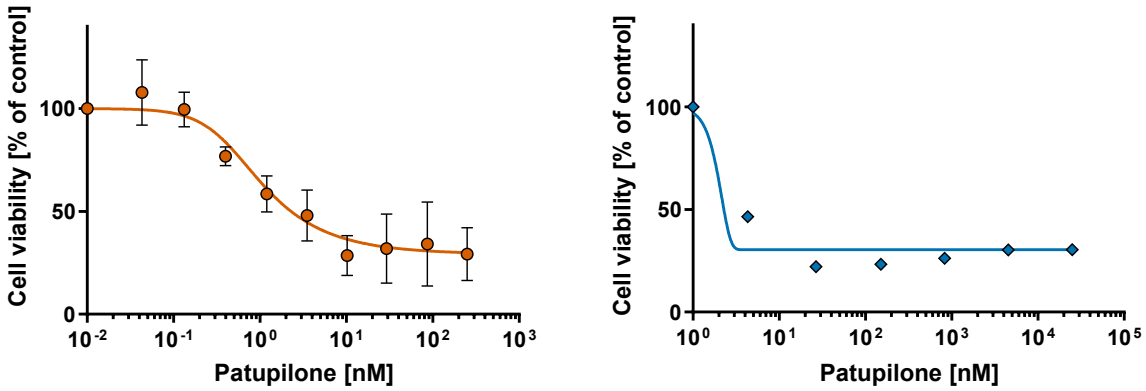

Patupilone				
Range [nM]	IC50 [nM]	Inhibition [%]	CIS	fAUC
0.05-250	1	70.78	0.71	0.37
5-25000	1.78	69.64	0.66	0.65

Figure 13. Dose-response curves of BT-16 cells treated with Patupilone. The curve on the right shows the results from the primary drug screening using the usual concentration range from 5 nM to 25,000 nM. On the contrary, the curve on the left is taken from the validation experiments using an individualized concentration range from 0.05 nM to 250 nM. While the CIS delivered comparable results in both experimental setups, the fAUC required adaption.

To simplify the analysis of experiments with non-equalized setups, another parameter was established by merging the bottom level (inhibition) and the IC50 using the following equation:

$$CIS = 1 - \frac{\log_{10}(IC_{50})}{\log_{10}(Conc_{max})} * \frac{100 - Bottom}{100}$$

Applying this combined inhibition score (CIS) to the dataset introduced in Figure 12 showed that it can deliver an adequate quantitative measure in any situation, just as the fAUC.

To determine and compare the performance of the described parameters in drug screening, a dataset including 495 drugs was reviewed. After filtering for a minimum inhibition of 80 %, manual annotation whether group A (n=6) had a superior response compared to group B (n=7) based on visual comparison of the corresponding dose-response curves was conducted. Next, the results were correlated with IC50, CIS and fAUC data to generate receiver operating characteristic (ROC) curves (Figure 14). Moreover, tAUC data was added to the analysis as a parameter independent from curve fitting. The evaluation using fAUC and tAUC data delivered the best results with almost equal areas under the ROC curve of 0.874 and 0.877, respectively. Both parameters performed slightly better than the CIS with an area under the ROC curve of 0.851. On the other hand, the IC50 was unable to clearly distinguish cases with superior activity and thus, provided an area under the ROC curve of only 0.649.

Taken together, these studies revealed two parameters to easily analyze larger dose-response datasets. While the fAUC was more precise, it required a unified experimental setup or additional calculations. The CIS on the other hand could also be used to compare datasets relying on different experimental setups without additional calculations, as long as the IC50 was calculated in an equal manner and inhibition as well as maximum drug concentrations were available. Still, it performed slightly less precise than the fAUC according to the ROC curve. As for most experiments of this thesis project, the experimental setup was equal, the fAUC was used for all further evaluations. When required, CIS and tAUC served as controls.

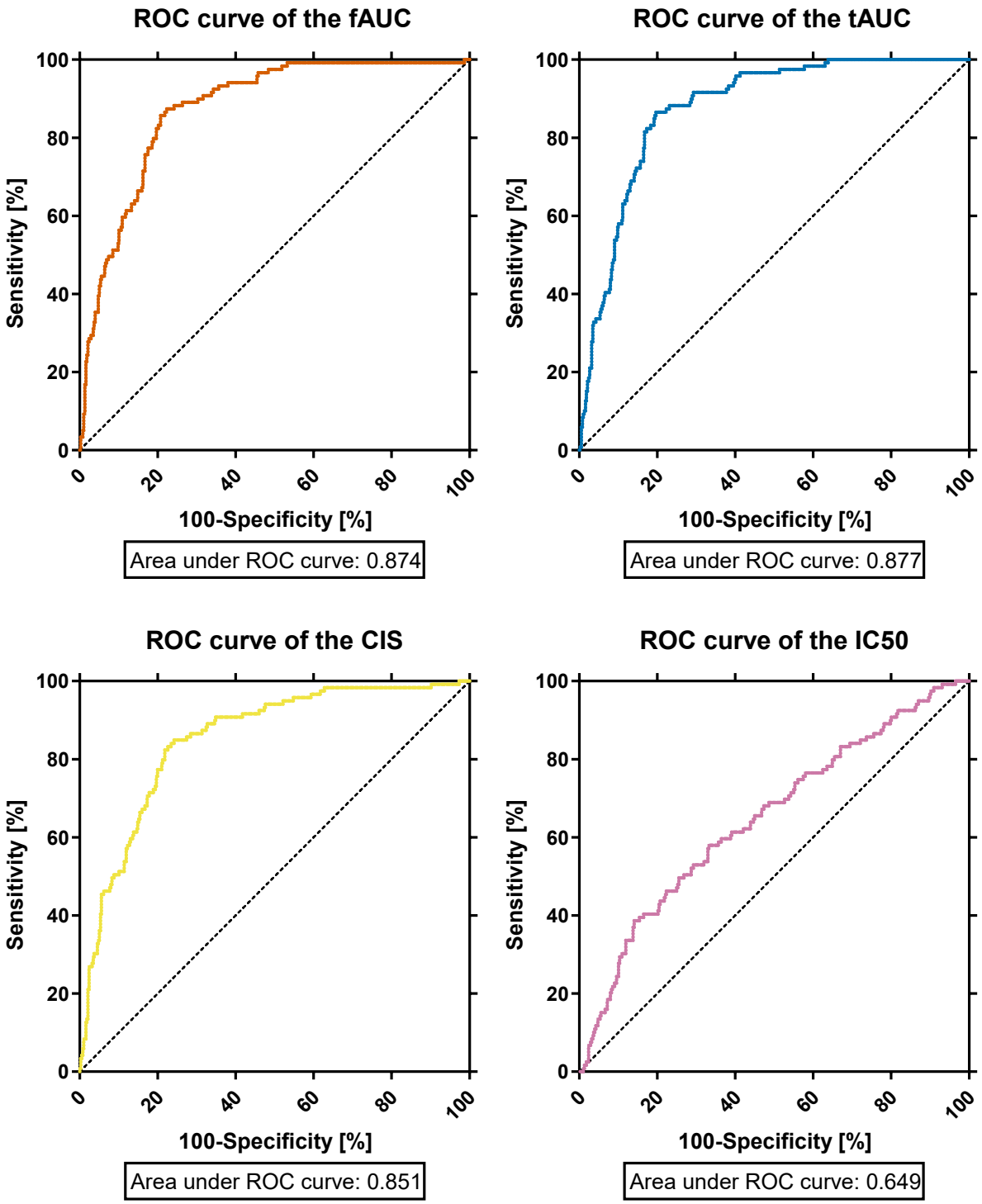

Figure 14. Receiver operating characteristic (ROC) curves of fAUC, tAUC, CIS and IC50 data derived from manual annotation of 495 dose-response curves comparing two groups of cell lines by visual comparison. AUC-based evaluation outperformed the CIS, and, most importantly, the IC50.

3.1.3. Comparison of pre-dispensed plates and plates dispensed directly

To elevate the experimental throughput of the drug screening workflow, a systematic plate preparation in batches of up to 70 plates was established by printing drugs into empty plates (pre-dispensed plates). After printing, the plates were sealed using Parafilm and then stored at -80 °C until needed, i.e., until cells were ready for screening. As a longer period between plate preparation and assay conduction in combination with a low total drug volume per well of only 0.075 µl (384-well plates with 30 µl working volume) could cause relevant evaporation of generally slow evaporating DMSO, the solubility of the drugs during the assay might be impaired, when the drug itself is not water soluble. Moreover, storage of such small drops of drugs in microplates is not ideal as it increases the exposure to ambient gas and humidity, which may cause rapid degradation. Thus, an experiment was set up to compare the assay performance either by printing drugs to plates filled with cell suspension (dispensed directly) or thawing plates from batch preparation (pre-dispensed plates). For this, four AT/RT cell lines (BT-12, CHLA-02, CHLA-04 and CHLA-266) were treated using the EG library. Notably, in the dispensed directly setup, the cells were allowed to incubate for 24 h after seeding and the exact treatment duration varied, as the printing process per se took some time. In either setting, we ensured an incubation period of at least 72 h for all drugs before the readout was conducted. In case of CHLA-02 eight drugs had to be removed from the analysis due to a handling error during preparation of directly dispensed plates. Overall, a Spearman correlation was calculated for each cell line which delivered r values ranging from 0.697 to 0.869 indicating a high similarity between both settings (Figure 15). Further evaluation of few outliers showed that these originated from fitting failure due to outliers or an uncommon dose-response pattern, thus leading to a false low (zero) fAUC value. However, manual comparison of dose-response curves indicated no major alteration. After consequent exclusion of these outliers, the alteration of the fAUC between pre-dispensed plates and plates dispensed directly stayed below 0.2 for all drugs and below 0.1 for 95,78 % of the drugs. Analyzing the cases with an fAUC alteration between 0.05 and 0.2 showed that the drugs tended to be more active in plates dispensed directly among screening data of BT-12, which grew adherently. For CHLA-02 and CHLA-04, which both grew in suspension, it seemed to be the other way round, as we observed higher activity in the pre-dispensed setup. CHLA-266 showed the least

alteration lacking an activity trend comparing pre-dispensed plates or plates dispensed directly. In plates dispensed directly, cells were incubated for 24 h before printing, and thus, the growth pattern and the underlying kinetics may explain the alterations that were observed. Moreover, most of the alterations happened at rather high concentrations, e.g. an onset of effect at 25,000 nM in one setup compared to no effect at all in the other setup. Thus, the measurable alterations were likely due to off-target effects rather than a specific increase or loss of sensitivity in either of the setups. Evaluation of data from DMSO and NT wells confirmed, that both settings delivered stable coefficients of variation (CoVs) of 8.35 % (CoV NT dispensed directly), 7.74 % (CoV DMSO dispensed directly), 7.51 % (CoV NT pre-dispensed) or 6.87 % (CoV DMSO pre-dispensed), respectively. However, the mean luminescence signal intensities appeared to vary between pre-dispensed plates and plates dispensed directly. While cell lines growing adherently tended to have a higher signal in plates dispensed directly, suspension cell lines showed the opposite (Figure 16). Probably, the incubation period of 24 h allowed faster evolving growth among cell lines growing adherently, making them also less susceptible to repetitive handling of the plates outside the incubator among plates dispensed directly. Moreover, different batches of CTG were used as the readouts of the pre-dispensed plates were not conducted on the same day. Regarding the effects of DMSO per se, the ratio of luminescence signal intensities derived from DMSO and NT wells was calculated, which ranged from 0.86 (BT-12 dispensed directly) to 0.98 (CHLA-02 dispensed directly). There was no significant alteration of the ratio comparing pre-dispensed plates vs. plates dispensed directly. In summary, both setups delivered well aligning data and comprehensive analyses did not reveal any systematic errors that would justify to prefer using the directly dispensed setup over the pre-dispensed setup.

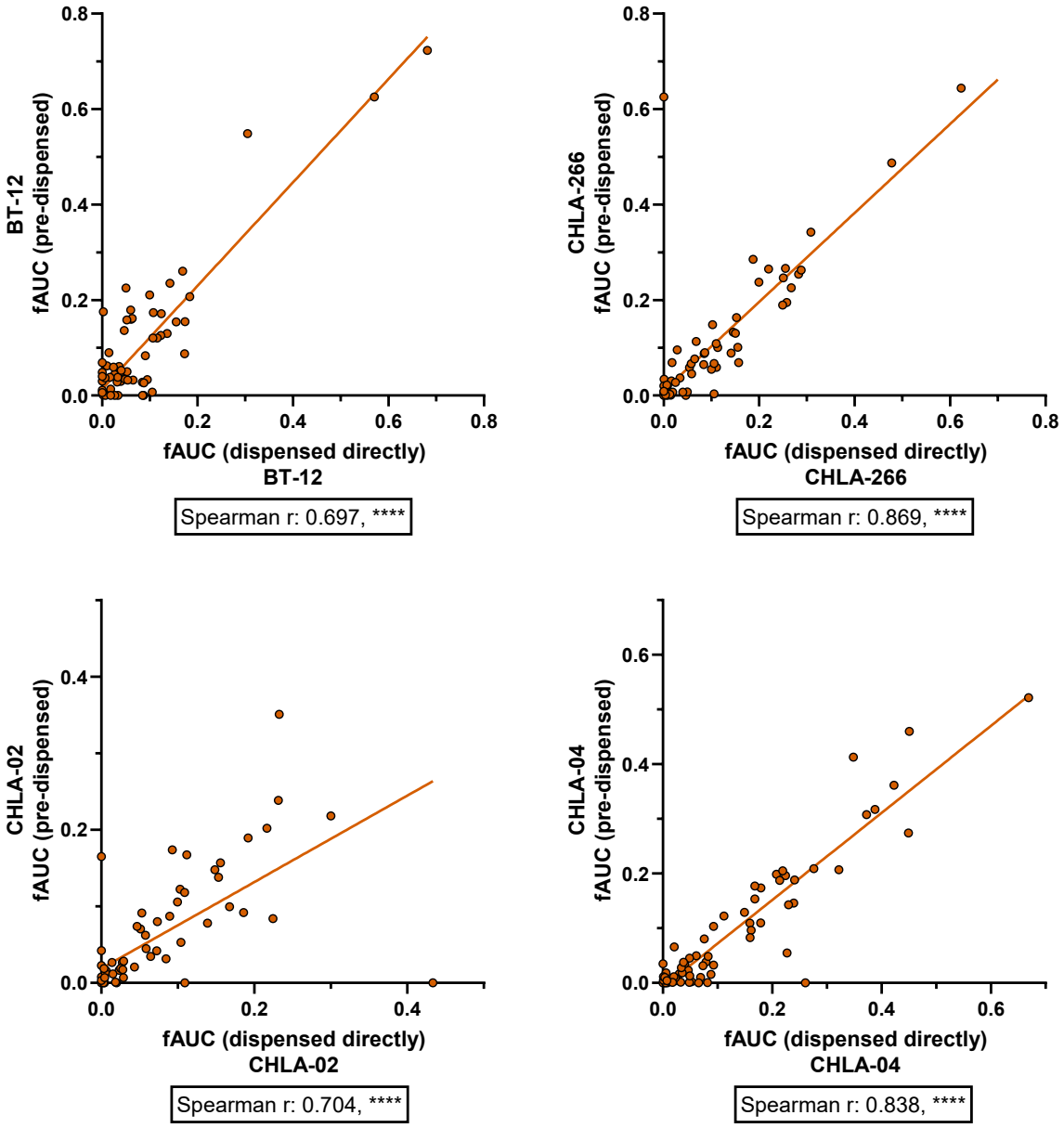

Figure 15. Correlation plots of pre-dispensed plates vs. plates dispensed directly. Significant Spearman correlations with high r values were obtained for all four cell lines indicating a high similarity of the data.

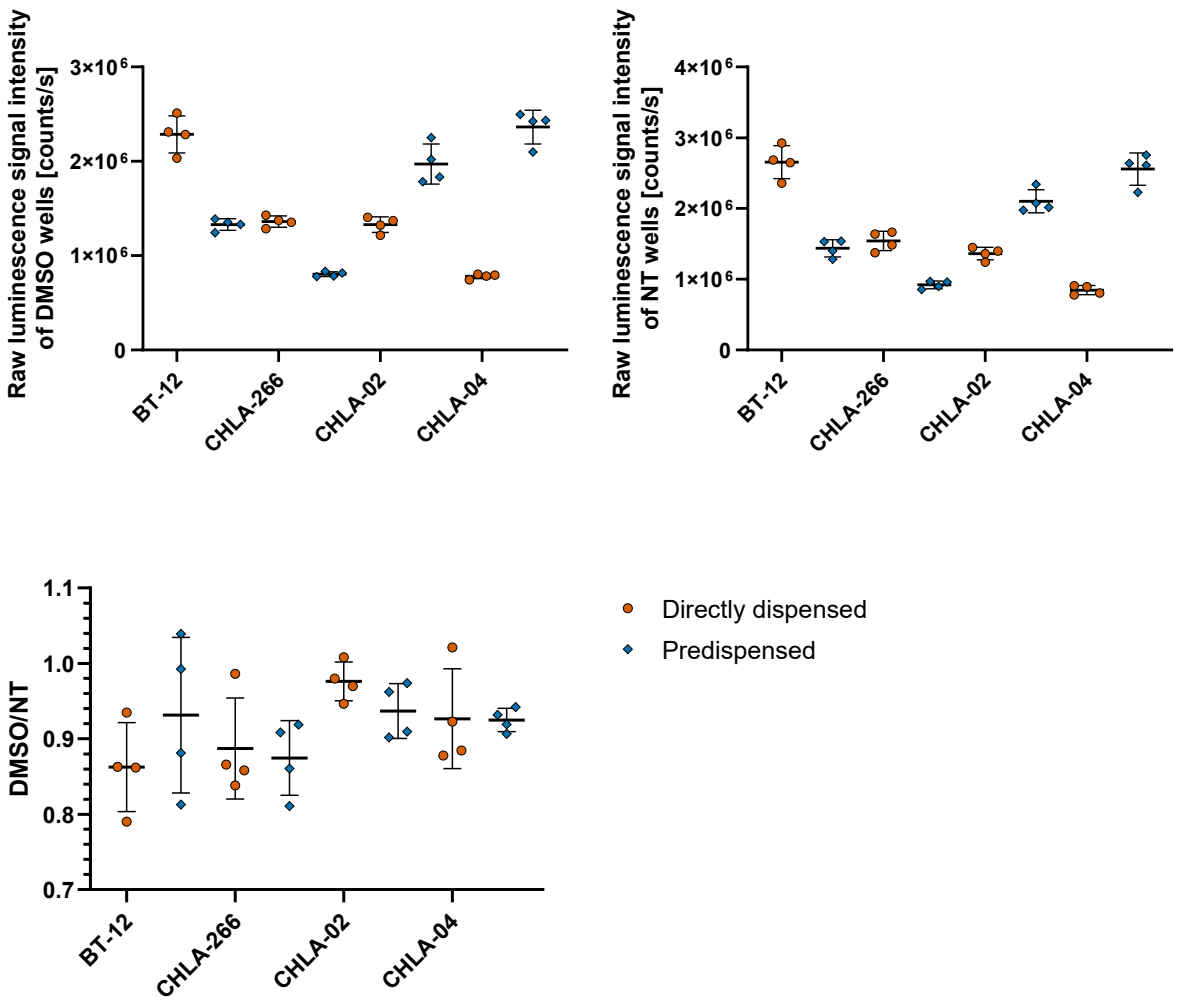

Figure 16. Mean DMSO and NT luminescence signal intensities per plate (upper). While luminescence signal intensities dropped in pre-dispensed plates among adherent cells, suspension cells displayed the opposite. DMSO/NT ratios from both setups (lower) did neither show an increased sensitivity vs. DMSO nor a significant influence of the setup (p-value = 0.174, one-way analysis of variance (ANOVA)).

3.1.4. Miniaturization of the plate format

Miniaturizing the plate format below 384-well plates reduces the resources required for drug screening, i.e., less media and CTG is consumed, and also fewer cells are required to screen the same number of drugs. Thus, drug screening becomes available to primary cultures and non-immortal controls, such as non-neoplastic cell culture models. However, reducing the well volume from 30 µl (384-well plates) to 4 µl (1536-well plates) is error-prone. Not only the reduced cell number per assay encourages higher variation, but also liquid handling operations become more complicated as a dispensing cassette with smaller tubing diameter is required, which might facilitate clogging. Nevertheless, considering the advantages, the performance of 1536-well plates in the own workflow was evaluated. For this, the AT/RT cell line BT-12

underwent drug screening in both, 1536- and 384-well plates using the CLS library. First, data quality was reviewed using CoVs of DMSO and NT wells, which increased from 5.6 % and 4.6 % in 384-well plates to 10.3 % and 11.5 % in 1536-well plates, respectively. The impact of DMSO was not altered as both formats showed a mild reduction in signal intensities of 4.5 % in 384-well plates and 4.9 % in 1536-well plates. Then a Spearman correlation of the fAUC data was calculated which delivered a Spearman r of 0.831, indicating a high correlation between both formats (Figure 17). Looking into the data more closely revealed that the fAUC varied fewer than 0.05 in 155 out of 197 cases (78.7 %) and fewer than 0.1 in 188 out of 197 cases (95.4 %). Manual review of the dose-response curves of drugs with an fAUC alteration of 0.1 or larger revealed that in three out of nine cases the alteration of the fAUC relied on the adaption of the dilution series. While the lowest concentration in 384-well plates was 5 nM it had to be elevated to 32.5 nM in 1536-well plates due to the minimum droplet size of the dispenser at 10 mM concentration. An early onset of effect thus indicated lower fAUC values in 384-well plates compared to 1536-well plates (Figure 18). In these cases, the measured alteration may be regarded as artifacts from the calculation of the fAUC. Three more of the reviewed dose-response curves revealed that the alteration of the fAUC was likely caused by increased variation of the assay as expected due to increased CoVs of DMSO and NT wells. For the other drugs, especially Homoharringtonine, minor alteration of their activity between plate formats was confirmed (Figure 18). In addition, a class-wise analysis of drug classes appearing multiple times was performed which did not reveal any clear trends (Figure 19). In summary, 1536-well plates performed well with the own workflow but delivered inferior screening quality compared to 384-well plates, as expected due to reduced assay volume and cell numbers. However, the alteration of the dose-response data remained minimal in the exemplary trial using the cell line BT-12.

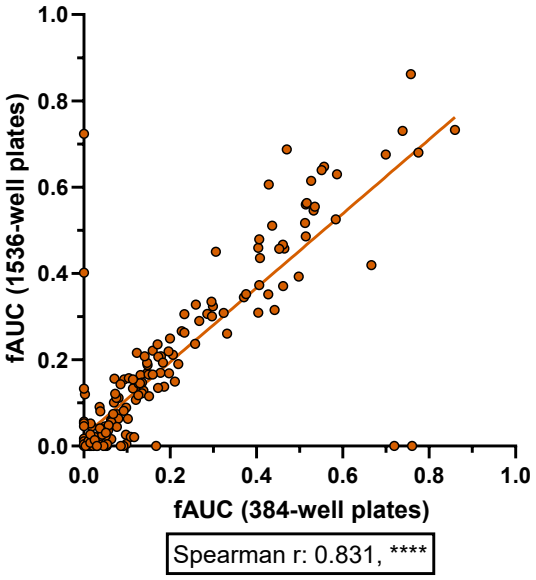

Figure 17. Correlation plot of CLS screening data of BT-12 cells in 384-well plates and 1536-well plates. A significant correlation with a Spearman r of 0.831 was obtained.

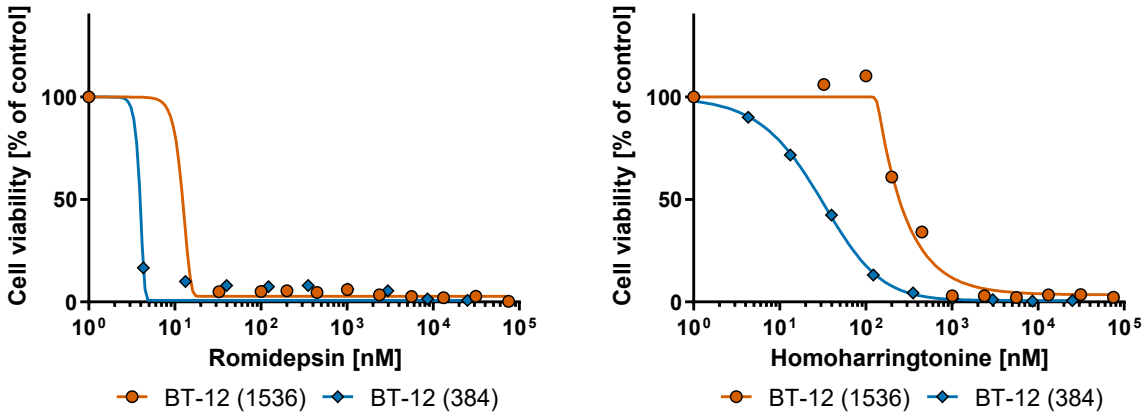

Figure 18. Overlapped dose-response curves of Romidepsin and Homoharringtonine in BT-12 cells comparing screening data from 384-well plates and 1536-well plates. Romidepsin exhibited an artificial alteration of the fAUC due to adaption of the lowest screening concentration (left). Homoharringtonine was one of few drugs that showed increased deviation between both formats (right).

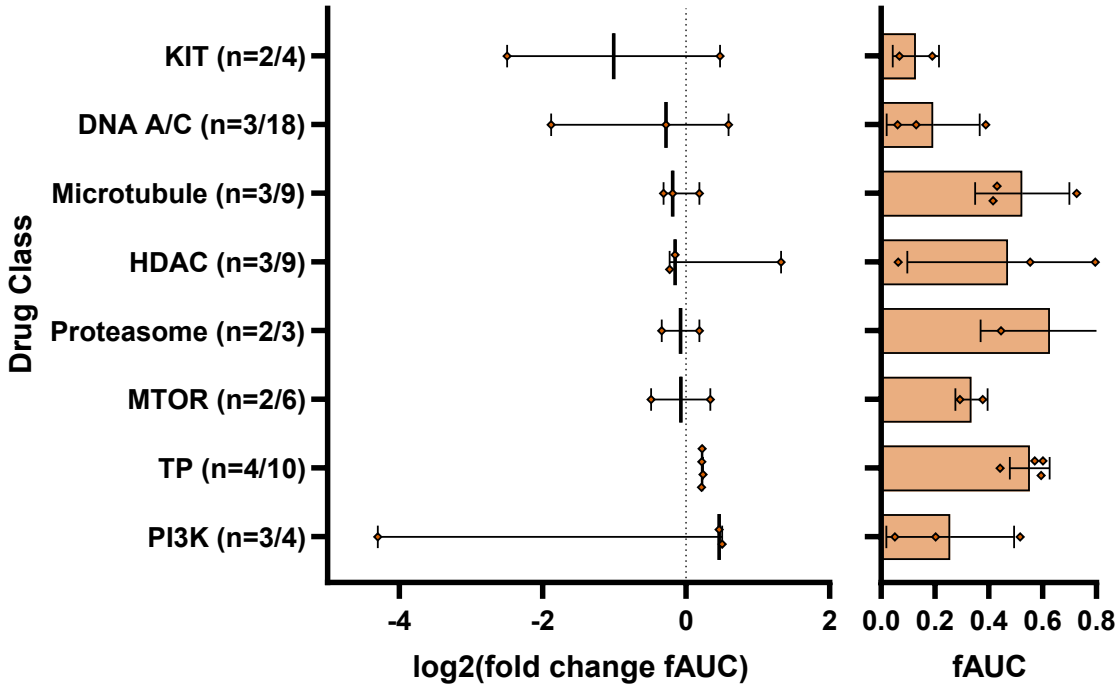

Figure 19. Drug class enrichment analysis (DCEA) of screening data from BT-12 cells, displayed as fold changes between 384-well plates and 1536-well plates (left), along with the corresponding fAUC values. Significant deviations were not observed. DNA A/C = DNA Alkylator/Crosslinker. TP = Topoisomerase.

3.1.5. Impact of diluting readout reagents

To reduce the resource consumption of the established workflow it was evaluated whether diluting CTG had an impact on dose-response data. For this, the AT/RT cell line BT-12 was seeded to three replicates of the EG library and CTG was used either in its undiluted state or at dilutions of 1:2 and 1:4 in PBS. A Spearman correlation (Figure 20) of the fAUC data was calculated, revealing r values of 0.851 (undiluted vs. 1:2) or 0.683 (undiluted vs. 1:4). Evaluation of the data from DMSO and NT wells revealed increased luminescence signal intensities upon dilution of CTG (Figure 21). However, the signal intensities did not further increase upon higher dilution. The CoVs of DMSO and NT wells remained stable. Furthermore, an fAUC alteration of lower than 0.05 was measured in 76 out of 80 (95 %) drugs in the comparison of undiluted CTG vs. 1:2 diluted CTG. For the comparison of undiluted CTG vs. 1:4 diluted CTG, 71 out of 80 (88.3 %) drugs obtained an fAUC alteration of 0.05 or lower. Taken together, a dilution of 1:2 over undiluted CTG was selected to reduce resource consumption, as the alteration of the dose-response data appeared minimal.

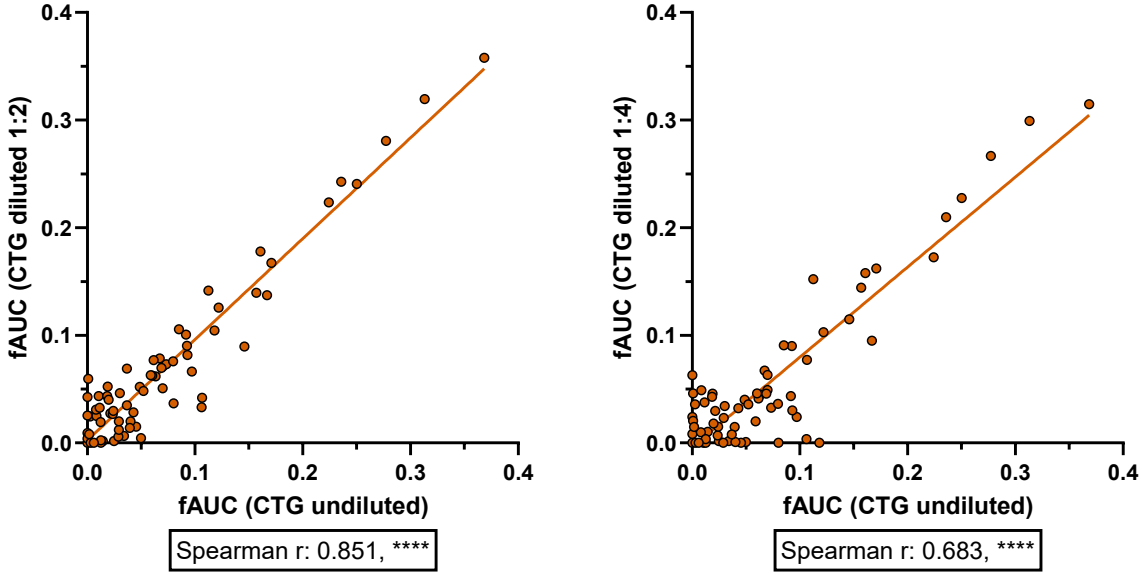

Figure 20. Correlation plots of EG screening data of BT-12 cells either using undiluted CTG or dilutions of 1:2 and 1:4, respectively. Both dilutions showed a significant correlation to undiluted CTG. The data from diluting 1:2 obtained a higher Spearman r of 0.851.

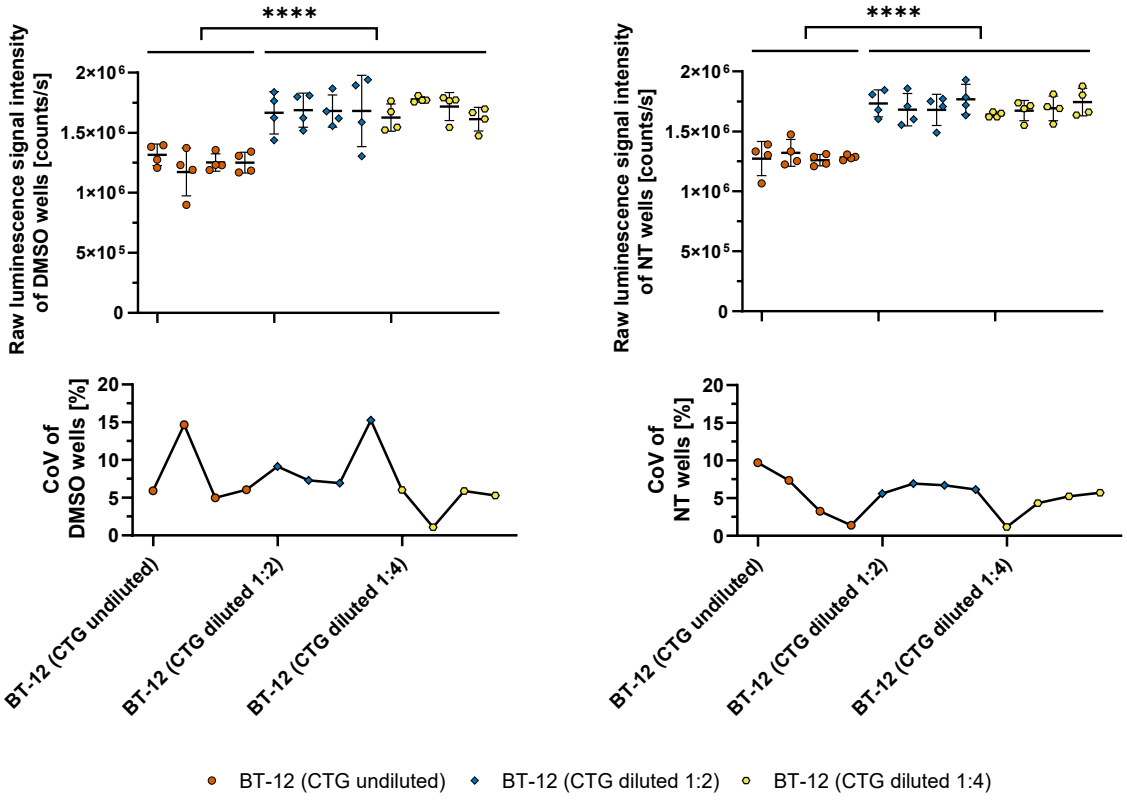

Figure 21. Raw luminescence signal intensities of NT and DMSO wells (upper) and corresponding CoVs (lower), displayed per plate (4 plates per library in total). A paradoxical increase of the luminescence signal intensities was observed upon dilution of CTG. CoVs remained stable.

3.1.6. Implications of supplementation of FBS on drug sensitivity profiles

Fetal bovine serum (FBS) has been shown to alter differentiation of stem cells and progenitors [136-138] and consequently, dose-response mechanisms of drugs in tumor cells may be altered as well. To analyze the effect of FBS supplementation on drug sensitivity profiles three cell lines, namely BT-12, BT-16 and CHLA-266, underwent drug screening in FBS-supplemented and serum-free media (cf. 2.4) using the EG, KI and CLS libraries resulting in a total number of 341 drugs. Correlation of the fAUC data revealed Spearman r values ranging from 0.690 to 0.807, indicating well aligning data for the most part (Figure 22). To further investigate the data for differential responses, the alteration of the fAUC was calculated between FBS-supplemented and serum-free culturing conditions, which revealed that 39.5 %, 33 % or 35.7 % of the drugs showed an fAUC alteration of larger than 0.05 in BT-12, BT-16 or CHLA-266, respectively. To eliminate any alteration relying on fitting issues, the alteration in fAUC data was aligned to the alteration in tAUC data and any drugs were removed that showed a deviation of 0.1 or more. This especially affected data points lying on the X or Y axes of the respective correlation plots (Figure 22). The data were then further filtered for drugs which showed an fAUC alteration in at least two out of three cell lines to focus on systemic effects, which held true for 123 out of 342 drugs (36 %). Figure 23 shows the fold change between FBS-supplemented and serum-free culturing conditions of these drugs arranged class-wise. Any classes represented by multiple drugs which only showed an fAUC alteration in a small subset were eliminated. Most prominently, this approach detected an increased activity of G9a/GLP inhibitors, a class of histone methyltransferases, Elesclomol, an apoptosis inducer, some of the CDK inhibitors and MTOR inhibitors in FBS-cultured cell lines compared to cell lines cultured under serum-free conditions, with mean fold changes of 3.13, 2.59, 1.96 or 1.57, respectively. Especially the increased activity of MTOR and CDK inhibitors may be related to a certain reduction in proliferation after switching the cells to serum-free conditions, which fits to reduced splitting factors observed during subculturing as well as higher cell numbers obtained through the seeding optimization procedure. Moreover, also epidermal growth factor receptor (EGFR) inhibitors showed a slightly increased activity under FBS-supplemented conditions, probably because of the specific addition of EGF to the serum-free medium and thus, higher dependence on EGF. On the other hand, some of the nucleoside antimetabolites (NA) and Cladribine,

an adenosine deaminase (ADA) inhibitor, exhibited reduced activity under FBS-supplemented conditions, which may be linked to a higher availability of nutrients in FBS-supplemented medium. However, for none of the classes there was a significant p-value in an MWU test. In summary, we detected minor alterations to drug sensitivity profiles among few classes of drugs induced by FBS supplementation, which remained non-significant in the investigated trial cohort (n=3).

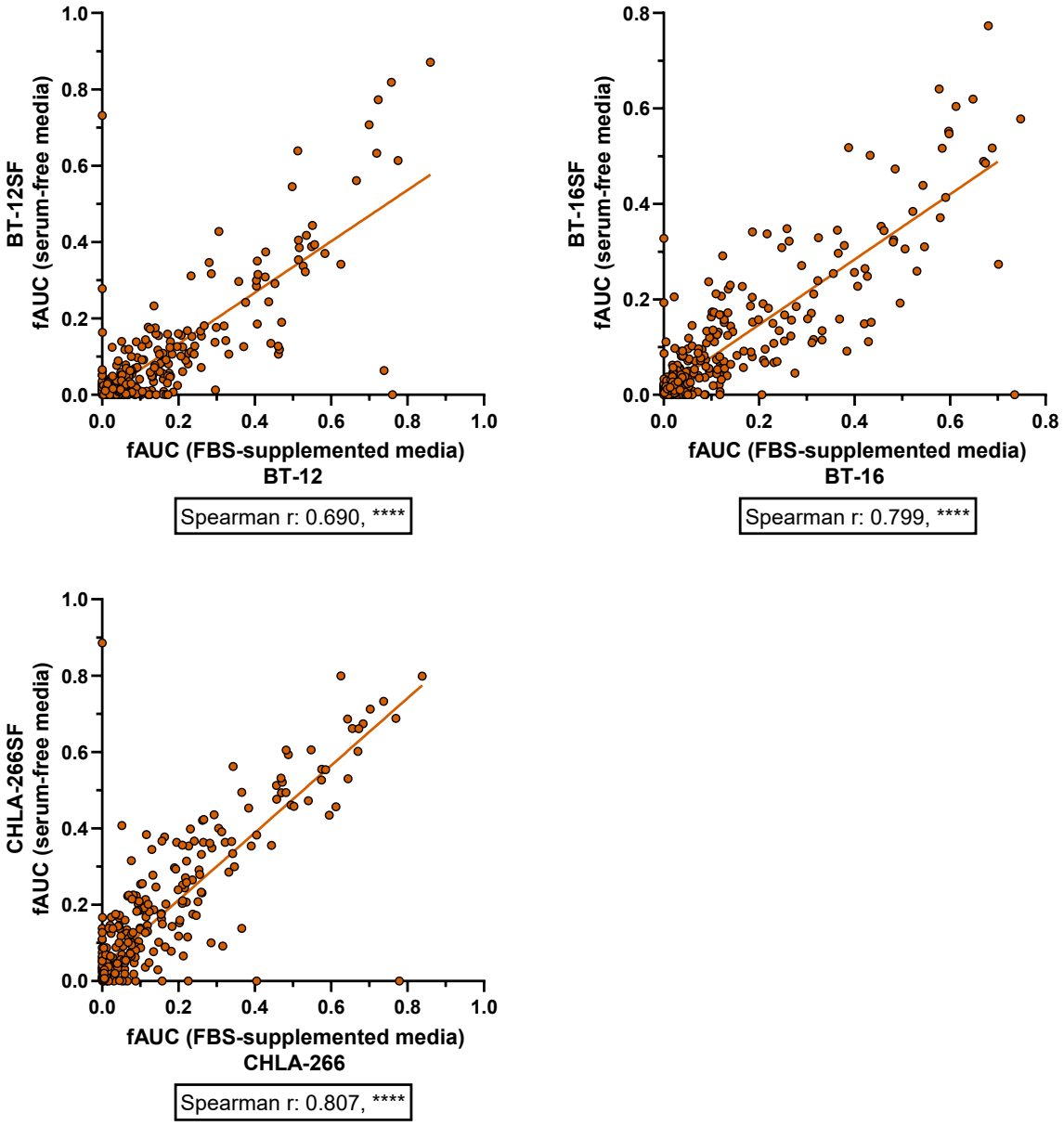

Figure 22. Correlation plots of combined EG, KI and CLS screening data of BT-12, BT-16 and CHLA-266 cells either using FBS-supplemented or serum-free media. All three cell lines obtained a significant correlation with high Spearman r values indicating highly overlapping data.

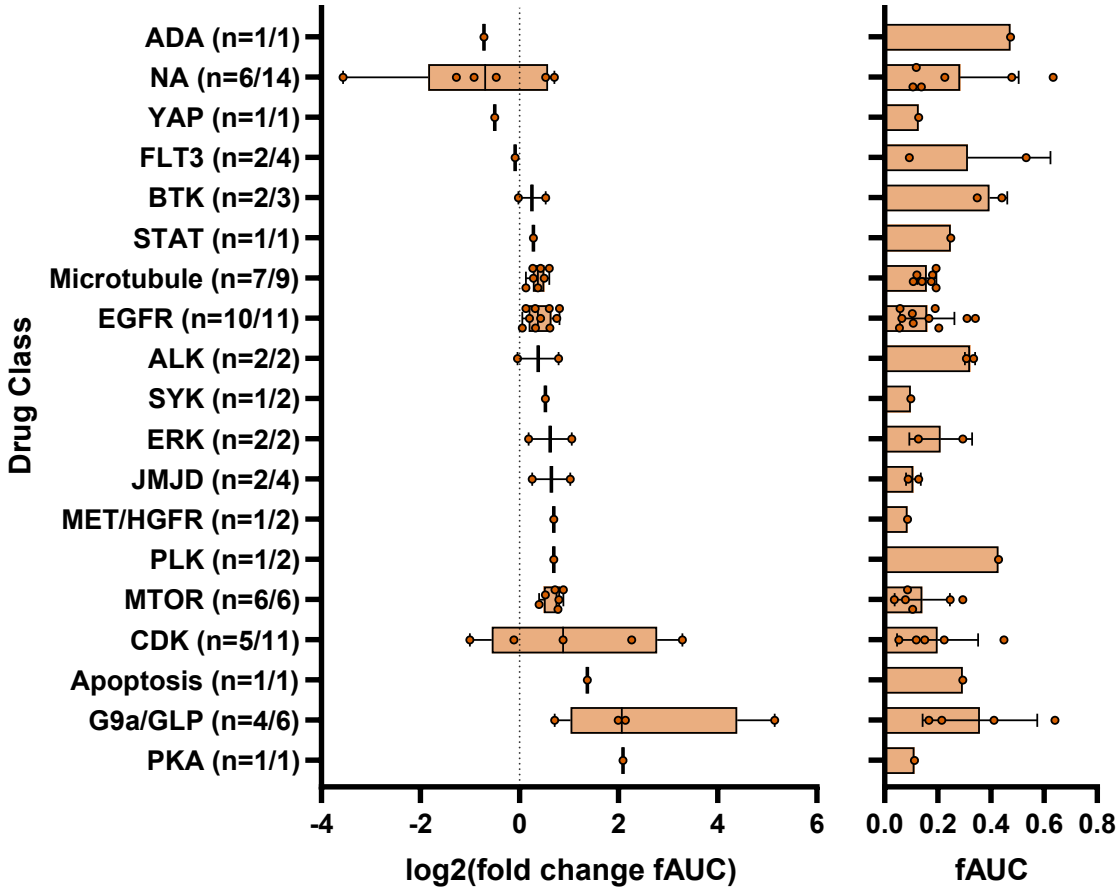

Figure 23. DCEA of screening data from BT-12, BT-16 and CHLA-266 cells in EG, KI and CLS libraries, displayed as fold changes between FBS-supplemented or serum-free conditions (left), along with the corresponding mean fAUC values (right). Significant differences (MWU test) were absent, but trends were observed, e.g. for G9a/GLP inhibitors, CDK inhibitors, MTOR inhibitors, EGFR inhibitors and nucleoside antimetabolites (NA).

3.2. Drug screening of AT/RT cell lines to identify targeted therapies

In total, data from 146 screens and 36 *in vitro* models were generated in this project. These included data from 13 AT/RT cell lines, 11 medulloblastoma cell lines, eight glioblastoma cell lines (including one pediatric glioblastoma cell line) and four non-neoplastic control models. Except for the healthy control models and the FBS-cultured derivatives of the AT/RT cell lines BT-12, BT-16 and CHLA-266, all cell lines were screened using four libraries (EG, KI, CLS, CLE). For the most part, screens of the different libraries were conducted using the same passage of cells. In case of CLE, the screens were usually conducted using another batch of cells, i.e., a different passage, as this library became available later than the others. CLE screens of medulloblastoma and glioblastoma cell lines were kindly performed by Mara Maue, Kübra Taban and Sarah Göbbels. In the following chapters each layer of data is analyzed separately.

3.2.1. Analysis of indicators of data quality

3.2.1.1. Variation among DMSO and NT controls

Before different cell lines were compared with each other to identify exceptional responses, indicators of data quality were evaluated. First, the variation among DMSO and NT wells was determined, of which at least three were included on each screening plate (range: 3-18 for DMSO and 3-6 for NT wells). For this, the CoVs were calculated based on the raw luminescence signal intensities [Counts/s] of each plate's DMSO and NT wells, and collected as mean values per cell line (Figure 24). The mean CoV per screen was 6.5 % among DMSO and 6 % among NT wells. 86.1 % of the screens showed a mean CoV of lower than 10 % among both, DMSO and NT wells. Analyzing the CoV per cell line revealed a mean CoV of 6.7 % and 6.4 % while staying below 10 % in 86.5 % and 91.9 % of the DMSO and NT wells, respectively. Highest values were reached for D425 cells in CLE with a CoV of 23.1 % and 18 %, DAOY cells in CLE with a CoV of 22.1 % and 23.7 %, YH-13 cells in EG with a CoV of 25.4 % and 15 % and Astrocytes-cerebellum in CLS with a CoV of 21.7 % and 14.3 % in DMSO and NT wells, respectively. In summary, the evaluation showed low variation across the individual screens indicating a high data quality with few exceptions, in which the CoV of DMSO and NT wells increased to a tolerable extent.

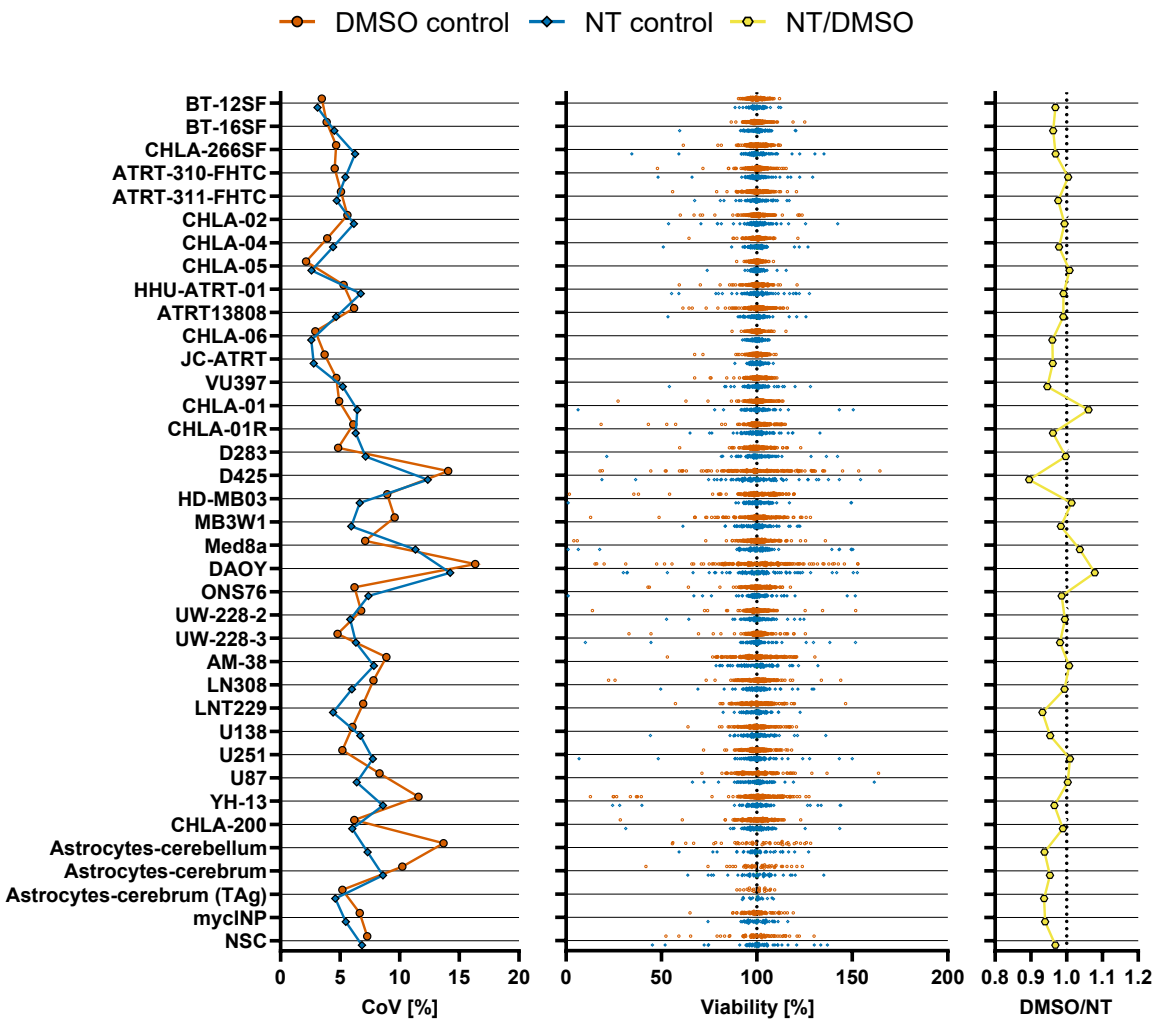

Figure 24. Mean CoVs per cell line (left), underlying raw luminescence signal intensities (middle) and the ratio of mean raw luminescence signal intensities of DMSO and non-treated (NT) wells (right). For the most part, low CoVs were achieved indicating high data quality. Highest CoVs occurred in D425, DAOY and Astrocytes-cerebellum. The DMSO/NT ratio remained low and stable.

Next, raw luminescence signal intensities of DMSO and NT wells were compared to reveal any impact of DMSO. Based on pre-experiments (data not shown) performed by Viktoria Marquardt, a DMSO concentration of 0.25 % was selected for the screening workflow, which did not display any DMSO-induced alteration of cell viability. To analyze whether the observations from the pre-experiments match with the data from drug screening, mean raw luminescence signal intensities were collected from DMSO and NT wells from a total of 927 plates and the DMSO/NT ratio was calculated for each plate. Taken together, the mean viability over all plates was 2.23 % lower in DMSO wells compared to NT wells (Figure 24). However, this finding was not statistically significant (Figure 25). Further summary of the data per screen showed that the ratio of DMSO and NT wells stayed between 0.85-1.15 in 96.6 % of the screens. Looking at individual screens, only D425 cells in EG showed a ratio below 0.85, namely 0.80. The

highest increase was detected for YH-13 cells in CLS with a ratio of 1.25, DAOY cells in CLS with a ratio of 1.33 and AM-38 cells in EG with a ratio of 1.21. Notably, there was a significant correlation between the CoVs of DMSO and NT well's luminescence signal intensities and the ratio of DMSO and NT wells with a Spearman r of 0.253 or 0.281, respectively. The correlation strengthened if smaller subsets with higher CoVs were chosen: For the top 10 % of highest CoVs among NT wells, the Spearman r was 0.583 (Figure 25). Thus, it is likely, that there was no variation in DMSO sensitivity but rather increased experimental noise. In summary, the data indicated that a DMSO percentage of 0.25 % was suitable for the own workflow.

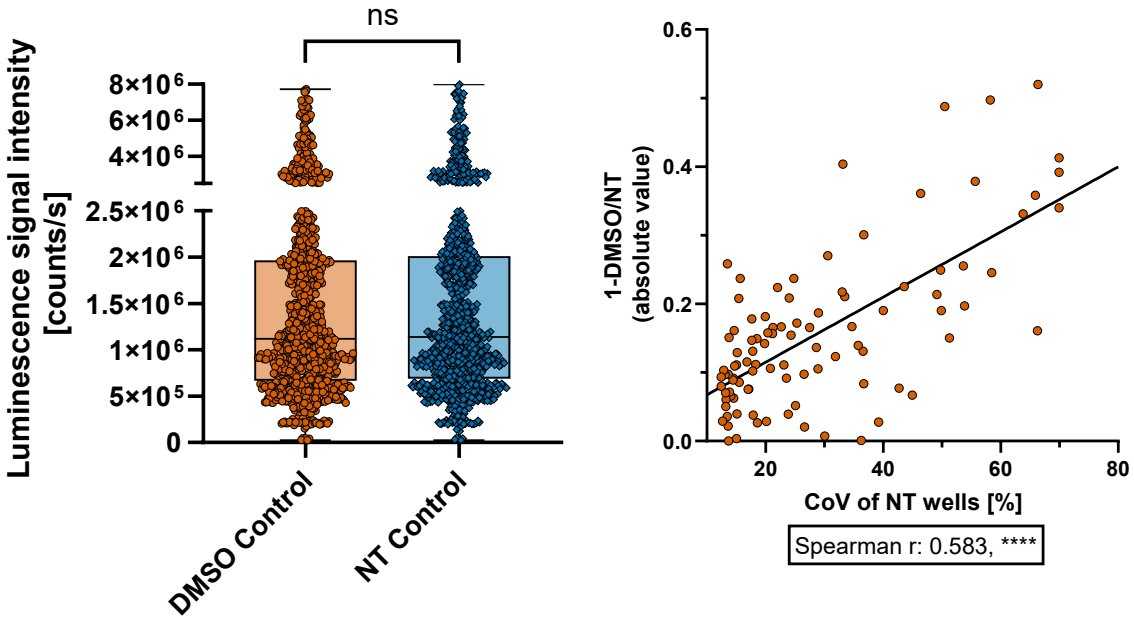

Figure 25. Mean luminescence signal intensities of DMSO and NT wells per plate (left). The observed difference is not significant (MWU test, p-value 0.583). A correlation of mean CoVs of NT wells per plate (highest 10 %) and the 1-DMSO/NT ratio (absolute value) (right) turned out significant with a Spearman r of 0.583 indicating a link between increased experimental noise and stronger alteration between DMSO and NT well's luminescence signal intensities.

3.2.1.2. Inter-plate effects

After ensuring the absence of unintended DMSO-induced effects, analyses for possible plate effects were carried out. As the plating process and the application of CTG after incubation had been conducted in a continuous, semi-automated fashion usually storing the whole cell suspension/CTG in a single large centrifuge tube and also using the same batch of CTG for all plates, it was to be expected that stronger inter-plate variations are absent. To proof this, the luminescence signal intensities of DMSO and NT wells were normalized by each of the screen's means and relative amplitudes per screen were calculated (Figure 26).

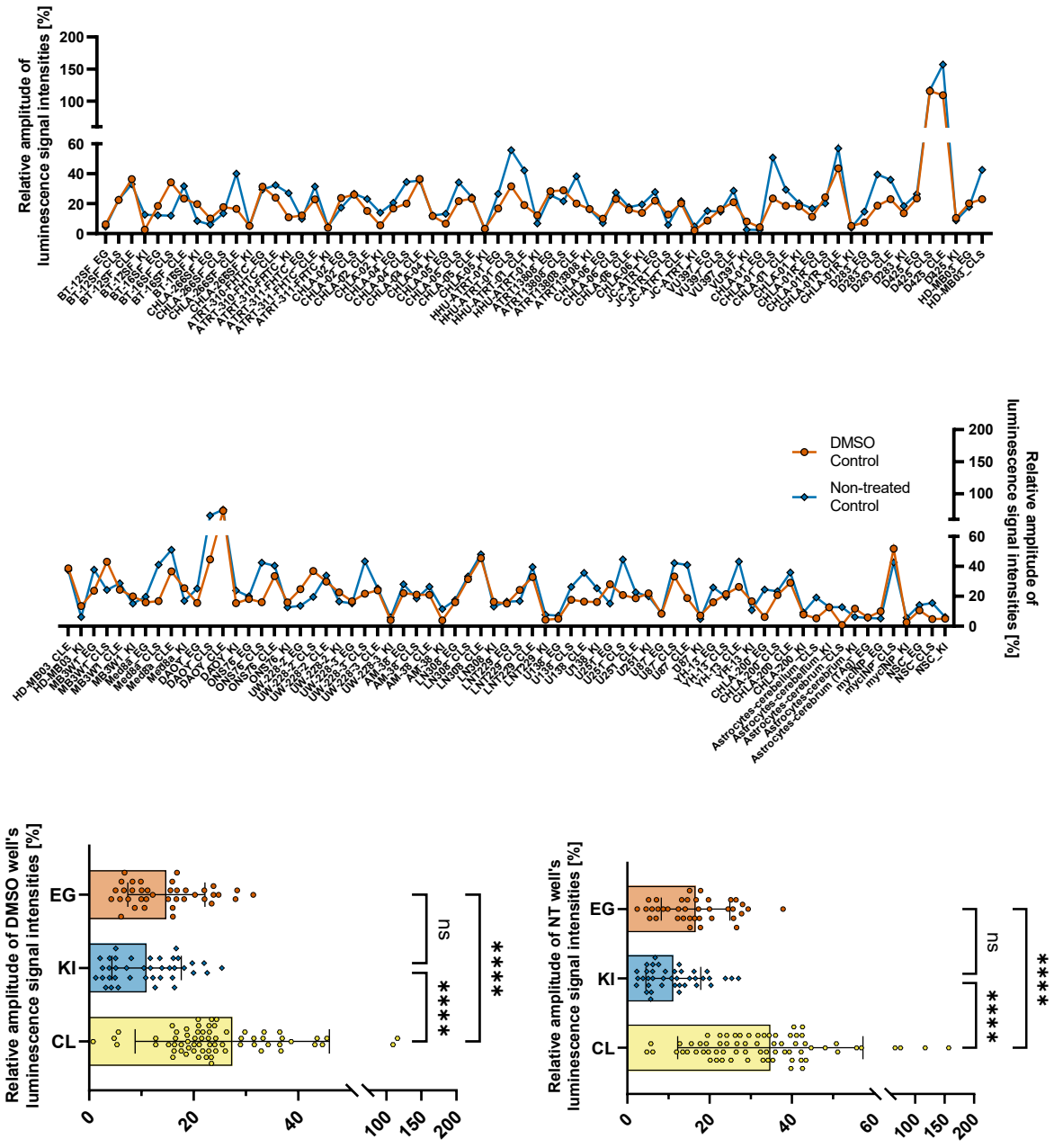

Figure 26. Relative amplitudes of DMSO and NT wells, i.e., the difference between the plates with highest and lowest mean luminescence signal intensities after normalization by the mean of all plates, displayed per screen (upper) or summarized per library (lower). Most screens stayed below 40 % indicating stable assay performance. The larger the libraries, the higher the relative amplitudes.

The mean relative amplitude was 20.4 % for DMSO wells and 24.6 % for NT wells. It stayed below 40 % in over 90 % of the screens in case of DMSO wells and over 80 % of the screens in case of NT wells. Notably, a library-wise analysis of the relative amplitudes revealed that the deviation significantly increased with the number of plates and thus, with the hands-on-time. This may result from a variety of factors: During plating of the cells the cell suspension modestly condenses due to the cells settling at the bottom of the tube, which even by employing gentle agitation cannot entirely be

avoided. This would cause the luminescence signal intensities to increase in the course of the plates and decrease again at the very end. On the other hand, during the readout process, it takes way longer to read a plate than to dispense CTG (using 500 ms integration time at least 2.5 minutes per plate for reading vs. about 20 seconds per plate for dispensing CTG). To decrease equipment wear and hands-on-time usually batches of plates were filled with CTG and then scanned gradually. Thus, with increasing batch size, there might be a measurable degradation of CTG which results in a reduction of the luminescence signal intensities of plates scanned later. Indeed, a significant alteration of the luminescence signal intensities was seen in the course of the plates with lower signals in the beginning and the end among CLE screens (Figure 27).

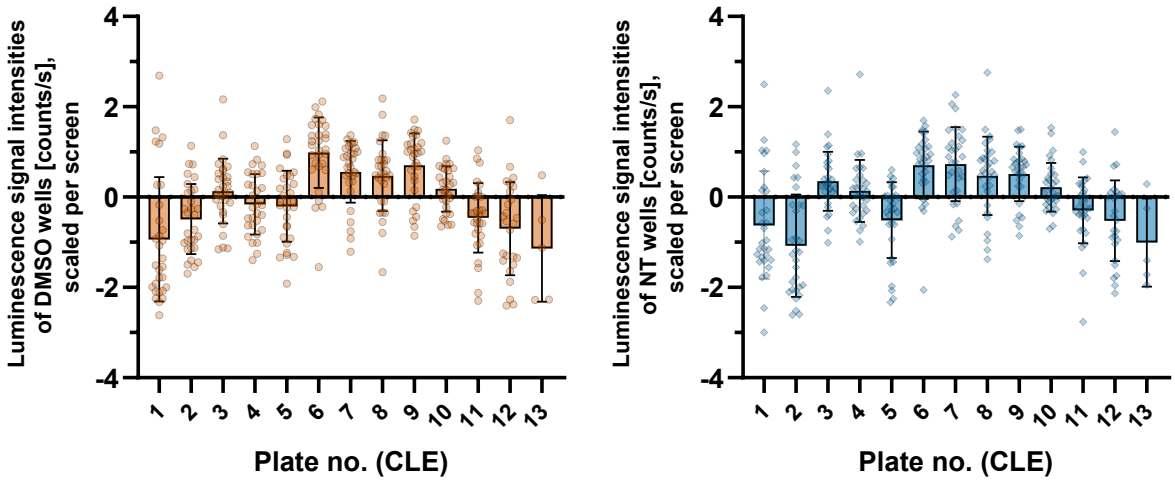

Figure 27. Luminescence signal intensities of DMSO and NT wells, scaled per screen and summarized by plate number. There was significant variation among the plates with lower signal intensities at the beginning and the end and increased signal intensities of the intermediate plates of the screens. P-values < 0.0001 each, according to one-way ANOVA.

Moreover, the variation of absolute luminescence signal intensities of DMSO and NT wells between screens was studied. Notably, the signal intensities varied significantly when screening of each library was conducted on different attempts, but also depending on the library/plate batch. Figure 28 exemplarily shows mean absolute luminescence signal intensities of DMSO and NT wells for BT-12SF, ATRT-310-FHTC and CHLA-04 cells. The screening of BT-12SF cells was conducted in two attempts. First, EG, KI and CLS libraries were screened. At a later time point, screening of the CLE library was conducted, displaying significantly higher luminescence signal intensities. In case of ATRT-310-FHTC cells, all screens were carried out on the same day, but still, the luminescence signal intensities appeared to vary significantly. As

ATRT-310-FHTC was a cell line obtained later, batches of EG and KI libraries had been stored frozen for longer at the time when ATRT-310-FHTC cells were screened. A correlation of plate age and luminescence signal intensities (scaled per cell line) revealed a weak, but significant correlation with a Spearman r of -0.209 among DMSO wells and -0.208 among NT wells (Figure 29). This indicated that older plates tended to deliver slightly lower luminescence signal intensities, potentially explaining the signal alteration observed for ATRT-310-FHTC cells. For CHLA-04 cells, each screen was conducted on a different day. While the earlier screens of the EG and KI libraries showed up to 5.4 (DMSO wells) or 5.8 (NT wells) times higher luminescence signal intensities, the difference among the HHUCL libraries appeared neglectable. However, in any case the deviation between the plates and the corresponding CoVs were stable, as previously described. The maximum fold change was calculated for each cell line which in the mean was 4.4 for DMSO and 4.6 for NT wells. Maximum fold changes were 14.6 in DAOY cells among DMSO wells and 13.8 among NT wells. Taken together, significant variation of the luminescence signal intensities was measured between screens, but not within screens indicating the absence of critical inter-plate effects, which would require adaptions of the workflow.

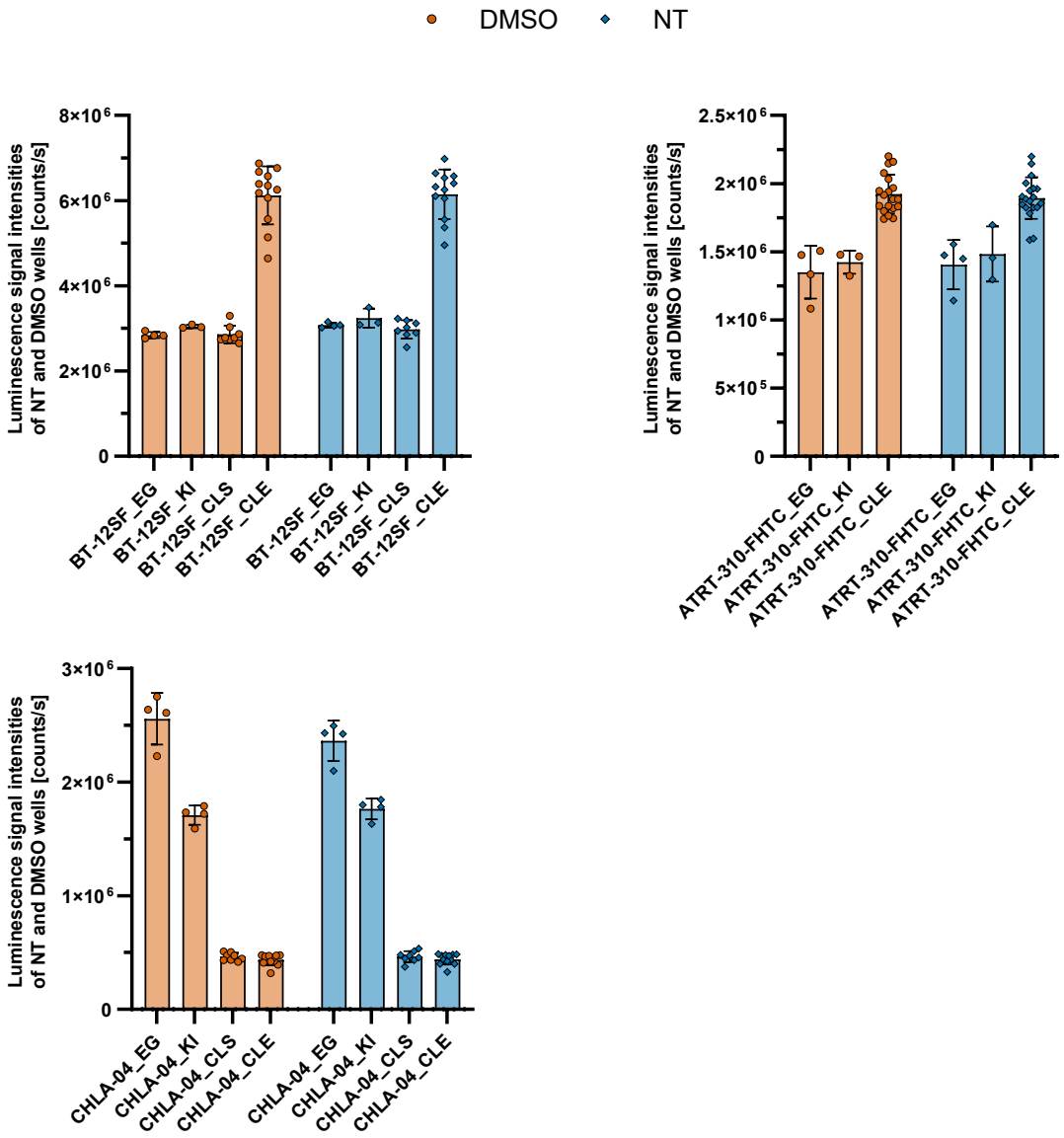

Figure 28. Mean luminescence signal intensities per plate collected per screen. All examples proved to vary significantly (p-value < 0.0001 each, according to one-way ANOVA). Different attempts of screening resulted in higher variation (BT-12SF, CHLA-04). In addition, variations were found between different batches of plates/libraries (ATRT-310-FHTC).

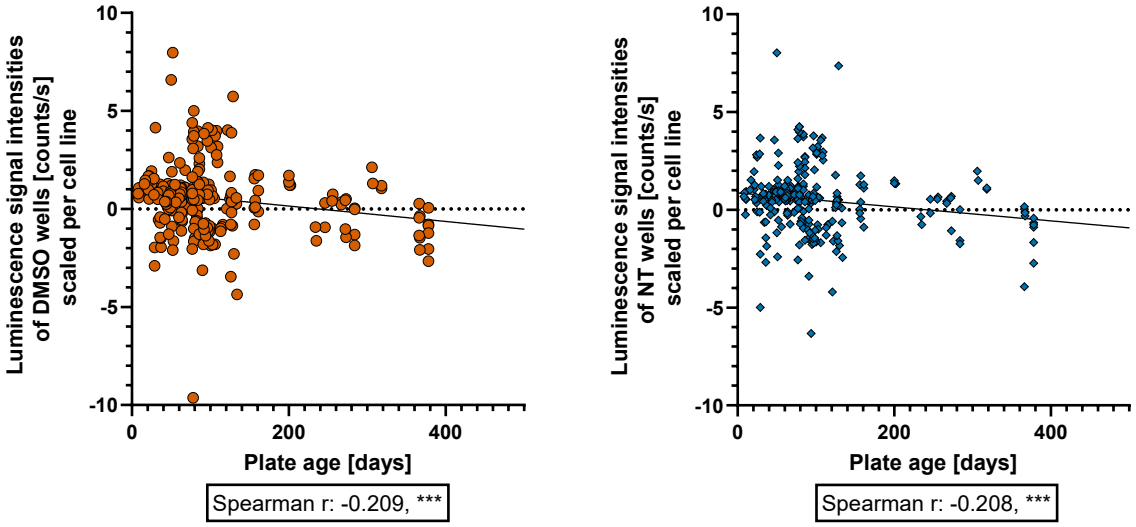

Figure 29. Correlation of luminescence signal intensities (scaled per cell line, y-axis) vs. plate age (x-axis). The data indicated significant correlations with Spearman r values of -0.209 and -0.208, respectively. *** = p-value < 0.001.

3.2.1.3. Intra-plate effects

As an uneven distribution of cells and/or CTG over the plate critically impairs data quality, the generated screening data were evaluated for such events. Due to randomization, means of each plate's rows and columns should nearly be equal, even when drug activity had caused reduced cell viability among certain wells. By calculating the fold changes of each row vs. all other rows and each column vs. all other columns, a sensitive marker for an uneven distribution of luminescence signal intensities was generated. From simulations, fold changes between 0.7-1.3 were expected to be very sensitive, e.g. for clogging, depletion of CTG or insufficient priming with cell suspension. The more frequent the fold change range of 0.7-1.3 was exceeded, the higher the probability for a real adverse event on a plate. Among 927 384-well plates in the own dataset, 246 plates were found to harbor at least one event. Only 48 plates showed three or more events. Among these, 29.2 % affected D425 and 14.6 % affected DAOY, both cell lines that exhibited higher variation in terms of CoVs and relative amplitudes beforehand. Still, manual review for variations of signal distribution of all plates with three events or more did not identify any circumscribed signal losses. Thus, the observed increase in row/column fold changes potentially relied on the increased overall variation, as indicated by increased CoVs and relative amplitudes of DMSO and NT wells among the respective cell lines. 1536-well plates delivered solid results as well staying at fold changes between 0.84 and 1.06 among all rows and columns. Moreover, no repeatedly increased fold changes of a specific plate were detected

indicating printing or randomization issues were absent as well. In summary, no obvious intra-plate effects were observed.

3.2.1.4. Stability of positive controls

As an additional layer of quality control, the stability of the dose-response profiles of the positive controls was analyzed, which were added to each plate, except for very early screens of the EG library. For most screens, variations among the corresponding fAUC values of Staurosporine or NH 125 were not observed (Figure 30). A manual review of few cases with low or absent Staurosporine activity showed that most of these cases were based on fitting issues showing retained activity in the underlying dose-response data. Only two cases, one among BT-12SF screening data, the other among ATRT-310-FHTC screening data, obtained no activity, indicating Staurosporine was absent on these plates, probably due to a handling error during plate preparation. Interestingly, cerebral astrocytes appeared to be entirely resistant vs. Staurosporine. In summary, the data further substantiated the reliability of the drug screening workflow.

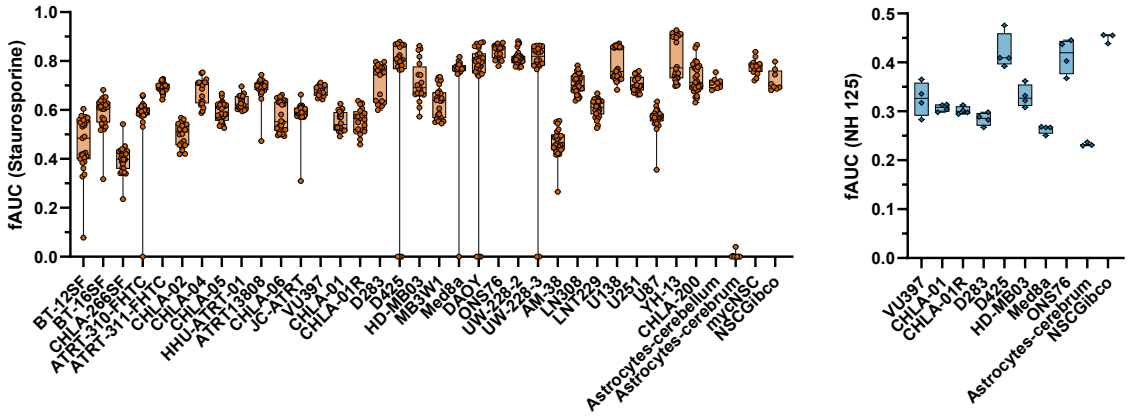

Figure 30. Collected fAUC values from positive controls. For most libraries, Staurosporine was used (left). Some of the EG libraries used NH 125 as positive control instead (right). Few plates exhibited loss or reduced activity of Staurosporine, mostly due to fitting issues. Cerebral astrocytes proved to be Staurosporine-resistant.

3.2.2. Overall drug activity across tumor entities

After a sufficient data quality was assured, the actual evaluation of the drug sensitivity profiles across various brain tumor cell lines was carried out. In total, dose-response data for 735 to 772 drugs in 32 tumor cell lines (13 AT/RT cell lines, 11 medulloblastoma cell lines and 8 glioblastoma cell lines) were generated using six to 11 dilution steps. The variation of the total number of drugs relied on the fact, that not all cell lines had been screened with the same version of the libraries and newer

versions had been updated with additional drugs. First, the distribution of the inhibition was examined using violin plots (Figure 31). This analysis revealed that the AT/RT drug screening data were well distributed with the median at 39.8 % and the third quartile at 74.4 %. While medulloblastoma cell lines appeared more sensitive with the third quartile at 81.1 %, glioblastoma cell lines exhibited a higher overall resistance reaching the third quartile at 64.1 %. Notably, as indicated by the low range of the first quartiles, there was a relevant number of drugs with low activity in all three entities. Thus, using a cut-off of at least 20 % growth inhibition, 40.1 % of the drugs were considered inactive in AT/RTs, with the percentage going down to 31 % when a cut-off of 10 % was used.

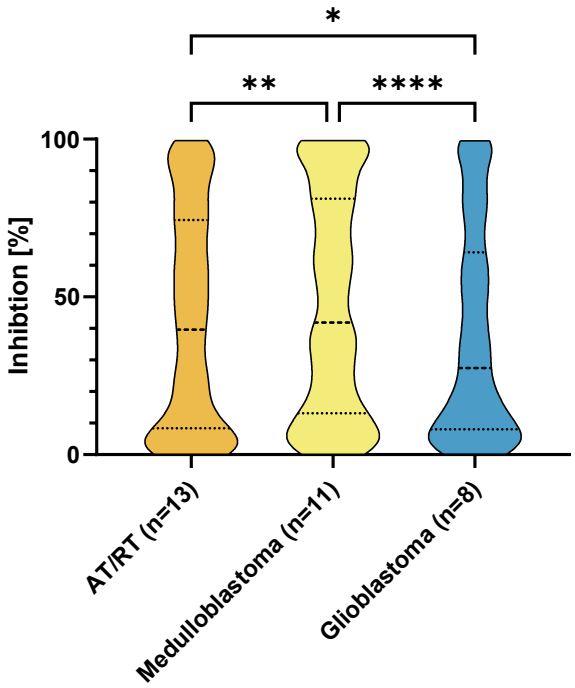

Figure 31. Violin plots of the inhibition, shown as mean values for each drug and collected per tumor entity. A significant variation was observed between the groups. * = p-value < 0.05, ** = p-value < 0.01, **** = p-value < 0.0001, Kruskal-Wallis test with uncorrected Dunn's test for post-hoc comparisons.

Table 9 lists the drugs with identified activity in AT/RT cell lines sorted by mean inhibition of all AT/RT cell lines. Notably, some classes appeared multiple times, like topoisomerase (TP) inhibitors (n=6), heat shock protein 90 (HSP90) inhibitors (n=5), proteasome inhibitors (n=5), MEK (mitogen-activated protein kinase kinase 1) inhibitors (n=4), DNA/RNA synthesis inhibitors (n=3) and microtubule inhibitors (n=3).

Table 9. List of the top 50 drugs in AT/RT cell lines with regards to mean inhibition.

Inhibitor	Class	Inhibition [%]	Inhibitor	Class	Inhibition [%]
Genz-644282	TP	99.53 (99.37 - 99.62)	Lurbinectedin	DNA/RNA S	90.4 (72.76 - 98.98)
YM-155 bromide	IAP	99.37 (98.62 - 99.52)	LY2874455	FGFR	90.36 (53.84 - 99.19)
VLX1570	Others	99.34 (99.07 - 99.66)	GSK2126458	MTOR	90.26 (73.58 - 98.88)
SB 743921 hcl	KSP	99.12 (98.98 - 99.27)	CUDC-907	HDAC	90.04 (0 - 99.03)
Alvespimycin hcl	HSP90	97.87 (87.14 - 99.5)	SN-38	ADC Cytotoxin	89.7 (72.24 - 98.93)
Romidepsin	HDAC	97.47 (88.48 - 99.65)	(S)-10-Hydroxycamptothecin	TP	89.64 (72.02 - 99.37)
Idarubicin hcl	TP	97.24 (84.22 - 99.45)	Exatecan mesylate	TP	88 (70.12 - 98.9)
Daunorubicin hcl	TP	96.29 (80.08 - 99.25)	Topotecan hcl	TP	87.65 (71.37 - 99.37)
BI-847325	ARK	95.9 (61.07 - 99.17)	Homoharringtonine	STAT	87.22 (50.65 - 98.52)
Quisinostat	HDAC	95.62 (90.3 - 98.97)	XL228	ARK	85.96 (68.02 - 99.34)
Delanzomib	Proteasome	95.47 (88.42 - 99.15)	Gemcitabine	NA	83.55 (56.22 - 97.79)
JIB 04	JMJD	95.34 (85.85 - 98.69)	TAK-733	MEK	79.8 (34.31 - 93.18)
Panobinostat	HDAC	94.79 (75.45 - 98.84)	AMG-232	MDM2	79.45 (55.26 - 93.72)
Cinobufotalin	EM	94.78 (88.23 - 99.34)	AZD-8330	MEK	79.24 (28.02 - 93.45)
BMS-214662	FTase	94.46 (83.53 - 99.42)	Actinomycin D	DNA/RNA S	79.18 (47.06 - 99.01)
NVP-AUY922	HSP90	94.4 (80.43 - 98.92)	GDC-0623	MEK	77.32 (38.51 - 92.94)
SJG-136	DNA A/C	93.96 (74.29 - 99.29)	Dinaciclib	CDK	75.17 (24.27 - 98.86)
FK866	Others	93.09 (78.21 - 98.95)	Triptolide	DNA/RNA S	74.55 (41.12 - 99.26)
Oprozomib	Proteasome	92.93 (66.8 - 99.14)	BMS-754807	IGF-1R	73.58 (28.94 - 97.31)
17-AAG	HSP90	92.91 (71.97 - 99.11)	Trametinib	MEK	72.84 (21.94 - 97.55)
Carfilzomib	Proteasome	92.03 (60.02 - 99.09)	Eribulin mesylate	Microtubule	67.57 (37.09 - 88.29)
AT13387	HSP90	91.97 (68.2 - 99.22)	Auristatin PE	Microtubule	64.94 (33.37 - 91.58)
Bortezomib	Proteasome	91.8 (56.64 - 99.37)	Plinabulin	Microtubule	60.83 (36.05 - 86)
MLN9708	Proteasome	91.54 (67.05 - 98.9)	Briciclib	eIF	58.57 (20.46 - 89)
Ganetespib	HSP90	90.58 (72.69 - 98.28)	Pralatrexate	Antifolate	49.72 (0 - 92.91)

(…) = Minimum and maximum values. DNA A/C = DNA Alkylator/Crosslinker. DNA/RNA S = DNA/RNA Synthesis. EM = Endogenous Metabolite. TP = Topoisomerase

3.2.3. Overall drug activity in healthy control models compared to tumor cell lines

In addition to AT/RT, medulloblastoma and glioblastoma tumor cell lines, four different non-neoplastic *in vitro* models were screened that served as controls and indicators of drug toxicity. Among these, there were an immortalized (by transduction of MYC) neural progenitor cell line (mycINP) and neural stem cells (NSC), which were both screened using KI, EG and CLS libraries. Moreover, screening of cerebellar astrocytes was conducted using the KI and CLS libraries and cerebral astrocytes underwent screening using the EG and CLS libraries (EG screen was conducted using an immortalized cell line derived from cerebral astrocytes by means of transduction of the SV40 large T antigen, astrocytes-cerebrum (TAg)). Taken together, each of the three libraries KI, EG and CLS were screened using at least three non-neoplastic *in vitro* models and in case of CLS using four non-neoplastic *in vitro* models. The CLE library was not screened using non-neoplastic *in vitro* models due to the availability of cells. Again, the distribution of the inhibition was analyzed using violin plots (Figure 32). Due to the reduced number of drugs used for screening the non-neoplastic *in vitro* models, results from the tumor cell lines showed minor alterations compared to the previous analysis (Figure 31), which included data from the CLE library. Non-neoplastic *in vitro* models exhibited similarities compared to tumor cell lines regarding the distribution of the quartiles with the first quartile at 12.9 %, indicating that 35.7 % or 21.4 % of the

drugs were regarded as inactive using a cut-off of 20 % or 10 % inhibition, respectively. The median was at 37.7 % and the third quartile at 67 %.

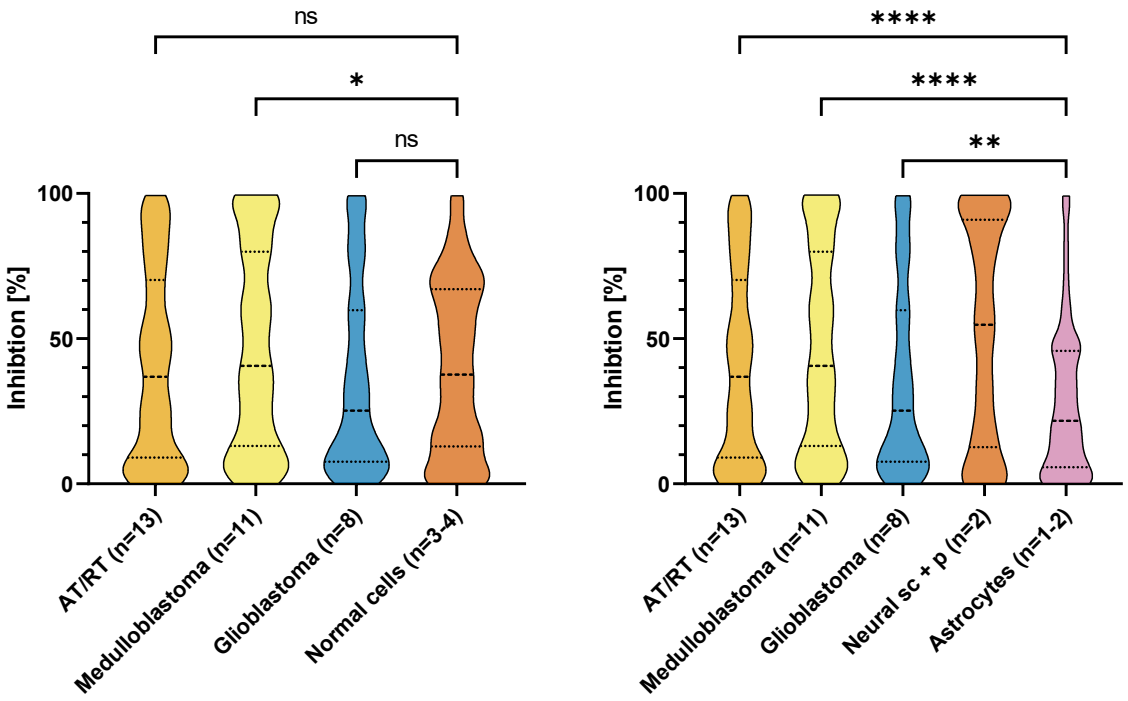

Figure 32. Violin plots of the inhibition, shown as mean values for each drug and collected per entity. If the non-neoplastic *in vitro* models were collected as one group (left), they exhibited a large proportion of drugs with submaximal activity. This group resolved once neural stem cells (sc) and neural progenitors (p) were analyzed separately (right). Astrocytes appeared more resistant, while neural stem cells and progenitors were very sensitive compared to tumor cell lines. * = p-value < 0.05, ** = p-value < 0.01, **** = p-value < 0.0001, Kruskal-Wallis test with uncorrected Dunn's test for post-hoc comparisons. Comparisons of neural stem cells and neural progenitors were also significant (asterisks not shown).

Notably, there was a group of drugs with submaximal activity, which resolved by separating the astrocytic *in vitro* models. While these were more resistant compared to tumor cell lines (third quartile changed from 67 % to 45.8 %), neural stem cells and progenitors exhibited an even increased overall drug sensitivity compared to tumor cell lines (third quartile changed from 67 % to 91 %). Taken together, the data indicated, that all non-neoplastic *in vitro* models that were screened were unsuitable for identifying drugs with selective activity in AT/RT cell lines, as the overall drug sensitivity was either significantly higher (neural stem cells and progenitors) or lower (astrocytes). However, the astrocytic *in vitro* models could be used as indicators of toxicity.

3.2.4. Cross entity analysis of dose-response data of AT/RT cell lines

To derive AT/RT-selective inhibitors, drug profiles derived from AT/RT cell lines were compared to a cohort of medulloblastoma cell lines (n=11) and glioblastoma cell lines (n=8). Drugs were excluded when they did not exceed an fAUC of 0.1 in any AT/RT cell line, reducing the number of drugs from 768 to 482 (62.8 %). A Mann-Whitney U (MWU) test was performed to generate a volcano plot, which showed numerous drugs with significantly increased activity in AT/RT cell lines compared to medulloblastoma and glioblastoma cell lines. Drug classes yielding three or more hits were highlighted, indicating a large active proportion among MEK inhibitors, fibroblast growth factor receptor (FGFR) inhibitors, HSP90 inhibitors, rapidly accelerated fibrosarcoma (RAF) inhibitors and Mouse double minute 2 homolog (MDM2) inhibitors (Figure 33).

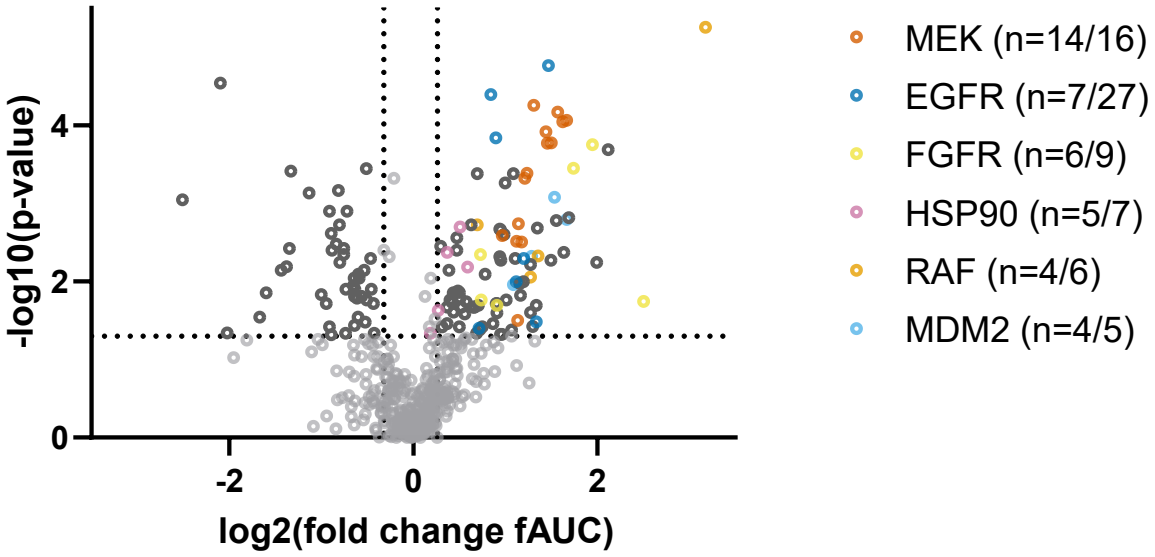

Figure 33. Volcano plot derived from the comparison of AT/RT cell lines with a pooled cohort of medulloblastoma and glioblastoma cell lines (MWU test). Multiple MEK, MDM2, RAF, EGFR, FGFR and HSP90 inhibitors were found to be enriched.

Evaluation of the selectively active drugs (Table 10) showed that MLN2480, a RAF inhibitor, was the top hit with a fold change of 9.04, but low inhibition and high IC50 values, alluding to low overall activity, as indicated by a mean fAUC of 0.15 and the dose-response curve depicted in Figure 34. Although at least few of the other RAF inhibitors yielded higher overall activity, they also achieved lower fold changes. The next six drugs according to fold change, TG100-801, ZM 306416 hydrochloride, GSK126, CH5183284, E-3810 and CX-5461, all showed a similar pattern and even lower fAUC values than MLN2480, which underlined that filtering for an fAUC of 0.1 in

any AT/RT cell line may be regarded as a very sensitive approach and that integrative review of all parameters was obligate. However, especially CH5183284, which is an FGFR inhibitor, and CX-5461, which is a specific ribosomal RNA (rRNA) synthesis inhibitor, in contrast to the other four drugs, showed a quite flat, almost linear, dose-response curve with an onset of effect at low micromolar range (Figure 34). This indicated that their effect might still be relevant for further evaluation under the perspective of a longer treatment schedule at low dosage. Moreover, the specific effect of inhibition of rRNA synthesis might even be of interest in terms of AT/RT biology. Thus, when data were filtered for higher fAUC values, both, especially CX-5461, would probably have been overlooked. Nevertheless, drugs with higher activity which still acquire a decent fold change deserved higher attention, like GDC-0623 (fold change 3.18), a MEK inhibitor, and RG7388 (fold change 3.17), an MDM2 inhibitor, whose dose-response curves are displayed in Figure 34 as well. While for MEK inhibition, the difference between AT/RT vs. medulloblastoma cell lines (the latter even exhibited discrete growth acceleratory effects) was larger than the difference of AT/RT vs. glioblastoma cell lines, MDM2 inhibition showed the opposite. MEK inhibitors appeared to be significantly enriched even when AT/RT cell lines were compared to medulloblastoma or glioblastoma cell lines separately. MDM2 inhibitors on the other hand yielded a significant difference vs. glioblastoma cell lines, but, in most cases, lacked a significant difference vs. medulloblastoma cell lines, i.e., out of all MDM2 inhibitors, only AMG-232 achieved a significant p-value of 0.043 when comparing AT/RT cell lines vs. medulloblastoma cell lines. Among the class of EGFR inhibitors (6/27 inhibitors enriched in AT/RT), Poziotinib showed the highest fold change (2.77) and a medium overall activity with a mean fAUC of 0.31. Its dose-response curve is depicted in Figure 34. Moreover, Salinomycin, an ionophore antibiotic drug which also comprises inhibitory effects on WNT signaling, was discovered to be significantly more active in AT/RT cell lines with a fold change of 2.24 and an early onset of effect at around 100 nM concentration. However, other WNT inhibitors were not enriched and WNT activation appears only as an established feature of the AT/RT-TYR subgroup, for which no models were included in this study according to DNA methylation profiling-based classification. Thus, the selective activity of Salinomycin is probably rather based on off-target effects. Like Salinomycin, also Endoxifen (an active form of the estrogen receptor modulator Tamoxifen), BEZ235 (an MTOR inhibitor), LB-100 (a phosphatase inhibitor), AZD-8186 (a PI3 kinase (PI3K) inhibitor), Ruboxistaurin hydrochloride (a protein kinase c (PKC) inhibitor), Fenretinide (a RAR/RXR inhibitor),

Voreloxin hydrochloride (a TP inhibitor) and Verteporfin (a YAP inhibitor) showed up as drugs with a significantly increased activity in AT/RT cell lines compared to medulloblastoma and glioblastoma cell lines, which were only represented once, either because there were no other drugs from the same class in the used libraries, or because other drugs from the same class were not enriched in AT/RTs.

Table 10. Descriptive parameters of drugs with significantly enriched activity in AT/RT cell lines vs. medulloblastoma and glioblastoma cell lines, sorted for fold change. P-value based on an MWU test. Higher fAUC values indicate higher activity.

Inhibitor	Class	Fold change	fAUC	IC50 [nM]	Inhibition [%]	P-value
MLN2480	RAF	9.04	0.15 (0.06 - 0.29)	4272 (1136 - 7067)	73.04 (44.58 - 95.42)	0.00001
TG100-801	FGFR	5.67	0.13 (0 - 0.35)	10150 (1 - 25000)	66.5 (0 - 99.09)	0.018
ZM 306416 hcl	VEGFR	4.33	0.07 (0.01 - 0.14)	4144 (1421 - 13988)	29.38 (3.84 - 53.78)	0.0002
GSK126	HMT	3.98	0.04 (0 - 0.1)	12103 (108 - 23267)	57.58 (0 - 97.93)	0.006
CH5183284	FGFR	3.85	0.22 (0.06 - 0.47)	1716 (192 - 8176)	62.47 (27.77 - 96.65)	0.0002
E-3810	FGFR	3.34	0.13 (0.04 - 0.29)	2370 (451 - 4545)	49.32 (17.13 - 92.64)	0.0004
CX-5461	DNA/RNA S	3.23	0.16 (0 - 0.33)	3199 (123 - 25000)	47.53 (5.46 - 98.96)	0.002
GDC-0623	MEK	3.18	0.45 (0.11 - 0.67)	243 (7 - 2369)	77.32 (38.51 - 92.94)	0.0001
RG7388	MDM2	3.17	0.41 (0.23 - 0.57)	82 (23 - 174)	71.02 (42.91 - 92.51)	0.002
BMS-708163	Notch	3.10	0.09 (0 - 0.22)	2846 (2 - 20536)	21.73 (5.96 - 46.75)	0.004
AS703026	MEK	3.08	0.33 (0.15 - 0.58)	578 (2 - 1584)	75.23 (15.61 - 90.59)	0.0001
Ro 5126766	MEK	2.96	0.26 (0.1 - 0.51)	512 (34 - 3477)	55.62 (34.4 - 83.43)	0.0001
Ro 08-2750	TRK	2.93	0.14 (0.01 - 0.24)	7283 (17 - 23022)	90.15 (4.35 - 99.22)	0.002
AMG-232	MDM2	2.90	0.43 (0.26 - 0.57)	101 (46 - 290)	79.45 (55.26 - 93.72)	0.001
TAK-733	MEK	2.83	0.43 (0.09 - 0.67)	319 (8 - 2580)	79.8 (34.31 - 93.18)	0.0002
MK-0752	Notch	2.82	0.04 (0 - 0.1)	3330 (9 - 25000)	11.71 (0 - 28.2)	0.005
Poziotinib	EGFR	2.77	0.31 (0.19 - 0.52)	1613 (64 - 3331)	89.3 (67.13 - 98.78)	0.00002
Refametinib	MEK	2.74	0.34 (0.09 - 0.56)	708 (36 - 5382)	75.67 (50.06 - 92.76)	0.0002
PD0325901	MEK	2.71	0.35 (0.08 - 0.59)	573 (15 - 2816)	77.31 (33.69 - 93.98)	0.0001
LGX818	RAF	2.56	0.08 (0 - 0.26)	1347 (2 - 3233)	28.38 (0 - 73.42)	0.005
GDC-0994	ERK	2.54	0.12 (0.01 - 0.31)	4401 (306 - 8712)	55.29 (10.78 - 94.2)	0.002
AZD-3759	EGFR	2.52	0.08 (0 - 0.2)	3386 (363 - 25000)	25.04 (0.3 - 53.61)	0.033
Bleomycin sulfate	DNA/RNA S	2.52	0.14 (0.01 - 0.34)	2489 (275 - 9736)	44.5 (9.86 - 89.92)	0.020
Trametinib	MEK	2.48	0.43 (0.08 - 0.78)	133 (4 - 670)	72.84 (21.94 - 97.55)	0.0001
LY3039478	Notch	2.46	0.07 (0 - 0.18)	2108 (5 - 25000)	9.34 (0 - 23.11)	0.038
MI-773	MDM2	2.44	0.32 (0.19 - 0.43)	883 (290 - 1990)	84.07 (59.92 - 95.52)	0.005
R788 d h	SYK	2.42	0.14 (0.01 - 0.3)	5075 (12 - 16131)	62.78 (5.94 - 98.23)	0.006
Dabrafenib mesylate	RAF	2.42	0.07 (0 - 0.21)	1668 (11 - 7552)	21.52 (0 - 69.74)	0.009
Tirapazamine	Others	2.42	0.05 (0 - 0.12)	6814 (663 - 19620)	28.38 (1.22 - 67.77)	0.025
Ro 4987655	MEK	2.35	0.35 (0.09 - 0.56)	304 (19 - 625)	74.36 (24.99 - 91.41)	0.0004
AZD-8330	MEK	2.32	0.47 (0.1 - 0.72)	89 (5 - 355)	79.24 (28.02 - 93.45)	0.0005
BMS-599626 hcl	EGFR	2.30	0.08 (0.01 - 0.15)	7383 (1304 - 22915)	51.31 (32.35 - 85.36)	0.005
Pazopanib hcl	CSF1R	2.29	0.09 (0.02 - 0.22)	3836 (1657 - 7980)	43.72 (10.18 - 82.99)	0.010
MEK162	MEK	2.26	0.2 (0.03 - 0.5)	1697 (59 - 4714)	57.42 (13.1 - 88.42)	0.003
Salinomycin	WNT	2.24	0.36 (0 - 0.57)	2282 (56 - 23044)	82.61 (0 - 98.85)	0.015
ABT-199	BCL2	2.23	0.1 (0.02 - 0.25)	5123 (963 - 13706)	49.95 (11.04 - 92.11)	0.011
U0126	MEK	2.21	0.06 (0.01 - 0.14)	5502 (921 - 14001)	32.12 (8.72 - 71.09)	0.002
CI-1040	MEK	2.20	0.19 (0 - 0.39)	3370 (20 - 25000)	56.96 (0 - 95.88)	0.032
Selumetinib	MEK	2.18	0.16 (0.03 - 0.43)	1698 (134 - 4374)	45.4 (16.1 - 80.13)	0.003
BMS-690514	EGFR	2.17	0.18 (0.01 - 0.4)	4050 (58 - 20810)	58.57 (29.1 - 88.43)	0.010
Ruboxistaurin hcl	PKC	2.16	0.39 (0.24 - 0.56)	152 (48 - 400)	76.4 (47.47 - 96.65)	0.005
RG7112	MDM2	2.12	0.25 (0.15 - 0.36)	2468 (826 - 4402)	92.68 (75.49 - 99.11)	0.011
LB-100	Phosphatase	2.12	0.27 (0.15 - 0.36)	1780 (110 - 3768)	88.15 (54.29 - 98.73)	0.0004
Luteolin	EM	2.09	0.05 (0 - 0.1)	12652 (5510 - 23807)	50.1 (7.08 - 83.95)	0.042
Xanthohumol	EM	2.01	0.13 (0 - 0.33)	7224 (883 - 23221)	73.59 (29.62 - 98.46)	0.017
Nedaplatin	DNA/RNA S	2.00	0.41 (0.28 - 0.54)	499 (124 - 1020)	98.72 (98.24 - 98.86)	0.001
Endoxifen (E-isomer)	ER	1.98	0.12 (0.08 - 0.19)	7304 (3259 - 11267)	93.18 (74.4 - 99.29)	0.003
Cobimetinib	MEK	1.95	0.3 (0.12 - 0.53)	1832 (65 - 8447)	86.6 (63.54 - 99.45)	0.003
CH5424802	ALK	1.95	0.07 (0 - 0.18)	8195 (30 - 25000)	39.75 (16.76 - 76.47)	0.047
PCI-32765	BTK	1.93	0.11 (0 - 0.18)	5209 (755 - 9947)	58.07 (0 - 85.17)	0.005
RGFP966	HDAC	1.93	0.13 (0.05 - 0.26)	3188 (272 - 5042)	56.98 (10.33 - 93.88)	0.002
KU-57788	CRISPR/Cas9	1.93	0.1 (0.05 - 0.21)	3937 (902 - 6727)	46.71 (25.82 - 78.75)	0.047
5-Azacytidine	NA	1.92	0.17 (0.08 - 0.29)	4359 (1484 - 7870)	86.35 (67.18 - 97.48)	0.002
Fenretinide	RAR/RXR	1.92	0.23 (0 - 0.33)	4335 (852 - 25000)	98.91 (96.96 - 99.41)	0.005
Voreloxin hcl	TP	1.88	0.18 (0.08 - 0.37)	1465 (31 - 3230)	50.92 (26.14 - 77.01)	0.019
CC-401 hcl	JNK	1.88	0.06 (0 - 0.12)	7824 (273 - 21552)	46.14 (14.36 - 71.24)	0.025
AZD-4547	FGFR	1.88	0.28 (0.03 - 0.61)	2103 (38 - 6266)	74.84 (16.26 - 99.33)	0.020
Navitoclax	BCL2	1.87	0.34 (0.07 - 0.66)	2565 (29 - 8820)	91.95 (48.54 - 99.17)	0.019

Inhibitor	Class	Fold change	fAUC	IC50 [nM]	Inhibition [%]	P-value
CO-1686	EGFR	1.86	0.25 (0.19 - 0.33)	2146 (837 - 3752)	95.03 (82.92 - 99.1)	0.0001
Purvalanol A	CDK	1.82	0.09 (0 - 0.16)	7346 (843 - 24864)	61.39 (0 - 96.8)	0.035
AZ5104	EGFR	1.79	0.36 (0.23 - 0.48)	1042 (177 - 3138)	98.23 (93.54 - 99.33)	0.00004
Verteporfin	YAP	1.72	0.16 (0.12 - 0.2)	5477 (3299 - 8362)	95.66 (88.3 - 99.24)	0.008
(-)-Terreic acid	BTK	1.68	0.12 (0.05 - 0.22)	7606 (2760 - 14072)	84.55 (43.92 - 98.75)	0.038
LY2784544	FGFR	1.67	0.18 (0.11 - 0.32)	2634 (1028 - 5597)	71.19 (36.91 - 98.91)	0.017
LY2874455	FGFR	1.66	0.54 (0.32 - 0.86)	244 (4 - 967)	90.36 (53.84 - 99.19)	0.005
Aprepitant	Others	1.65	0.08 (0.01 - 0.13)	8050 (5349 - 21354)	65.54 (46.53 - 91.38)	0.041
Gefitinib	EGFR	1.64	0.09 (0 - 0.17)	6902 (1373 - 25000)	46.55 (16.24 - 69.2)	0.040
ZM 323881 hcl	VEGFR	1.63	0.06 (0 - 0.14)	7700 (1033 - 23539)	43.9 (0 - 80.79)	0.020
LY3009120	RAF	1.62	0.3 (0.1 - 0.51)	463 (58 - 1319)	69.91 (25.62 - 91.81)	0.002
GSK1059615	MTOR	1.62	0.24 (0.18 - 0.37)	2396 (685 - 3889)	91.78 (73.26 - 98.01)	0.0004
TAK-632	ARK	1.61	0.21 (0.1 - 0.41)	1673 (304 - 3666)	70.73 (47.08 - 96.89)	0.046
C 646	HAT	1.58	0.08 (0.02 - 0.2)	9521 (2737 - 15887)	70.52 (16.22 - 97.88)	0.021
PND-1186	FAK	1.58	0.2 (0.09 - 0.3)	1827 (677 - 4369)	68.54 (27.15 - 92.66)	0.021
BMS-754807	IGF-1R	1.56	0.42 (0.17 - 0.66)	122 (10 - 332)	73.58 (28.94 - 97.31)	0.021
AVL-292	BTK	1.54	0.21 (0.13 - 0.3)	2970 (1105 - 7337)	88.76 (66.67 - 99.37)	0.002
17-AAG	HSP90	1.51	0.52 (0.23 - 0.7)	289 (16 - 2256)	92.91 (71.97 - 99.11)	0.007
CX-4945	Others	1.49	0.15 (0.1 - 0.22)	3970 (2648 - 5076)	75.34 (56.18 - 90.61)	0.018
Toceranib phosphate	KIT	1.47	0.1 (0 - 0.17)	8455 (4589 - 23579)	78.88 (34.89 - 99.07)	0.026
Entrectinib	ALK	1.44	0.17 (0.1 - 0.26)	5167 (2001 - 9596)	96.51 (81.5 - 99.02)	0.021
BIIB021	HSP90	1.42	0.4 (0.24 - 0.54)	380 (98 - 837)	91.91 (69.29 - 99.23)	0.002
BEZ235	MTOR	1.42	0.26 (0 - 0.39)	2278 (45 - 25000)	59.93 (39.04 - 83.96)	0.016
Ellipticine hcl	TP	1.41	0.22 (0.16 - 0.34)	3355 (1016 - 5654)	98.68 (96.67 - 99.15)	0.014
Dovitinib	KIT	1.41	0.21 (0.1 - 0.36)	2758 (645 - 5490)	81.11 (47.55 - 99.5)	0.038
Tamoxifen	ER	1.40	0.09 (0.01 - 0.14)	10962 (5910 - 23071)	95.37 (84.33 - 98.93)	0.013
CGK 733	ATM/ATR	1.39	0.19 (0.14 - 0.24)	3943 (2349 - 6408)	97.9 (92.7 - 99.2)	0.004
ZSTK474	PI3K	1.39	0.27 (0.19 - 0.36)	418 (244 - 665)	64.18 (52.42 - 80.97)	0.003
JIB 04	JMJD	1.37	0.43 (0.19 - 0.61)	664 (42 - 3827)	95.34 (85.85 - 98.69)	0.014
Ryuvidine	CDK	1.36	0.2 (0.12 - 0.36)	4363 (713 - 6688)	94.36 (81.67 - 99.06)	0.025
PKC412	PKC	1.35	0.28 (0.16 - 0.42)	581 (32 - 1019)	70.34 (40.02 - 96.19)	0.014
Bendamustine hcl	DNA A/C	1.34	0.05 (0 - 0.13)	5980 (1 - 13473)	31.66 (0 - 65.44)	0.019
BI-847325	ARK	1.32	0.48 (0.29 - 0.62)	270 (23 - 1280)	95.9 (61.07 - 99.17)	0.017
Brivanib	VEGFR	1.31	0.05 (0.02 - 0.14)	6918 (2 - 9965)	37.16 (2.27 - 88.81)	0.007
AZD-8186	PI3K	1.29	0.24 (0.12 - 0.36)	1962 (440 - 4099)	80.25 (50.18 - 95.91)	0.021
Alvespimycin hcl	HSP90	1.29	0.69 (0.34 - 0.85)	46 (3 - 334)	97.87 (87.14 - 99.5)	0.004
Genz-644282	TP	1.29	0.65 (0.5 - 0.8)	29 (4 - 89)	99.53 (99.37 - 99.62)	0.035
Toremifene citrate	ER	1.24	0.09 (0.01 - 0.14)	9198 (6230 - 21397)	77.33 (46.39 - 98.75)	0.038
IMD 0354	IKK	1.23	0.33 (0.27 - 0.41)	868 (401 - 1623)	97.52 (90.79 - 99.44)	0.004
Ganetespib	HSP90	1.21	0.62 (0.41 - 0.74)	37 (13 - 187)	90.58 (72.69 - 98.28)	0.024
Cinobufotalin	EM	1.18	0.52 (0.39 - 0.66)	108 (25 - 223)	94.78 (88.23 - 99.34)	0.030
BMS-214662	FTase	1.14	0.45 (0 - 0.56)	2062 (65 - 25000)	94.46 (83.53 - 99.42)	0.009
Debio 0932	HSP90	1.14	0.36 (0.26 - 0.42)	579 (347 - 963)	94.08 (71.3 - 98.59)	0.046
CH5132799	PI3K	1.13	0.24 (0.18 - 0.34)	961 (393 - 1423)	70.48 (54.96 - 89.9)	0.038

(…) = Minimum and maximum values. DNA A/C = DNA Alkylator/Crosslinker. DNA/RNA S = DNA/RNA Synthesis. EM = Endogenous Metabolite. TP = Topoisomerase

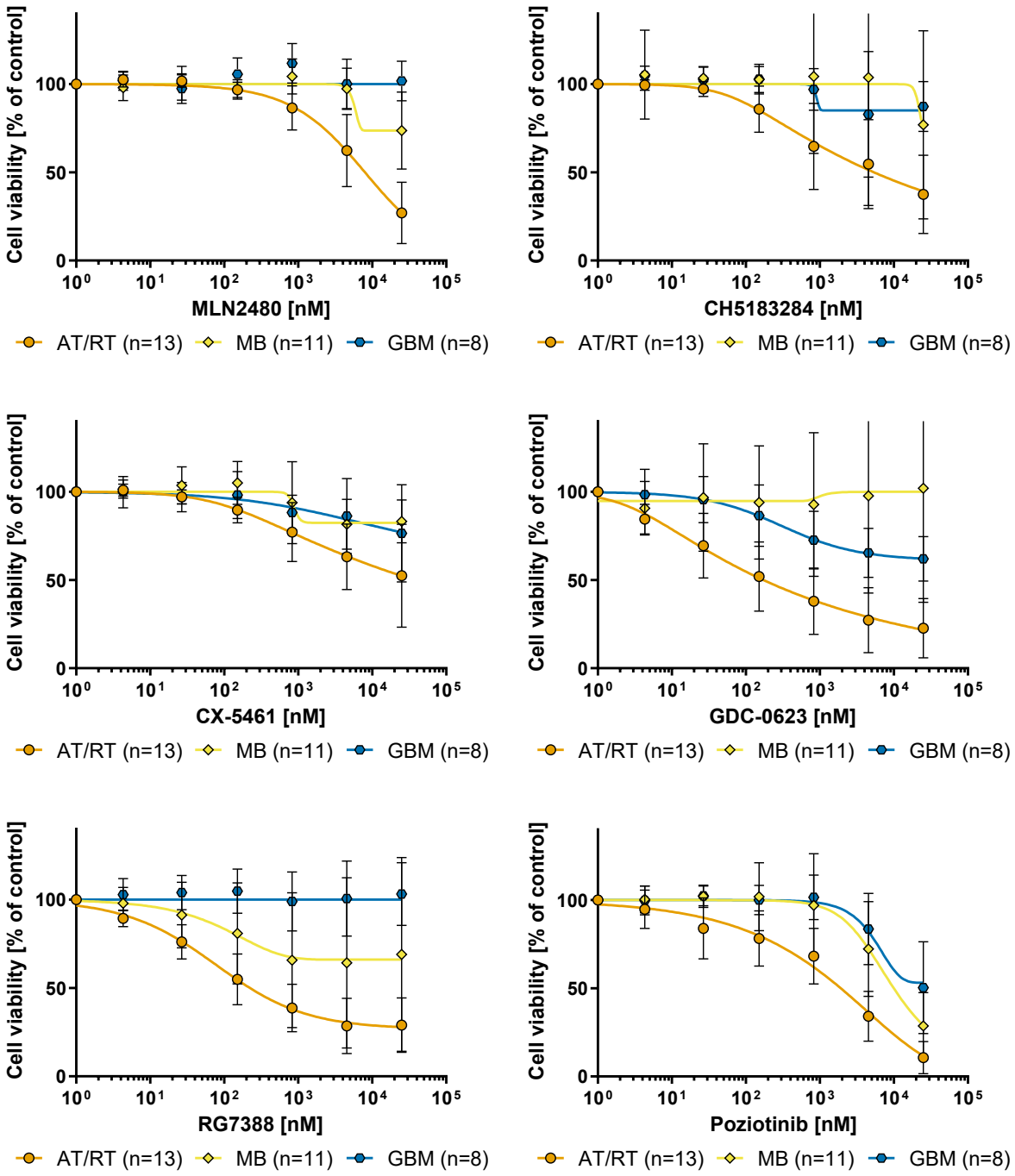

Figure 34. Selected dose-response curves comparing AT/RT cell lines vs. medulloblastoma and glioblastoma cell lines. MLN2480 = RAF inhibitor. CH5183284 = FGFR inhibitor. CX-5461 = ribosomal RNA synthesis inhibitor. GDC-0623 = MEK inhibitor. RG7388 = MDM2 inhibitor. Poziotinib = EGFR inhibitor.

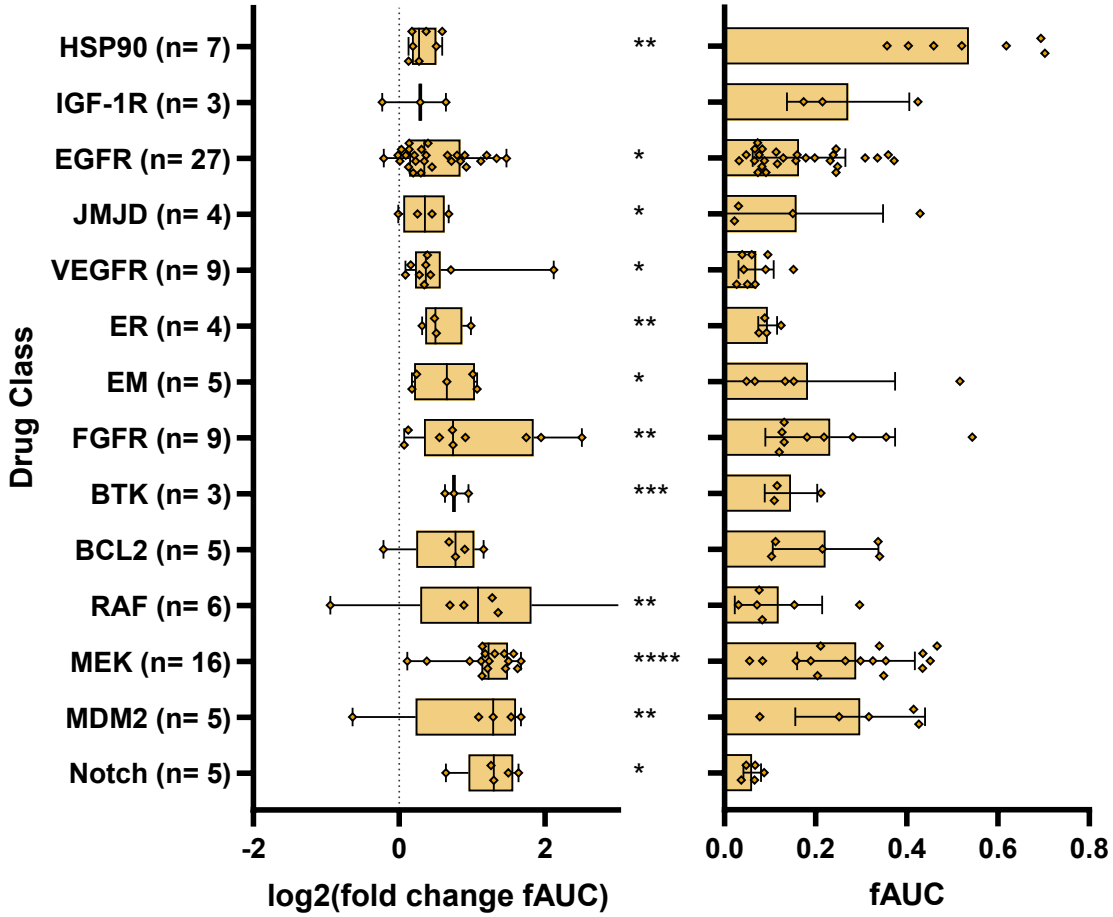

Figure 35. DCEA of AT/RT cell lines vs. medulloblastoma and glioblastoma cell lines depicted as fold change per inhibitor (left) along with mean fAUC values in AT/RT cell lines (right). Drug classes consisting of at least four drugs and showing a fold change of 1.1 or larger are displayed. * = p-value < 0.05, ** = p-value < 0.01, *** = p-value < 0.001, **** = p-value < 0.0001, MWU test. EM = Endogenous Metabolite. ER = Estrogen Receptor.

A class-wise analysis, including all drug classes which consisted of at least four drugs achieving a fold change of 1.1 or larger, confirmed MDM2 and MEK inhibitors as the top candidates showing the highest group-wise enrichment in AT/RT cell lines compared to medulloblastoma and glioblastoma cell lines (Figure 35), disregarding Notch inhibition. Notch inhibitors underwent further evaluation among subgroup-stratified analyses, as their selective activity appeared to rely on affiliation to the AT/RT-SHH subgroup. The partial response pattern of Notch inhibitors became evident when repeating the group-wise analysis using fAUC fold changes calculated per cell line (Figure 36) instead of per inhibitor, like before (Figure 35). Notch inhibitors showed a widespread activity with only 8/13 cell lines achieving a fold change of 1.2 or higher, whereas MEK and MDM2 inhibitors yielded a homogeneous response with an increased fold change in (almost) all AT/RT cell lines. Only ATRT-310-FHTC seemed to be mostly resistant against MEK inhibitors. The partial response pattern observed

among Notch inhibitors appeared to apply to even more classes, especially B-cell lymphoma 2 (BCL2) inhibitors, which were identified among subgroup-stratified analyses as well.

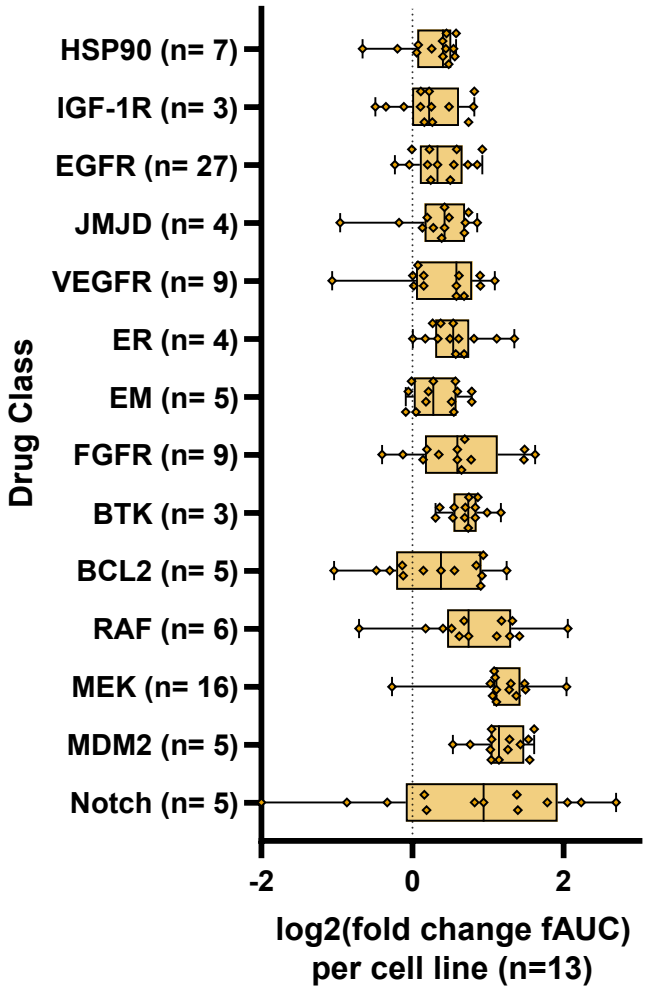

Class	Cell lines with fold change > 1.2
Notch	8/13
MDM2	13/13
MEK	12/13
RAF	11/13
BCL2	7/13
BTK	13/13
FGFR	9/13
EM	7/13
ER	11/13
VEGFR	7/13
JMJD	9/13
EGFR	7/13
IGF-1R	4/13
HSP90	8/13

Figure 36. DCEA of AT/RT cell lines vs. medulloblastoma and glioblastoma cell lines depicted as fold change per cell line (left). Drug classes consisting of at least four drugs and showing a fold change of 1.1 or larger are displayed. The table on the right gives the number of cell lines per class that exceeded a fold change of 1.2, thereby highlighting heterogenous responses in AT/RT cell lines for some drug classes. EM = Endogenous Metabolite. ER = Estrogen Receptor.

RAF inhibitors yielded a significant enrichment in AT/RT, but, as indicated above, their fold change was highly variable and additionally their activity appeared to vary among AT/RT cell lines as well. The pattern of distribution indicated a certain RAF-sensitive cohort. To elucidate whether RAF inhibitors exhibited a cell line-specific activity, an unsupervised hierarchical clustering (HCL) analysis was performed (Figure 37). The clustering showed that ATRT13808 comprised an increased sensitivity vs. most RAF inhibitors, including pan-RAF as well as V600E-specific RAF inhibitors, a finding indicative of a RAF mutation. However, ATRT13808 appeared to be resistant vs.

Vemurafenib, one of the BRAF V600E-specific RAF inhibitors. Upon exclusion of Vemurafenib the effect was significant (Figure 37). Furthermore, limited activity of some RAF inhibitors was observed in CHLA-04 and JC-ATRT cells.

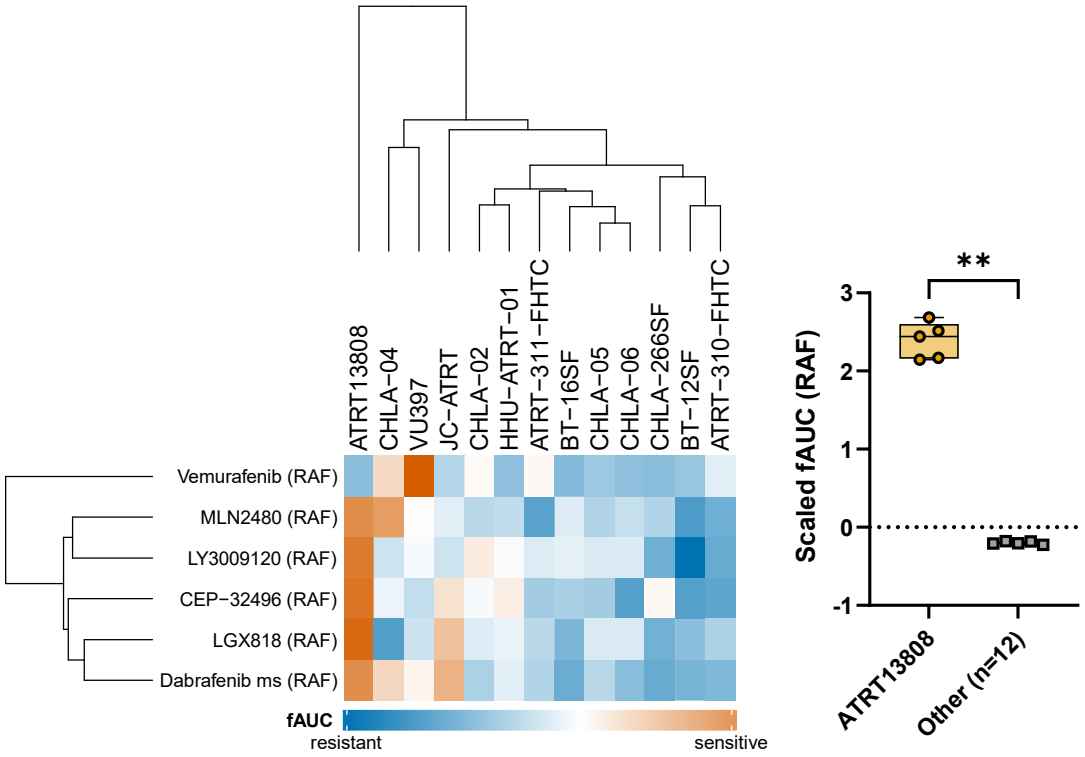

Figure 37. Unsupervised hierarchical clustering (HCL) analysis of RAF inhibitors in AT/RT cell lines after scaling per inhibitor (left, Manhattan distance, average linkage). Most RAF inhibitors showed a selective activity in ATRT13808. The strong signal for Vemurafenib in VU397 relied on low overall activity of Vemurafenib and hence did not indicate a selective effect. The selective activity of RAF inhibitors in ATRT13808 was significant when Vemurafenib was excluded. (right, ** = p-value < 0.01, MWU test on scaled fAUC data). ms = mesylate.

Additional unsupervised hierarchical clustering analyses were performed for EGFR (Figure 38), FGFR (Figure 39) and VEGFR (Figure 40) inhibitors, revealing a significantly increased activity of EGFR inhibitors in BT-16SF, CHLA-266SF and VU397 cells, and a significantly increased activity of FGFR inhibitors in CHLA-04, HHU-ATRT-01 and ATRT13808 cells. None of the cell lines showed a significant enrichment for VEGFR inhibitors.

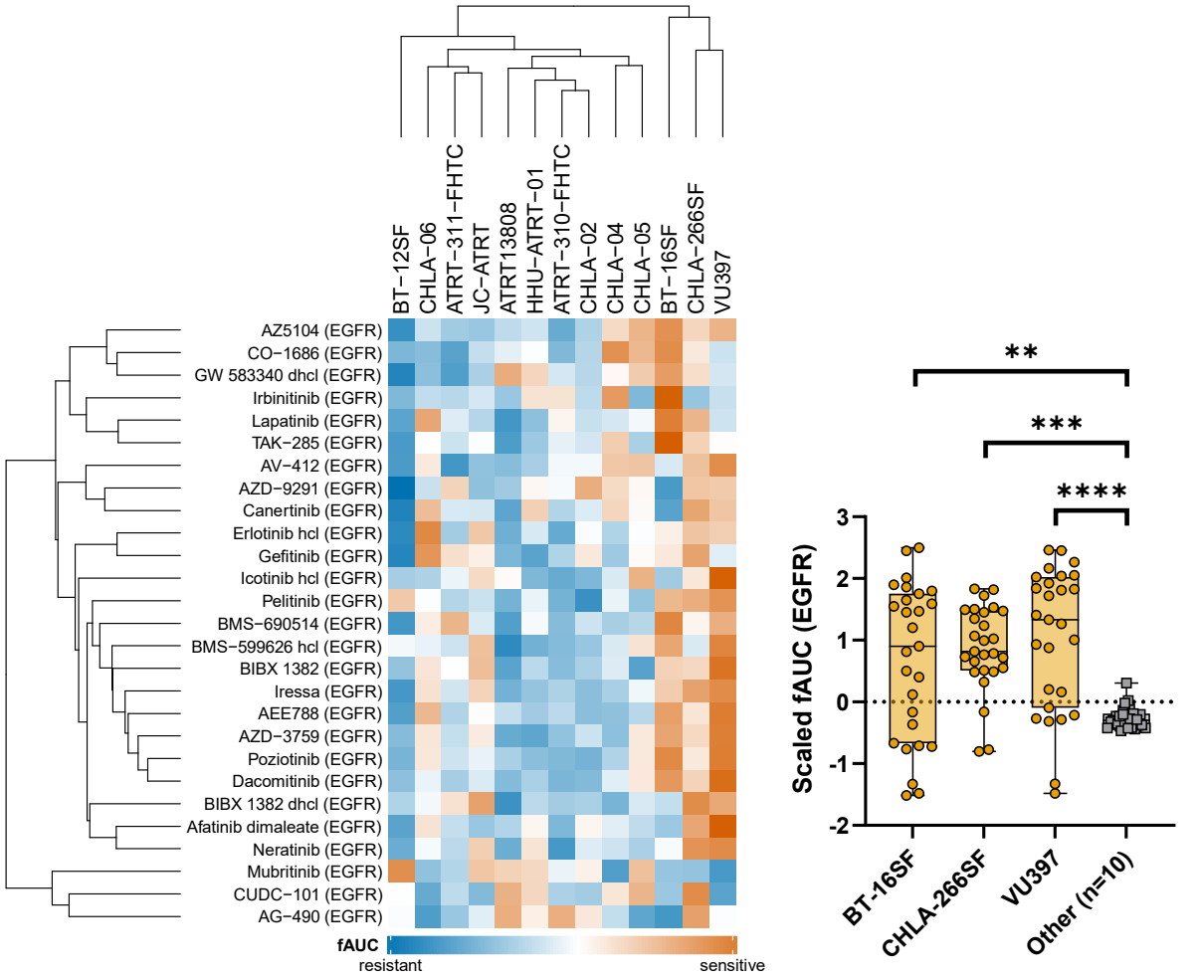

Figure 38. Unsupervised HCL analysis of EGFR drug screening data in AT/RT cell lines (left, Manhattan distance, average linkage). BT-16SF, CHLA-266SF and VU397 cells exhibited an increased sensitivity for EGFR inhibitors (right, Kruskal-Wallis test with uncorrected Dunn's test for post-hoc comparisons). hcl = hydrochloride. dhcl = dihydrochloride.

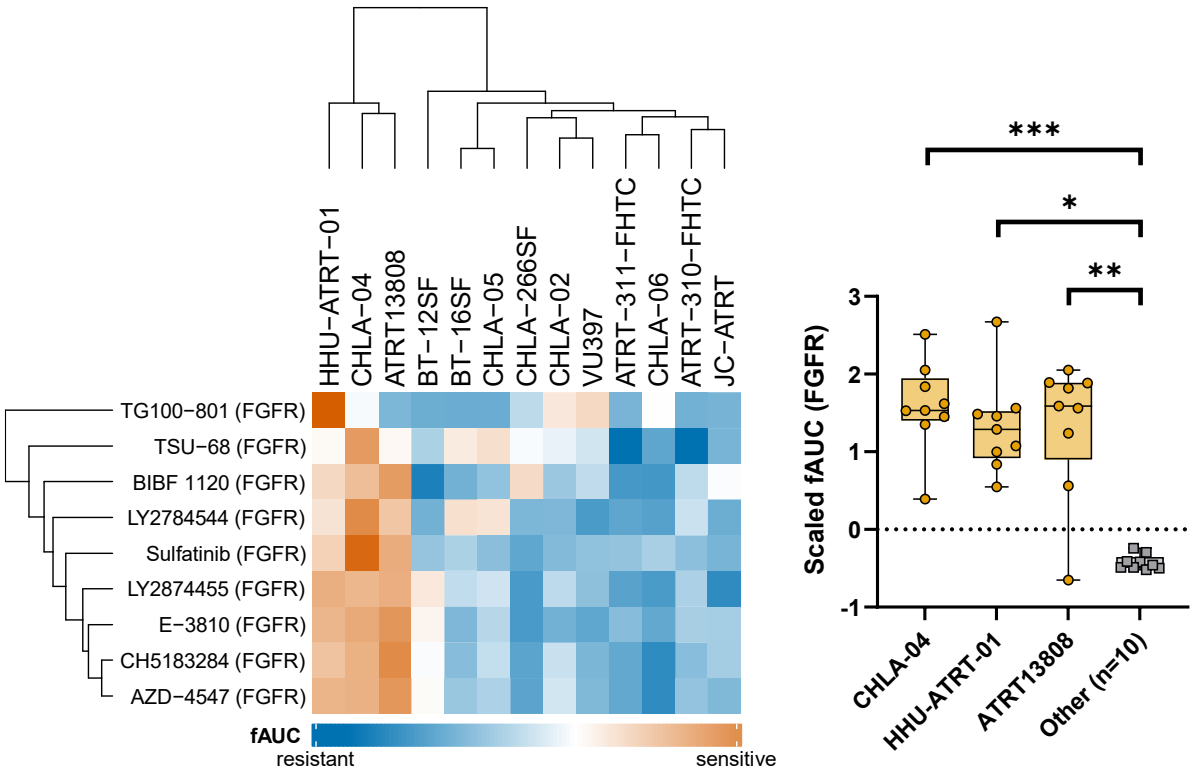

Figure 39. Unsupervised HCL analysis of FGFR drug screening data in AT/RT cell lines (left, Manhattan distance, average linkage). CHLA-04, HHU-ATRT-01 and ATRT13808 cells exhibited an increased sensitivity for FGFR inhibitors (right, Kruskal-Wallis test with uncorrected Dunn's test for post-hoc comparisons).

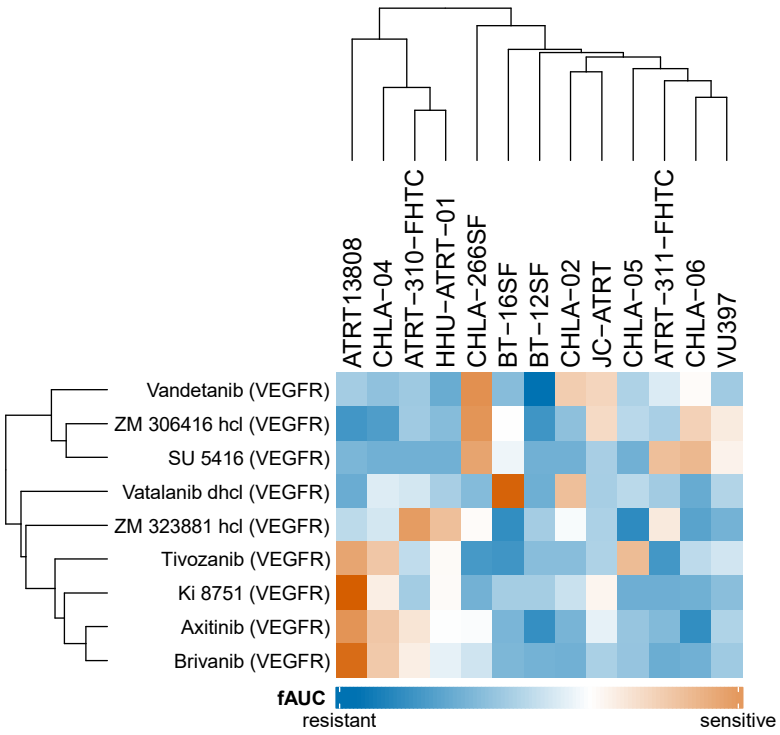

Figure 40. Unsupervised HCL of VEGFR drug screening data in AT/RT cell lines (Manhattan distance, average linkage). Significantly enriched cell lines were not detected. hcl = hydrochloride. dhcl = dihydrochloride.

Lastly, Bruton's tyrosine kinase (BTK) inhibitors were significantly more active in AT/RT cell lines with a stable fold change. However, even the top drug from this class, which was PCI-32765, required high concentrations to yield an effect and the separation from medulloblastoma cell lines appeared less pronounced, as depicted in Figure 41.

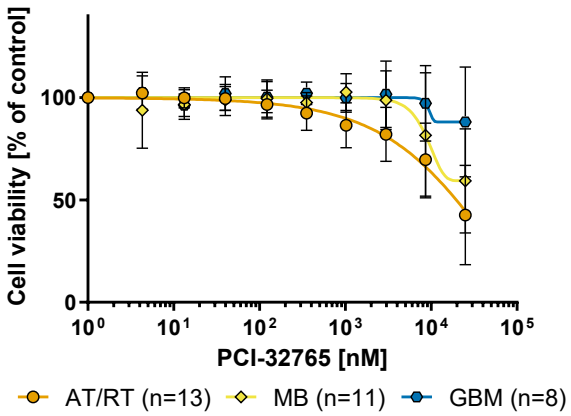

Figure 41. Dose-response curve of the BTK inhibitor PCI-32765 in AT/RT cell lines compared to medulloblastoma and glioblastoma cell lines. The separation from medulloblastoma cell lines appeared marginal.

In summary, cross entity analyses revealed selective and potent inhibition of AT/RT cell lines through MEK and MDM2 inhibition and, with limitations, BTK inhibition. Moreover, a subset of AT/RT cell lines showed a sensitivity for EGFR and FGFR inhibitors and one cell line proved to be targetable by RAF inhibitors.

3.2.5. Subgroup-stratified analysis of dose-response data of AT/RT cell lines

3.2.5.1. Intra-entity subgroup-stratified analysis

After evaluating specific drug responses across AT/RT cell lines using a comparison to medulloblastoma and glioblastoma cell lines, specific drug responses were evaluated according to subgroups of AT/RT cell lines, as previous analyses indicated heterogeneity among certain classes of drugs. An unsupervised HCL analysis with Spearman correlation-based distance calculation and average linkage method for agglomeration was performed on AT/RT drug screening data applying the same pre-filters as before, namely the exclusion of any drugs which did not exceed an fAUC of 0.1 in at least one AT/RT cell line. The data were then scaled for each inhibitor to reduce it to response patterns rather than giving higher impact to drugs with higher overall activity. The analysis revealed two major clusters, one of which aligns with

AT/RT-SHH cell lines whereas the other covers AT/RT-MYC cell lines according to classification based on DNA methylation profiling (cf. 3.4.1). While Figure 42 shows the 50 drugs with highest standard deviation, larger proportions (top 100, top 150, top 200) yielded comparable results with only minor changes in group alignment, if any. Clustering the whole dataset weakened the distinctness of the clusters. Notably, some of the vertical clusters were frequently comprised of drugs belonging to the same class, thus giving first hints that AT/RT subgroups were linked to sensitivity to certain drug classes.

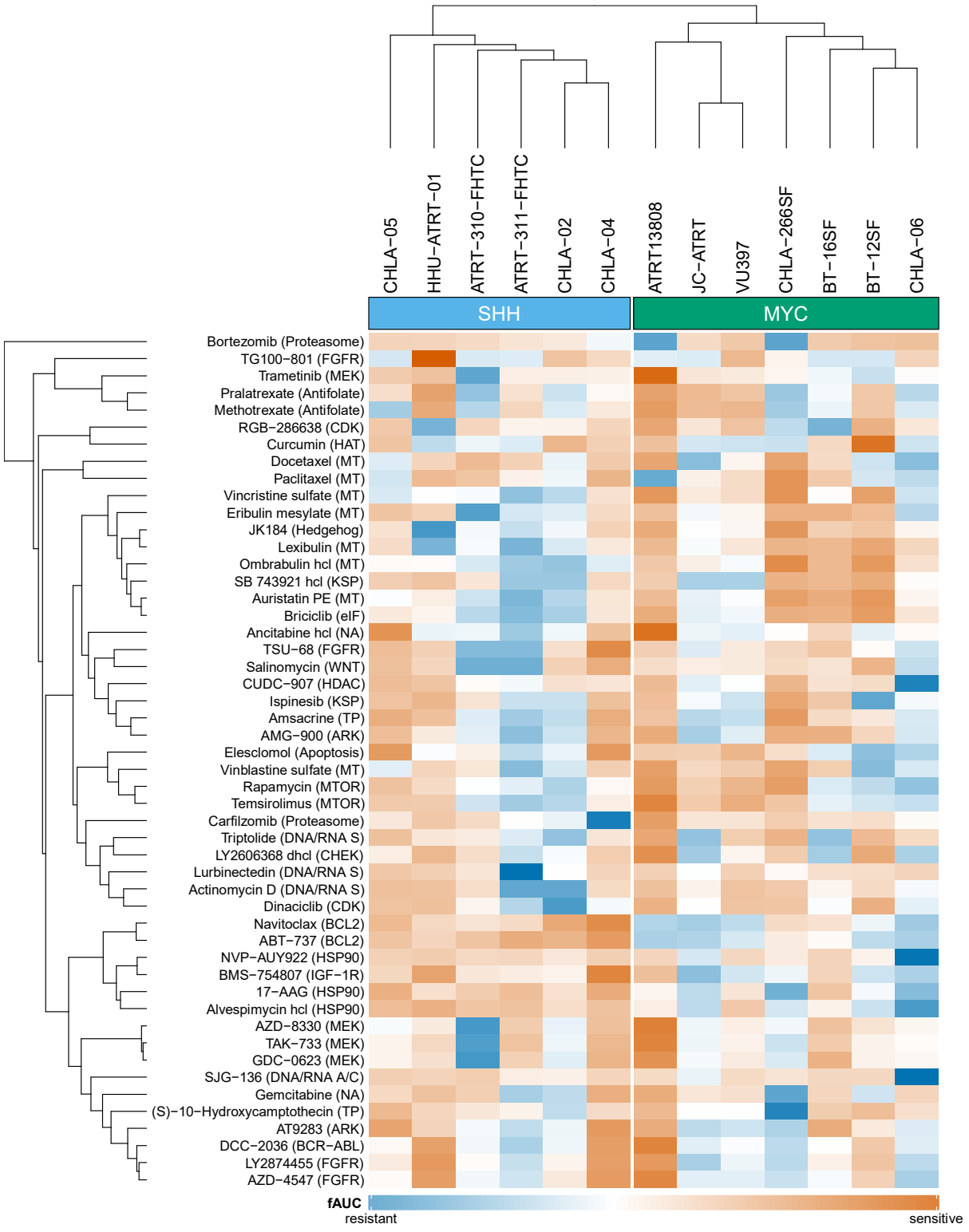

Figure 42. Unsupervised HCL analysis of AT/RT drug screening data (top 50 drugs based on standard deviation, Spearman correlation, average linkage). Two clusters emerged corroborating AT/RT-SHH and AT/RT-MYC affiliations of the cell lines as derived from classification through DNA methylation profiling. hcl = hydrochloride. dhcl = dihydrochloride. DNA/RNA S = DNA/RNA Synthesis. DNA A/C = DNA Alkylator/Crosslinker. MT = Microtubule. TP = Topoisomerase.

To further delineate the association of AT/RT subgroups and drug sensitivities, an MWU test comparing AT/RT-SHH cell lines vs. AT/RT-MYC cell lines was performed.

A volcano plot depicts the resulting p-values and the corresponding fold changes (Figure 43). Drugs with at least two hits were highlighted, indicating an increased occurrence of HSP90, BCL2, Notch, Janus kinase (JAK) and Protein kinase B (PKB or, more commonly, AKT) inhibitors.

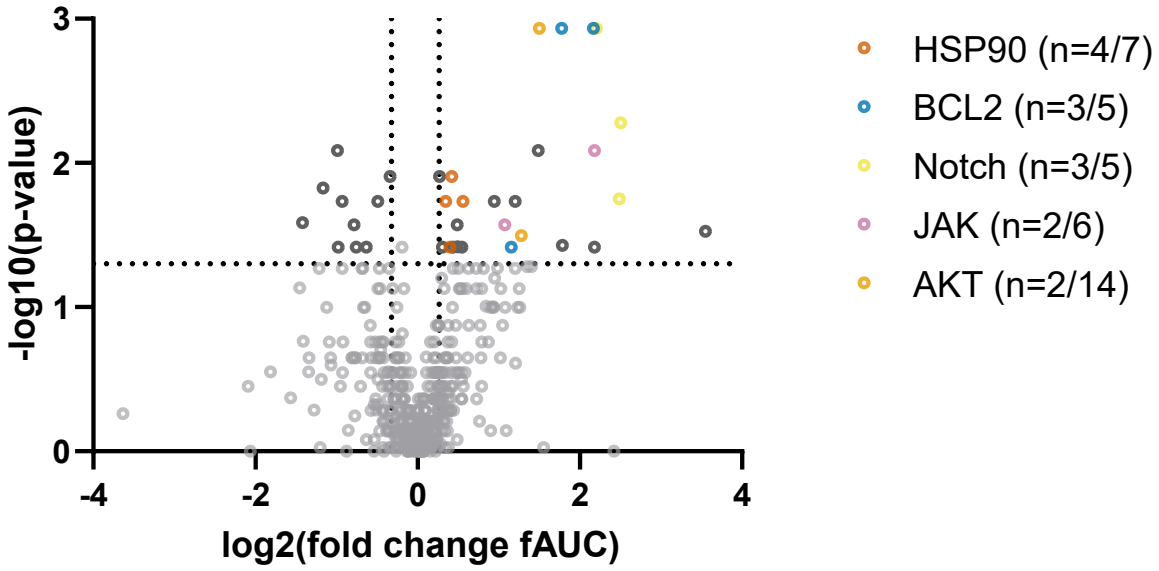

Figure 43. Volcano plot derived from the comparison of AT/RT-SHH cell lines with AT/RT-MYC cell lines (MWU test). Multiple HSP90, BCL2, Notch, JAK and AKT inhibitors were found to be enriched.

A comprehensive collection of the respective activity parameters is depicted in Table 11. The top four candidates (with regards to fold change) showed a comparable profile with low IC50 values but also rather low inhibition and consisted of three Notch inhibitors and one MCT1 inhibitor (AZD-3965). An association of MCT1 inhibition and Notch signaling was previously reported [139]. In conclusion, four Notch-related inhibitors appeared to specifically inhibit AT/RT-SHH cell lines at nano-molar range achieving submaximal inhibition, which may increase upon longer treatment time. Figure 44 visualizes the effect in actual dose-response curves derived from the two top candidates, AZD-3965 and LY3039478. Next came one of the two enriched JAK inhibitors, ZM 449829, which obtained varying inhibition and late onset of effect, as indicated by very high IC50 values. Its dose-response curve is depicted in Figure 44 as well. Just as done for the cross entity analyses, it was perceived that the analysis parameters were very sensitive, as an integrative analysis of JAK inhibitors seemed less convincing in terms of their specificity. With regards to drugs achieving higher fAUC values, ABT-737 and Navitoclax (both BCL2 inhibitors), 17-AAG, Alvespimycin hydrochloride, NVP-AUY922 and Ganetespib (all HSP90 inhibitors), and API-2 and FPA124 (both AKT inhibitors) were found. While BCL2 inhibitors delivered higher fold

changes, HSP90 inhibitors showed very low IC50 values. Overall, these two classes stood out as prime candidates in AT/RT-SHH cell lines. Their performance in dose-response curves is depicted for exemplarily drugs from both classes in Figure 44. For the two AKT inhibitors, there were variable IC50 values and medium inhibition. Their dose-response curves indicated high standard deviation (Figure 44). Separation of highly responsive from resistant cell lines revealed a specific activity of AKT inhibition in CHLA-04 cells. However, no consistent AKT sensitivity was detected in the other AT/RT-SHH cell lines, and neither were there AKT-sensitive cell lines in the AT/RT-MYC group. Thus, sensitivity to AKT inhibition may rather be regarded as individually acquired feature than a systemically relevant effect in AT/RTs.

Table 11. Descriptive parameters of drugs with significantly enriched activity in AT/RT-SHH cell lines vs. AT/RT-MYC cell lines, sorted for fold change. P-value based on an MWU test. Higher fAUC values indicate higher activity.

Inhibitor	Class	Fold change	fAUC	IC50 [nM]	Inhibition [%]	P-value
AZD-3965	Others	11.69	0.19 (0 - 0.43)	355 (3 - 2006)	25.89 (0 - 49.66)	0.030
LY3039478	Notch	5.68	0.12 (0.05 - 0.18)	22 (9 - 37)	17.06 (7.03 - 23.11)	0.005
Ro 4929097	Notch	5.61	0.12 (0.03 - 0.24)	46 (18 - 129)	19.83 (4.26 - 34.45)	0.018
MK-0752	Notch	4.59	0.06 (0.03 - 0.1)	1288 (9 - 3833)	18.76 (10.94 - 28.2)	0.001
ZM 449829	JAK	4.53	0.1 (0.04 - 0.12)	8052 (4786 - 10748)	85.22 (24.12 - 99.53)	0.008
CTS-1027	MMP	4.53	0.07 (0.01 - 0.14)	8371 (6016 - 11398)	56.45 (7.48 - 93.13)	0.038
ABT-737	BCL2	4.49	0.37 (0.29 - 0.47)	510 (202 - 817)	92.42 (84.01 - 98.96)	0.001
Flumatinib	BCR-ABL	3.45	0.08 (0.01 - 0.14)	8229 (1073 - 22914)	69.95 (12.65 - 99.36)	0.037
ABT-199	BCL2	3.42	0.17 (0.08 - 0.25)	2761 (994 - 4063)	63.98 (39.41 - 92.11)	0.001
API-2	AKT	2.83	0.31 (0.2 - 0.55)	97 (81 - 118)	57.7 (38.06 - 98.26)	0.001
CGP 53353	PKC	2.80	0.09 (0.04 - 0.26)	7206 (1910 - 12932)	55.69 (31.77 - 95.79)	0.008
FPA 124	AKT	2.43	0.06 (0.02 - 0.13)	7215 (3285 - 14810)	42.47 (7.07 - 71)	0.032
AZD-1208	PIM	2.30	0.15 (0.07 - 0.25)	45 (29 - 72)	24.09 (11.81 - 36.91)	0.018
Navitoclax	BCL2	2.23	0.48 (0.36 - 0.66)	268 (29 - 569)	98.05 (96.05 - 99)	0.038
ZM 39923 hcl	JAK	2.11	0.13 (0.02 - 0.18)	7441 (3500 - 17841)	90.09 (47.12 - 99.2)	0.027
(-)-Terreic acid	BTK	1.93	0.16 (0.07 - 0.22)	6094 (2760 - 13226)	96.82 (92.78 - 98.75)	0.018
17-AAG	HSP90	1.47	0.63 (0.53 - 0.7)	36 (16 - 71)	96.85 (90.2 - 99.11)	0.018
BYL-719	PI3K	1.46	0.2 (0.16 - 0.32)	1495 (27 - 2567)	59.84 (26.93 - 89.36)	0.038
Entrectinib	ALK	1.40	0.2 (0.15 - 0.26)	3779 (2001 - 5187)	98.44 (96.38 - 99.02)	0.038
Auranofin	Others	1.40	0.41 (0.3 - 0.48)	573 (180 - 1353)	98.89 (98.67 - 99.06)	0.027
BI-78D3	JNK	1.35	0.32 (0.29 - 0.35)	1064 (783 - 1474)	99.2 (99.12 - 99.29)	0.038
Alvespimycin hcl	HSP90	1.34	0.8 (0.73 - 0.85)	6 (3 - 11)	99.14 (98.54 - 99.42)	0.012
NVP-AUY922	HSP90	1.32	0.81 (0.72 - 0.86)	5 (4 - 6)	96.32 (89.37 - 98.92)	0.038
Ganetespib	HSP90	1.27	0.7 (0.6 - 0.74)	17 (13 - 21)	95.22 (87.86 - 98.28)	0.018
CGK 733	ATM/ATR	1.23	0.21 (0.17 - 0.24)	3289 (2349 - 4672)	98.62 (97.87 - 99.2)	0.038
VLX1570	Others	1.20	0.54 (0.46 - 0.58)	101 (53 - 191)	99.48 (99.31 - 99.66)	0.012

(…) = Minimum and maximum values

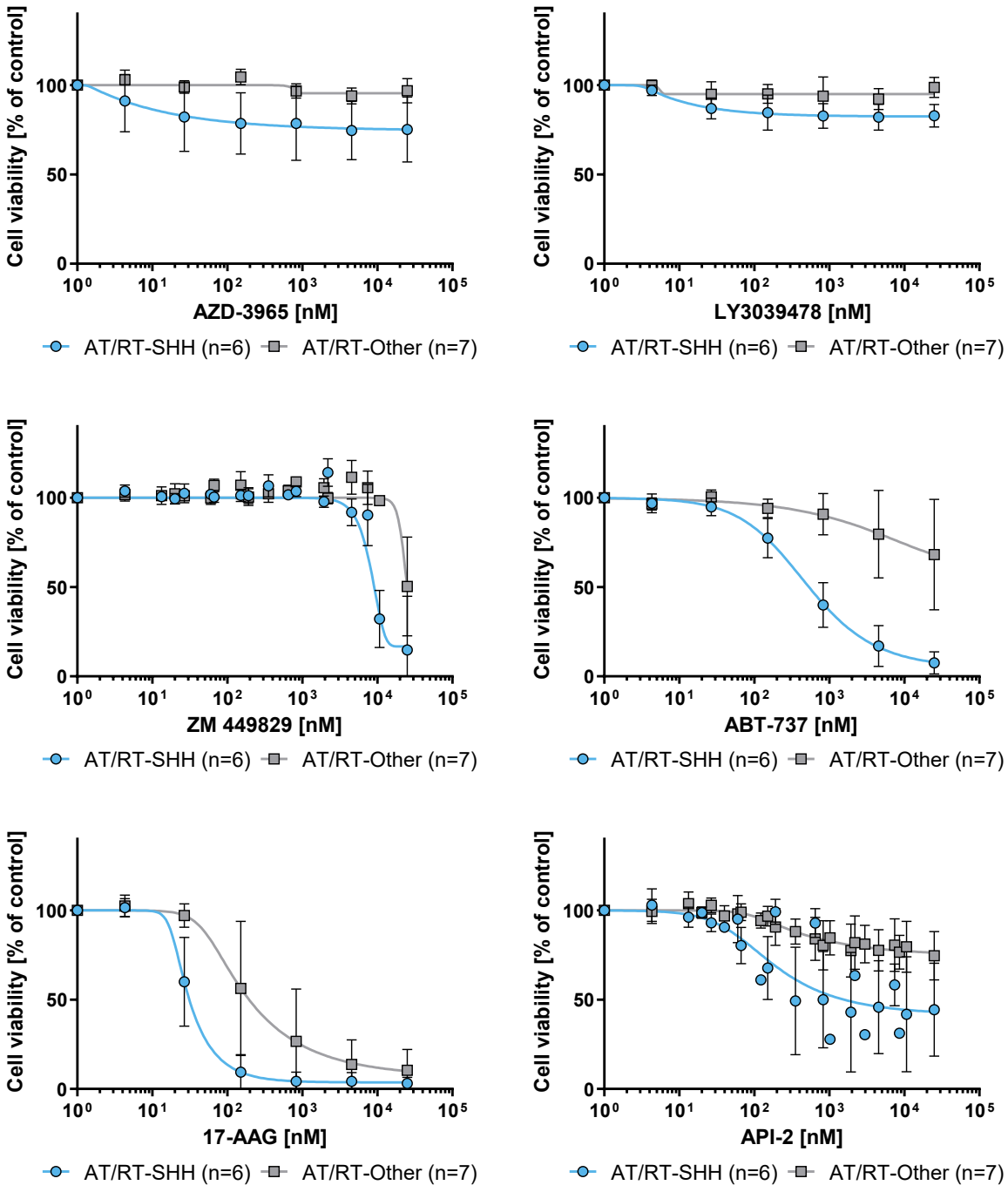

Figure 44. Dose-response curves of selected AT/RT-SHH-specific inhibitors. AZD-3965 and LY3039478 = Notch inhibitors. ZM 449829 = JAK inhibitor. ABT-737 = BCL2 inhibitor. 17-AAG = HSP90 inhibitor. API-2 = AKT inhibitor.

In addition, analysis of the dose-response data was performed in a class-wise manner. Figure 45 displays drug classes represented by at least four members which delivered a mean fold change of at least 1.1. An MWU test revealed that Notch, BCL2 and HSP90 inhibitors yielded a significant enrichment in AT/RT-SHH cell lines. While Notch inhibition showed a high fold change, it achieved low overall activity, as indicated by low fAUC values. There was no further enrichment of FGFR and EGFR inhibitors, which ruled out a subgroup-mediated response to these classes (cf. HCL analyses in

3.2.4). In conclusion, HSP90 and BCL2 inhibitors as well as, with limitations, Notch inhibitors turned out as the prime candidates for the treatment of AT/RT-SHH cell lines.

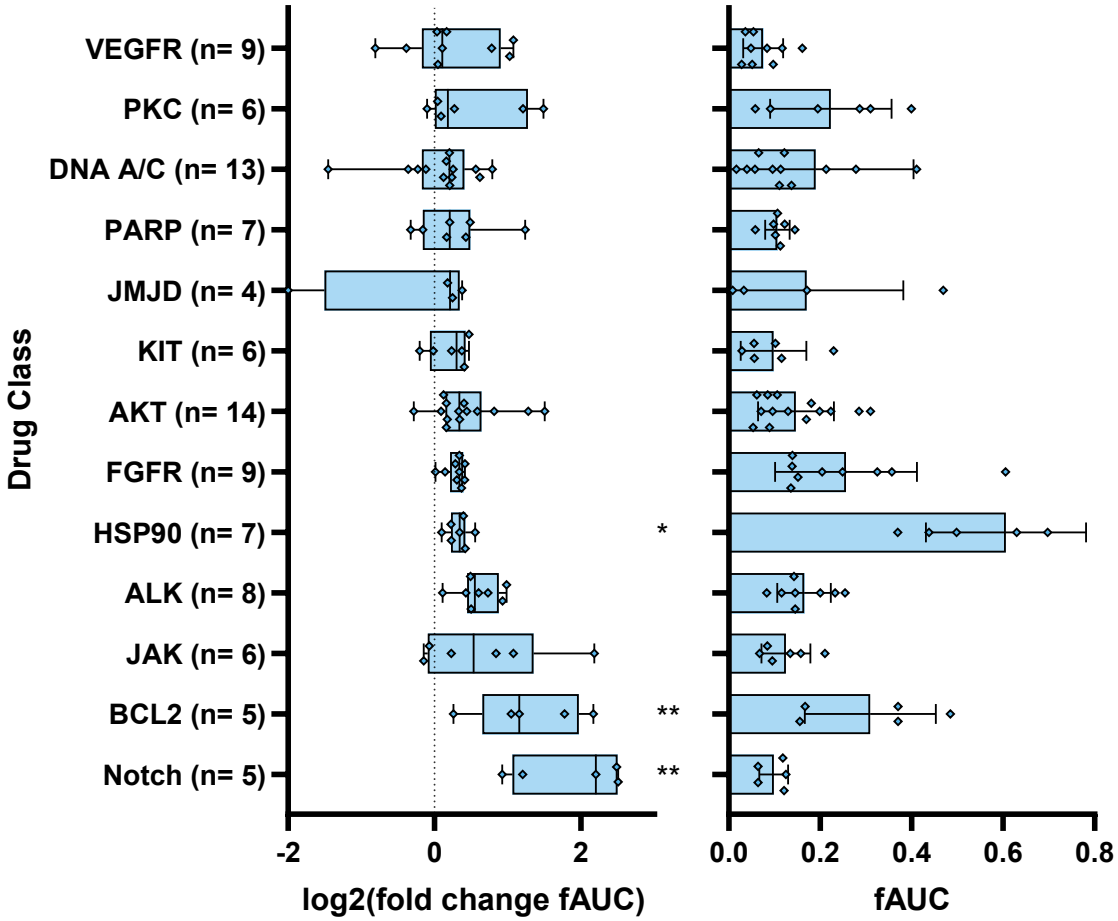

Figure 45. DCEA of AT/RT-SHH cell lines vs. AT/RT-MYC cell lines depicted as fold change per inhibitor (left) along with mean fAUC values in AT/RT-SHH cell lines (right). Drug classes consisting of at least four drugs and showing a fold change of 1.1 or larger are displayed. * = p-value < 0.05, ** = p-value < 0.01, MWU test. DNA A/C = DNA Alkylator/Crosslinker.

Next, the analysis was repeated with a focus on specific inhibitory effects in AT/RT-MYC cell lines. A corresponding volcano plot was generated, indicating few drugs with significantly higher activity in AT/RT-MYC cell lines compared to AT/RT-SHH cell lines according to an MWU test. Among these, drugs from classes occurring more than one time were highlighted, which held true for four (out of 19) microtubule inhibitors, two (out of 27) EGFR inhibitors and two (out of 5) proteasome inhibitors.

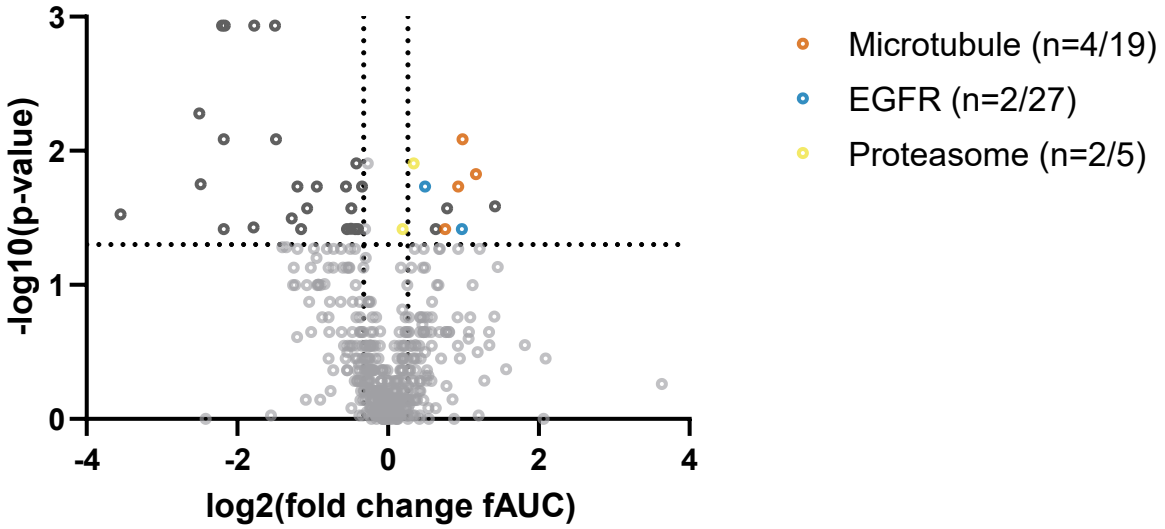

Figure 46. Volcano plot derived from the comparison of AT/RT-MYC cell lines with AT/RT-SHH cell lines (MWU test). Multiple microtubule, EGFR and proteasome inhibitors were found to be enriched.

Table 12 displays detailed information about the drugs with a significant enrichment. The top candidate, RX-3117, which is a nucleoside antimetabolite (NA), appeared to be a false positive after visual inspection of an overlapped dose-response curve (Figure 47) and comparison with tAUC data (fold change: 1.24, n.s. according to an MWU test). Its relatively high fold change relied on misfitting of highly variable data highlighting the limitations of working with fitted data. The following two candidates, namely Lexibulin and Ombrabulin hydrochloride, which both are microtubule inhibitors, may be regarded as the prime candidates for the treatment of AT/RT-MYC cell lines as they showed the highest fold changes along with high activity, as indicated by high fAUC values. Their dose-response curves are depicted in Figure 47. Interestingly, the eukaryotic initiation factor 4E (eIF4E) inhibitor Briciclib and the PI3K inhibitor Rigosertib sodium showed a comparable profile plateauing at submaximal inhibition requiring low IC50s without exhibiting further reduction of viability at higher concentrations (Figure 47). Furthermore, we found the two EGFR inhibitors AEE788 and Pelitinib to obtain similar dose-response profiles in the sense of a flat dose-response curve with an early onset of effect, as depicted in the corresponding dose-response curve of Pelitinib (Figure 47), which showed higher overall activity compared to AEE788. As it had been shown previously, this effect relied on the increased sensitivity of BT-16SF, CHLA-266SF and VU397 vs. EGFR inhibitors (cf. 3.2.4). Proteasome inhibitors on the other hand may rather be rejected, as they delivered marginal fold changes and similar curve progressions compared to AT/RT-SHH cell lines, as indicated by the dose-response

curve of MLN9708 (Figure 47). A group-wise analysis was unable to detect any drug classes with a significantly enriched activity in AT/RT-MYC cell lines. In accordance with previous findings there was a strong trend for microtubule inhibitors (Figure 48).

Table 12. Descriptive parameters of drugs with significantly enriched activity in AT/RT-MYC cell lines vs. AT/RT-SHH cell lines, sorted for fold change. P-value based on an MWU test. Higher fAUC values indicate higher activity.

Inhibitor	Class	Fold change	fAUC	IC50 [nM]	Inhibition [%]	P-value
RX-3117	NA	2.68	0.28 (0.18 - 0.41)	640 (298 - 1916)	75 (58.04 - 96.09)	0.026
Lexibulin	Microtubule	2.25	0.41 (0.24 - 0.53)	71 (50 - 119)	71.05 (46.25 - 86.73)	0.015
Ombrabulin hcl	Microtubule	1.98	0.48 (0.31 - 0.64)	19 (11 - 26)	67.73 (44.09 - 87.53)	0.008
AEE788	EGFR	1.97	0.17 (0.02 - 0.26)	3933 (877 - 9597)	68.57 (23.39 - 91.71)	0.038
Fosbretabulin disodium	Microtubule	1.91	0.34 (0.19 - 0.52)	124 (23 - 359)	59.65 (34.75 - 81.36)	0.018
Rigosertib sodium	PI3K	1.72	0.36 (0.22 - 0.5)	86 (45 - 141)	62.74 (40.63 - 82.25)	0.027
Vincristine sulfate	Microtubule	1.69	0.5 (0.26 - 0.71)	15 (4 - 64)	64.25 (43.94 - 85.23)	0.038
Briciclib	eIF	1.55	0.51 (0.32 - 0.64)	15 (7 - 22)	70 (48.54 - 89)	0.038
Pelitinib	EGFR	1.41	0.39 (0.26 - 0.47)	711 (162 - 2275)	98.54 (96.97 - 99.26)	0.018
MLN9708	Proteasome	1.27	0.51 (0.43 - 0.55)	108 (76 - 142)	96.18 (88.53 - 98.9)	0.012
Delanzomib	Proteasome	1.14	0.74 (0.68 - 0.82)	8 (5 - 12)	96.23 (88.62 - 99.15)	0.038

(…) = Minimum and maximum values. NA = Nucleoside Antimetabolite

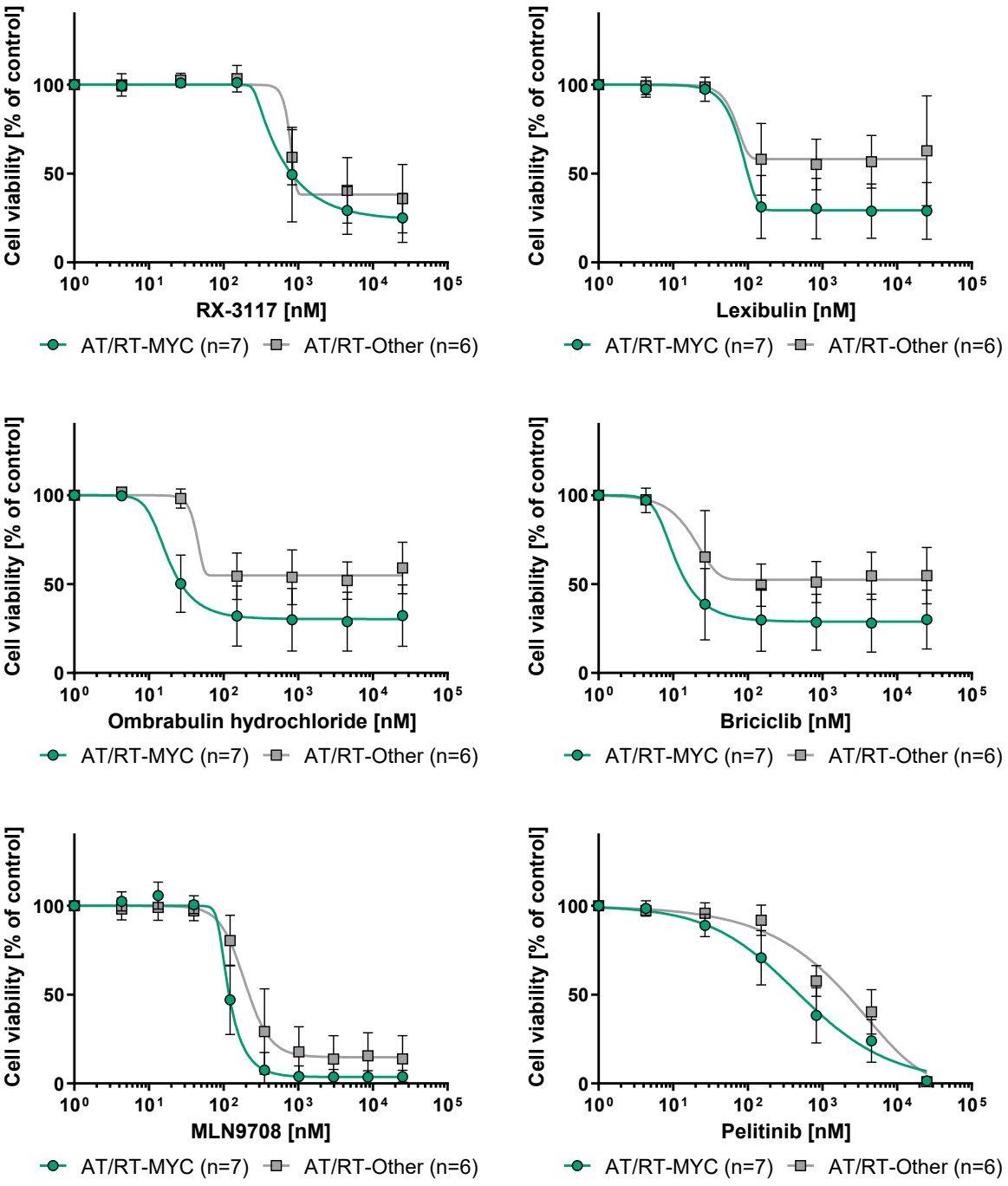

Figure 47. Dose-response curves of selected AT/RT-MYC-specific inhibitors. RX-3117 = nucleoside antimetabolite. Lexibulin and Ombrabulin hydrochloride = microtubule inhibitors. Briciclib = eIF4E inhibitor. MLN9708 = proteasome inhibitor. Pelitinib = EGFR inhibitor.

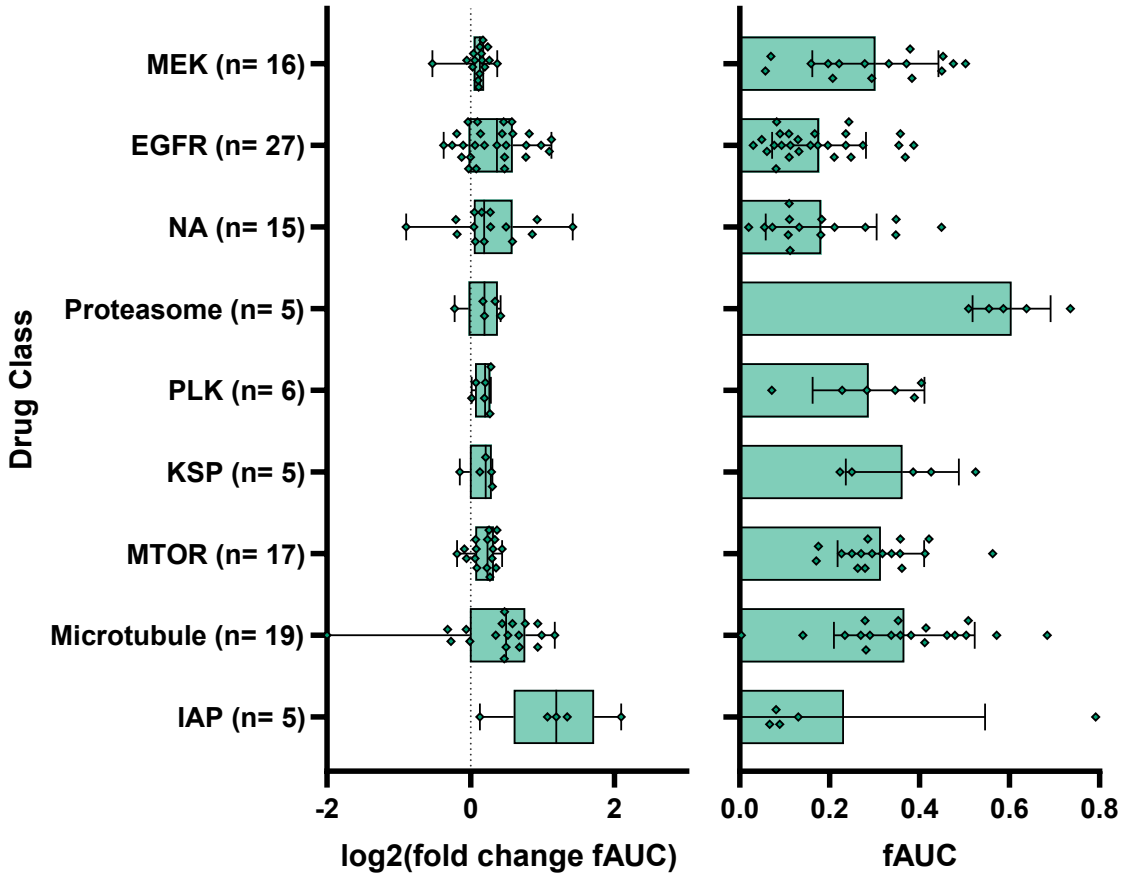

Figure 48. DCEA of AT/RT-MYC cell lines vs. AT/RT-SHH cell lines depicted as fold change per inhibitor (left) along with mean fAUC values in AT/RT-MYC cell lines (right). Drug classes consisting of at least three drugs and showing a fold change of 1.1 or larger are displayed. All results turned out non-significant according to an MWU test. NA = Nucleoside Antimetabolite. IAP = Inhibitor of apoptosis.

Microtubule inhibitors emerged as the top candidates for the treatment of AT/RT-MYC cell lines. Thus, it was aimed to characterize their activity profile among AT/RT-MYC cell lines in more detail revealing significant heterogeneity (Figure 49). It appeared that the specific effect was limited to four out of seven cell lines. While CHLA-06, JC-ATRT and VU397 had a similar sensitivity compared to AT/RT-SHH cell lines, ATRT13808, BT-12SF, BT-16SF and CHLA-266SF were significantly more sensitive.

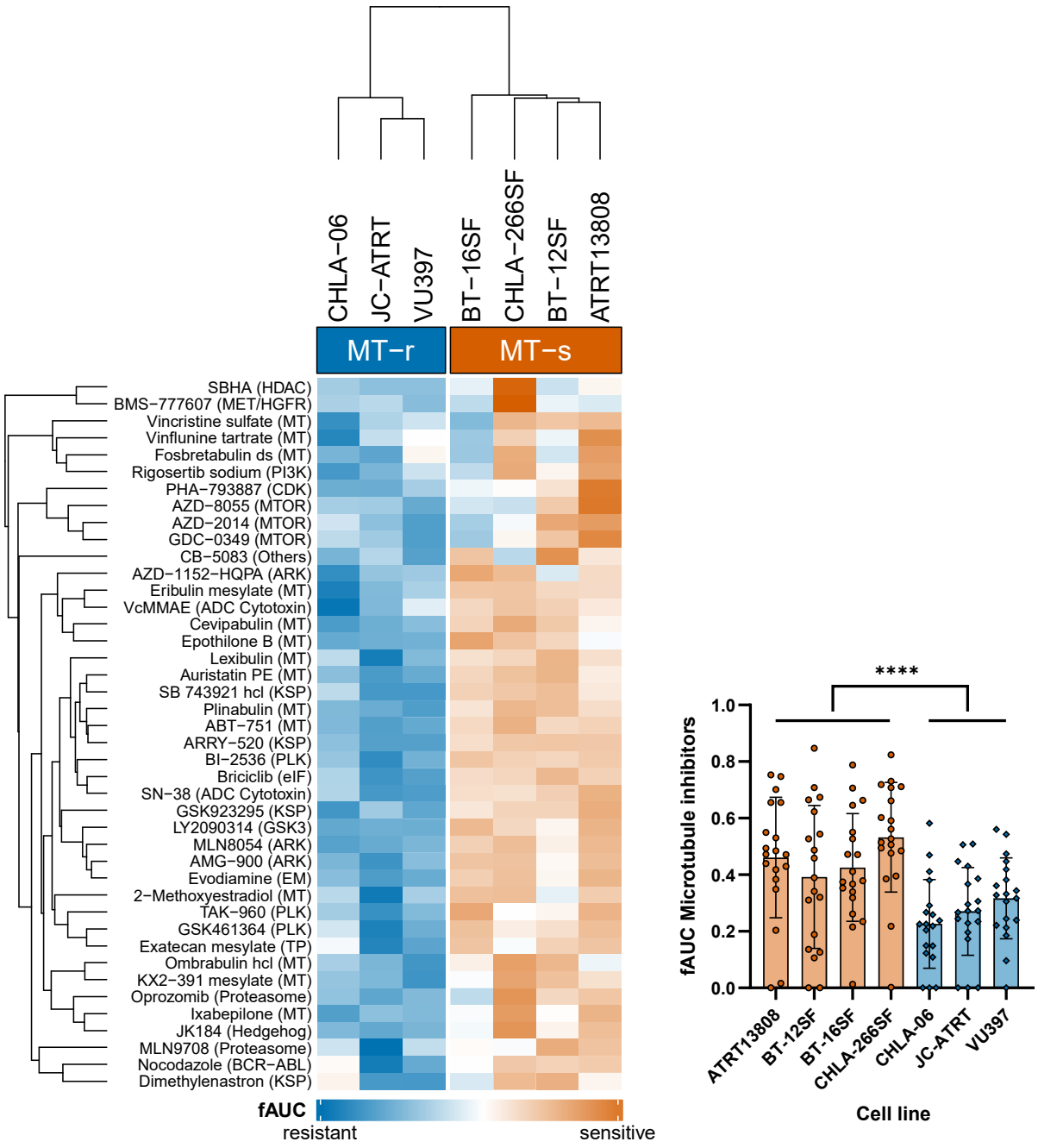

Figure 49. An MWU test on fAUC data from microtubule inhibitors showed significantly higher activity in ATRT13808, BT-12SF, BT-16SF and CHLA-266SF compared to other AT/RT-MYC cell lines (right). Supervised HCL analysis (Manhattan distance, average linkage) of significantly enriched drugs in ATRT13808, BT-12SF, BT-16SF and CHLA-266SF (microtubule inhibitor-sensitive cohort = MT-s) vs. other AT/RT-MYC cell lines (microtubule inhibitor-resistant cohort = MT-r) revealed even more drug classes with increased sensitivity including spindle kinesin protein (KSP) inhibitors. **** = p-value < 0.0001, MWU test. ds = disodium. hcl = hydrochloride. MT = Microtubule. TP = Topoisomerase.

As a subset of AT/RT-MYC cell lines showed a higher sensitivity for the treatment with microtubule inhibitors, the MWU analysis was repeated comparing microtubule inhibitor-sensitive (MT-s) cell lines (ATRT13808, BT-12SF, BT-16SF and CHLA-266SF) vs. all other AT/RT cell lines (microtubule inhibitor-resistant = MT-r), in order

to generate another volcano plot (Figure 50). Highlighting all classes represented by at least three significantly enriched drugs, an increase of the number of microtubule inhibitors from two out of 19 inhibitors to 14 out of 19 inhibitors was detected. Additionally, there were significantly higher activities of Spindle kinesin protein (KSP) inhibitors (4/5), ARK inhibitors (3/20), Polo-like kinase (PLK) inhibitors (3/6), MTOR inhibitors (3/17) and cytotoxic drugs used in antibody drug conjugates (ADC, 2/3). Notably, all of these drug classes (except for MTOR inhibitors) are directly or indirectly acting through disruption of mitosis.

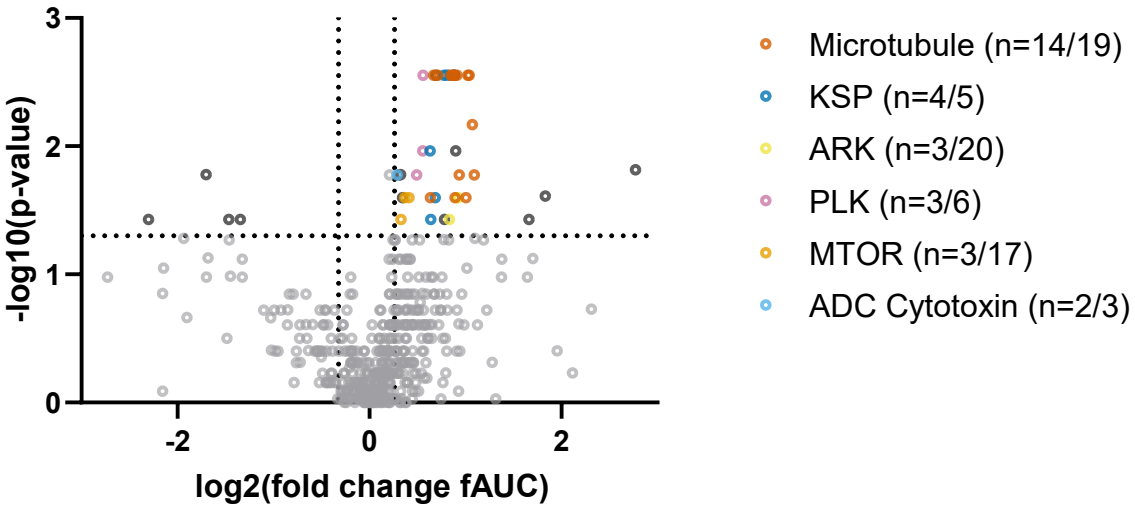

Figure 50. Volcano plot derived from the comparison of the MT-s cohort of AT/RT-MYC cell lines with all other AT/RT cell lines (MWU test). Multiple microtubule, KSP, ARK, PLK and MTOR inhibitors as well as ADC cytotoxins were found to be enriched.

The respective activity parameters of individual drugs were evaluated in detail (Table 13). Again, the top three candidate drugs in terms of fold change (SBHA, LY2090314 and BMS-777607) showed very low overall activity, as indicated by low fAUC values, which in turn led to an overestimation of their fold changes. Moreover, they did not reach a significant difference in tAUC-based evaluation and visual inspection of the corresponding dose-response curves revealed a very tight difference (data not shown). Taken together, the first three drugs from Table 13 may be regarded as false positives due to the sensitive parameters used in this analysis, as already explained before. The next six drugs all belonged to the class of microtubule inhibitors. The first one, 2-Methoxyestradiol, a metabolite of the steroid hormone estradiol, showed the highest fold change (2.13), but its overall activity with an fAUC of 0.2 appeared lower than the activity of the other microtubule inhibitors. Thus, both Lexibulin and Ombrabulin hydrochloride as well as Ixabepilone emerged as the top candidates in the MT-s cohort of AT/RT-MYC cell lines. Their dose-response curves are depicted in Figure 51. ARK

inhibitors and KSP inhibitors displayed lower fold changes but obtained a similar dose-response pattern compared to microtubule inhibitors, with an activity plateau at submaximal inhibition. Interestingly, also the PI3K inhibitor Rigosertib sodium and the Hedgehog inhibitor JK184 exhibited similar profiles and delivered a medium fold change between those of microtubule and KSP inhibitors. As JK184 mediates its activity through microtubule depolymerization [140] and Rigosertib sodium preparations have been shown to contain contaminants of microtubule polymerization inhibitors from production, both drugs probably acted through disruption of mitosis as well, and thus, did not indicate a certain sensitivity of AT/RT-MYC cell lines vs. Hedgehog or PI3K inhibition. The eIF4E inhibitor Briciclib also yielded a comparable dose-response profile to microtubule inhibitors (Figure 51), but as it is a selective inhibitor of eIF4E, it may imply an important role of eIF4E in the mechanism of microtubule inhibitors among the MT-s cohort of AT/RT-MYC cell lines. Furthermore, PLK inhibitors showed lower but stable fold changes between 1.41 and 1.47. They also exhibited an interesting dose-response profile with an early onset of effect at lower than 100 nM concentration, but a loss of selectivity at higher concentrations, indicating off-target effects at maximum concentrations, as exemplarily depicted for BI-2536 in Figure 51. MTOR inhibitors obtained the lowest fold changes (1.26-1.33) and displayed only minor differences in the dose-response curves with similar curve progressions in the MT-s cohort of AT/RT-MYC cell lines and other AT/RT cell lines (Figure 51).

Table 13. Descriptive parameters of drugs with significantly enriched activity in the MT-s cohort of AT/RT-MYC cell lines vs. other AT/RT cell lines, sorted for fold change. P-value based on an MWU test. Higher fAUC values indicate higher activity.

Inhibitor	Class	Fold change	fAUC	IC50 [nM]	Inhibition [%]	P-value
SBHA	HDAC	6.83	0.06 (0.02 - 0.14)	5208 (3259 - 8758)	36.04 (11.07 - 76.77)	0.015
LY2090314	GSK3	3.56	0.1 (0.08 - 0.13)	2800 (149 - 5055)	40.98 (17.23 - 56.49)	0.024
BMS-777607	MET/HGFR	3.17	0.11 (0.04 - 0.24)	1910 (16 - 6535)	32.82 (16.79 - 45.69)	0.037
2-Methoxyestradiol	Microtubule	2.13	0.2 (0.14 - 0.22)	1206 (863 - 1913)	63.14 (53.78 - 70.71)	0.017
Lexibulin	Microtubule	2.10	0.48 (0.41 - 0.53)	64 (53 - 85)	82.71 (77.8 - 86.73)	0.007
Ombrabulin hcl	Microtubule	2.05	0.57 (0.49 - 0.64)	19 (11 - 23)	80.05 (69.43 - 87.53)	0.003
Ixabepilone	Microtubule	2.03	0.47 (0.34 - 0.61)	26 (9 - 45)	67.77 (60.69 - 77.14)	0.003
Vinflunine tartrate	Microtubule	2.01	0.35 (0.24 - 0.47)	197 (60 - 291)	71.41 (53.38 - 82.86)	0.025
Fosbretabulin disodium	Microtubule	1.91	0.39 (0.26 - 0.52)	113 (25 - 228)	70.1 (51.99 - 81.36)	0.017
AZD-1152-HQPA	ARK	1.90	0.28 (0.2 - 0.31)	832 (39 - 1763)	65.74 (47.5 - 89.95)	0.025
ABT-751	Microtubule	1.88	0.34 (0.32 - 0.38)	309 (208 - 453)	80.96 (73.63 - 86.18)	0.003
AMG-900	ARK	1.88	0.41 (0.35 - 0.45)	4 (2 - 8)	48.87 (36.79 - 58.01)	0.025
Rigosertib sodium	PI3K	1.87	0.42 (0.33 - 0.5)	79 (45 - 121)	73.27 (57.92 - 82.25)	0.011
Vincristine sulfate	Microtubule	1.85	0.6 (0.37 - 0.71)	7 (4 - 12)	74.25 (48.82 - 85.23)	0.025
Evodiamine	EM	1.85	0.22 (0.19 - 0.25)	941 (452 - 1278)	65.94 (59.82 - 77.68)	0.003
JK184	Hedgehog	1.84	0.61 (0.52 - 0.71)	17 (6 - 32)	84.43 (80.53 - 88.62)	0.003
KX2-391 mesylate	Microtubule	1.84	0.43 (0.38 - 0.49)	95 (64 - 123)	78.85 (71.41 - 86.8)	0.003
Eribulin mesylate	Microtubule	1.82	0.64 (0.58 - 0.67)	7 (4 - 9)	83.85 (77.53 - 88.29)	0.003
Cevipabulin	Microtubule	1.80	0.46 (0.42 - 0.49)	67 (50 - 89)	81.9 (70.04 - 89.52)	0.003
MLN8054	ARK	1.78	0.24 (0.21 - 0.27)	176 (133 - 214)	49.63 (39.59 - 56.02)	0.037
Briciclib	eIF	1.76	0.61 (0.6 - 0.64)	13 (7 - 19)	82.33 (76.28 - 89)	0.003
VcMMAE	ADC Cytotoxin	1.74	0.33 (0.31 - 0.34)	376 (330 - 446)	78.05 (73.3 - 86.34)	0.003
PHA-793887	CDK	1.72	0.29 (0.22 - 0.42)	917 (239 - 1593)	87.57 (68.07 - 98.87)	0.037
ARRY-520	KSP	1.71	0.55 (0.51 - 0.57)	18 (3 - 31)	74.79 (61.74 - 81.69)	0.003
Plinabulin	Microtubule	1.64	0.68 (0.65 - 0.71)	4 (4 - 6)	79.94 (75.36 - 86)	0.003
Nocodazole	BCR-ABL	1.62	0.45 (0.42 - 0.49)	108 (74 - 141)	85.93 (81.59 - 89.97)	0.003
GSK923295	KSP	1.61	0.33 (0.31 - 0.34)	191 (102 - 335)	67.98 (60.37 - 76.52)	0.025
Auristatin PE	Microtubule	1.59	0.8 (0.75 - 0.85)	2 (2 - 2)	85.85 (79.86 - 91.58)	0.003
Dimethylenastron	KSP	1.56	0.27 (0.21 - 0.32)	694 (342 - 1315)	72.26 (64.71 - 82.48)	0.037
Patupilone	Microtubule	1.55	0.55 (0.44 - 0.66)	3 (2 - 4)	61.89 (47.67 - 73.29)	0.025
SB 743921 hcl	KSP	1.55	0.65 (0.56 - 0.75)	20 (11 - 37)	99.1 (99.07 - 99.16)	0.011
BI-2536	PLK	1.47	0.49 (0.46 - 0.54)	106 (90 - 126)	99.05 (98.43 - 99.44)	0.003
GSK461364	PLK	1.47	0.46 (0.4 - 0.53)	121 (86 - 163)	95.01 (91.8 - 99.1)	0.011
TAK-960	PLK	1.41	0.41 (0.36 - 0.47)	160 (97 - 199)	88.18 (77.79 - 98.89)	0.017
AZD-2014	MTOR	1.33	0.34 (0.29 - 0.39)	230 (131 - 341)	71.09 (60 - 83.92)	0.025
GDC-0349	MTOR	1.29	0.27 (0.23 - 0.31)	608 (436 - 745)	70.9 (62.64 - 84.83)	0.025
CB-5083	Others	1.27	0.18 (0.16 - 0.2)	4317 (3528 - 5237)	98.89 (97.9 - 99.26)	0.025
AZD-8055	MTOR	1.26	0.45 (0.4 - 0.52)	44 (20 - 67)	69.95 (55.45 - 84.58)	0.037
Exatecan mesylate	TP	1.25	0.81 (0.77 - 0.85)	4 (3 - 5)	95.7 (90.02 - 98.9)	0.017
MLN9708	Proteasome	1.24	0.53 (0.5 - 0.55)	88 (76 - 95)	96.94 (95.28 - 98.48)	0.017
SN-38	ADC Cytotoxin	1.22	0.79 (0.75 - 0.85)	5 (4 - 6)	96.89 (92.52 - 98.93)	0.017
Oprozomib	Proteasome	1.15	0.61 (0.59 - 0.63)	46 (27 - 65)	97.65 (94.63 - 99.14)	0.017

(…) = Minimum and maximum values. EM = Endogenous Metabolite. TP = Topoisomerase

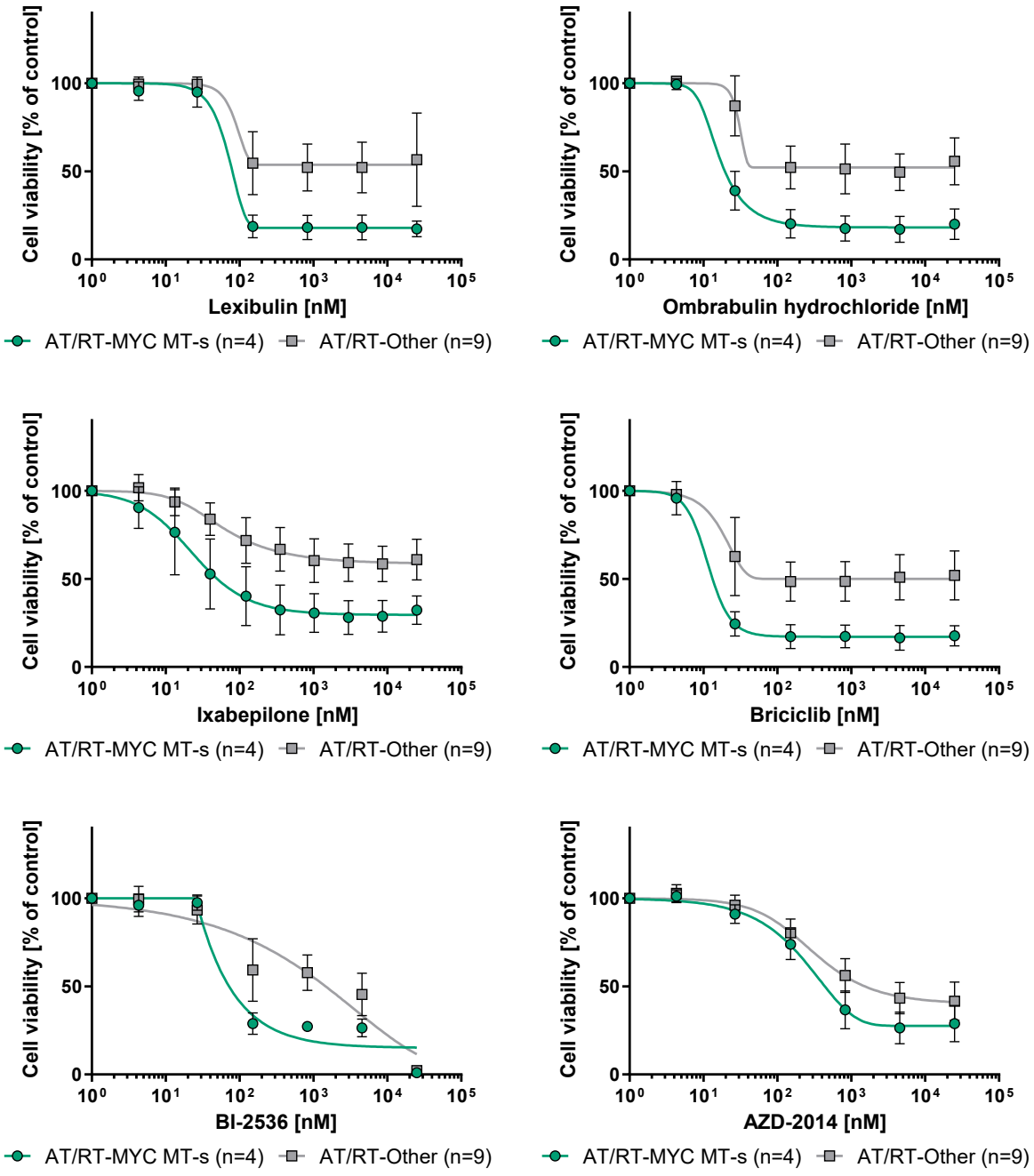

Figure 51. Dose-response curves of selected MT-s-specific inhibitors. Lexibulin, Ombrabulin hydrochloride and Ixabepilone = microtubule inhibitors. Briciclib = eIF4E inhibitor. BI-2536 = PLK inhibitor. AZD-2014 = MTOR inhibitor.

Group-wise analyses showed a significant enrichment for microtubule inhibitors and KSP inhibitors as well as PLK inhibitors (Figure 52). There was a strong trend for inhibitors of apoptosis (IAP), but even when evaluated individually none of the class members reached a significant difference. MTOR and ARK inhibitors were unable to

achieve a significant enrichment as well, which was to be expected as the active proportion according to the volcano plot (Figure 50) was low.

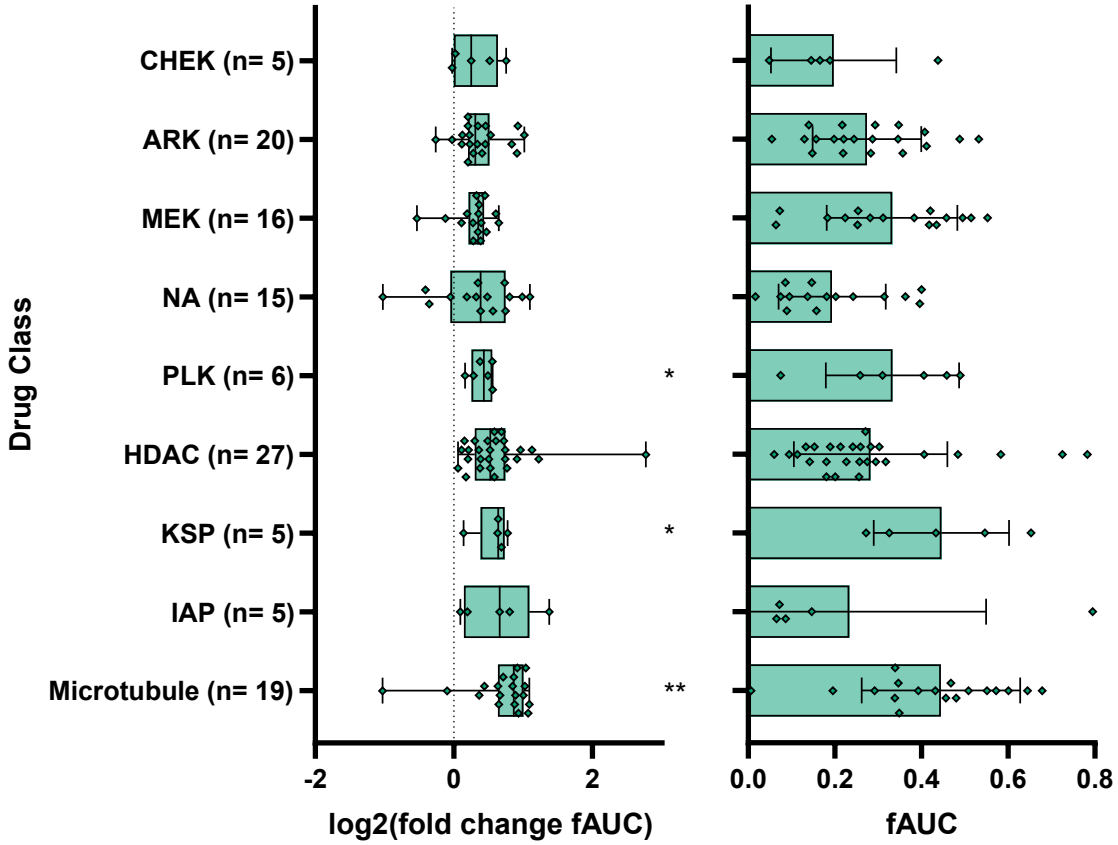

Figure 52. DCEA of the MT-s cohort of AT/RT-MYC cell lines vs. other AT/RT cell lines depicted as fold change per inhibitor (left) along with mean fAUC values in AT/RT-MYC MT-s cell lines (right). Drug classes consisting of at least four drugs and showing a fold change of 1.2 or larger are displayed. * = p-value < 0.05, ** = p-value < 0.01, MWU test. NA = Nucleoside Antimetabolite. IAP = Inhibitor of apoptosis.

3.2.5.2. Inter-entity subgroup-stratified analysis

To strengthen the potential of drugs with subgroup-specific inhibitory effects subgroup-stratified analyses were conducted comparing AT/RT-SHH and -MYC cell lines vs. medulloblastoma and glioblastoma cell lines. Starting off with AT/RT-SHH, another volcano plot was generated which is depicted in Figure 53. Drug classes consisting of at least three drugs which exceeded a fold change of 1.3 were highlighted. As expected, the analysis yielded multiple MEK inhibitors, as they were enriched across AT/RT cell lines. This applied to MDM2 inhibitors as well. On the other hand, the drug classes HSP90, Notch and BCL2 showed an increased proportion of active drugs, thus indicating superior activity in AT/RT-SHH cell lines even if compared to medulloblastoma and glioblastoma cell lines, i.e. their effect was specific intra- and inter-entity-wise.

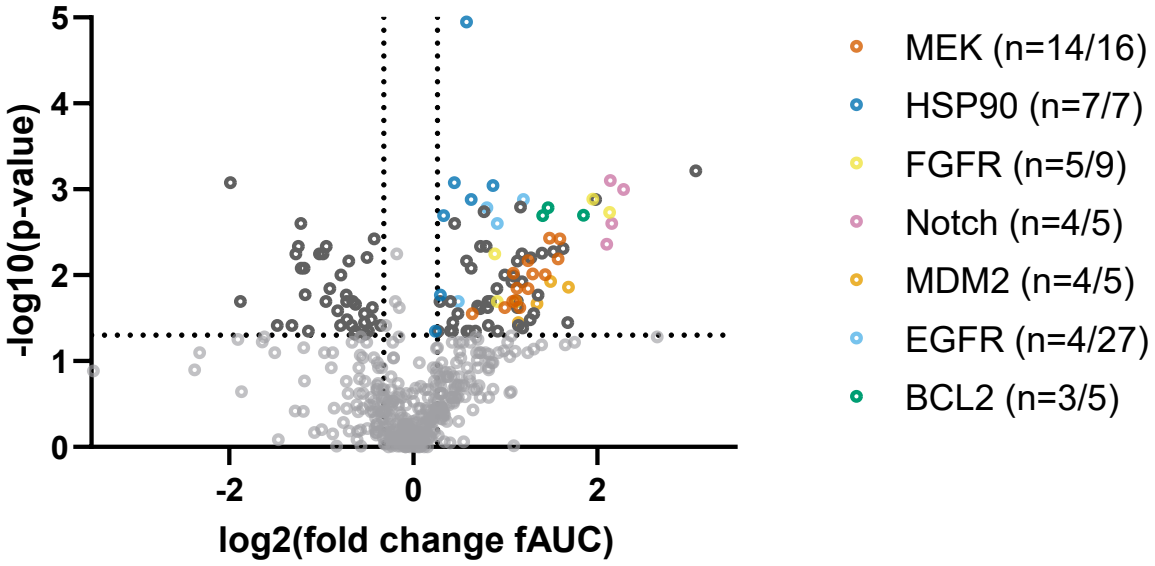

Figure 53. Volcano plot derived from the comparison of AT/RT-SHH cell lines with medulloblastoma and glioblastoma cell lines (MWU test). Multiple MEK, HSP90, FGFR, Notch, MDM2, EGFR and BCL2 inhibitors were found to be enriched.

In-depth analyses yielded MLN2480 as the prime candidate again (Table 14), however, with a lower fold change than in non-subgroup-stratified analyses (all AT/RT cell lines vs. medulloblastoma and glioblastoma cell lines), which, in corroboration of previous results, substantiated that RAF sensitivity was not AT/RT-SHH-mediated. The next six candidates were comprised of four Notch inhibitors (fold change 4.29-4.87), further supporting the specificity of Notch inhibition as a therapeutic target in the AT/RT-SHH subgroup. Additionally, a significantly increased activity was detected for Ro 08-2750 (Figure 54), which inhibits binding of nerve growth factor (NGF) to p75 neurotrophin receptor (p75NTR) and neurotrophic receptor tyrosine kinase 1 (NTRK1), thus being referred to as a TRK inhibitor. After manual review of the corresponding dose-response curves the same trend was seen in the comparison of AT/RT-SHH vs. AT/RT-MYC cell lines, but it had not been previously detected as it did not achieve a significant p-value. Ro 08-2750 showed a significant enrichment among non-stratified analyses (all AT/RT cell lines vs. medulloblastoma and glioblastoma cell lines) as well with a reduced fold change of 2.93 (vs. 3.95 here), thus indicating its effect might be subgroup-mediated. Shortly after, the BCL2 inhibitor ABT-199 turned up with a relatively high fold change of 3.60 (compared to 3.42 in intra-AT/RT analyses), promoting also BCL2 inhibitors as specific inhibitors in inter- and intra-entity analyses. Similarly, HSP90 inhibitors, which had been discovered among subgroup-stratified analyses as well, showed a stronger selectivity with a fold change of 1.82 (compared to 1.47 in intra-AT/RT analyses) in

case of the first appearing HSP90 inhibitor 17-AAG. The corresponding dose-response curves are depicted in Figure 54. In addition to previous analyses, the insulin-like growth factor 1 receptor (IGF-1R) inhibitor BMS-754807 (Figure 54) was significantly enriched, as compared to intra-AT/RT analyses in which it obtained a non-significant p-value (0.074), just like Ro 08-2750. Its fold change increased to 1.88 compared to 1.46 in intra-AT/RT analyses and 1.56 in non-stratified analyses (all AT/RT cell lines vs. medulloblastoma and glioblastoma cell lines). Furthermore, weak but significant increases of activity were detected for AZD-1208 (a Pim kinase (PIM) inhibitor), CC-401 hydrochloride, BI-78D3 (both c-Jun N-terminal kinase (JNK) inhibitors) and Brigatinib (an anaplastic lymphoma kinase (ALK) inhibitor). JAK inhibitors and AKT inhibitors both yielded lower fold changes, reinforcing the impression that they were of minor interest for further evaluation.

Table 14. Descriptive parameters of drugs with significantly enriched activity in AT/RT-SHH cell lines vs. medulloblastoma and glioblastoma cell lines, sorted for fold change. P-value based on an MWU test. Higher fAUC values indicate higher activity.

Inhibitor	Class	Fold change	fAUC	IC50 [nM]	Inhibition [%]	P-value
MLN2480	RAF	8.40	0.14 (0.07 - 0.28)	4803 (1433 - 6907)	71.7 (49.11 - 95.42)	0.001
MK-0752	Notch	4.87	0.06 (0.03 - 0.1)	1288 (9 - 3833)	18.76 (10.94 - 28.2)	0.001
BMS-708163	Notch	4.46	0.12 (0.04 - 0.22)	2025 (16 - 6550)	33.27 (22.45 - 46.75)	0.002
LY3039478	Notch	4.41	0.12 (0.05 - 0.18)	22 (9 - 37)	17.06 (7.03 - 23.11)	0.001
CH5183284	FGFR	4.38	0.25 (0.11 - 0.42)	1117 (201 - 2524)	67.7 (27.77 - 91.2)	0.002
Ro 4929097	Notch	4.29	0.12 (0.03 - 0.24)	46 (18 - 129)	19.83 (4.26 - 34.45)	0.004
Ro 08-2750	TRK	3.95	0.18 (0.06 - 0.24)	5089 (2327 - 13806)	98.88 (98.46 - 99.22)	0.001
E-3810	FGFR	3.86	0.15 (0.07 - 0.27)	3086 (927 - 4545)	61.61 (37.82 - 87.97)	0.001
ABT-199	BCL2	3.60	0.17 (0.08 - 0.25)	2761 (994 - 4063)	63.98 (39.41 - 92.11)	0.002
RG7388	MDM2	3.22	0.42 (0.3 - 0.57)	68 (23 - 115)	71 (54.6 - 89.83)	0.014
Tirapazamine	Others	3.20	0.06 (0.02 - 0.12)	5869 (4290 - 10816)	37.53 (15.28 - 67.77)	0.036
ZM 306416 hcl	VEGFR	3.09	0.05 (0.02 - 0.06)	4620 (1624 - 10457)	22.76 (17.75 - 30.01)	0.005
AS703026	MEK	3.01	0.32 (0.15 - 0.42)	460 (2 - 1119)	70.69 (15.61 - 89.86)	0.004
GDC-0623	MEK	2.98	0.42 (0.11 - 0.57)	446 (11 - 2369)	74.55 (38.51 - 92.94)	0.006
GDC-0994	ERK	2.87	0.13 (0.08 - 0.2)	5236 (2984 - 6729)	78.47 (36.97 - 94.2)	0.005
AMG-232	MDM2	2.81	0.41 (0.26 - 0.54)	120 (46 - 290)	78.68 (62.63 - 93.58)	0.012
Ro 5126766	MEK	2.79	0.25 (0.1 - 0.4)	748 (71 - 3477)	54.99 (37.45 - 72.2)	0.004
ABT-737	BCL2	2.76	0.37 (0.29 - 0.47)	510 (202 - 817)	92.42 (84.01 - 98.96)	0.002
TAK-733	MEK	2.70	0.42 (0.09 - 0.55)	508 (23 - 2580)	76.7 (34.31 - 93.18)	0.010
Navitoclax	BCL2	2.65	0.48 (0.36 - 0.66)	268 (29 - 569)	98.05 (96.05 - 99)	0.002
AZD-1208	PIM	2.63	0.15 (0.07 - 0.25)	45 (29 - 72)	24.09 (11.81 - 36.91)	0.006
Pazopanib hcl	CSF1R	2.56	0.1 (0.04 - 0.17)	3941 (1811 - 7980)	50.13 (16.71 - 81.91)	0.017
MI-773	MDM2	2.54	0.33 (0.25 - 0.43)	841 (290 - 1990)	87.15 (72.09 - 95.52)	0.021
R788 d h	SYK	2.48	0.14 (0.04 - 0.29)	3406 (12 - 9059)	58.16 (5.94 - 85.46)	0.028
PD0325901	MEK	2.45	0.32 (0.08 - 0.44)	765 (91 - 2816)	73.31 (33.69 - 93.21)	0.010
CC-401 hcl	JNK	2.43	0.08 (0.05 - 0.12)	6291 (5194 - 7993)	52.81 (41.01 - 70.67)	0.006
Lenvatinib	KIT	2.41	0.12 (0.02 - 0.24)	1439 (836 - 2136)	38.38 (6.12 - 68.06)	0.033
Trametinib	MEK	2.38	0.42 (0.08 - 0.56)	123 (29 - 369)	71.74 (21.94 - 94.55)	0.007
Refametinib	MEK	2.37	0.29 (0.09 - 0.42)	1169 (100 - 5382)	70.15 (50.06 - 87.66)	0.014
Poziotinib	EGFR	2.29	0.26 (0.2 - 0.39)	2303 (697 - 3331)	91.3 (84.09 - 97.5)	0.001
ZM 323881 hcl	VEGFR	2.28	0.08 (0 - 0.14)	5894 (4124 - 9395)	52.49 (0 - 80.79)	0.041
RGFP966	HDAC	2.27	0.15 (0.08 - 0.26)	3283 (1737 - 5042)	67.19 (47.57 - 93.88)	0.006
(-)-Terreic acid	BTK	2.27	0.16 (0.07 - 0.22)	6094 (2760 - 13226)	96.82 (92.78 - 98.75)	0.012
Nedaplatin	DNA/RNA S	2.24	0.46 (0.34 - 0.54)	309 (124 - 753)	98.69 (98.24 - 98.86)	0.002
MEK162	MEK	2.23	0.2 (0.03 - 0.3)	1349 (777 - 2107)	59.37 (13.1 - 88.42)	0.024
CGP 53353	PKC	2.21	0.09 (0.04 - 0.26)	7206 (1910 - 12932)	55.69 (31.77 - 95.79)	0.039
RG7112	MDM2	2.20	0.26 (0.17 - 0.36)	2432 (826 - 4373)	94.89 (87.74 - 98.84)	0.036
Ruboxistaurin hcl	PKC	2.19	0.4 (0.27 - 0.56)	132 (49 - 284)	75.86 (47.47 - 96.65)	0.024
LB-100	Phosphatase	2.19	0.27 (0.2 - 0.32)	1508 (110 - 3664)	84.56 (54.29 - 95.86)	0.007
Dabrafenib mesylate	RAF	2.19	0.06 (0.02 - 0.15)	1360 (57 - 3037)	19.55 (4.66 - 30.36)	0.020
Ro 4987655	MEK	2.18	0.32 (0.09 - 0.45)	283 (47 - 464)	70.2 (24.99 - 90.72)	0.014
AZD-4547	FGFR	2.16	0.32 (0.13 - 0.54)	1800 (68 - 6266)	84.85 (61.53 - 97.54)	0.020
Selumetinib	MEK	2.16	0.16 (0.03 - 0.21)	1744 (243 - 4374)	48.9 (16.1 - 80.13)	0.020

Inhibitor	Class	Fold change	fAUC	IC50 [nM]	Inhibition [%]	P-value
Endoxifen (E-isomer)	ER	2.13	0.13 (0.08 - 0.19)	7359 (3259 - 11267)	98.15 (93.99 - 99.25)	0.010
U0126	MEK	2.12	0.05 (0.03 - 0.09)	5753 (1806 - 9749)	35.16 (13.16 - 49.82)	0.009
AZD-8330	MEK	2.11	0.43 (0.1 - 0.57)	122 (21 - 355)	75.09 (28.02 - 93.45)	0.020
API-2	AKT	2.10	0.31 (0.2 - 0.55)	97 (81 - 118)	57.7 (38.06 - 98.26)	0.012
Cobimetinib	MEK	1.99	0.3 (0.12 - 0.48)	2120 (172 - 8447)	91.09 (80.94 - 99.45)	0.024
PCI-32765	BTK	1.99	0.11 (0.08 - 0.15)	6522 (2502 - 9460)	68.49 (49.76 - 85.17)	0.010
Icaritin	EM	1.89	0.08 (0.01 - 0.13)	11747 (7670 - 23102)	86.1 (71.33 - 95.41)	0.045
CO-1686	EGFR	1.88	0.25 (0.19 - 0.32)	2063 (837 - 3752)	93.61 (82.92 - 98.48)	0.003
LY2784544	FGFR	1.88	0.2 (0.11 - 0.32)	2218 (1028 - 4158)	76.65 (40.71 - 97.18)	0.020
BMS-754807	IGF-1R	1.88	0.51 (0.42 - 0.66)	57 (10 - 109)	82.42 (65 - 94.46)	0.014
LY2874455	FGFR	1.85	0.61 (0.35 - 0.86)	134 (4 - 578)	92.28 (84.85 - 98.23)	0.006
17-AAG	HSP90	1.82	0.63 (0.53 - 0.7)	36 (16 - 71)	96.85 (90.2 - 99.11)	0.001
5-Azacytidine	NA	1.79	0.16 (0.11 - 0.18)	4692 (3964 - 5786)	86 (73.24 - 94.37)	0.020
Verteporfin	YAP	1.76	0.16 (0.12 - 0.19)	5273 (3602 - 8362)	96.39 (88.3 - 99.18)	0.039
PND-1186	FAK	1.75	0.22 (0.18 - 0.3)	1838 (884 - 3024)	76.98 (60.1 - 92.66)	0.020
AZ5104	EGFR	1.74	0.35 (0.25 - 0.47)	1042 (272 - 2066)	98.38 (97.18 - 99.33)	0.002
GSK1059615	MTOR	1.73	0.26 (0.21 - 0.37)	2233 (685 - 3439)	94.81 (87.39 - 98.01)	0.005
Entrectinib	ALK	1.70	0.2 (0.15 - 0.26)	3779 (2001 - 5187)	98.44 (96.38 - 99.02)	0.002
LY3009120	RAF	1.66	0.3 (0.21 - 0.38)	569 (199 - 1319)	75.11 (66.88 - 83.44)	0.005
Brigatinib	ALK	1.65	0.14 (0.09 - 0.19)	5079 (3595 - 7267)	82.45 (58.72 - 94.97)	0.025
Bendamustine hcl	DNA A/C	1.62	0.06 (0.03 - 0.13)	6320 (4272 - 8844)	35.75 (22.45 - 65.44)	0.023
Melphalan	DNA A/C	1.60	0.12 (0.06 - 0.21)	3612 (1522 - 6575)	54.98 (37.03 - 78.61)	0.045
Arctigenin	MEK	1.56	0.1 (0.07 - 0.15)	1025 (156 - 1888)	29.86 (21.03 - 40.08)	0.028
CGK 733	ATM/ATR	1.55	0.21 (0.17 - 0.24)	3289 (2349 - 4672)	98.62 (97.87 - 99.2)	0.008
BIIB021	HSP90	1.55	0.44 (0.35 - 0.52)	282 (98 - 624)	96.02 (87.7 - 99.23)	0.001
AVL-292	BTK	1.53	0.21 (0.13 - 0.3)	3405 (1105 - 7337)	90.57 (79.07 - 96.91)	0.045
ZM 449829	JAK	1.50	0.1 (0.04 - 0.12)	8052 (4786 - 10748)	85.22 (24.12 - 99.53)	0.045
Alvespimycin hcl	HSP90	1.49	0.8 (0.73 - 0.85)	6 (3 - 11)	99.14 (98.54 - 99.42)	0.000
JIB 04	JMJD	1.49	0.47 (0.35 - 0.61)	230 (42 - 753)	94.5 (89.15 - 97.59)	0.007
AZD-9291	EGFR	1.40	0.23 (0.2 - 0.29)	3225 (2254 - 3893)	99.02 (98.27 - 99.37)	0.020
PKC412	PKC	1.40	0.29 (0.22 - 0.42)	605 (354 - 1019)	74.24 (55.86 - 94.22)	0.028
BI-78D3	JNK	1.36	0.32 (0.29 - 0.35)	1064 (783 - 1474)	99.2 (99.12 - 99.29)	0.003
Ganetespib	HSP90	1.36	0.7 (0.6 - 0.74)	17 (13 - 21)	95.22 (87.86 - 98.28)	0.001
Ryuvidine	CDK	1.35	0.19 (0.16 - 0.26)	4139 (1927 - 5311)	96.84 (95.28 - 98.37)	0.036
ZSTK474	PI3K	1.34	0.27 (0.19 - 0.36)	447 (252 - 665)	63.6 (52.42 - 80.97)	0.045
Ponatinib	BCR-ABL	1.32	0.37 (0.31 - 0.44)	754 (337 - 1448)	99.28 (99.04 - 99.45)	0.020
Brivanib	VEGFR	1.32	0.05 (0.02 - 0.09)	6579 (2 - 9819)	38.8 (2.27 - 65.19)	0.045
NVP-AUY922	HSP90	1.25	0.81 (0.72 - 0.86)	5 (4 - 6)	96.32 (89.37 - 98.92)	0.002
AT13387	HSP90	1.22	0.5 (0.39 - 0.55)	157 (76 - 358)	96.06 (86.91 - 99.22)	0.017
IMD 0354	IKK	1.22	0.33 (0.28 - 0.4)	816 (401 - 1306)	97.41 (93.88 - 99.3)	0.020
GSK2126458	MTOR	1.21	0.6 (0.49 - 0.7)	31 (9 - 46)	91.52 (77.41 - 96.78)	0.045
Debio 0932	HSP90	1.18	0.37 (0.32 - 0.42)	566 (347 - 963)	96.61 (89.51 - 98.59)	0.045

(…) = Minimum and maximum values. d h = disodium hexahydrate. DNA A/C = DNA Alkylator/Crosslinker. DNA/RNA S = DNA/RNA Synthesis. EM = Endogenous Metabolite. ER = Estrogen Receptor. TP = Topoisomerase

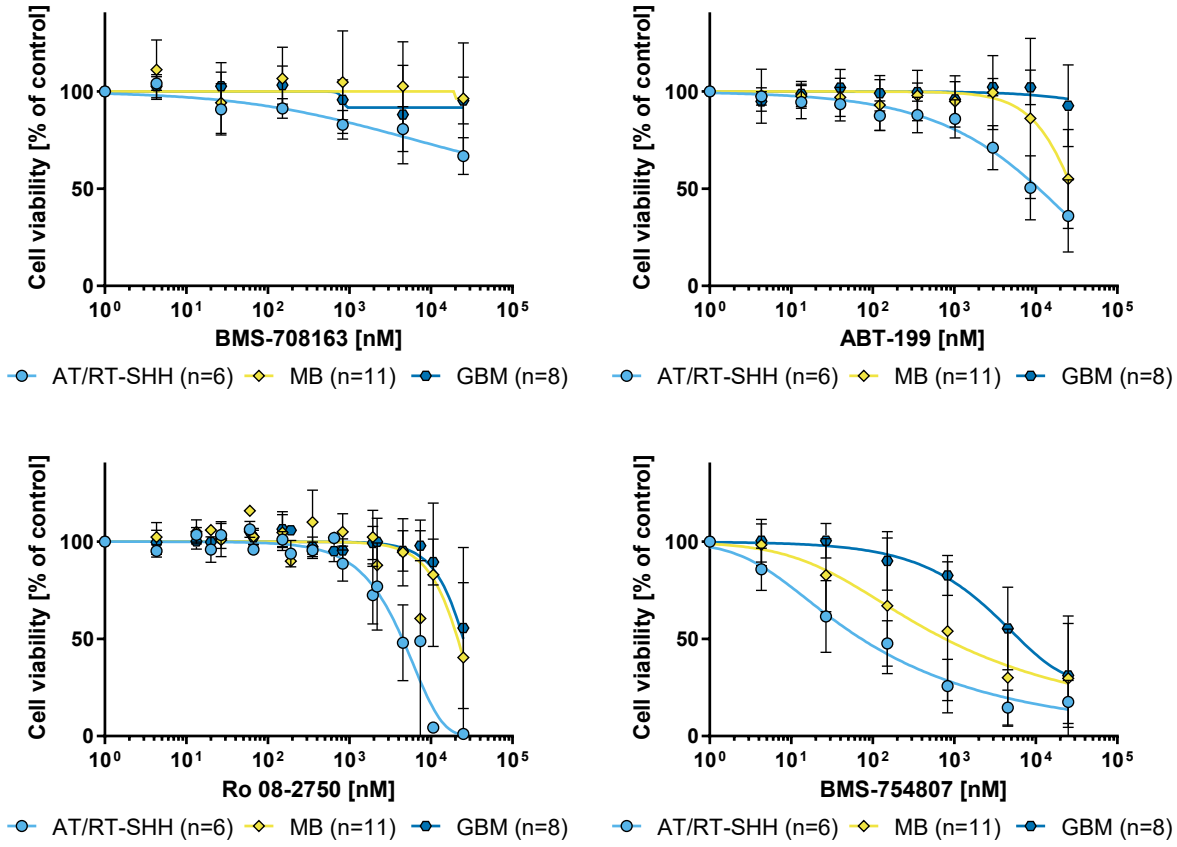

Figure 54. Dose-response curves of selected AT/RT-SHH-specific inhibitors. BMS-708163 = Notch inhibitor. ABT-199 = BCL2 inhibitor. Ro 08-2750 = TRK inhibitor. BMS-754807 = IGF-1R inhibitor.

Group-wise analyses validated a significant difference for Notch inhibitors as well as BCL2 and HSP90 inhibitors (Figure 55). Moreover, a discrete increase in fold change of IGF-1R inhibitors from 1.22 (all AT/RT cell lines vs. medulloblastoma and glioblastoma cell lines) to 1.38 (AT/RT-SHH cell lines vs. medulloblastoma and glioblastoma cell lines) was detected yielding a significant p-value, which was in line with the individual evaluation of the IGF-1R inhibitor BMS-754807. There was no further enrichment of other classes or enrichment of classes that had not been discovered before.

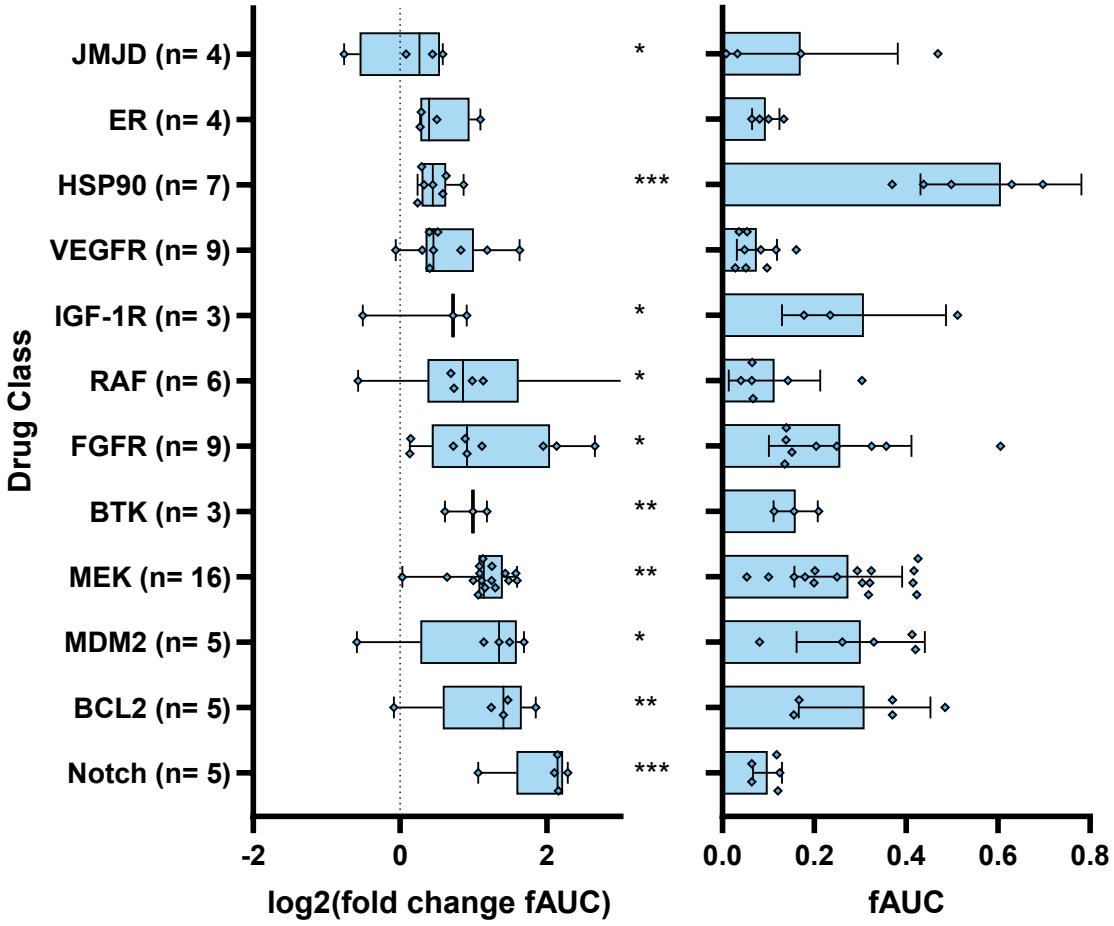

Figure 55. DCEA of AT/RT-SHH cell lines vs. medulloblastoma and glioblastoma cell lines depicted as fold change per inhibitor (left) along with mean fAUC values in AT/RT-SHH cell lines (right). Drug classes consisting of at least three drugs and showing a fold change of 1.3 or larger are displayed. * = p-value < 0.05, ** = p-value < 0.01, *** = p-value < 0.001, MWU test. ER = Estrogen Receptor.

As a next step, AT/RT-MYC cell lines were compared to medulloblastoma and glioblastoma cell lines to validate intra-AT/RT observations made in this subset. The overlap compared to the non-stratified analyses (all AT/RT cell lines vs. medulloblastoma and glioblastoma cell lines) was quite extensive, as indicated by few changes in the volcano plot (Figure 56).

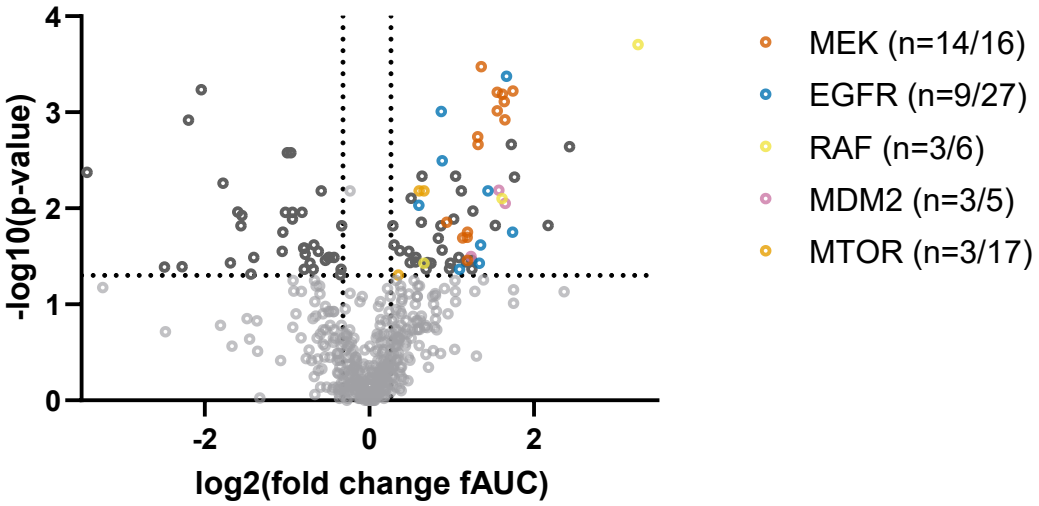

Figure 56. Volcano plot derived from the comparison of AT/RT-MYC cell lines with medulloblastoma and glioblastoma cell lines (MWU test). Multiple MEK, EGFR, RAF, MDM2 and MTOR inhibitors were found to be enriched.

A detailed evaluation using Table 15 showed that only minor differences were measured among EGFR and VEGFR inhibitors, which partially displayed a slight increase of sensitivity compared to non-stratified analyses (all AT/RT cell lines vs. medulloblastoma and glioblastoma cell lines). Pelitinib remained significantly more active in AT/RT-MYC cell lines even when compared to medulloblastoma and glioblastoma cell lines, indicating an intra- and inter-entity-wise enrichment with a fold change of 1.55 and 1.52, respectively. Furthermore, a significant enrichment was detected for the Sirtuin (SIRT) inhibitor Tenovin-1, which showed a trend in non-stratified analyses (all AT/RT cell lines vs. medulloblastoma and glioblastoma cell lines) but did not yield a significant p-value (0.11). This is interesting as Tenovin-1, besides its HDAC inhibitory activity, inhibits MDM2-mediated degradation of p53 [141], which is in line with increased activity of MDM2 inhibitors in AT/RT cell lines as elaborated above. However, the fold change of Tenovin-1 was quite low. Dose-response curves of Tenovin-1 and Pelitinib are depicted in Figure 57. Notably, microtubule inhibitors did not reach a significant p-value in this comparison.

Table 15. Descriptive parameters of drugs with significantly enriched activity in AT/RT-MYC cell lines vs. medulloblastoma and glioblastoma cell lines, sorted for fold change. P-value based on an MWU test. Higher fAUC values indicate higher activity.

Inhibitor	Class	Fold change	fAUC	IC50 [nM]	Inhibition [%]	P-value
MLN2480	RAF	9.60	0.16 (0.06 - 0.29)	3817 (1136 - 7067)	74.19 (44.58 - 94.01)	0.0002
ZM 306416 hcl	VEGFR	5.40	0.08 (0.01 - 0.14)	3736 (1421 - 13988)	35.06 (3.84 - 53.78)	0.002
GSK126	HMT	4.50	0.05 (0 - 0.1)	9122 (108 - 14461)	51.88 (0 - 97.71)	0.015
CH5183284	FGFR	3.39	0.19 (0.06 - 0.47)	2230 (192 - 8176)	57.99 (33.92 - 96.65)	0.005
GDC-0623	MEK	3.35	0.48 (0.36 - 0.67)	69 (7 - 139)	79.7 (53.48 - 90.67)	0.001
AZD-3759	EGFR	3.34	0.11 (0.01 - 0.2)	1179 (363 - 4550)	31.48 (3.06 - 53.61)	0.018
CX-5461	DNA/RNA S	3.30	0.16 (0.07 - 0.24)	1178 (147 - 2599)	46.7 (14.73 - 62.51)	0.002
Poziotinib	EGFR	3.18	0.35 (0.19 - 0.52)	1021 (64 - 3176)	87.58 (67.13 - 98.78)	0.000
RG7388	MDM2	3.14	0.41 (0.23 - 0.54)	95 (40 - 174)	71.04 (42.91 - 92.51)	0.009
AS703026	MEK	3.14	0.33 (0.25 - 0.58)	680 (14 - 1584)	79.13 (57.12 - 90.59)	0.001
Ro 5126766	MEK	3.11	0.28 (0.17 - 0.51)	309 (34 - 789)	56.16 (34.4 - 83.43)	0.001
Refametinib	MEK	3.06	0.38 (0.28 - 0.56)	314 (36 - 673)	80.4 (54.59 - 92.76)	0.001
LGX818	RAF	3.06	0.1 (0.02 - 0.26)	1099 (656 - 2775)	30.65 (6.38 - 73.42)	0.008
AMG-232	MDM2	2.97	0.44 (0.28 - 0.57)	84 (51 - 165)	80.11 (55.26 - 93.72)	0.006
TAK-733	MEK	2.94	0.45 (0.32 - 0.67)	158 (8 - 370)	82.47 (54.24 - 92.82)	0.001
PD0325901	MEK	2.93	0.38 (0.3 - 0.59)	408 (15 - 977)	80.74 (50.94 - 93.98)	0.001
E-3810	FGFR	2.89	0.11 (0.04 - 0.29)	1756 (451 - 3722)	38.79 (17.13 - 92.64)	0.015
BMS-599626 hcl	EGFR	2.71	0.09 (0.01 - 0.15)	6304 (1304 - 22915)	51.05 (35.3 - 66.14)	0.007
Trametinib	MEK	2.56	0.45 (0.32 - 0.78)	142 (4 - 670)	73.79 (53.95 - 97.55)	0.0003
BMS-690514	EGFR	2.55	0.21 (0.01 - 0.4)	5647 (58 - 20810)	60.15 (29.1 - 88.43)	0.024
BIBX 1382	EGFR	2.52	0.11 (0 - 0.22)	6474 (1157 - 24389)	48.62 (27.92 - 78.43)	0.037
Ro 4987655	MEK	2.50	0.37 (0.29 - 0.56)	321 (19 - 625)	77.92 (51.75 - 91.41)	0.002
AZD-8330	MEK	2.49	0.5 (0.38 - 0.72)	60 (5 - 124)	82.8 (58.01 - 93.28)	0.002
Salinomycin	WNT	2.39	0.38 (0.21 - 0.54)	794 (70 - 3713)	97.03 (91.87 - 98.79)	0.011
Luteolin	EM	2.38	0.05 (0 - 0.1)	10531 (5510 - 22202)	49.19 (29.42 - 72.67)	0.043
R788 d h	SYK	2.37	0.13 (0.01 - 0.3)	6505 (1403 - 16131)	66.74 (18.05 - 98.23)	0.035
MI-773	MDM2	2.35	0.31 (0.19 - 0.4)	919 (322 - 1628)	81.43 (59.92 - 93.81)	0.032
CI-1040	MEK	2.29	0.2 (0 - 0.39)	899 (20 - 2409)	53.11 (0 - 87.46)	0.035
MEK162	MEK	2.29	0.21 (0.06 - 0.5)	1995 (59 - 4714)	55.75 (26.14 - 87.57)	0.018
U0126	MEK	2.28	0.06 (0.01 - 0.14)	5288 (921 - 14001)	29.52 (8.72 - 71.09)	0.020
GDC-0994	ERK	2.26	0.11 (0.01 - 0.31)	3686 (306 - 8712)	35.42 (10.78 - 76.97)	0.036
Selumetinib	MEK	2.20	0.16 (0.05 - 0.43)	1658 (134 - 3405)	42.39 (18.6 - 80.03)	0.020
Fenretinide	RAR/RXR	2.17	0.26 (0.14 - 0.33)	2341 (852 - 5981)	99.03 (98.1 - 99.34)	0.007
Iressa	EGFR	2.14	0.11 (0.02 - 0.2)	5732 (971 - 11957)	53.38 (20.33 - 84.09)	0.043
Ruboxistaurin hcl	PKC	2.13	0.39 (0.24 - 0.49)	170 (48 - 400)	76.86 (55.41 - 95.07)	0.032
LB-100	Phosphatase	2.07	0.26 (0.15 - 0.36)	2013 (384 - 3768)	91.23 (71.78 - 98.73)	0.005
5-Azacytidine	NA	2.03	0.18 (0.08 - 0.29)	4073 (1484 - 7870)	86.65 (67.18 - 97.48)	0.013
Voreloxin hcl	TP	1.98	0.19 (0.08 - 0.37)	1736 (31 - 3230)	54.19 (28.41 - 77.01)	0.037
Xanthohumol	EM	1.97	0.13 (0.02 - 0.26)	6975 (1877 - 20897)	77.04 (29.62 - 98.18)	0.043
Cobimetinib	MEK	1.92	0.29 (0.14 - 0.53)	1585 (65 - 5794)	82.75 (63.54 - 99.04)	0.014
Endoxifen (E-isomer)	ER	1.85	0.12 (0.08 - 0.15)	7257 (5238 - 9664)	88.92 (74.4 - 99.29)	0.027
CO-1686	EGFR	1.84	0.24 (0.21 - 0.33)	2218 (1004 - 3238)	96.25 (86.38 - 99.1)	0.003
AZ5104	EGFR	1.83	0.37 (0.23 - 0.48)	1042 (177 - 3138)	98.11 (93.54 - 99.3)	0.001
RX-3117	NA	1.82	0.28 (0.18 - 0.41)	640 (298 - 1916)	75 (58.04 - 96.09)	0.015
Nedaplatin	DNA/RNA S	1.79	0.37 (0.28 - 0.47)	661 (243 - 1020)	98.74 (98.64 - 98.86)	0.021
Verteporfin	YAP	1.68	0.15 (0.12 - 0.2)	5652 (3299 - 8056)	95.02 (88.72 - 99.24)	0.037
RGFP966	HDAC	1.63	0.11 (0.05 - 0.23)	3107 (272 - 4869)	48.23 (10.33 - 89.62)	0.037
Tenovin-1	SIRT	1.61	0.21 (0.09 - 0.34)	1303 (463 - 3087)	66.57 (37 - 92.43)	0.043
LY3009120	RAF	1.59	0.29 (0.1 - 0.51)	371 (58 - 743)	65.46 (25.62 - 91.81)	0.037
BEZ235	MTOR	1.58	0.29 (0.19 - 0.38)	348 (104 - 1055)	62.9 (52.62 - 83.96)	0.007
AVL-292	BTK	1.56	0.21 (0.16 - 0.26)	2597 (1260 - 4413)	87.2 (66.67 - 99.37)	0.005
Tamoxifen	ER	1.55	0.1 (0.07 - 0.14)	9464 (5931 - 13431)	93.58 (84.33 - 98.91)	0.014
GSK1059615	MTOR	1.52	0.23 (0.18 - 0.28)	2535 (1677 - 3889)	89.18 (73.26 - 97.52)	0.007
Pelitinib	EGFR	1.52	0.39 (0.26 - 0.47)	711 (162 - 2275)	98.54 (96.97 - 99.26)	0.009
Toceranib phosphate	KIT	1.48	0.1 (0.07 - 0.15)	5976 (5099 - 7312)	71.35 (41.9 - 96.12)	0.032
Cisplatin	DNA A/C	1.48	0.05 (0.02 - 0.09)	1090 (40 - 2664)	15.75 (6.59 - 43.17)	0.036
ZSTK474	PI3K	1.42	0.28 (0.23 - 0.32)	393 (244 - 586)	64.69 (57.06 - 80.19)	0.008
Ellipticine hcl	TP	1.41	0.22 (0.18 - 0.34)	3316 (1016 - 5006)	98.66 (96.67 - 99.15)	0.037
AZD-8186	PI3K	1.40	0.26 (0.16 - 0.36)	1694 (440 - 4099)	81.83 (65.51 - 95.91)	0.028
Brivanib	VEGFR	1.29	0.05 (0.02 - 0.14)	7209 (1079 - 9965)	35.75 (16.4 - 88.81)	0.028
OSI-027	MTOR	1.28	0.27 (0.2 - 0.35)	463 (220 - 899)	63.95 (43.52 - 87.74)	0.049
IMD 0354	IKK	1.23	0.33 (0.27 - 0.41)	912 (456 - 1623)	97.62 (90.79 - 99.44)	0.024
BMS-214662	FTase	1.22	0.48 (0.42 - 0.56)	177 (88 - 240)	96.02 (83.53 - 99.42)	0.015

(…) = Minimum and maximum values. d h = disodium hexahydrate. DNA A/C = DNA Alkylator/Crosslinker. DNA/RNA S = DNA/RNA Synthesis. EM = Endogenous Metabolite. TP = Topoisomerase

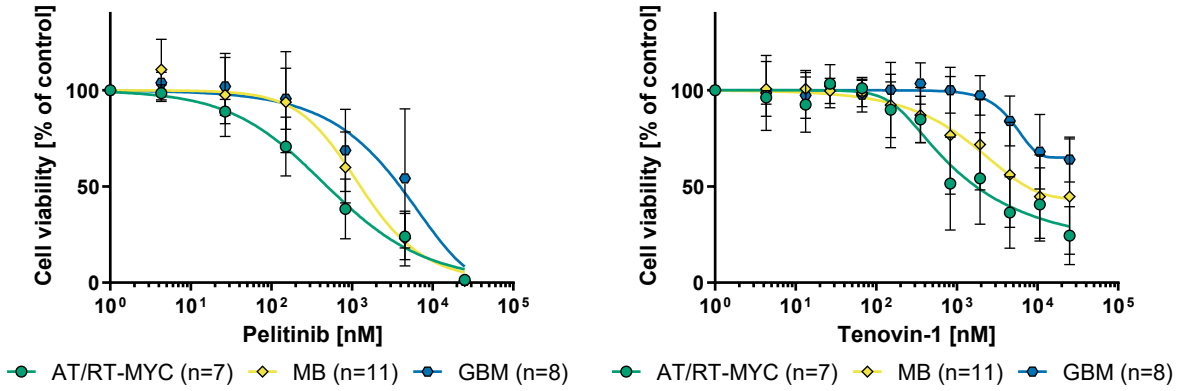

Figure 57. Dose-response curves of selected AT/RT-MYC-specific inhibitors. Pelitinib = EGFR inhibitor. Tenovin-1 = SIRT inhibitor.

A group-wise analysis showed a slightly higher sensitivity of AT/RT-MYC cell lines vs. MEK inhibitors with a fold change of 2.67 vs. 2.36 in non-stratified analyses (all AT/RT cell lines vs. medulloblastoma and glioblastoma cell lines) as well as RAF inhibitors with a fold change of 2.3 vs. 1.96 in non-stratified analyses (all AT/RT cell lines vs. medulloblastoma and glioblastoma cell lines), as depicted in Figure 58. Classes with further enrichment were not detected.

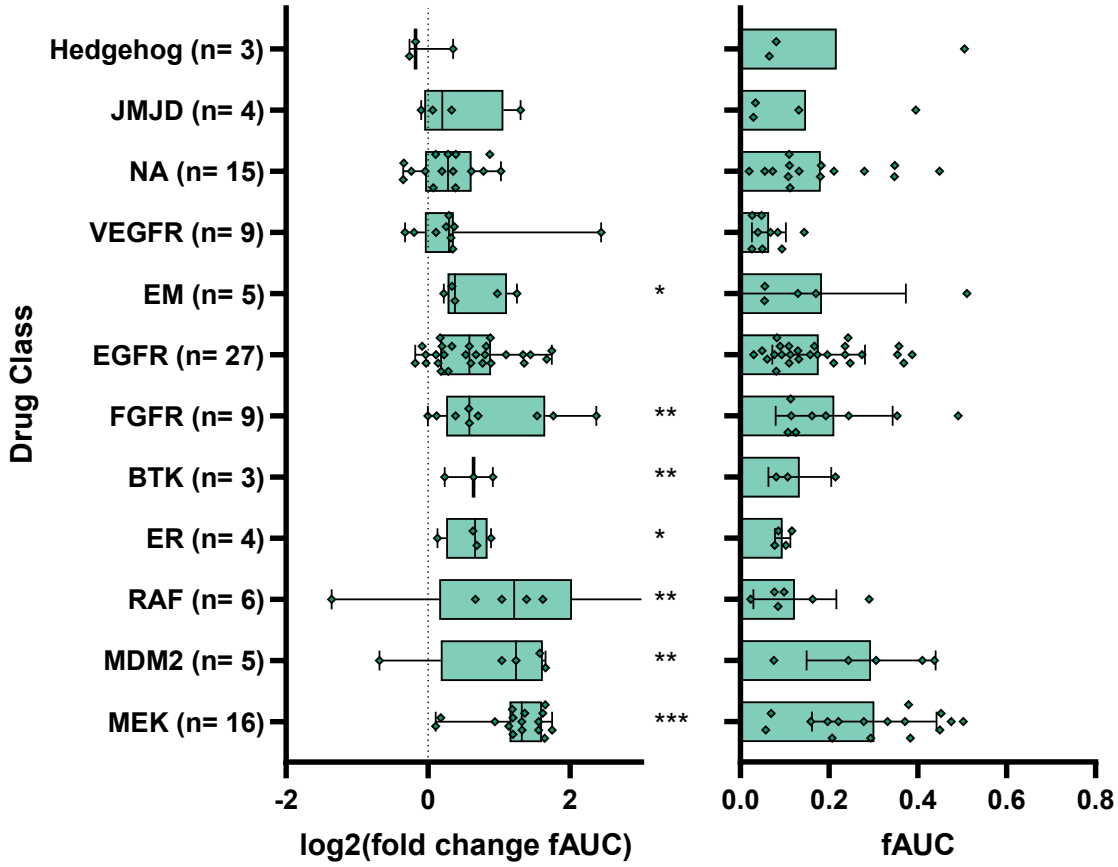

Figure 58. DCEA of AT/RT-MYC cell lines vs. medulloblastoma and glioblastoma cell lines depicted as fold change per inhibitor (left) along with mean fAUC values in AT/RT-MYC cell lines (right). Drug classes consisting of at least three drugs and showing a fold change of 1.2 or larger are displayed. * = p-value < 0.05, ** = p-value < 0.01, *** = p-value < 0.001, MWU test. EM = Endogenous Metabolite. ER = Estrogen Receptor. NA = Nucleoside Antimetabolite.

Lastly, a comparison of the MT-s cohort of AT/RT-MYC cell lines to medulloblastoma and glioblastoma cell lines was performed to validate the detected enrichments. The volcano plot already implied that the proportion of enriched microtubule inhibitors was drastically lower and neither were there many KSP inhibitors enriched (Figure 59).

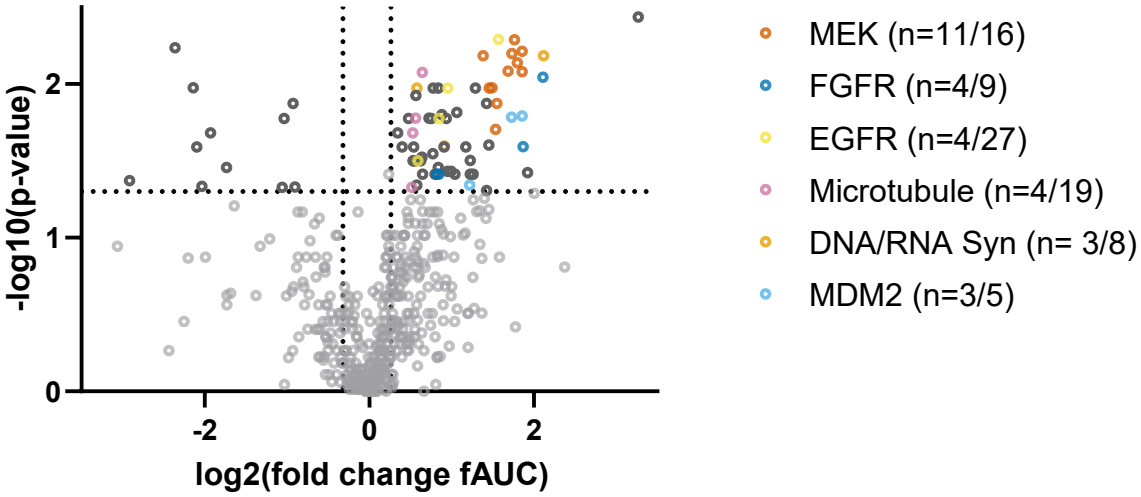

Figure 59. Volcano plot derived from the comparison of AT/RT-MYC cell lines (MT-s cohort) with medulloblastoma and glioblastoma cell lines (MWU test). Multiple MEK, FGFR, EGFR, DNA/RNA synthesis and MDM2 inhibitors but only few microtubule inhibitors were found to be enriched.

Further in-depth analyses using Table 16 showed that CX-5461 (Figure 60) was the top hit, disregarding MLN2480, which did not yield any additional enrichment. CX-5461 had previously been detected among non-stratified analyses (all AT/RT cell lines vs. medulloblastoma and glioblastoma cell lines) but exhibited further enrichment with an increase of its fold change from 3.23 to 4.34. However, the difference measured between AT/RT-SHH and AT/RT-MYC cell lines was not significant, neither when the whole subgroup (p-value 0.83) nor the MT-s cohort (p-value 0.14) was used. Furthermore, the class of IAP had shown a trend to be enriched in the MT-s cohort of AT/RT-MYC cell lines in intra-AT/RT analyses. Compared to medulloblastoma and glioblastoma cell lines, an IAP class member, namely Birinapant (Figure 60), finally yielded a slightly significant result (p-value 0.038) with a fold change of 3.79. Moreover, Salinomycin (antibiotic/WNT inhibitor), Voreloxin hydrochloride (TP inhibitor), BEZ235 (MTOR inhibitor), Tamoxifen (selective estrogen receptor modulator) and AZD-8186 (selective PI3K inhibitor) exhibited a significant enrichment with a mildly increased fold change in comparison to non-stratified analyses (all AT/RT cell lines vs. medulloblastoma and glioblastoma cell lines). However, the enrichment appeared to be too neat to indicate a subgroup-related mechanism. Two of the previously discovered ARK inhibitors, AMG-900 and AZD-1152-HQPA, showed similar fold changes in intra- and inter-entity analyses. Among the class of microtubule inhibitors, only four (out of 19) candidates remained significantly enriched with a reduced fold change, i.e., the fold change of Lexibulin dropped from 2.1 to 1.43 and the fold change

of Ombrabulin hydrochloride (Figure 60) dropped from 2.05 to 1.44. The other two candidates, ABT-751 and Plinabulin (Figure 60), obtained a milder reduction of their fold changes (1.88 to 1.56 and 1.64 to 1.48, respectively). Interestingly, the only KSP inhibitor with a significant enrichment, which was Dimethylenastron, did not exhibit a relevant decrease of its fold change (reduction from 1.56 to 1.49). The remaining fold changes of drug classes acting through disruption of mitosis appeared equal on average comparing the results from inter- and intra-entity analyses.

Table 16. Descriptive parameters of drugs with significantly enriched activity in AT/RT-MYC cell lines (MT-s cohort) vs. medulloblastoma and glioblastoma cell lines, sorted for fold change. P-value based on an MWU test. Higher fAUC values indicate higher activity.

Inhibitor	Class	Fold change	fAUC	IC50 [nM]	Inhibition [%]	P-value
MLN2480	RAF	9.63	0.16 (0.06 - 0.29)	4267 (1136 - 7067)	74.22 (44.58 - 94.01)	0.004
CX-5461	DNA/RNA S	4.34	0.22 (0.18 - 0.24)	943 (324 - 1995)	59.45 (55.28 - 62.51)	0.007
CH5183284	FGFR	4.32	0.25 (0.11 - 0.47)	1413 (192 - 3571)	67.3 (33.92 - 96.65)	0.009
Birinapant	IAP	3.79	0.15 (0.03 - 0.26)	673 (4 - 1446)	34.61 (8.01 - 65.97)	0.038
E-3810	FGFR	3.65	0.14 (0.04 - 0.29)	1667 (1134 - 2765)	49.27 (17.13 - 92.64)	0.026
AS703026	MEK	3.63	0.38 (0.25 - 0.58)	612 (14 - 1121)	82.93 (71.18 - 90.59)	0.008
GDC-0623	MEK	3.62	0.51 (0.36 - 0.67)	62 (7 - 139)	83.35 (63 - 90.67)	0.006
RG7388	MDM2	3.62	0.47 (0.37 - 0.54)	69 (40 - 105)	79.84 (57.22 - 92.51)	0.016
Ro 5126766	MEK	3.48	0.31 (0.17 - 0.51)	290 (34 - 789)	58.95 (34.4 - 83.43)	0.007
Refametinib	MEK	3.40	0.42 (0.3 - 0.56)	261 (36 - 472)	84.46 (65.88 - 92.76)	0.005
PD0325901	MEK	3.33	0.43 (0.3 - 0.59)	278 (15 - 632)	84.71 (64.24 - 93.98)	0.006
AMG-232	MDM2	3.32	0.49 (0.39 - 0.57)	89 (51 - 165)	90.48 (86.18 - 93.72)	0.016
TAK-733	MEK	3.22	0.49 (0.32 - 0.67)	163 (8 - 370)	86.91 (72.01 - 92.82)	0.008
Poziotinib	EGFR	2.97	0.33 (0.19 - 0.52)	1511 (140 - 3176)	89.67 (80.25 - 97.95)	0.005
CI-1040	MEK	2.93	0.25 (0.14 - 0.39)	1051 (261 - 2409)	66.06 (51.51 - 87.46)	0.013
U0126	MEK	2.89	0.07 (0.03 - 0.14)	3887 (921 - 8775)	36.17 (15.45 - 71.09)	0.020
Ro 4987655	MEK	2.81	0.42 (0.29 - 0.56)	268 (19 - 541)	83.14 (65.75 - 91.41)	0.011
AZD-8330	MEK	2.74	0.55 (0.4 - 0.72)	49 (5 - 85)	87.11 (71.1 - 93.28)	0.011
Salinomycin	WNT	2.74	0.44 (0.38 - 0.54)	249 (70 - 357)	98.45 (97.62 - 98.79)	0.025
LGX818	RAF	2.69	0.09 (0.02 - 0.26)	832 (656 - 915)	24.83 (6.38 - 73.42)	0.049
Voreloxin hcl	TP	2.69	0.25 (0.15 - 0.37)	1271 (31 - 2877)	66.49 (61.79 - 77.01)	0.013
Trametinib	MEK	2.61	0.46 (0.32 - 0.78)	208 (4 - 670)	76.6 (53.95 - 97.55)	0.007
LB-100	Phosphatase	2.44	0.31 (0.26 - 0.36)	1204 (384 - 1617)	94.29 (84.66 - 98.73)	0.011
Ruboxistaurin hcl	PKC	2.40	0.44 (0.33 - 0.49)	104 (48 - 150)	83.49 (60.84 - 95.07)	0.039
Purvalanol A	CDK	2.34	0.12 (0.06 - 0.16)	7347 (4387 - 11470)	89.86 (81.89 - 96.8)	0.031
Fenretinide	RAR/RXR	2.34	0.28 (0.14 - 0.33)	2187 (852 - 5981)	99.25 (99.16 - 99.34)	0.039
RG7112	MDM2	2.33	0.28 (0.21 - 0.31)	2092 (1070 - 3954)	96.7 (93.99 - 99.11)	0.045
5-Azacytidine	NA	2.26	0.2 (0.15 - 0.29)	3718 (1484 - 5659)	94.46 (88.05 - 97.48)	0.026
RGFP966	HDAC	2.09	0.14 (0.1 - 0.23)	3577 (2138 - 4869)	63.99 (42.81 - 89.62)	0.015
RX-3117	NA	2.05	0.31 (0.18 - 0.41)	726 (298 - 1916)	84.24 (75.7 - 96.09)	0.039
Endoxifen (E-isomer)	ER	1.99	0.12 (0.08 - 0.15)	6981 (5514 - 9664)	93.07 (76.47 - 99.29)	0.037
CO-1686	EGFR	1.94	0.26 (0.21 - 0.33)	2018 (1004 - 3238)	97.61 (95.01 - 99.1)	0.011
Cisplatin	DNA A/C	1.93	0.06 (0.04 - 0.09)	1369 (344 - 2664)	21.66 (11.95 - 43.17)	0.037
VAL-083	DNA A/C	1.91	0.19 (0.15 - 0.21)	2837 (1729 - 4972)	80.41 (65.66 - 87.76)	0.017
Nedaplatin	DNA/RNA S	1.88	0.39 (0.34 - 0.47)	569 (243 - 756)	98.76 (98.69 - 98.86)	0.025
AMG-900	ARK	1.88	0.41 (0.35 - 0.45)	4 (2 - 8)	48.87 (36.79 - 58.01)	0.026
AZD-1152-HQPA	ARK	1.84	0.28 (0.2 - 0.31)	832 (39 - 1763)	65.74 (47.5 - 89.95)	0.016
LY2784544	FGFR	1.80	0.2 (0.13 - 0.28)	2321 (1459 - 3604)	75.32 (44.09 - 98.91)	0.039
AZ5104	EGFR	1.80	0.36 (0.23 - 0.48)	1197 (177 - 3138)	98.72 (97.08 - 99.3)	0.017
Tenovin-1	SIRT	1.79	0.23 (0.14 - 0.34)	1408 (463 - 3087)	75.52 (63.58 - 92.43)	0.035
BEZ235	MTOR	1.79	0.33 (0.28 - 0.38)	253 (154 - 457)	69.23 (58.97 - 83.96)	0.011
LY2874455	FGFR	1.77	0.58 (0.32 - 0.86)	46 (4 - 83)	86.16 (53.84 - 99.19)	0.039
Toceranib phosphate	KIT	1.74	0.12 (0.09 - 0.15)	6199 (5340 - 7312)	84.89 (68.48 - 96.12)	0.039
GSK1059615	MTOR	1.71	0.26 (0.23 - 0.28)	2157 (1677 - 2738)	95.67 (94.53 - 97.52)	0.011
Tamoxifen	ER	1.71	0.11 (0.07 - 0.14)	8578 (5931 - 12346)	95.67 (86.12 - 98.89)	0.028
AVL-292	BTK	1.69	0.23 (0.16 - 0.26)	2538 (1387 - 4413)	91.14 (83.29 - 99.37)	0.017
Evodiamine	EM	1.65	0.22 (0.19 - 0.25)	941 (452 - 1278)	65.94 (59.82 - 77.68)	0.017
AZD-8186	PI3K	1.57	0.29 (0.18 - 0.36)	1179 (440 - 2230)	84.36 (65.51 - 95.91)	0.039
ABT-751	Microtubule	1.56	0.34 (0.32 - 0.38)	309 (208 - 453)	80.96 (73.63 - 86.18)	0.008
Ellipticine hcl	TP	1.56	0.25 (0.21 - 0.34)	2564 (1016 - 3171)	98.98 (98.86 - 99.15)	0.030
JK184	Hedgehog	1.54	0.61 (0.52 - 0.71)	17 (6 - 32)	84.43 (80.53 - 88.62)	0.031
Pelitinib	EGFR	1.50	0.38 (0.26 - 0.46)	775 (220 - 2275)	98.91 (98.06 - 99.26)	0.032
Dimethylenastron	KSP	1.49	0.27 (0.21 - 0.32)	694 (342 - 1315)	72.26 (64.71 - 82.48)	0.045
AVN-944	DNA/RNA S	1.49	0.41 (0.36 - 0.43)	170 (151 - 193)	85.93 (71.13 - 94.07)	0.011
BIIB021	HSP90	1.48	0.42 (0.35 - 0.54)	424 (132 - 837)	94.92 (86.01 - 98.15)	0.012
PKC412	PKC	1.48	0.3 (0.23 - 0.39)	509 (32 - 879)	73.53 (40.02 - 96.19)	0.032
Plinabulin	Microtubule	1.48	0.68 (0.65 - 0.71)	4 (4 - 6)	79.94 (75.36 - 86)	0.017
ZSTK474	PI3K	1.45	0.29 (0.23 - 0.32)	441 (244 - 586)	67.58 (57.06 - 80.19)	0.032
BI-847325	ARK	1.45	0.53 (0.43 - 0.58)	141 (40 - 422)	98.68 (97.67 - 99.11)	0.026
Genz-644282	TP	1.45	0.73 (0.64 - 0.8)	9 (4 - 16)	99.6 (99.56 - 99.62)	0.032
Ombrabulin hcl	Microtubule	1.44	0.57 (0.49 - 0.64)	19 (11 - 23)	80.05 (69.43 - 87.53)	0.021
Lexibulin	Microtubule	1.43	0.48 (0.41 - 0.53)	64 (53 - 85)	82.71 (77.8 - 86.73)	0.047
INNO-206	ADC Cytotoxin	1.39	0.47 (0.39 - 0.53)	292 (120 - 532)	96.99 (93.18 - 98.87)	0.017
IMD 0354	IKK	1.32	0.36 (0.28 - 0.41)	856 (456 - 1623)	99.03 (97.98 - 99.44)	0.026
BMS-214662	FTase	1.27	0.5 (0.47 - 0.56)	171 (88 - 240)	97.93 (96.36 - 99.42)	0.021
VS-5584	MTOR	1.18	0.39 (0.37 - 0.41)	170 (140 - 203)	80.97 (74.01 - 92.48)	0.039

(…) = Minimum and maximum values. DNA A/C = DNA Alkylator/Crosslinker. DNA/RNA S = DNA/RNA Synthesis. EM = Endogenous Metabolite. TP = Topoisomerase

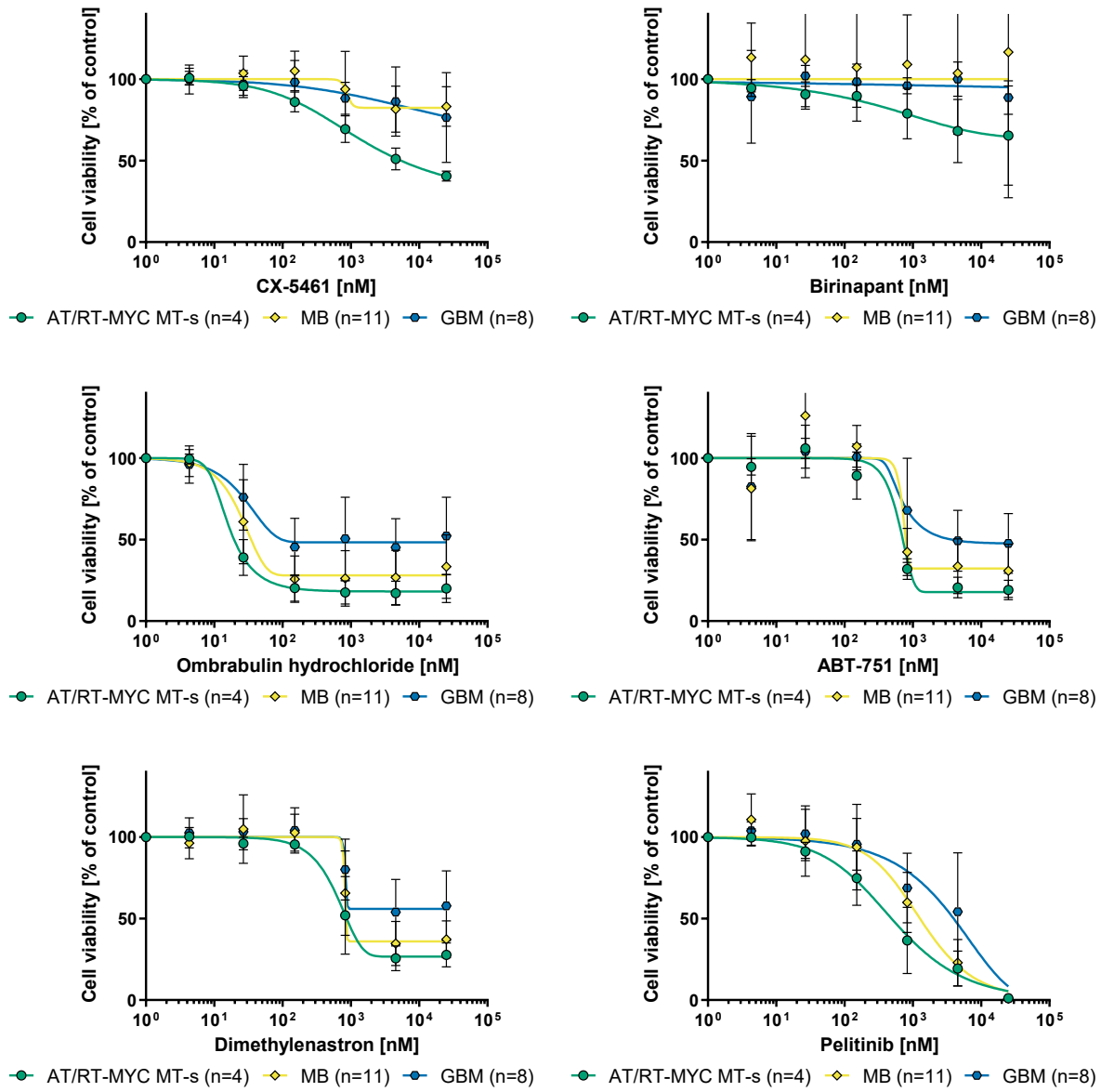

Figure 60. Dose-response curves of selected MT-s-specific inhibitors. CX-5461 = ribosomal RNA synthesis inhibitor. Birinapant = inhibitor of apoptosis (IAP). Ombrabulin hydrochloride and ABT-751 = microtubule inhibitors. Dimethylenastron = KSP inhibitor. Pelitinib = EGFR inhibitor.

In group-wise analyses (Figure 61) no additional enrichment was revealed in comparison to non-stratified analyses (all AT/RT cell lines vs. medulloblastoma and glioblastoma cell lines).

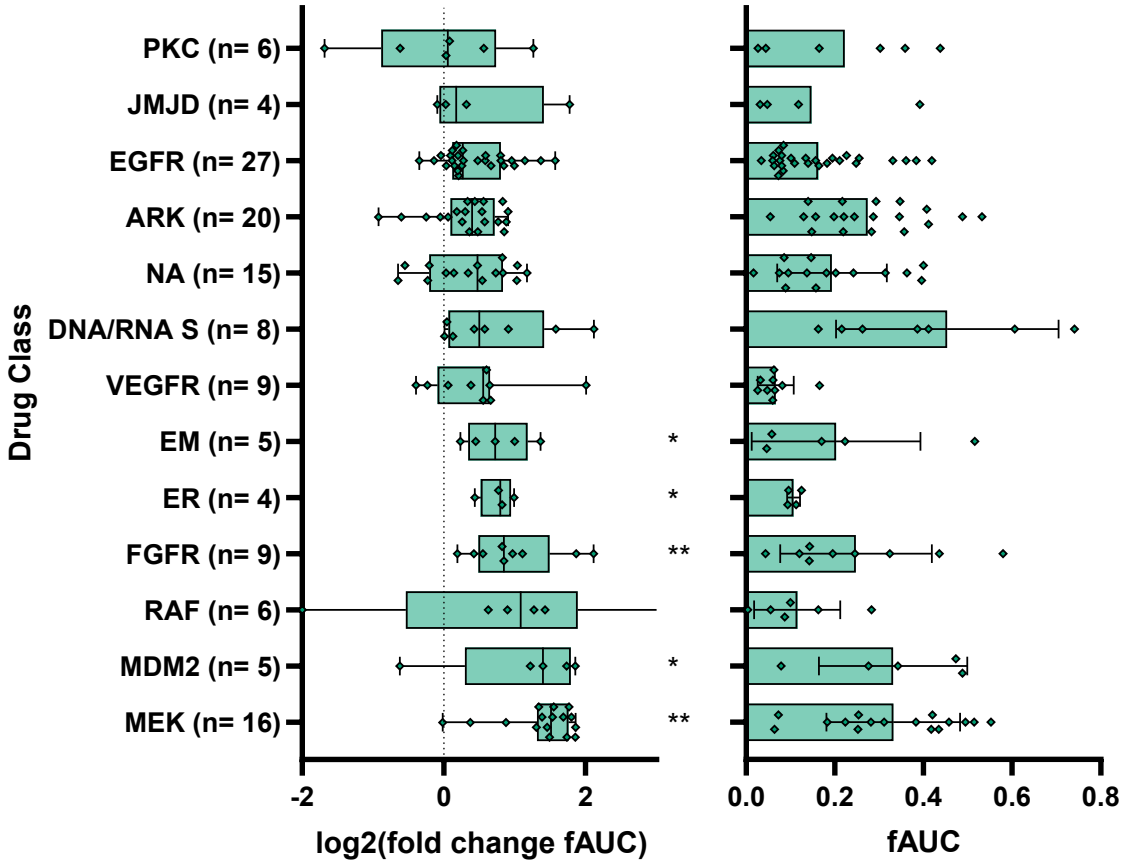

Figure 61. DCEA of AT/RT-MYC cell lines (MT-s cohort) vs. medulloblastoma and glioblastoma cell lines depicted as fold change per inhibitor (left) along with mean fAUC values in AT/RT-MYC cell lines (MT-s cohort, right). Drug classes consisting of at least four drugs and showing a fold change of 1.2 or larger are displayed. * = p-value < 0.05, ** = p-value < 0.01, MWU test. EM = Endogenous Metabolite. ER = Estrogen Receptor. NA = Nucleoside Antimetabolite. DNA/RNA Syn = DNA/RNA Synthesis.

3.3. Validation of drug screening results

To validate the hits identified in drug screening the CTG-based viability readouts were substantiated with additional parameters.

3.3.1. Time course of caspase activation and viability after Patupilone treatment

Apoptosis and necroptosis are regarded as the main mechanisms by which chemotherapeutic drugs promote their antitumoral effects [142-146]. Thus, the induction of apoptosis was evaluated for the prime candidates derived from drug screening. Due to the availability of *in vivo* models, validation experiments were focused on the AT/RT-MYC MT-s cohort. At the time when the validation experiments were initiated, screening results of the CLE library were not yet available. Consequently, there were no data for Lexibulin and Ombrabulin hydrochloride, which is why Ixabepilone was regarded as the prime candidate for the treatment of the MT-s cohort of AT/RT-MYC. As a derivative of Ixabepilone with known blood-brain barrier penetration, Patupilone, also known as Epothilone B, was preferred over Ixabepilone for validation experiments [147-149]. As apoptosis is an active process with the end stage of cellular destruction, detection of apoptosis incorporates a timing issue, as one must choose a treatment period long enough for the drug to induce measurable effects but not too long to avoid a loss of signal by cellular degradation. Consequently, the time course of Caspase activation was examined by means of the Caspase-Glo 3/7 Assay in the cell lines BT-12SF, BT-16SF and CHLA-266SF at different time points between 6 h and 72 h after exposure to a dilution series of Patupilone. As a control and a factor for normalization, cell viability was simultaneously measured using CTG along with caspase activation at any time point. The results are depicted in Figure 62. Caspase activation levels reached maximum intensity at 24-36 h. Notably, the 72 h data for caspase activity are not shown as inconsistent signals emerged indicating progressed cellular decay. While BT-12SF and BT-16SF reached peak signals earlier (24 h time point each), CHLA-266SF required a longer exposure time to reach maximum signal intensity (36 h time point). Moreover, the viability readout at 72 h corroborated the results from drug screening, reinforcing the reliability of the own workflow.

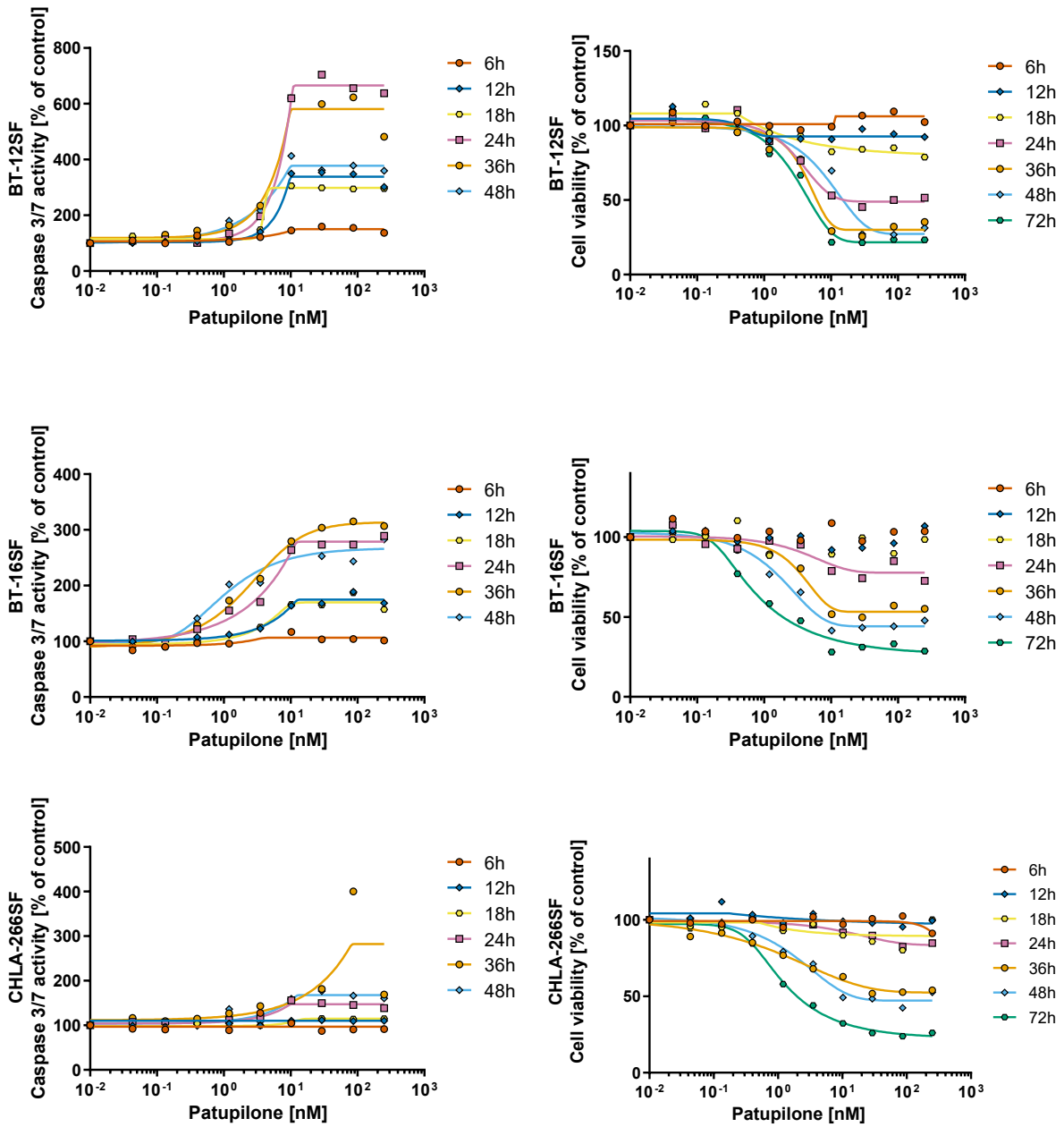

Figure 62. Dose-response curves of caspase activation and viability of BT-12SF, BT-16SF and CHLA-266SF cells after exposure to a dilution series of Patupilone. Maximum signal intensities were reached at 24 h (BT-12SF, BT-16SF) or 36 h (CHLA-266SF).

3.3.2. Flow-cytometric analysis of Patupilone-treated AT/RT cells

To further substantiate and stage apoptosis upon Patupilone treatment, the relocalization of Annexin V in the cell membrane was determined using fluorescence-activated cell sorting (FACS). The treatment period was chosen to correspond to a time point that yielded high signals in all three cell lines used (BT-12, BT-16 and CHLA-266) according to the previous time course experiments, namely 30 h of exposure time

using 100 nM of Patupilone. After co-staining with Annexin V and propidium iodide 40,000-50,000 events were captured per sample and the experiments were performed in three biological replicates with three technical replicates each. Figure 63 displays the results. All three cell lines showed a significant increase of both, the early and the late apoptotic fractions, along with a consequent reduction of viable cells. DMSO controls performed as expected. Consistent with the previous time course experiments, BT-12 and BT-16 exhibited a higher fraction of cells undergoing apoptosis than CHLA-266. Exemplary dot plots are depicted in Supplementary Figure 3. In conclusion, Patupilone induced apoptosis in all three AT/RT-MYC cell lines, thus making it a suitable candidate for further preclinical evaluation using *in vivo* models of AT/RT-MYC.

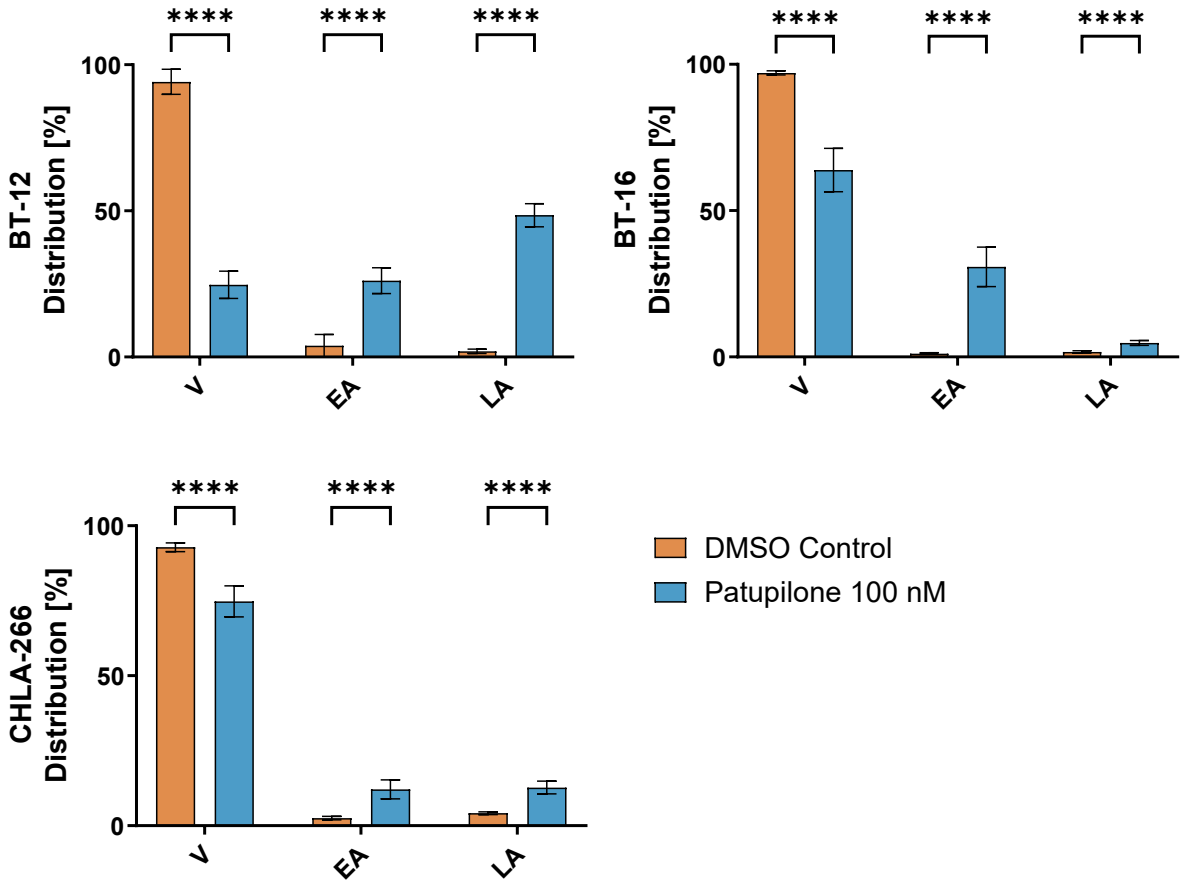

Figure 63. FACS analysis using Annexin V-/propidium iodide-costaining. All three AT/RT-MYC cell lines showed an increased fraction of early- and late-stage apoptotic cells upon treatment using 100 nM Patupilone for 30 h.

3.3.1. Incucyte Apoptosis Assay

To further evaluate the cellular responses of AT/RT-MYC cell lines to drug treatments, live-cell imaging studies using the Incucyte Apoptosis Assay were performed. Therefore, BT-12, BT-16 and CHLA-266 cells were treated using a dilution series of

Patupilone and monitored for over 96 h. As these experiments were conducted later than previous apoptosis studies, when CLE data had indicated Briciclib activity, Briciclib was evaluated in addition. All three cell lines showed increased total integrated fluorescence signal intensities upon treatment compared to DMSO controls (Figure 64 and Figure 65). While for BT-12 and CHLA-266 cells the time of highest signal intensities matched with the previously conducted time course experiments using the Caspase 3/7 Glo Assay, the highest signal intensity was reached later for BT-16 cells. Notably, for this experiment a high DMSO percentage of 1.1 % (including 0.1 % DMSO content obtained from the addition of the Incucyte Caspase-3/7 Green Reagent) was required to simultaneously cover the dilution ranges of Patupilone and Briciclib, thus causing increased apoptosis signals among the DMSO controls of CHLA-266, which were absent in the corresponding NT control. BT-12 and BT-16 cells on the other hand did not show increased apoptosis signals among DMSO controls. Moreover, all three cell lines exhibited reduced confluency in the course of the experiment when treated with Patupilone or Briciclib (data not shown). Interestingly, a population of cells remained alive in the treated wells, in line with the residual viability signals observed in drug screening (cf. Figure 51). According to optical evaluation these cells did not proliferate any longer indicating they likely became senescent. In conclusion, the data further validated the results obtained by drug screening and indicated that both, Patupilone and Briciclib, act through induction of apoptosis.

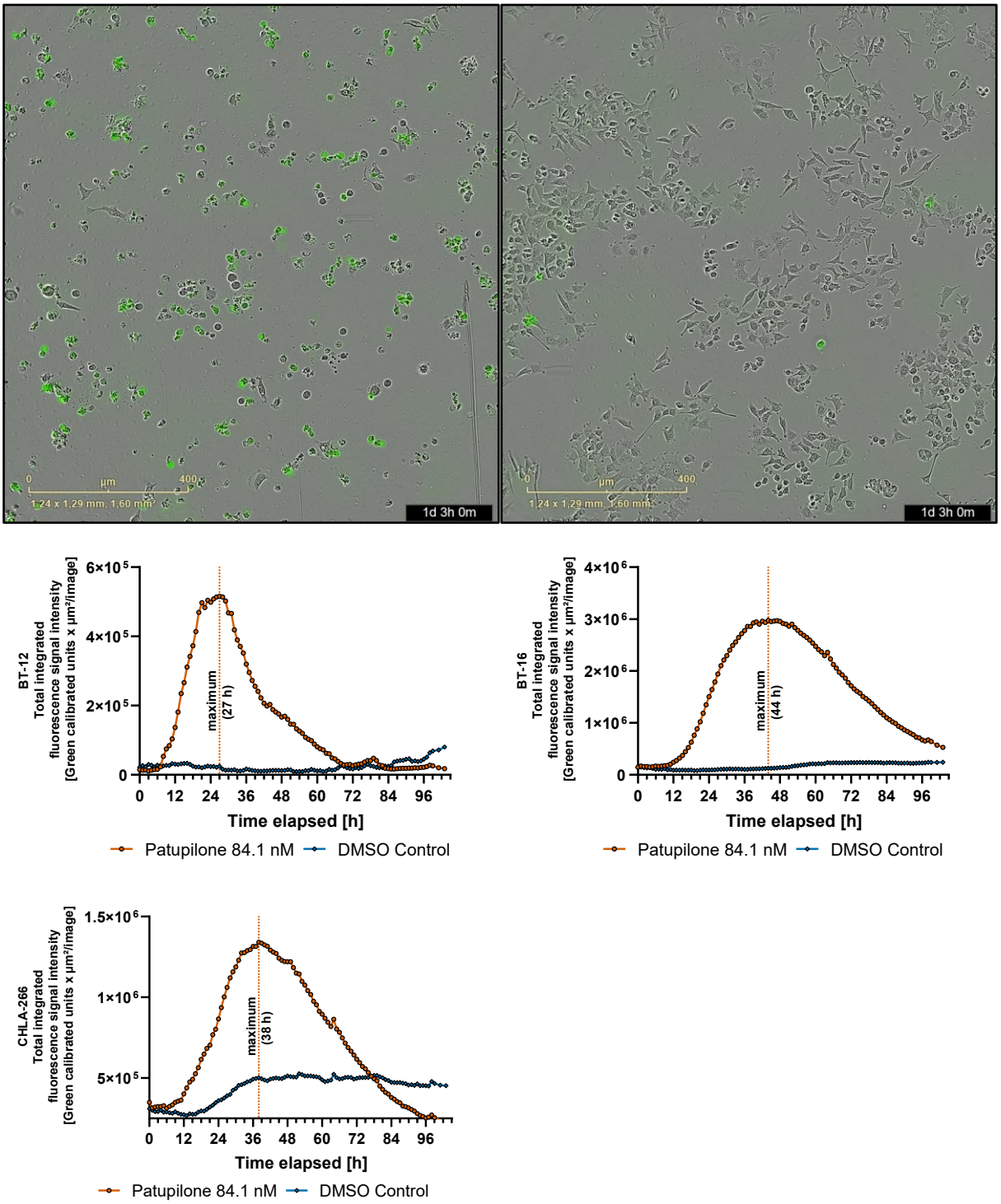

Figure 64. Incucyte apoptosis assay from treating BT-12, BT-16 and CHLA-266 cells using 84.1 nM Patupilone. The data indicated induction of apoptosis, reaching maximum total integrated fluorescence signal intensities at 27, 44 or 38 h, respectively (lower). Exemplary images from BT-12 cells after 27 h of treatment duration using Patupilone (upper left) or DMSO (upper right). Images from BT-16 and CHLA-266 cells are provided in Supplementary Figure 1 and Supplementary Figure 2.

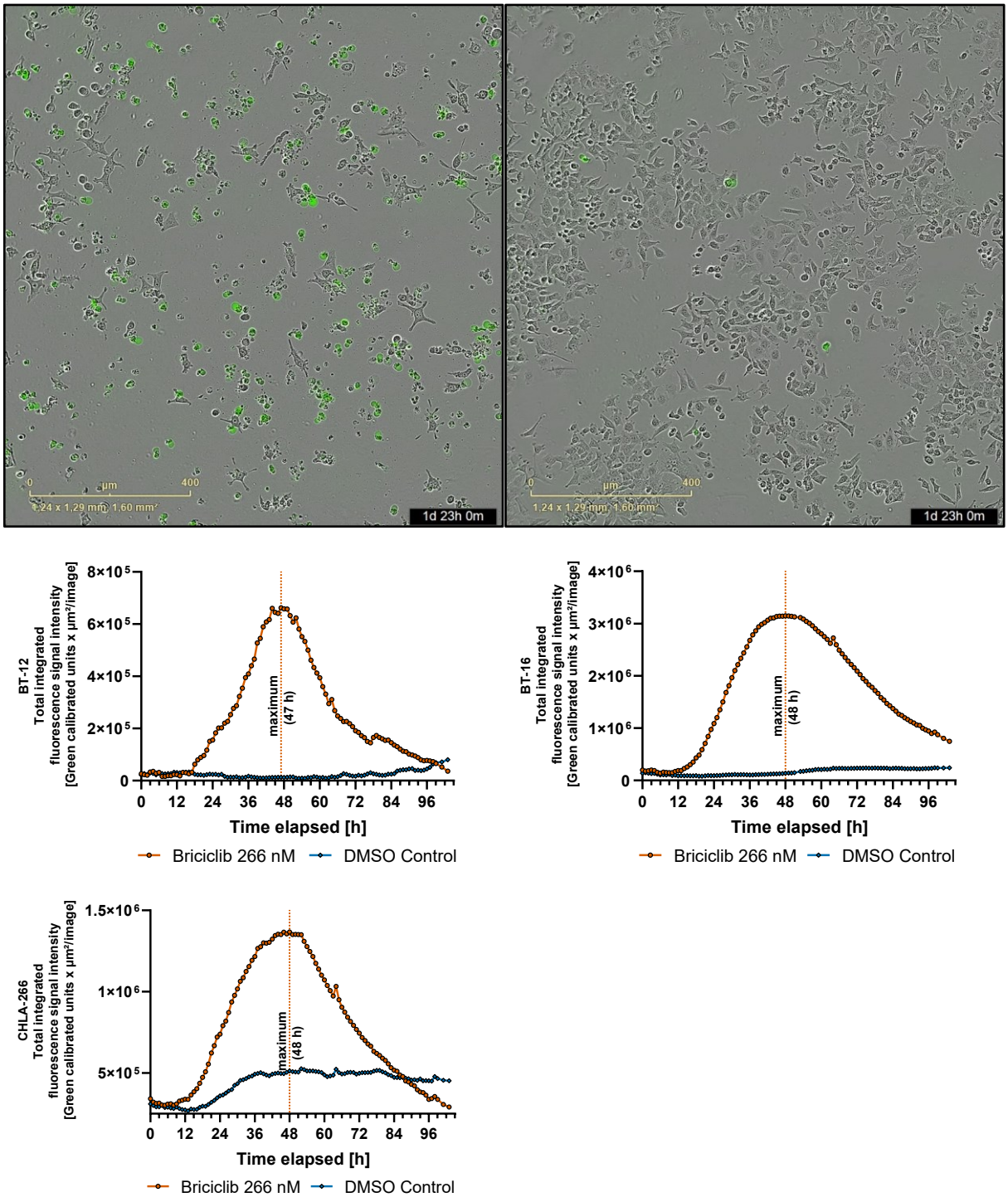

Figure 65. Incucyte apoptosis assay from treating BT-12, BT-16 and CHLA-266 cells using 266 nM Briciclib. The data indicated induction of apoptosis, reaching maximum total integrated fluorescence signal intensities at 47 and 48 h, respectively (lower). Exemplary images from BT-12 cells after 47 h of treatment duration using Patupilone (upper left) or DMSO (upper right). Images from BT-16 and CHLA-266 cells are provided in Supplementary Figure 1 and Supplementary Figure 2.

3.4. Identification of biomarkers

As it has been implied at numerous occasions during the evaluation of the drug screening data, biomarkers of drug activity were assessed using further genetic and epigenetic profiling. Most prominently, it was pursued to associate AT/RT cell lines to established molecular subgroups.

3.4.1. Assigning AT/RT cell lines to established molecular subgroups using multi-omics

To enable subgroup-stratified analyses of the dose-response data from AT/RT drug screening, DNA methylation profiles were generated using Infinium MethylationEPIC arrays as well as gene expression profiles using RNASeq. DNA/RNA isolation and sample processing were kindly performed by Frauke Meyer (RNASeq) and Nadezhda Bogodukhova (DNA methylation profiling). The DNA methylation data were analyzed using the platform Molecular Neuropathology 2.0 [132]. The cell lines ATRT13808, BT-12SF, BT-16SF, CHLA-06, CHLA-266SF, JC-ATRT and VU397 exhibited the highest calibrated classifier scores for the methylation class of AT/RT-MYC, whereas the cell lines ATRT-310-FHTC, ATRT-311-FHTC, CHLA-02, CHLA-04, CHLA-05 and HHU-ATRT-01 were assigned to the methylation class AT/RT-SHH. Not all cell lines reached a significant calibrated classifier score (cut-off 0.9, Table 17). AT/RT-TYR cell lines were not detected among the available models according to DNA methylation profiles. Notably, the subgroup affiliations of ATRT-310-FHTC, ATRT-311-FHTC and HHU-ATRT-01 were previously determined using DNA methylation data derived from primary tumor tissues, matching with the data obtained from the respective cell lines. The RNASeq data were kindly analyzed by Daniel Picard. An unsupervised HCL analysis employing Pearson dissimilarity to calculate a distance matrix and average linkage to agglomerate clusters was performed. A subset of 10 % of the most differentially regulated genes according to standard deviation projected two major clusters, again showing, that only two subgroups were represented in the available cohort of cell lines (Figure 66). The similarity of the own data was compared to publicly available AT/RT expression data employing a submap analysis (Figure 66). Two datasets were incorporated, both generated using the Affymetrix GeneChip Human Genome U133 Plus 2.0 Array (Birks et al. (18 AT/RT tumor samples) [150], Johann et al. (49 AT/RT tumor samples) [113]). These analyses revealed consistent expression profiles between AT/RT-SHH tumors and cell lines but a contradictive overlap of gene

signatures of AT/RT-TYR tumors and AT/RT-MYC cell lines. None of the cell line groups showed features of AT/RT-MYC tumors according to the sub-map analysis. Table 17 summarizes the results from each analysis as well as the subgroup affiliation according to the current published consensus [151]. Due to the consistent results of DNA methylation profiling and the established consensus, it was decided, that these outweigh the contradictive results among RNASeq data. In summary, the clusters of cell lines derived from the HCL analysis of the drug screening data (Figure 42) were finally assigned to AT/RT-SHH and AT/RT-MYC subgroups.

Table 17. Summary of subgroup affiliations based on RNASeq data and DNA methylation profiling either from primary tissue (left) or cell lines (right) along with the current consensus [151].

	Primary tumor tissue	Cell lines		
Cell line	**MNP 2.0 classifier**	**MNP 2.0 classifier (Calibrated classifier score)**	**RNASeq**	**Ho et. al**
ATRT13808	-	MYC (0.9473)	Non-SHH	-
ATRT-310-FHTC	SHH	SHH (0.99727)	SHH	-
ATRT-311-FHTC	SHH	SHH (0.94502)	SHH	-
BT-12SF	-	MYC (0.73581)	Non-SHH	MYC
BT-16SF	-	MYC (0.88533)	Non-SHH	MYC
CHLA-02	-	SHH (0.39382)	SHH	SHH
CHLA-04	-	SHH (0.57165)	SHH	SHH
CHLA-05	-	SHH (0.98818)	SHH	SHH
CHLA-06	-	MYC (0.88772)	Non-SHH	MYC
CHLA-266SF	-	MYC (0.82484)	Non-SHH	MYC
HHU-ATRT-01	SHH	SHH (0.99957)	SHH	-
JC-ATRT	-	MYC (0.84985)	Non-SHH	-
VU397	-	MYC (0.99298)	Non-SHH	-

- = data not available, MNP 2.0 classifier = Molecular Neuropathology 2.0 (Brain Tumor Classifier v12.5).

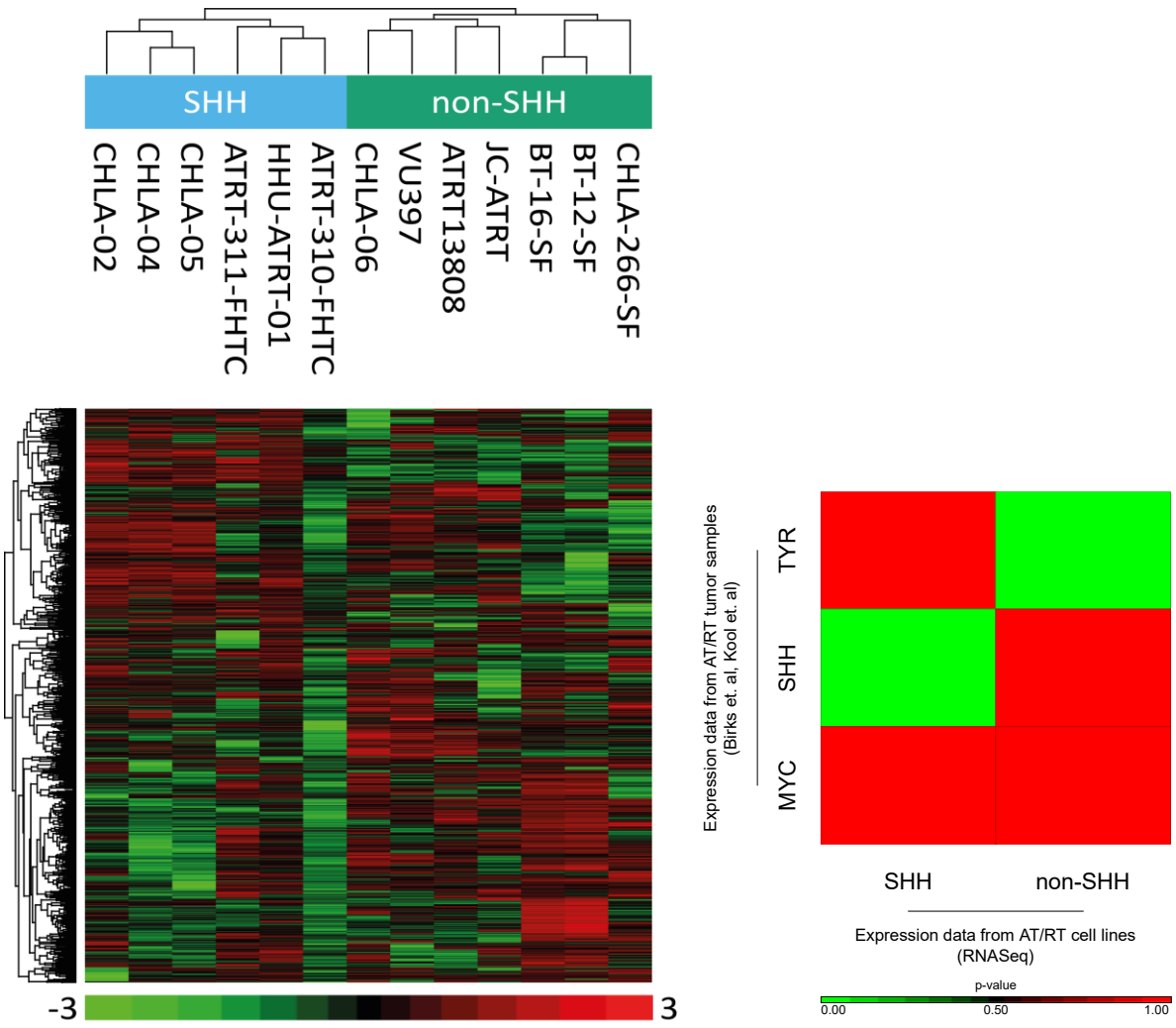

Figure 66. Unsupervised HCL analysis of RNASeq data using 10 % of most differentially regulated genes according to standard deviation (left). Based on a sub-map analysis (right), the left cluster represented cell lines derived from AT/RT-SHH tumors, whereas the right cluster of cell lines originated from AT/RT-TYR tumors. The latter disagreed with the current published consensus. P-value was calculated and corrected using Bonferroni correction.

3.4.2. Further exploration of RNASeq data for biomarkers of drug activity

To investigate the molecular background of the observed selective drug activities obtained from drug screening expression profiles of AT/RT cell lines generated using RNASeq data were reviewed for biomarkers of drug activity. For this, genes were collected that showed a consistent regulation comparing AT/RT-SHH and AT/RT-MYC subgroups in cell line data and publicly available AT/RT expression data derived from the two datasets introduced before (cf. 3.4.1), i.e., genes that showed a conserved regulation from tumors to cell lines. Filtering for a significant q-value and fold changes of at least +/- 2 obtained a list of 109 genes (Supplementary Table 1). Amongst these,

few genes were discovered that are known to be associated to different pathways involved in AT/RT drug sensitivities. Concerning the eIF4E inhibitor Briciclib, an increased expression of *IL4R* [152] and *VCL* [153] was found in the AT/RT-MYC subgroup compared to the AT/RT-SHH subgroup. The trend for *IL4R* increased, when AT/RT-MYC cell lines were separated into Briciclib-sensitive (MT-s cohort) and Briciclib-resistant (MT-r cohort) cell lines (Figure 67).

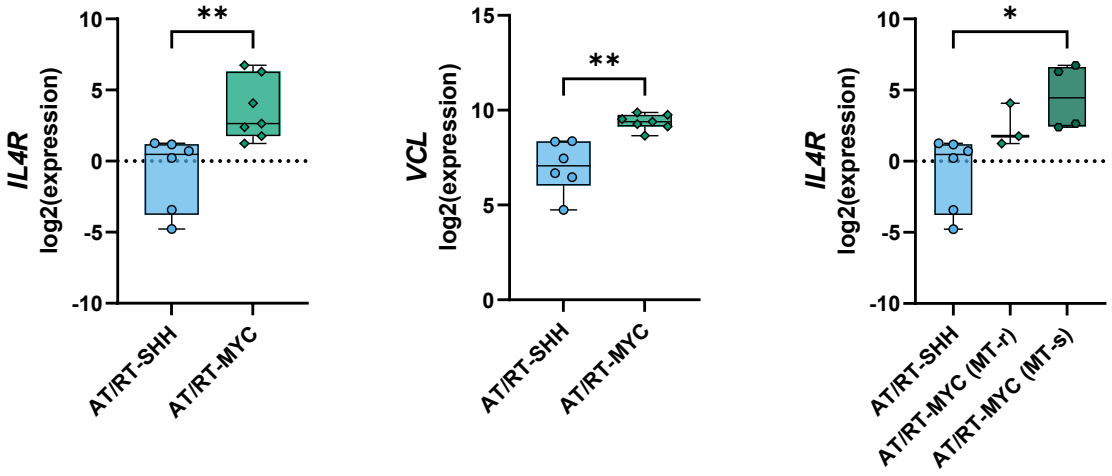

Figure 67. Expression data of *IL4R* and *VCL* derived from RNASeq indicated increased expression in AT/RT-MYC cell lines. Notably, Briciclib-sensitive cell lines showed the highest expression of *IL4R*. * = p-value < 0.05, ** = p-value < 0.01, t-test.

Other genes with conserved differential expression in the AT/RT-MYC subgroup comprised associations to microtubule functioning, including *CCDC69* [154], *ADAP2* [155], *ADM* [156], *GLCCI1* [157] and *B4GALT1* [158] (Figure 68). Notably, just as *IL4R*, all these candidate genes showed the highest expression in the MT-s cohort of AT/RT-MYC cell lines.

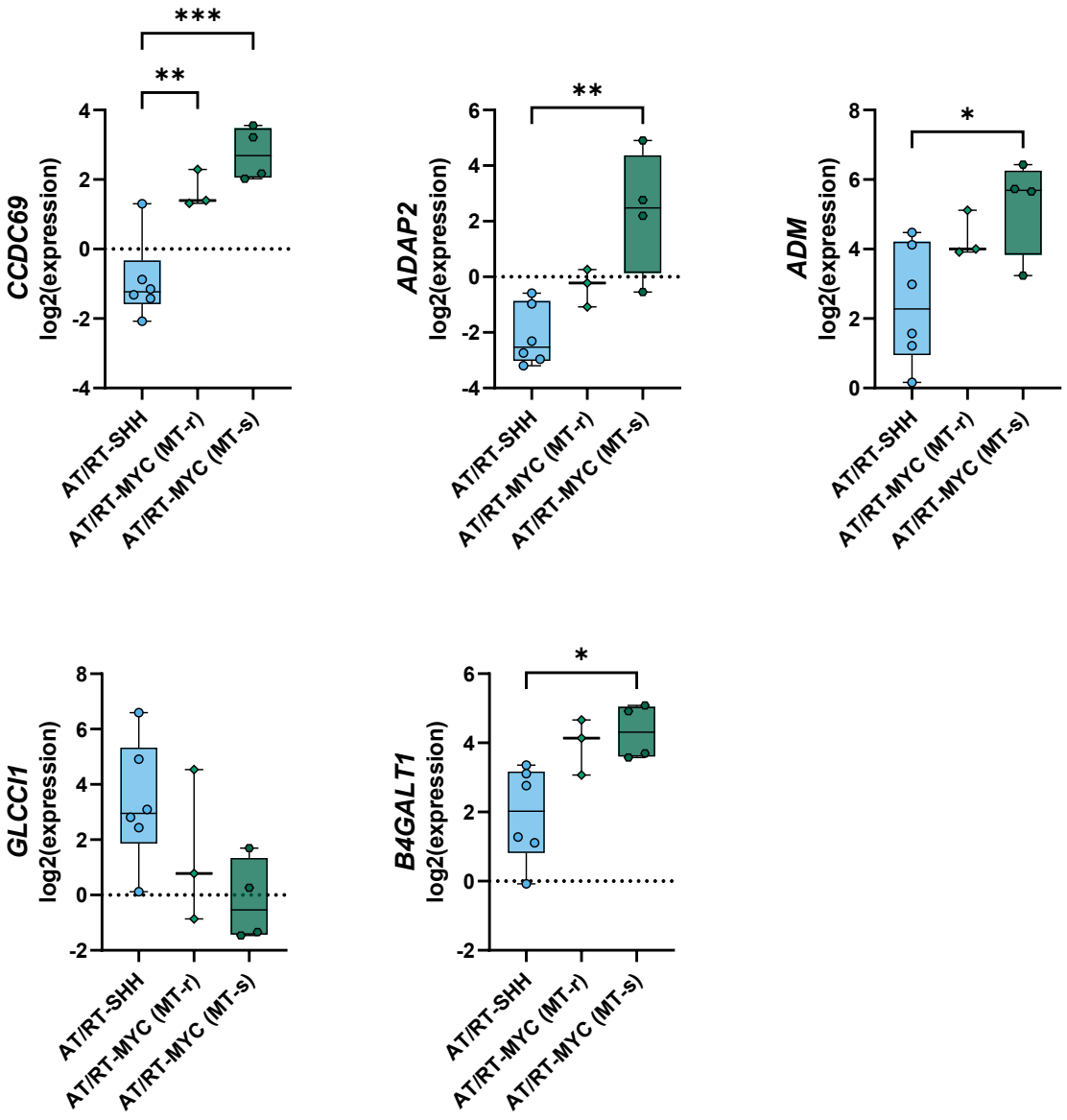

Figure 68. Expression of genes with an association to microtubule functioning in AT/RT-SHH cell lines compared to AT/RT-MYC cell lines derived from RNASeq data. Highest/lowest expression levels were observed in the MT-s cohort of AT/RT-MYC cell lines. * = p-value < 0.05, ** = p-value < 0.01, *** = p-value < 0.001, t-test.

Moreover, multiple genes that harbor known associations to BCL2 signaling (*LINC01315* [159], *NOVA1* [160], *LMO4* [161], Figure 69) or HSP90 signaling (*TAGLN* [162], *MYL12A* [163], Figure 70) exhibited differential expression in the AT/RT-SHH subgroup. Correlations of mean activities of BCL2 inhibitors and the corresponding genes were calculated which obtained partially significant results with Pearson r values ranging from 0.504 to 0.610 (Figure 69).

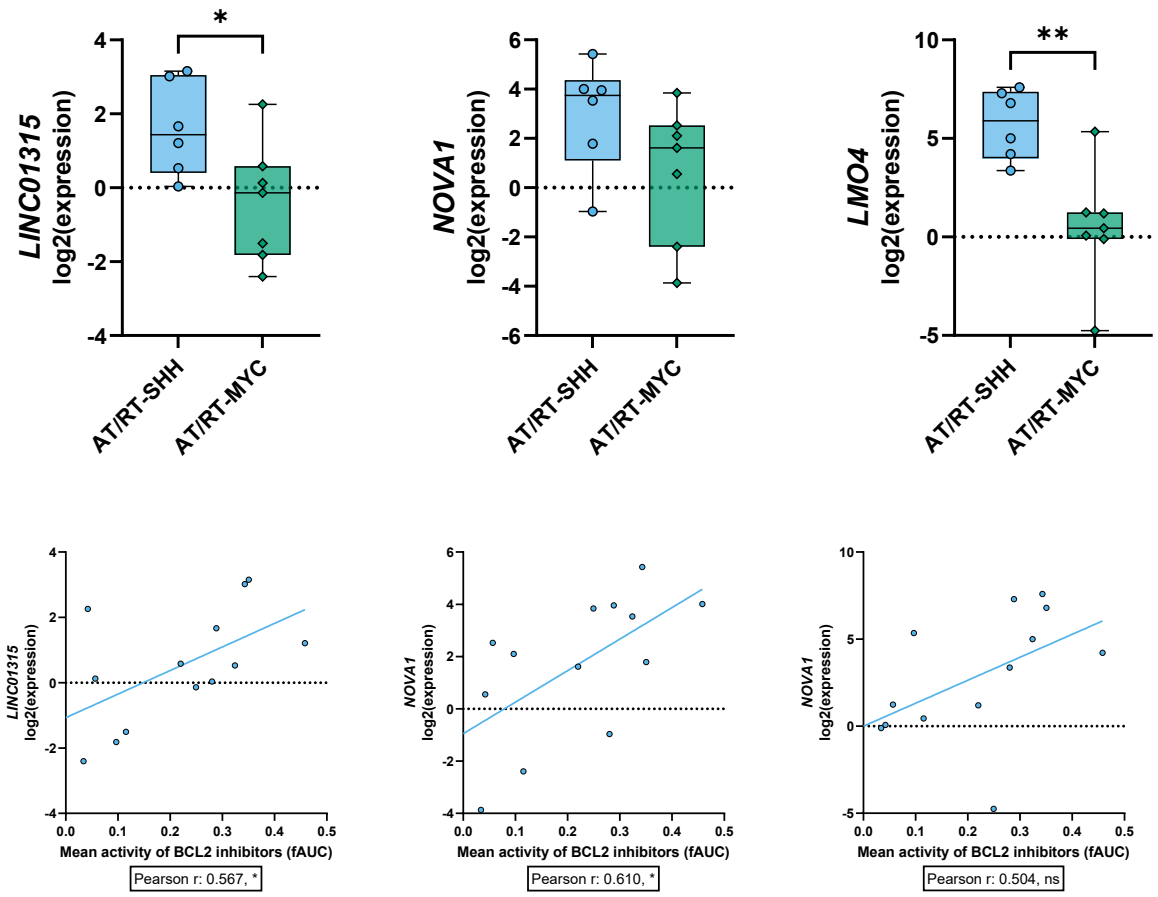

Figure 69. Expression of genes associated with BCL2 signaling in AT/RT-SHH cell lines compared to AT/RT-MYC cell lines derived from RNASeq data (upper). Increased gene expression was correlated with increased activity of BCL2 inhibitors (lower). * = p-value < 0.05, ** = p-value < 0.01, t-test.

Moreover, mean HSP90 inhibitor activities were correlated with reduced expression of *TAGLN* and *MYL12A* with Pearson r values of -0.535 and -0.455 (Figure 70).

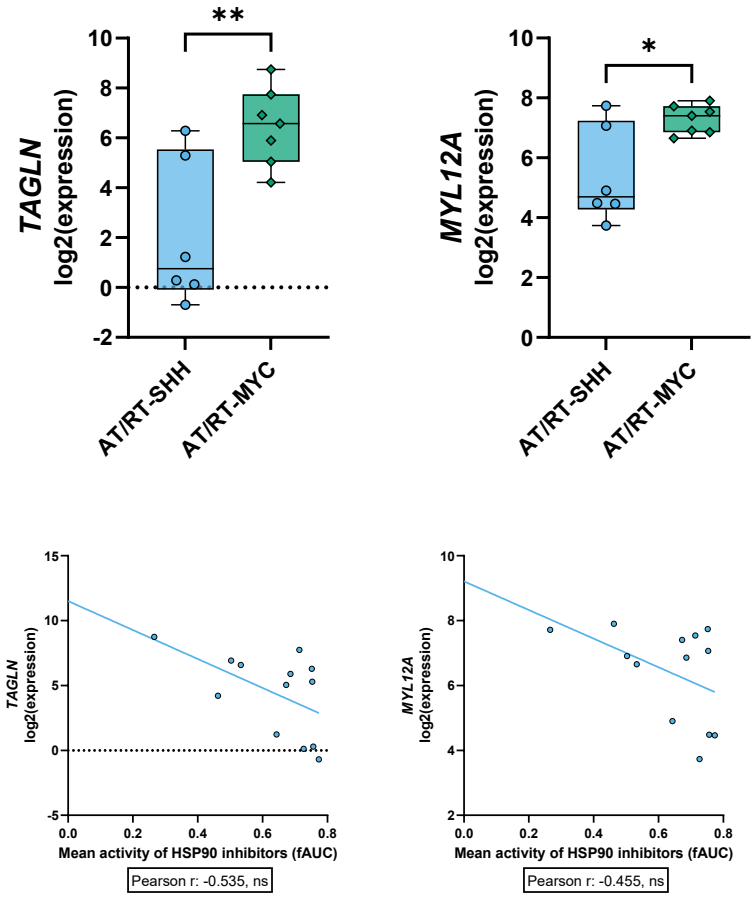

Figure 70. Expression of genes associated with HSP90 signaling in AT/RT-SHH cell lines compared to AT/RT-MYC cell lines derived from RNASeq data (upper). Increased gene expression was anti-correlated with the activity of HSP90 inhibitors (lower). * = p-value < 0.05, ** = p-value < 0.01, t-test.

4. Discussion and Conclusion

AT/RT represents a rare pediatric brain tumor with dismal prognosis. In recent years, emerging knowledge of AT/RT biology has gathered, including the identification of molecular subgroups associated with distinct expression and methylation profiles as well as underlying pathways. Moreover, a potential link between these epigenetic alterations and AT/RT's bland genome with *SMARCB1* and, in rare cases, *SMARCA4* being the only recurrent aberrations has been reported. However, targeted therapeutic approaches are still lacking. Thus, this thesis project aimed to identify targeted therapeutic approaches in AT/RTs by means of drug screening.

For this purpose, a workflow was developed that was capable of screening *in vitro* cell lines using libraries comprised of drugs in clinical use as well as early and late stages of development, thus facilitating drug repurposing. To obtain dose-response data from raw data, the DSA software was developed for processing, storing and arranging drug screening data. In agreement with the literature, fAUC values were calculated for all analyses as a measure of drug activity employing five-parametric logistic fitting, which exhibited major superiority compared to evaluation by means of the IC50. The underlying curve fitting was optimized by carefully evaluated constraints. A major requirement to enable screening of larger cohorts of cell lines was the introduction of batch preparation of plates with intermittent frozen storage. To rule out an impaired performance of this concept compared to individual plate preparation, results were compared from both concepts derived from four different cell lines, revealing highly correlative data with Spearman r values between 0.697 to 0.869. Minor alterations were observed among overall luminescence signal intensities and activity of few drugs, mostly of those with low fAUC values. The trends among both observations appeared to be linked to the growth pattern of the corresponding cell lines and thus, probably relied on the alteration of their growth kinetics in each of the two concepts. However, neither failure of drugs nor larger systemic deviation was evident, so that the following experiments were conducted using batch-prepared plates. To further reduce the costs of the workflow, it was evaluated whether dilutions of CTG affected the screening results. Except for a paradoxical increase of the overall luminescence signal intensities, no relevant alteration was detected. While a 1:2 dilution delivered a Spearman r of 0.851, a 1:4 dilution performed slightly worse with a Spearman r of 0.683. Thus, it was decided to perform further experiments using a 1:2 dilution of CTG. As most AT/RT cell lines used in this thesis project were grown in serum-free media,

we adjusted the remaining FBS-grown cell lines (BT-12, BT-16, CHLA-266) to serum-free conditions as well. Along with their adaption, the effects of FBS-based culturing on drug screening results was evaluated, revealing an increased activity of certain drug classes, including G9a/GLP inhibitors, inducers of apoptosis, CDK inhibitors, MTOR inhibitors, EGFR inhibitors and microtubule inhibitors as well as a decreased activity of nucleoside antimetabolites and an ADA inhibitor. Most of the classes with increased activity among the FBS-cultured cell lines were linked to mitosis and proliferation, thus indicating that their increase of activity may be explained through the increased proliferation under FBS-supplemented conditions. This hypothesis aligns well to the results from the repeated seeding optimization procedure after adaption to serum-free conditions, which indicted a higher cell number to be required to reach confluency after 72 h. Moreover, the decreased activity of nucleoside antimetabolites and an ADA inhibitor in FBS-cultured cell lines may result from the increased availability of nutrients in FBS-supplemented media. Regarding the increased activity of G9a/GLP inhibitors, serum starvation was confirmed to reduce the expression of the G9a protein through autophagy as a matter of increased cellular stress, thus potentially explaining the increased activity after switching to serum-free conditions [164]. This hypothesis also fits to the increased activity of Elesclomol, an apoptosis inducer [165]. To allow screening of non-neoplastic astrocytes, the miniaturization of the plate format from 384-well plates to 1536-well plates was inevitable. Thus, a trial was conducted to compare the performance using the cell line BT-12 which delivered a robust Spearman r of 0.831. Most of the few drugs with aberrant activity could be traced back to either fitting-related issues or increased variation due to the smaller assay volume. Finally, only few drugs showed convincing, but minor alteration between the two formats, thus making 1536-well plates a suitable alternative for screening of cells with non-infinite growth properties, such as non-neoplastic astrocytes and, in the future, primary cultures.

An actual screening was then carried out using 13 AT/RT cell lines, 11 medulloblastoma cell lines and 8 glioblastoma cell lines as well as a neural progenitor cell line, neural stem cells and two non-neoplastic astrocyte models. Data quality was assured at multiple layers. The analysis of CoVs of DMSO and NT wells showed low variation, with only few exceptions exhibiting moderately increased CoVs. Serious DMSO-induced reduction of viability seemed absent with a mean reduction of viability over all plates of about 2.23 %. To exclude inter-plate effects, relative amplitudes of luminescence signal intensities between plates were reviewed, which revealed mostly

stable results within screens and moderate variation among screening of larger libraries (CLE library). It remains questionable if increased priming and left-over volumes would decrease the latter. However, it may not be worthwhile, as the alteration of the luminescence signal intensities remained low and this adaption to the workflow would significantly increase the resource consumption as more media needs to be prepared and higher cell numbers to be grown. If screening of even larger libraries with a higher number of plates is conducted, however, improved mixing and larger priming and left-over volumes should be considered. Moreover, the own experiments revealed variation of DMSO and NT well's luminescence signal intensities between different screening attempts and library batches, the origin of which remained mostly unclear. Evidently, different batches of plates and CTG were used, along with working at slightly varying ambient temperatures and light exposure. Although the aim was to reduce the latter as far as possible, light exposure could not be entirely avoided. However, clearly identifying the background of the inter-screen signal alterations requires further experiments to be conducted. To exclude any liquid handling errors, an intra-plate analysis was performed which reported minor increased signals among some plates with lower CoVs, but no liquid handling errors at all after manual review.

The actual analysis of AT/RT drug screening data revealed that 40.14 % of drugs may be regarded as (almost) inactive. On the contrary, multiple drug classes with activity in AT/RTs were discovered including topoisomerase inhibitors, HSP90 inhibitors, proteasome inhibitors, MEK inhibitors, DNA/RNA synthesis inhibitors and microtubule inhibitors. Against expectations, the overlap with non-neoplastic cells was extensive. Further evaluations showed, that neural stem cells as well as neural progenitors were unsuitable as controls, as they appeared to be even more sensitive vs. most drugs than tumor cell lines. Astrocytes on the other hand were resistant vs. the majority of drugs, as expected due to their terminal differentiation. In conclusion, astrocytes may give an idea of toxicity to normal cells, but neither astrocytes nor neural stem cells nor neural progenitors were suitable to discriminate AT/RT-selective drugs. Consequently, the analyses were focused on the comparison of AT/RT cell lines vs. medulloblastoma and glioblastoma cell lines. Among these cross entity comparisons, AT/RT cell lines turned out to be more sensitive to MEK and MDM2 inhibitors and, with limitations, to BTK inhibitors. It has recently been published, that MDM2 inhibitors reduce growth of AT/RT cell lines *in vitro* and *in vivo* [125]. Moreover, also *in vitro* activity of MEK inhibitors has been previously reported [166]. The fact, that the own data thus corroborated observations made in other studies was very encouraging concerning the

validity of the own drug screening workflow. It may be of interest to further evaluate the resistance against MEK inhibitors observed in ATRT-310-FHTC, as resistance mechanisms are highly relevant upon clinical translation. Moreover, a relatively low, but specific activity was detected for CX-5461, also referred to as Pidnarulex, a specific ribosomal RNA (rRNA) synthesis inhibitor. Interestingly, Pidnarulex has very recently been shown to have anti-tumoral effects on MYCN-amplified neuroblastoma [167]. Additionally, two clinical trials (NCT05425862 and NCT04890613) are recruiting patients to elucidate the activity of Pidnarulex in solid cancers Thus, in the future, it may be worthwhile to further pursue the applicability of this drug for the treatment of AT/RTs as well. Lastly, few cell lines exhibited sensitivity to EGFR and FGFR inhibition and one cell line was targetable by RAF inhibitors. Further studies are required to elucidate whether these targets may be regarded as individually acquired phenomenon of the respective cell lines and/or tumors or a higher frequency of sensitivity to these drugs may be discovered in larger cohorts.

As heterogeneity of AT/RTs was shown before, evident by the presence of molecular subgroups [113], an unsupervised HCL analysis revealed two clusters in the obtained drug screening data. Alignment of the drug sensitivity-based groups to those derived from RNASeq data and DNA methylation profiling revealed distinct, subgroup-mediated drug responses. Notably, the subgroup affiliation derived from DNA methylation profiling also matched with the current consensus [151]. AT/RT-SHH cell lines showed an increased sensitivity to Notch inhibitors, which fits to the upregulation of Notch signaling in this subgroup as reported [113, 151]. However, previous clinical trials which aimed to evaluate the efficacy of Notch inhibitors in pediatric cancer patients indicated a lack of activity [168], but neither these studies focused on AT/RT nor did they incorporate their molecular classification. Thus, further evaluation of other Notch inhibitors for the treatment of AT/RT-SHH may be considered, especially as an add-on therapy in light of their rather mild effects in drug screening. Furthermore, AT/RT-SHH cell lines showed an increased sensitivity to BCL2 and HSP90 inhibitors, a finding that to our knowledge has not been reported to date. Through the evaluation of RNASeq data a potential link was found between increased expression of *LINC01315*, *NOVA1* and *LMO4* and BCL2 inhibitor activity and reduced expression of *TAGLN* and *MYL12A* and HSP90 inhibitor activity. Notably, only genes with conserved regulation in cell lines and expression profiles derived from publicly available AT/RT tumor data were evaluated. As AT/RT-SHH was shown to be among the groups with worse prognosis [97], these results may be of particular interest for further (pre-)clinical

evaluation. Furthermore, a mild selectivity of Ro 08-2750 was observed for AT/RT-SHH cell lines in comparison with medulloblastoma and glioblastoma cell lines. A role of neurogenesis signaling has been implied in AT/RT-SHH [151]. However, because of its quite high IC50 values and low overall activity, Ro 08-2750 is less attractive for further evaluation. Regarding the other cell lines, which apparently represented members of the AT/RT-MYC subgroup, no drug classes showed a significant enrichment. However, a trend was observed for microtubule inhibitors, which proved to rely on sensitivity of a sub-population (n=4) of AT/RT-MYC cell lines (MT-s), while the other cell lines were significantly more resistant (MT-r). Interestingly, even more drug classes exhibiting the same profile were identified when the two subpopulations of AT/RT-MYC cell lines were analyzed in more detail, including a significant enrichment of KSP and PLK inhibitors in the MT-s cohort of AT/RT-MYC cell lines. Notably, Vincristine sulfate, which is another microtubule inhibitor and frequently used for the treatment of AT/RT, showed inferior fold change compared to Ombrabulin hydrochloride, Lexibulin and Ixabepilone, the top hits among the class of microtubule inhibitors. This may indicate that the microtubule inhibitors identified in this project exhibit a higher specificity for AT/RTs, or rather AT/RT-MYC. However, comparison of the MT-s cohort of AT/RT-MYC cell lines to the drug sensitivity profiles derived from medulloblastoma and glioblastoma cell lines indicated a much neater selectivity, which only remained significant for four out of 19 microtubule inhibitors, including the prime candidates from the previous analysis, Ombrabulin hydrochloride und Lexibulin. In expression profiles from RNASeq data, few genes associated with microtubule functioning (*CCDC69*, *ADAP2*, *ADM*, *GLCCI1* and *B4GALT1*) were discovered that showed a differential expression in the MT-s cohort of AT/RT-MYC cell lines and a conserved regulation between cell lines and publicly available AT/RT expression data, thus harboring potential to serve as biomarkers of microtubule inhibitor activity. Moreover, the activity of the eIF4E inhibitor Briciclib in the MT-s cohort of AT/RT-MYC cell lines was interesting, as it showed a similar selectivity compared to microtubule inhibitors along with a similar dose-response profile. This indicates the mechanism of microtubule inhibitors may be linked to eIF4E. Unfortunately, the available libraries did not contain other eIF4E-specific inhibitors for comparison to the activity of Briciclib. An exploratory investigation revealed that only few other specific eIF4E inhibitors are commercially available and of the available ones most are unsuitable for the established own workflow, as proclaimed IC50 values exceed the working range. Among the RNASeq data, no increase of eIF4E's expression levels was detected but

Ingenuity Pathway Analysis identified a consistent regulation of upstream regulators and downstream targets alluding to upregulated eIF4E signaling activity (data not shown). Moreover, analyses of genes with conserved regulation in cell lines compared to publicly available AT/RT expression data indicated *IL4R* as a potential biomarker of eIF4E activity. Further validation of all RNASeq findings on the protein level is urgently required, especially concerning the role of potential biomarkers of microtubule and eIF4E inhibitor activity, as subgroup affiliation to the AT/RT-MYC subgroup alone is not specific according to drug sensitivities observed in the respective cell lines.

At the time when follow-up experiments of this thesis project were initiated, drug screening of the CLE library was only partially conducted. As also data for Ombrabulin hydrochloride and Lexibulin were absent at that time point, Ixabepilone, another microtubule inhibitor, appeared to be the prime candidate for the treatment of the MT-s cohort of AT/RT-MYC cell lines. As another derivative of Ixabepilone, namely Patupilone, also referred to as Epothilone B, was shown to cross the blood-brain barrier, it was preferred over Ixabepilone for validation experiments [147-149]. Among the final analyses, Ixabepilone (fold change 2.03) performed almost equally compared to Ombrabulin hydrochloride (fold change 2.05) and Lexibulin (fold change 2.10), but only reached significance after separation of the MT-s cohort of AT/RT-MYC cell lines. Moreover, Ixabepilone did not yield a significant effect in the comparison with medulloblastoma and glioblastoma cell lines at all. Regarding Patupilone, the own experiments unfortunately found inferior selectivity (fold change 1.55) and it did not achieve a significant result when compared to medulloblastoma and glioblastoma cell lines as well. As studies reliably characterizing the blood-brain barrier penetrance of Ombrabulin hydrochloride and Lexibulin are still lacking, Patupilone may still represent a suitable candidate, but due to its reduced selectivity in final analyses it is unlikely, that Patupilone outperforms Vincristine sulfate, which is already in use among the treatment of AT/RT. However, this may only be elucidated through further *in vivo* studies. In the follow-up experiments, the induction of apoptosis using Patupilone was evaluated by means of a time course experiment, revealing maximum caspase activity after 24 to 36 h. These results were validated for the most part through continuous live-cell imaging-based measurement of caspase activity for over 96 h. The following flow-cytometric analysis regarding the translocation of Annexin V in the cellular membrane after 30 h of treatment using Patupilone assured the induction of apoptosis through another method with Patupilone significantly increasing the fraction of early and late apoptotic cells compared to DMSO controls.

5. Outlook

In summary, the drug screening experiments conducted in this thesis project revealed multiple targeted therapeutic approaches in AT/RT cell lines. While MDM2 and MEK inhibitors as well as Pidnarulex were active across AT/RTs, other drugs exhibited a subgroup selectivity. Most prominently, BCL2 and HSP90 inhibitors showed increased activity in AT/RT-SHH cell lines, while microtubule and eIF4E inhibitors preferentially inhibited a subset of AT/RT-MYC cell lines. Further evaluation of the underlying mechanisms is required, including the validation of biomarkers discovered in RNASeq data.

Due to these promising results, an *in vivo* validation has been initiated in cooperation with Johanna Theruvath and Siddhartha Mitra. Preliminary results showed a striking effect in orthotopic xenografts of BT-16 cells, in which Patupilone almost entirely abrogated tumor growth (Figure 71). However, up to now, the colleagues were unable to reproduce the results obtained from the first attempt and another model, BT-12, showed no sensitivity *in vivo*. Nevertheless, the findings are worthwhile to be further investigated in upcoming collaborative studies.

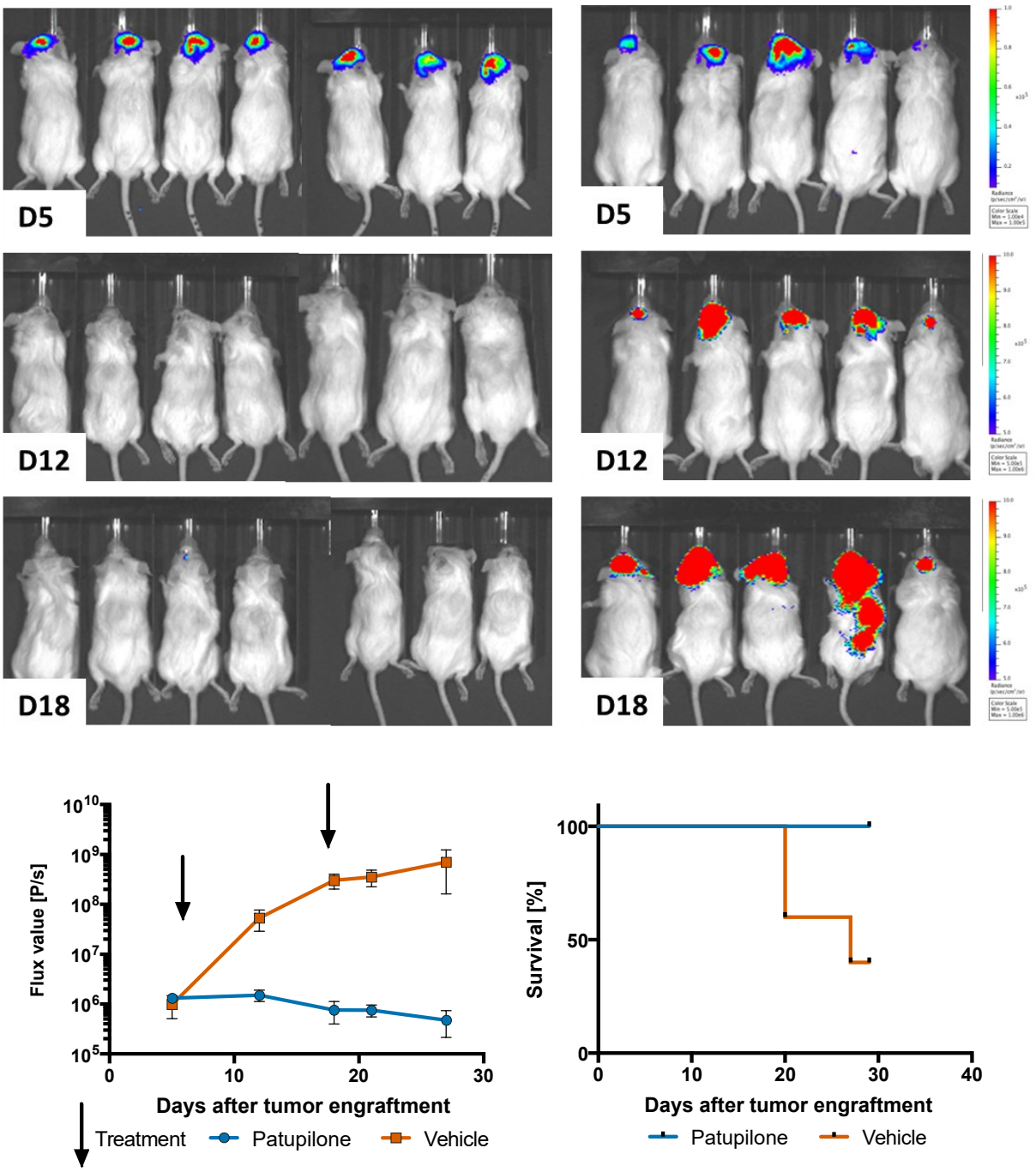

Figure 71. Spectrum *in vivo* imaging (IVIS scans) of mice bearing orthotopic xenografts of BT-16 cells on different days (upper). Two treatments using Patupilone were conducted on days 6 and 19 yielding a significant reduction of tumor volume (lower left) as well as increased survival (lower right).

6. References

1. Hanahan, D. and R.A. Weinberg, *Hallmarks of cancer: the next generation.* Cell, 2011. **144**(5): p. 646-74.
2. Hanahan, D. and R.A. Weinberg, *The hallmarks of cancer.* Cell, 2000. **100**(1): p. 57-70.
3. De Palma, M. and D. Hanahan, *The biology of personalized cancer medicine: facing individual complexities underlying hallmark capabilities.* Mol Oncol, 2012. **6**(2): p. 111-27.
4. Orozco, J.I.J., et al., *Epigenetic profiling for the molecular classification of metastatic brain tumors.* Nat Commun, 2018. **9**(1): p. 4627.
5. Zaky, W., *Revisiting Management of Pediatric Brain Tumors with New Molecular Insights.* Cell, 2016. **164**(5): p. 844-6.
6. Pu, X., Y. Ye, and X. Wu, *Development and validation of risk models and molecular diagnostics to permit personalized management of cancer.* Cancer, 2014. **120**(1): p. 11-9.
7. Velázquez Vega, J.E. and D.J. Brat, *Molecular-Genetic Classification of Gliomas and Its Practical Application to Diagnostic Neuropathology*, in *Diffuse Low-Grade Gliomas in Adults*, H. Duffau, Editor. 2017, Springer International Publishing: Cham. p. 73-100.
8. Riemenschneider, M.J. and G. Reifenberger, *Molecular neuropathology of gliomas.* International journal of molecular sciences, 2009. **10**(1): p. 184-212.
9. Tabatabai, G., et al., *Clinical implications of molecular neuropathology and biomarkers for malignant glioma.* Curr Neurol Neurosci Rep, 2012. **12**(3): p. 302-7.
10. Shiraishi, T. and K. Tabuchi, *Genetic alterations of human brain tumors as molecular prognostic factors.* Neuropathology, 2003. **23**(1): p. 95-108.
11. Riemenschneider, M.J. and G. Reifenberger, *Molecular neuropathology of low-grade gliomas and its clinical impact*, in *Low-Grade Gliomas*, J. Schramm, Editor. 2010, Springer Vienna: Vienna. p. 35-64.
12. Wood, M.D., A.M. Halfpenny, and S.R. Moore, *Applications of molecular neuro-oncology - a review of diffuse glioma integrated diagnosis and emerging molecular entities.* Diagnostic Pathology, 2019. **14**(1): p. 29.
13. Dixon, S.B., et al., *Reduced Morbidity and Mortality in Survivors of Childhood Acute Lymphoblastic Leukemia: A Report From the Childhood Cancer Survivor Study.* J Clin Oncol, 2020. **38**(29): p. 3418-3429.
14. Ramaswamy, V., et al., *Risk stratification of childhood medulloblastoma in the molecular era: the current consensus.* Acta Neuropathol, 2016. **131**(6): p. 821-31.
15. Slamon, D.J., et al., *Studies of the HER-2/neu proto-oncogene in human breast and ovarian cancer.* Science, 1989. **244**(4905): p. 707-12.
16. Bazell, R., A. Bernstein, and M.C. King, *Her-2: The Making of Herceptin, a Revolutionary Treatment for Breast Cancer*. 1998: Random House.
17. Li, Y.Y. and S.J. Jones, *Drug repositioning for personalized medicine.* Genome Med, 2012. **4**(3): p. 27.
18. Zhang, Z., J. Ji, and H. Liu, *Drug Repurposing in Oncology: Current Evidence and Future Direction.* Curr Med Chem, 2021. **28**(11): p. 2175-2194.
19. Bhattarai, D., et al., *An Insight into Drug Repositioning for the Development of Novel Anti-Cancer Drugs.* Curr Top Med Chem, 2016. **16**(19): p. 2156-68.
20. Yang, E.J., et al., *Revisiting Non-Cancer Drugs for Cancer Therapy.* Curr Top Med Chem, 2016. **16**(19): p. 2144-55.

21. Shim, J.S. and J.O. Liu, *Recent advances in drug repositioning for the discovery of new anticancer drugs.* Int J Biol Sci, 2014. **10**(7): p. 654-63.
22. Rose, J.S. and T.S. Bekaii-Saab, *New developments in the treatment of metastatic gastric cancer: focus on trastuzumab.* Onco Targets Ther, 2011. **4**: p. 21-6.
23. Sun, G., et al., *Drug repositioning: A bibliometric analysis.* Front Pharmacol, 2022. **13**: p. 974849.
24. Friedman, A.A., et al., *Feasibility of Ultra-High-Throughput Functional Screening of Melanoma Biopsies for Discovery of Novel Cancer Drug Combinations.* Clinical Cancer Research, 2017. **23**(16): p. 4680.
25. Narasimhan, V., et al., *Medium-throughput Drug Screening of Patient-derived Organoids from Colorectal Peritoneal Metastases to Direct Personalized Therapy.* Clinical Cancer Research, 2020. **26**(14): p. 3662.
26. Coussens, N.P., et al., *Small-Molecule Screens: A Gateway to Cancer Therapeutic Agents with Case Studies of Food and Drug Administration–Approved Drugs.* Pharmacological Reviews, 2017. **69**(4): p. 479.
27. Iljin, K., et al., *High-Throughput Cell-Based Screening of 4910 Known Drugs and Drug-like Small Molecules Identifies Disulfiram as an Inhibitor of Prostate Cancer Cell Growth.* Clinical Cancer Research, 2009. **15**(19): p. 6070.
28. Gorshkov, K., et al., *Advancing precision medicine with personalized drug screening.* Drug Discov Today, 2019. **24**(1): p. 272-278.
29. International Agency for Research on Cancer: Global Cancer Observatory *Cancer Today*. 2018 11.01.2023]; Available from: https://gco.iarc.fr/today/home.
30. Wilne, S., et al., *Presentation of childhood CNS tumours: a systematic review and meta-analysis.* Lancet Oncol, 2007. **8**(8): p. 685-95.
31. Albright, A.L., *Pediatric brain tumors.* CA Cancer J Clin, 1993. **43**(5): p. 272-88.
32. Barnes, P.D., *Magnetic resonance in pediatric and adolescent neuroimaging.* Neurol Clin, 1990. **8**(3): p. 741-57.
33. Shiminski-Maher, T., *Brain tumors in childhood: implications for nursing practice.* J Pediatr Health Care, 1990. **4**(3): p. 122-30.
34. Shiminski-Maher, T. and M. Shields, *Pediatric brain tumors: diagnosis and management.* J Pediatr Oncol Nurs, 1995. **12**(4): p. 188-98; quiz 199-202.
35. Zimmerman, R.A. and L.T. Bilaniuk, *Applications of magnetic resonance imaging in diseases of the pediatric central nervous system.* Magn Reson Imaging, 1986. **4**(1): p. 11-24.
36. Rao, P., *Role of MRI in paediatric neurooncology.* Eur J Radiol, 2008. **68**(2): p. 259-70.
37. Louis, D.N., et al., *The 2021 WHO Classification of Tumors of the Central Nervous System: a summary.* Neuro Oncol, 2021. **23**(8): p. 1231-1251.
38. Lutz, K., S.T. Jünger, and M. Messing-Jünger, *Essential Management of Pediatric Brain Tumors.* Children (Basel), 2022. **9**(4).
39. Silva, A.H.D. and K. Aquilina, *Surgical approaches in pediatric neuro-oncology.* Cancer Metastasis Rev, 2019. **38**(4): p. 723-747.
40. Zebian, B., et al., *Recent technological advances in pediatric brain tumor surgery.* CNS Oncol, 2017. **6**(1): p. 71-82.
41. Schwake, M., et al., *5-ALA fluorescence-guided surgery in pediatric brain tumors-a systematic review.* Acta Neurochir (Wien), 2019. **161**(6): p. 1099-1108.
42. Radcliffe, J., et al., *Cognitive deficits in long-term survivors of childhood medulloblastoma and other noncortical tumors: age-dependent effects of whole brain radiation.* Int J Dev Neurosci, 1994. **12**(4): p. 327-34.

43. Radcliffe, J., et al., *Three- and four-year cognitive outcome in children with noncortical brain tumors treated with whole-brain radiotherapy.* Ann Neurol, 1992. **32**(4): p. 551-4.
44. Mabbott, D.J., et al., *Serial evaluation of academic and behavioral outcome after treatment with cranial radiation in childhood.* J Clin Oncol, 2005. **23**(10): p. 2256-63.
45. Ris, M.D. and R.B. Noll, *Long-term neurobehavioral outcome in pediatric brain-tumor patients: review and methodological critique.* J Clin Exp Neuropsychol, 1994. **16**(1): p. 21-42.
46. Duffner, P.K., *Long-term effects of radiation therapy on cognitive and endocrine function in children with leukemia and brain tumors.* Neurologist, 2004. **10**(6): p. 293-310.
47. Merchant, T.E., et al., *Late effects of conformal radiation therapy for pediatric patients with low-grade glioma: prospective evaluation of cognitive, endocrine, and hearing deficits.* J Clin Oncol, 2009. **27**(22): p. 3691-7.
48. Butler, R.W. and R.K. Mulhern, *Neurocognitive interventions for children and adolescents surviving cancer.* J Pediatr Psychol, 2005. **30**(1): p. 65-78.
49. Danoff, B.F., et al., *Assessment of the long-term effects of primary radiation therapy for brain tumors in children.* Cancer, 1982. **49**(8): p. 1580-6.
50. Packer, R.J. and G. Vezina, *Management of and prognosis with medulloblastoma: therapy at a crossroads.* Arch Neurol, 2008. **65**(11): p. 1419-24.
51. Packer, R.J., et al., *Long-term neurologic and neurosensory sequelae in adult survivors of a childhood brain tumor: childhood cancer survivor study.* J Clin Oncol, 2003. **21**(17): p. 3255-61.
52. Turner, C.D., et al., *Late Effects of Therapy for Pediatric Brain Tumor Survivors.* Journal of Child Neurology, 2009. **24**(11): p. 1455-1463.
53. Ris, M.D. and R.B. Noll, *Long-term neurobehavioral outcome in pediatric brain-tumor patients: Review and methodological critique.* Journal of Clinical and Experimental Neuropsychology, 1994. **16**(1): p. 21-42.
54. Kenborg, L., et al., *Neurologic disorders in 4858 survivors of central nervous system tumors in childhood-an Adult Life after Childhood Cancer in Scandinavia (ALiCCS) study.* Neuro Oncol, 2019. **21**(1): p. 125-136.
55. Wells, E.M., et al., *Longitudinal assessment of late-onset neurologic conditions in survivors of childhood central nervous system tumors: a Childhood Cancer Survivor Study report.* Neuro Oncol, 2018. **20**(1): p. 132-142.
56. Patel, S.K., et al., *Neuropsychological differences between survivors of supratentorial and infratentorial brain tumours.* J Intellect Disabil Res, 2011. **55**(1): p. 30-40.
57. Butler, R.W., et al., *Intellectual functioning and multi-dimensional attentional processes in long-term survivors of a central nervous system related pediatric malignancy.* Life Sci, 2013. **93**(17): p. 611-6.
58. Ellenberg, L., et al., *Neurocognitive status in long-term survivors of childhood CNS malignancies: a report from the Childhood Cancer Survivor Study.* Neuropsychology, 2009. **23**(6): p. 705-17.
59. Reeves, C.B., et al., *Attention and memory functioning among pediatric patients with medulloblastoma.* J Pediatr Psychol, 2006. **31**(3): p. 272-80.
60. Robinson, K.E., et al., *A quantitative meta-analysis of neurocognitive sequelae in survivors of pediatric brain tumors.* Pediatr Blood Cancer, 2010. **55**(3): p. 525-31.

61. Brinkman, T.M., et al., *Long-Term Neurocognitive Functioning and Social Attainment in Adult Survivors of Pediatric CNS Tumors: Results From the St Jude Lifetime Cohort Study.* J Clin Oncol, 2016. **34**(12): p. 1358-67.
62. Bhakta, N., et al., *The cumulative burden of surviving childhood cancer: an initial report from the St Jude Lifetime Cohort Study (SJLIFE).* Lancet, 2017. **390**(10112): p. 2569-2582.
63. Le Deley, M.C., et al., *Risk of secondary leukemia after a solid tumor in childhood according to the dose of epipodophyllotoxins and anthracyclines: a case-control study by the Société Française d'Oncologie Pédiatrique.* J Clin Oncol, 2003. **21**(6): p. 1074-81.
64. Turcotte, L.M., et al., *Chemotherapy and Risk of Subsequent Malignant Neoplasms in the Childhood Cancer Survivor Study Cohort.* J Clin Oncol, 2019. **37**(34): p. 3310-3319.
65. Thirman, M.J. and R.A. Larson, *Therapy-related myeloid leukemia.* Hematol Oncol Clin North Am, 1996. **10**(2): p. 293-320.
66. Pedersen-Bjergaard, J. and P. Philip, *Balanced translocations involving chromosome bands 11q23 and 21q22 are highly characteristic of myelodysplasia and leukemia following therapy with cytostatic agents targeting at DNA-topoisomerase II.* Blood, 1991. **78**(4): p. 1147-8.
67. Teepen, J.C., et al., *Long-Term Risk of Subsequent Malignant Neoplasms After Treatment of Childhood Cancer in the DCOG LATER Study Cohort: Role of Chemotherapy.* J Clin Oncol, 2017. **35**(20): p. 2288-2298.
68. Majhail, N.S., et al., *Secondary solid cancers after allogeneic hematopoietic cell transplantation using busulfan-cyclophosphamide conditioning.* Blood, 2011. **117**(1): p. 316-22.
69. Neglia, J.P., et al., *New primary neoplasms of the central nervous system in survivors of childhood cancer: a report from the Childhood Cancer Survivor Study.* J Natl Cancer Inst, 2006. **98**(21): p. 1528-37.
70. Zin, F., et al., *Histopathological patterns in atypical teratoid/rhabdoid tumors are related to molecular subgroup.* Brain Pathol, 2021. **31**(5): p. e12967.
71. Erdmann, F., et al., *German Childhood Cancer Registry - Annual Report 2019 (1980-2018).* 2020: Institute of Medical Biostatistics, Epidemiology and Informatics (IMBEI) at the University Medical Center of the Johannes Gutenberg University Mainz.
72. Frühwald, M.C., et al., *Atypical teratoid/rhabdoid tumors-current concepts, advances in biology, and potential future therapies.* Neuro Oncol, 2016. **18**(6): p. 764-78.
73. Tulla, M., et al., *Incidence, Trends, and Survival of Children With Embryonal Tumors.* Pediatrics, 2015. **136**(3): p. e623-32.
74. Almalki, M.H., et al., *Atypical Teratoid/Rhabdoid Tumor of the Sellar Region in an Adult With Long Survival: Case Report and Review of the Literature.* J Clin Med Res, 2017. **9**(3): p. 216-220.
75. Alzoubi, H., et al., *Dural-based atypical teratoid/rhabdoid tumor in an adult: DNA methylation profiling as a tool for the diagnosis.* CNS Oncol, 2020. **9**(2): p. CNS54.
76. Chen, F., et al., *Atypical Teratoid/Rhabdoid Tumor Originated From the Trigeminal Nerve in a Young Male Adult: Case Report and Review of the Literature.* Front Neurol, 2020. **11**: p. 265.
77. Dardis, C., et al., *Atypical Teratoid Rhabdoid Tumor: Two Case Reports and an Analysis of Adult Cases with Implications for Pathophysiology and Treatment.* Front Neurol, 2017. **8**: p. 247.

78. Doi, M., et al., *A case of an atypical teratoid/rhabdoid tumor with distinctive histology in the pineal region in an adult patient.* Pathol Int, 2021. **71**(11): p. 777-782.
79. Duan, Z., et al., *Primary adult sellar SMARCB1/INI1-deficient tumor represents a subtype of atypical teratoid/rhabdoid tumor.* Mod Pathol, 2022. **35**(12): p. 1910-1920.
80. Fukuda, N., et al., *An Adult Case of Sellar Atypical Teratoid/Rhabdoid Tumor Presenting with Lung Metastasis, Harboring a Compound Heterozygous Mutation in INI1.* NMC Case Rep J, 2021. **8**(1): p. 267-274.
81. Greeneway, G.P., et al., *Atypical Teratoid/Rhabdoid Tumor of the Cerebellum in an Adult: Case Report and Literature Review.* World Neurosurg, 2021. **145**: p. 57-63.
82. Larran-Escandon, L., et al., *Pituitary apoplexy as presentation of atypical teratoid/rhabdoid tumor in an adult.* Endocrinol Nutr, 2016. **63**(7): p. 364-5.
83. Mathkour, M., et al., *Adult Pineal Region Atypical Teratoid Rhabdoid Tumor: A Case for Aggressive Surgical and Chemoradiation Management with Comprehensive Literature Review.* World Neurosurg, 2020. **142**: p. 117-127.
84. Monteiro, J., et al., *Adult Atypical Teratoid/Rhabdoid Tumor in the Pineal Region: Case Report and Literature Review.* World Neurosurg, 2020. **134**: p. 428-433.
85. Moujahed, R., et al., *Brain atypical teratoid rhabdoid tumor in an adult with long-term survival: Case report and review of literature.* J Cancer Res Ther, 2020. **16**(Supplement): p. S243-S245.
86. Neromyliotis, E., et al., *Spinal Atypical Rhabdoid Teratoid Tumor in an Adult Woman: Case Report and Review of the Literature.* World Neurosurg, 2019. **128**: p. 196-199.
87. Peng, A.J., et al., *Atypical teratoid/rhabdoid tumor in adult: case series and an integrated survival analysis.* Br J Neurosurg, 2021: p. 1-16.
88. Pesantez, D., G. Frigola, and D. Cazar, *Multifocal atypical teratoid rhabdoid tumor of the central nervous system in an adult patient.* Med Clin (Barc), 2018. **150**(7): p. e15-e16.
89. Shaaban, A., et al., *Purely Suprasellar (Hypothalamic) Atypical Teratoid Rhabdoid Tumor Presenting with Diabetes Insipidus and Panhypopituitarism in an Adult Male: A Case Report and Review of Literature.* Asian J Neurosurg, 2021. **16**(4): p. 846-849.
90. Yu, F., F. Chiang, and C. Bazan, 3rd, *Atypical teratoid/rhabdoid tumor arising from the trigeminal nerve in an adult.* Neuroradiol J, 2016. **29**(6): p. 447-449.
91. McGinity, M., et al., *Primary atypical teratoid rhabdoid tumor in the adult spine.* Surgical Neurology International, 2017. **8**(1): p. 34.
92. Dho, Y.S., et al., *Investigation of the location of atypical teratoid/rhabdoid tumor.* Childs Nerv Syst, 2015. **31**(8): p. 1305-11.
93. Tsitsopoulos, P.P., et al., *Infantile Atypical Teratoid Rhabdoid Tumor of the Spine Presenting with Acute Hydrocephalus.* Pediatr Neurosurg, 2020: p. 1-6.
94. Moeller, K.K., et al., *Atypical teratoid/rhabdoid tumor of the spine.* AJNR Am J Neuroradiol, 2007. **28**(3): p. 593-5.
95. Zarovnaya, E.L., et al., *Atypical teratoid/rhabdoid tumor of the spine in an adult: case report and review of the literature.* J Neurooncol, 2007. **84**(1): p. 49-55.
96. Wykoff, C.C., et al., *Atypical teratoid/rhabdoid tumor arising from the third cranial nerve.* J Neuroophthalmol, 2008. **28**(3): p. 207-11.
97. Frühwald, M.C., et al., *Age and DNA methylation subgroup as potential independent risk factors for treatment stratification in children with atypical teratoid/rhabdoid tumors.* Neuro Oncol, 2020. **22**(7): p. 1006-1017.

98. Bartelheim, K., et al., *Improved 6-year overall survival in AT/RT - results of the registry study Rhabdoid 2007.* Cancer Med, 2016. **5**(8): p. 1765-75.
99. Hilden, J.M., et al., *Central nervous system atypical teratoid/rhabdoid tumor: results of therapy in children enrolled in a registry.* J Clin Oncol, 2004. **22**(14): p. 2877-84.
100. Lafay-Cousin, L., et al., *Neurocognitive evaluation of long term survivors of atypical teratoid rhabdoid tumors (ATRT): The Canadian registry experience.* Pediatr Blood Cancer, 2015. **62**(7): p. 1265-9.
101. Hoell, J.I., et al., *Whole-genome paired-end analysis confirms remarkable genomic stability of atypical teratoid/rhabdoid tumors.* Genes Chromosomes Cancer, 2013. **52**(10): p. 983-5.
102. Hasselblatt, M., et al., *High-resolution genomic analysis suggests the absence of recurrent genomic alterations other than SMARCB1 aberrations in atypical teratoid/rhabdoid tumors.* Genes Chromosomes Cancer, 2013. **52**(2): p. 185-90.
103. Biegel, J.A., *Molecular genetics of atypical teratoid/rhabdoid tumor.* Neurosurg Focus, 2006. **20**(1): p. E11.
104. Louis, D.N., et al., *The 2016 World Health Organization Classification of Tumors of the Central Nervous System: a summary.* Acta Neuropathologica, 2016. **131**(6): p. 803-820.
105. Judkins, A.R., *Immunohistochemistry of INI1 expression: a new tool for old challenges in CNS and soft tissue pathology.* Adv Anat Pathol, 2007. **14**(5): p. 335-9.
106. Hasselblatt, M., et al., *Nonsense mutation and inactivation of SMARCA4 (BRG1) in an atypical teratoid/rhabdoid tumor showing retained SMARCB1 (INI1) expression.* Am J Surg Pathol, 2011. **35**(6): p. 933-5.
107. Kim, K.H. and C.W. Roberts, *Mechanisms by which SMARCB1 loss drives rhabdoid tumor growth.* Cancer Genet, 2014. **207**(9): p. 365-72.
108. Nakayama, R.T., et al., *SMARCB1 is required for widespread BAF complex-mediated activation of enhancers and bivalent promoters.* Nat Genet, 2017. **49**(11): p. 1613-1623.
109. Hashimoto, Y., et al., *Expression profiles of melanogenesis-related genes and proteins in acquired melanocytic nevus.* J Cutan Pathol, 2006. **33**(3): p. 207-15.
110. Ruiz i Altaba, A., P. Sánchez, and N. Dahmane, *Gli and hedgehog in cancer: tumours, embryos and stem cells.* Nat Rev Cancer, 2002. **2**(5): p. 361-72.
111. Eva, A., et al., *Cellular genes analogous to retroviral onc genes are transcribed in human tumour cells.* Nature, 1982. **295**(5845): p. 116-9.
112. Donati, G. and B. Amati, *MYC and therapy resistance in cancer: risks and opportunities.* Mol Oncol, 2022. **16**(21): p. 3828-3854.
113. Johann, P.D., et al., *Atypical Teratoid/Rhabdoid Tumors Are Comprised of Three Epigenetic Subgroups with Distinct Enhancer Landscapes.* Cancer Cell, 2016. **29**(3): p. 379-93.
114. Erkek, S., et al., *Comprehensive Analysis of Chromatin States in Atypical Teratoid/Rhabdoid Tumor Identifies Diverging Roles for SWI/SNF and Polycomb in Gene Regulation.* Cancer Cell, 2019. **35**(1): p. 95-110.e8.
115. Frühwald, M.C. and R. Furtwängler, *European Rhabdoid Registry (EU-RHAB), Part I: Therapy recommendations*. 2021.
116. Geoerger, B., et al., *A Phase I Study of the CDK4/6 Inhibitor Ribociclib (LEE011) in Pediatric Patients with Malignant Rhabdoid Tumors, Neuroblastoma, and Other Solid Tumors.* Clin Cancer Res, 2017. **23**(10): p. 2433-2441.

117. DeWire, M.D., et al., *A Phase I and Surgical Study of Ribociclib and Everolimus in Children with Recurrent or Refractory Malignant Brain Tumors: A Pediatric Brain Tumor Consortium Study.* Clin Cancer Res, 2021. **27**(9): p. 2442-2451.
118. Maris, J.M., et al., *Initial testing of the aurora kinase A inhibitor MLN8237 by the Pediatric Preclinical Testing Program (PPTP).* Pediatr Blood Cancer, 2010. **55**(1): p. 26-34.
119. Venkataraman, S., et al., *Targeting Aurora Kinase A enhances radiation sensitivity of atypical teratoid rhabdoid tumor cells.* J Neurooncol, 2012. **107**(3): p. 517-26.
120. Wetmore, C., et al., *Alisertib is active as single agent in recurrent atypical teratoid rhabdoid tumors in 4 children.* Neuro Oncol, 2015. **17**(6): p. 882-8.
121. Upadhyaya, S.A., et al., *Phase II study of alisertib as a single agent for treating recurrent or progressive atypical teratoid/rhabdoid tumor.* Neuro Oncol, 2022.
122. American Association for Cancer Research *Rare Tumors in Kids May Respond to Tazemetostat.* Cancer Discov, 2018. **8**(1): p. Of5.
123. Hummel, T.R., et al., *A pediatric phase 1 trial of vorinostat and temozolomide in relapsed or refractory primary brain or spinal cord tumors: a Children's Oncology Group phase 1 consortium study.* Pediatr Blood Cancer, 2013. **60**(9): p. 1452-7.
124. Leary, S.E.S., et al., *Vorinostat and isotretinoin with chemotherapy in young children with embryonal brain tumors: A report from the Pediatric Brain Tumor Consortium (PBTC-026).* Neuro Oncol, 2022. **24**(7): p. 1178-1190.
125. Alimova, I., et al., *Targeting the TP53/MDM2 axis enhances radiation sensitivity in atypical teratoid rhabdoid tumors.* Int J Oncol, 2022. **60**(3).
126. Bindslev, N., *Drug-Acceptor Interactions: Modeling Theoretical Tools to Test and Evaluate Experimental Equilibrium Effects (1st ed.).* CRC Press, 2008.
127. Sebaugh, J.L., *Guidelines for accurate EC50/IC50 estimation.* Pharmaceutical Statistics, 2011. **10**(2): p. 128-134.
128. National Cancer Institute *Developmental Therapeutics Program: COMPARE Analysis*. 2015 25.01.2021]; Available from: https://dtp.cancer.gov/databases_tools/docs/compare/compare_methodology.htm.
129. Cumberland, W.N., et al., *Nonlinear Calibration Model Choice between the Four and Five-Parameter Logistic Models.* Journal of biopharmaceutical statistics, 2015. **25**(5): p. 972-983.
130. Gottschalk, P.G. and J.R. Dunn, *The five-parameter logistic: A characterization and comparison with the four-parameter logistic.* Analytical Biochemistry, 2005. **343**(1): p. 54-65.
131. Huang, S. and L. Pang, *Comparing statistical methods for quantifying drug sensitivity based on in vitro dose-response assays.* Assay Drug Dev Technol, 2012. **10**(1): p. 88-96.
132. Capper, D., et al., *DNA methylation-based classification of central nervous system tumours.* Nature, 2018. **555**(7697): p. 469-474.
133. Forget, A., et al., *Aberrant ERBB4-SRC Signaling as a Hallmark of Group 4 Medulloblastoma Revealed by Integrative Phosphoproteomic Profiling.* Cancer Cell, 2018. **34**(3): p. 379-395.e7.
134. Sievert, A.J., et al., *Paradoxical activation and RAF inhibitor resistance of BRAF protein kinase fusions characterizing pediatric astrocytomas.* Proceedings of the National Academy of Sciences of the United States of America, 2013. **110**(15): p. 5957-5962.
135. Fallahi-Sichani, M., et al., *Metrics other than potency reveal systematic variation in responses to cancer drugs.* Nat Chem Biol, 2013. **9**(11): p. 708-14.

136. Le, H.M., et al., *Differential Development of Umbilical Cord-Derived Mesenchymal Stem Cells During Long-Term Maintenance in Fetal Bovine Serum-Supplemented Medium and Xeno- and Serum-Free Culture Medium.* Cell Reprogram, 2021. **23**(6): p. 359-369.
137. Chiang, Y.H., V. Silani, and F.C. Zhou, *Morphological differentiation of astroglial progenitor cells from EGF-responsive neurospheres in response to fetal calf serum, basic fibroblast growth factor, and retinol.* Cell Transplant, 1996. **5**(2): p. 179-89.
138. Yokoyama, M., et al., *Influence of fetal calf serum on differentiation of mesenchymal stem cells to chondrocytes during expansion.* J Biosci Bioeng, 2008. **106**(1): p. 46-50.
139. Liu, Z., et al., *Regulation of Monocarboxylic Acid Transporter 1 Trafficking by the Canonical Wnt/β-Catenin Pathway in Rat Brain Endothelial Cells Requires Cross-talk with Notch Signaling.* J Biol Chem, 2016. **291**(15): p. 8059-69.
140. Cupido, T., et al., *The imidazopyridine derivative JK184 reveals dual roles for microtubules in Hedgehog signaling.* Angew Chem Int Ed Engl, 2009. **48**(13): p. 2321-4.
141. Lain, S., et al., *Discovery, in vivo activity, and mechanism of action of a small-molecule p53 activator.* Cancer Cell, 2008. **13**(5): p. 454-63.
142. Elmore, S., *Apoptosis: a review of programmed cell death.* Toxicologic pathology, 2007. **35**(4): p. 495-516.
143. Gong, Y., et al., *The role of necroptosis in cancer biology and therapy.* Molecular Cancer, 2019. **18**(1): p. 100.
144. Hannun, Y.A., *Apoptosis and the Dilemma of Cancer Chemotherapy.* Blood, 1997. **89**(6): p. 1845-1853.
145. Kerr, J.F., C.M. Winterford, and B.V. Harmon, *Apoptosis. Its significance in cancer and cancer therapy.* Cancer, 1994. **73**(8): p. 2013-26.
146. Sen, S. and M. D'Incalci, *Apoptosis. Biochemical events and relevance to cancer chemotherapy.* FEBS Lett, 1992. **307**(1): p. 122-7.
147. Ruschel, J., et al., *Systemic administration of epothilone B promotes axon regeneration after spinal cord injury.* Science, 2015. **348**(6232): p. 347.
148. Abrey, L.E., et al., *Patupilone for the treatment of recurrent/progressive brain metastases in patients (pts) with non-small cell lung cancer (NSCLC): An open-label phase II study.* Journal of Clinical Oncology, 2008. **26**(15_suppl): p. 2033-2033.
149. Conlin, A.K., et al., *Phase II trial of patupilone in patients (pts) with breast cancer brain metastases (BCBM) progressing or recurring after whole brain radiation therapy (WBXRT).* Journal of Clinical Oncology, 2008. **26**(15_suppl): p. 1086-1086.
150. Birks, D.K., et al., *High expression of BMP pathway genes distinguishes a subset of atypical teratoid/rhabdoid tumors associated with shorter survival.* Neuro Oncol, 2011. **13**(12): p. 1296-307.
151. Ho, B., et al., *Molecular subgrouping of atypical teratoid/rhabdoid tumors-a reinvestigation and current consensus.* Neuro Oncol, 2020. **22**(5): p. 613-624.
152. Ghram, M., et al., *The eukaryotic translation initiation factor eIF4E reprograms alternative splicing.* Embo j, 2023: p. e110496.
153. Kraemer, B.F., et al., *Extracellular Matrix-Specific Platelet Activation Leads to a Differential Translational Response and Protein De Novo Synthesis in Human Platelets.* Int J Mol Sci, 2020. **21**(21).
154. Pal, D., et al., *Role of a novel coiled-coil domain-containing protein CCDC69 in regulating central spindle assembly.* Cell Cycle, 2010. **9**(20): p. 4117-29.

155. Zuccotti, P., et al., *Centaurin-α_2 interacts with β-tubulin and stabilizes microtubules.* PLoS One, 2012. **7**(12): p. e52867.
156. Ferrero, H., et al., *Reduced Adrenomedullin Parallels Microtubule Dismantlement in Frontotemporal Lobar Degeneration.* Mol Neurobiol, 2018. **55**(12): p. 9328-9333.
157. Kiuchi, Z., et al., *GLCCI1 is a novel protector against glucocorticoid-induced apoptosis in T cells.* Faseb j, 2019. **33**(6): p. 7387-7402.
158. Dai, Z., K. Wang, and Y. Gao, *The critical role of B4GALT4 in promoting microtubule spindle assembly in HCC through the regulation of PLK1 and RHAMM expression.* J Cell Physiol, 2022. **237**(1): p. 617-636.
159. Li, Y., et al., *Colorectal cancer stem cell-derived exosomal long intergenic noncoding RNA 01315 (LINC01315) promotes proliferation, migration, and stemness of colorectal cancer cells.* Bioengineered, 2022. **13**(4): p. 10827-10842.
160. Li, H., et al., *Nova1 mediates resistance of rat pheochromocytoma cells to hypoxia-induced apoptosis via the Bax/Bcl-2/caspase-3 pathway.* Int J Mol Med, 2017. **40**(4): p. 1125-1133.
161. Ding, K., et al., *LMO4 mediates trastuzumab resistance in HER2 positive breast cancer cells.* Am J Cancer Res, 2018. **8**(4): p. 594-609.
162. Raymundo, B.R., et al., *Transgelin (TAGLN) Regulates IQGAP1 and Alters the Functions of Breast Cancer Cells.* Bulletin of the Korean Chemical Society, 2020. **41**(10): p. 1019-1026.
163. Marrugal, Á., et al., *Identification of Predictive Biomarkers of Response to HSP90 Inhibitors in Lung Adenocarcinoma.* Int J Mol Sci, 2021. **22**(5).
164. Kim, C.-H., et al., *G9a/GLP methyltransferases inhibit autophagy by methylation-mediated ATG12 protein degradation.* bioRxiv, 2021: p. 2021.02.05.430008.
165. Kirshner, J.R., et al., *Elesclomol induces cancer cell apoptosis through oxidative stress.* Mol Cancer Ther, 2008. **7**(8): p. 2319-27.
166. Shahab, S., et al., *MEK Inhibition Suppresses Growth of Atypical Teratoid/Rhabdoid Tumors.* J Neuropathol Exp Neurol, 2020. **79**(7): p. 746-753.
167. Hald Ø, H., et al., *Inhibitors of ribosome biogenesis repress the growth of MYCN-amplified neuroblastoma.* Oncogene, 2019. **38**(15): p. 2800-2813.
168. Fouladi, M., et al., *Phase I trial of MK-0752 in children with refractory CNS malignancies: a pediatric brain tumor consortium study.* J Clin Oncol, 2011. **29**(26): p. 3529-34.

7. Appendix

7.1. Supplementary Figures and Tables

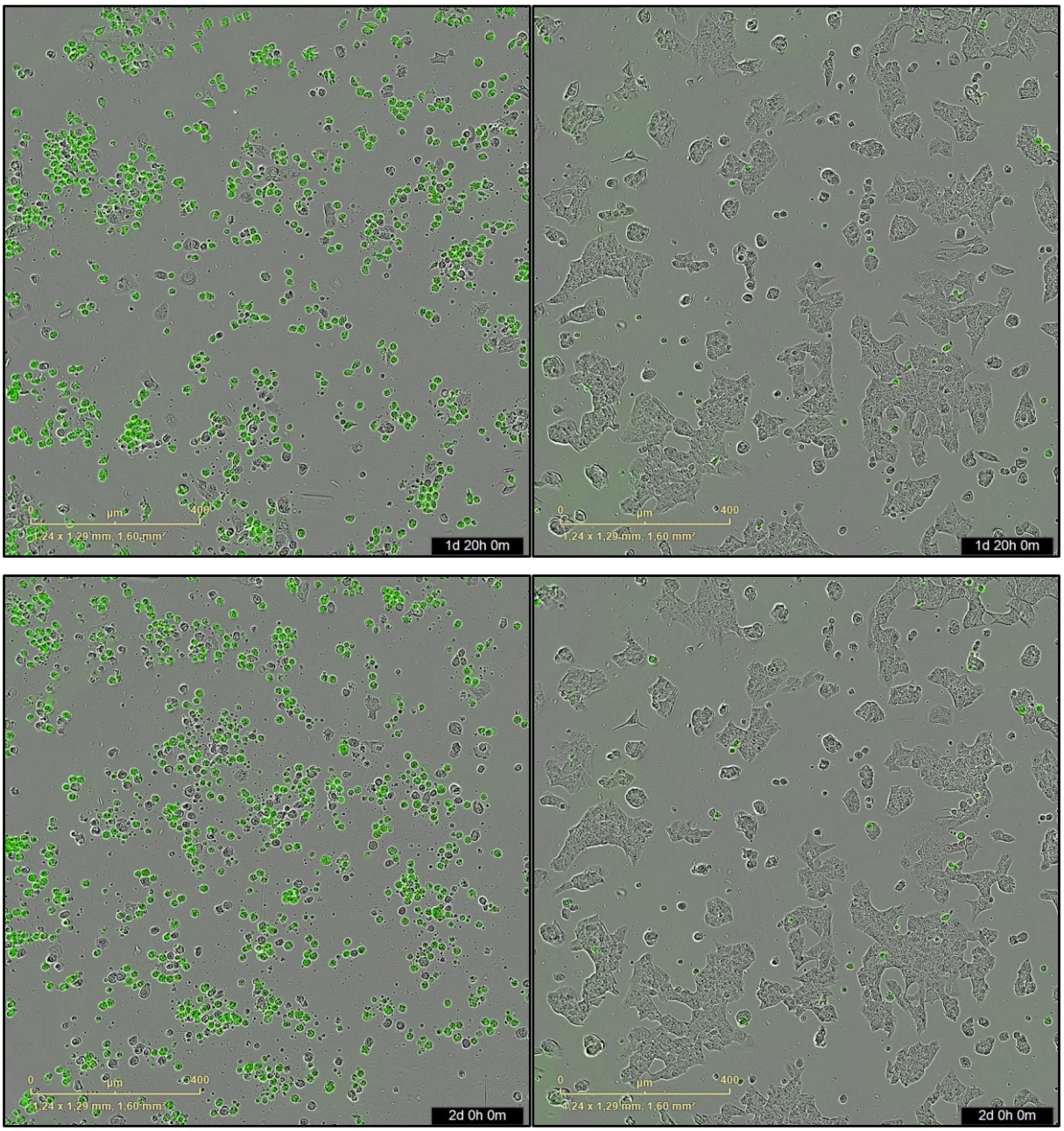

Supplementary Figure 1. Incucyte images from treating BT-16 cells using 84.1 nM Patupilone (upper left) or 266 nM Briciclib (lower left), along with corresponding time-matched DMSO controls (right). Both drugs yielded increased fluorescence signal intensities, indicating induction of apoptosis.

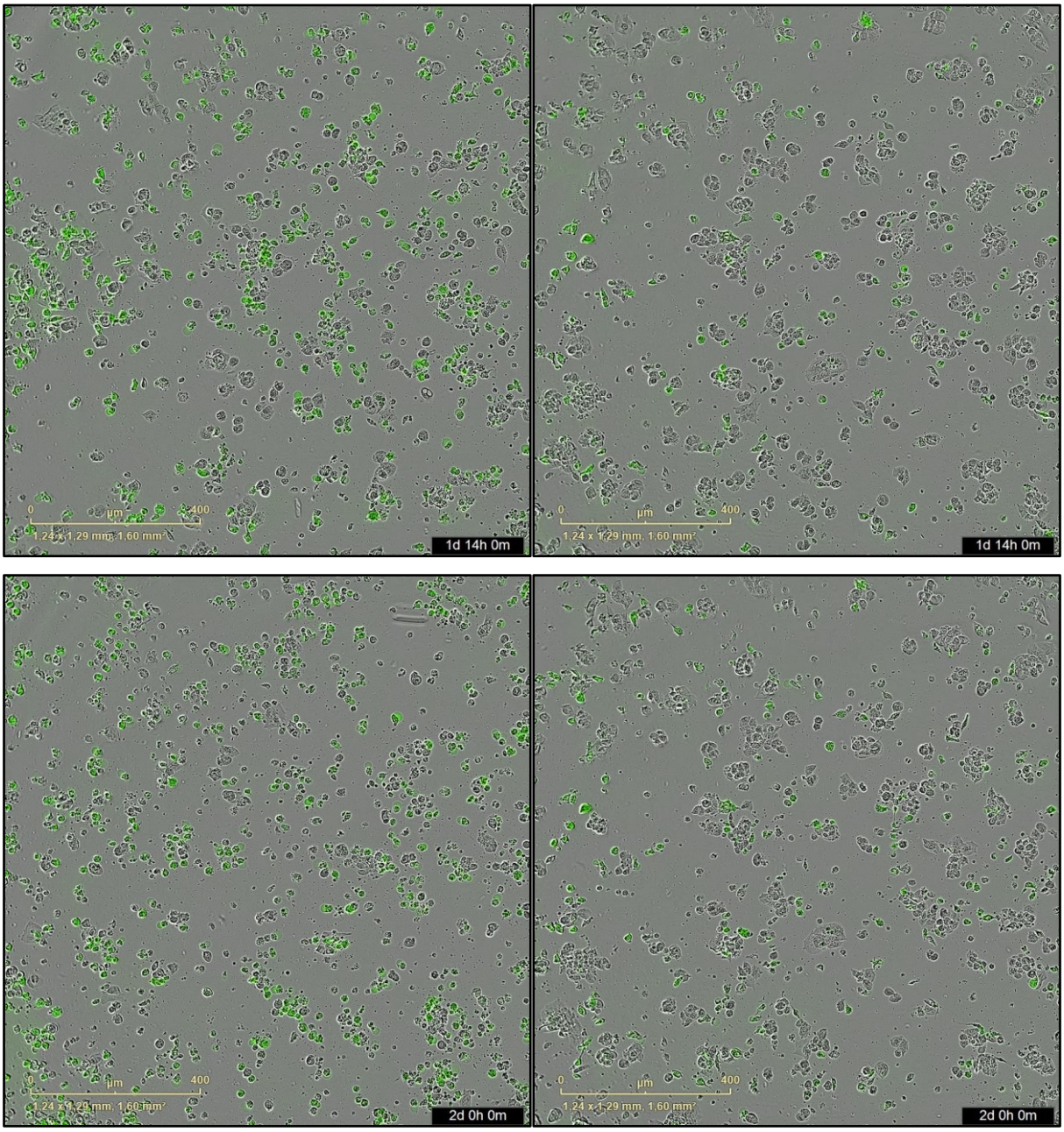

Supplementary Figure 2. Incucyte images from treating CHLA-266 cells using 84.1 nM Patupilone (upper left) or 266 nM Briciclib (lower left), along with corresponding time-matched DMSO controls (right). Both drugs yielded increased fluorescence signal intensities, indicating induction of apoptosis.

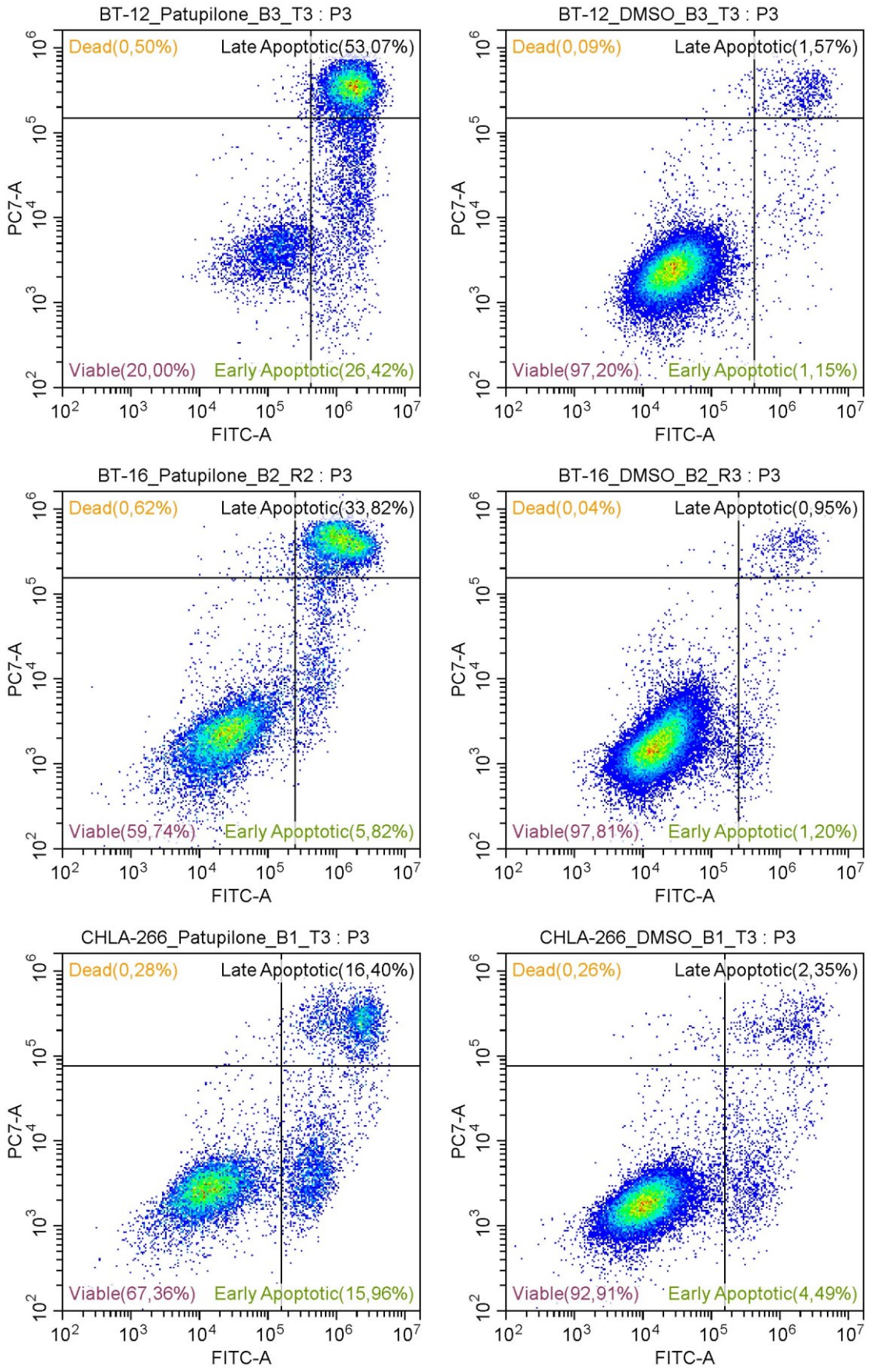

Supplementary Figure 3. Exemplary dot plots of FACS analyses using Annexin V-/propidium iodide-costaining. All three AT/RT-MYC cell lines showed an increased fraction of early- and late-stage apoptotic cells upon treatment using 100 nM Patupilone (left) for 30 h compared to DMSO controls (right).

Supplementary Table 1. List of genes with conserved regulation in AT/RT cell lines compared to publicly available AT/RT tumor data (cf. 3.4.2).

	AT/RT tumor data				AT/RT cell line data			
Probeset ID	**Log2(expression)**		**Fold change**	**q-value**	**Log2(expression)**		**Fold change**	**q-value**
	AT/RT-SHH	AT/RT-MYC	SHH/MYC	SHH vs MYC	AT/RT-SHH	AT/RT-MYC	SHH/MYC	SHH vs MYC
LINC01315	7.39	5.24	4.45	1.79E-05	1.92	-0.41	5.03	7.54E-02
TFDP2	10.29	8.29	3.99	3.91E-05	8.05	5.88	4.49	4.66E-02
FAM95B1	5.06	2.62	5.41	8.68E-05	3.98	1.85	4.38	6.42E-02
SLC35F2	5.55	7.53	-3.95	1.01E-04	2.23	5.82	-12.05	7.19E-02
MYOF	6.84	9.61	-6.81	1.08E-04	5.83	8.32	-5.64	9.77E-02
TLCD2	5.05	6.37	-2.50	1.32E-04	1.02	2.77	-3.37	9.70E-02
SLIT1	8.97	6.39	5.98	1.47E-04	0.30	-2.75	8.32	7.17E-02
PTCH1	11.00	9.27	3.31	1.97E-04	6.06	4.24	3.54	1.05E-01
MYC	6.47	8.91	-5.44	2.04E-04	2.22	6.48	-19.17	6.47E-02
S100A13	6.80	8.68	-3.67	2.68E-04	2.70	6.33	-12.35	3.72E-02
JAK3	4.37	5.87	-2.84	3.27E-04	0.34	2.42	-4.22	7.16E-02
SBF2-AS1	3.30	5.10	-3.47	3.28E-04	-0.48	1.82	-4.94	7.57E-02
VCL	9.98	11.01	-2.04	3.28E-04	7.46	9.37	-3.76	2.61E-02
TMEM109	6.49	7.54	-2.06	3.96E-04	4.17	5.59	-2.66	6.48E-02
AGPAT4	7.30	6.20	2.15	4.23E-04	4.59	3.27	2.50	1.01E-01
ADM	7.85	9.67	-3.52	4.34E-04	2.87	4.87	-3.99	8.34E-02
FHOD1	4.78	6.30	-2.86	4.34E-04	0.92	3.18	-4.79	1.07E-01
DPY19L2P2	8.33	7.08	2.37	4.53E-04	2.51	1.08	2.69	1.12E-01
DRAXIN	6.34	4.05	4.89	4.57E-04	6.24	2.81	10.77	4.69E-02
QPRT	4.39	6.44	-4.13	4.72E-04	-3.01	3.29	-78.90	6.77E-02
FAM19A5	7.32	5.51	3.53	4.72E-04	1.74	-1.40	8.85	9.45E-02
GJA3	3.69	5.54	-3.62	6.31E-04	-1.37	2.24	-12.14	1.16E-01
CTDSP1	6.63	7.66	-2.04	8.59E-04	4.36	5.38	-2.02	5.01E-02
AUTS2	10.86	9.49	2.58	1.08E-03	4.51	-0.20	26.11	5.74E-02
KIF21A	9.97	7.52	5.43	1.11E-03	7.20	1.97	37.61	2.84E-02
CDC42EP5	3.63	6.34	-6.52	1.16E-03	-0.42	2.27	-6.50	9.35E-02
PPM1E	8.40	6.85	2.93	1.18E-03	2.85	0.19	6.32	1.13E-01
IL4R	4.17	5.84	-3.19	1.21E-03	-1.11	3.59	-26.02	5.47E-02
HES6	8.89	6.17	6.61	1.36E-03	7.43	2.77	25.14	7.64E-03
PBX1	10.01	8.76	2.39	1.52E-03	6.20	-0.39	96.32	1.19E-02
PRKCD	1.56	3.33	-3.42	1.62E-03	-0.49	2.10	-6.05	3.35E-02
SLC39A4	4.76	6.14	-2.61	1.81E-03	-2.24	1.78	-16.24	9.16E-02
NOVA1	8.97	7.80	2.25	1.83E-03	3.74	0.62	8.68	1.09E-01
FBXW7	9.41	8.00	2.66	2.22E-03	6.60	4.29	4.97	7.04E-02
TNNT1	2.67	6.07	-10.53	2.26E-03	2.66	5.63	-7.82	4.60E-02
SLC50A1	5.11	6.18	-2.10	2.36E-03	3.97	5.33	-2.58	6.35E-02
NAGS	3.79	5.01	-2.33	2.52E-03	-0.59	0.79	-2.61	7.83E-02
TAGLN	6.79	8.53	-3.32	2.61E-03	2.48	6.45	-15.65	6.65E-02
TGM2	5.31	6.48	-2.26	2.62E-03	-1.62	3.01	-24.76	5.77E-02
MYADM	8.85	9.97	-2.17	2.80E-03	3.58	5.42	-3.58	9.63E-02
WSCD1	8.86	6.80	4.15	2.81E-03	5.50	1.91	12.01	6.83E-02
TSPAN4	6.81	8.00	-2.28	3.08E-03	3.00	5.23	-4.70	4.03E-02
DLGAP1-AS1	4.39	5.52	-2.18	3.08E-03	0.38	2.10	-3.30	2.84E-02
GPC2	5.81	4.79	2.03	3.29E-03	3.20	-0.05	9.50	2.01E-03
NUDT11	8.63	7.56	2.10	3.43E-03	4.26	3.11	2.22	1.13E-01
NIN	8.86	7.74	2.18	3.49E-03	6.41	4.49	3.78	9.58E-02
ZC3H12C	8.53	7.32	2.31	3.79E-03	4.94	3.16	3.44	1.03E-01
LRRC17	8.39	6.93	2.75	4.04E-03	3.04	-0.96	16.01	1.12E-01
SLC4A8	7.39	6.22	2.26	4.52E-03	4.74	3.01	3.31	8.46E-02
SERPINH1	8.36	9.56	-2.29	4.54E-03	7.43	8.59	-2.23	1.02E-01
TLE4	9.65	8.52	2.19	4.81E-03	5.31	-0.52	56.96	5.79E-02
KIAA0895L	6.35	5.15	2.30	4.87E-03	3.60	2.34	2.39	3.87E-02
GLCCI1	9.14	7.80	2.52	4.96E-03	3.97	0.52	10.96	6.47E-02
ARPC1B	7.06	8.19	-2.19	5.68E-03	3.35	6.00	-6.30	7.44E-02
IFIT1	7.47	8.98	-2.85	5.79E-03	4.35	6.75	-5.27	1.02E-01
ATL1	8.09	6.83	2.39	6.07E-03	2.55	-0.49	8.20	8.78E-02
CCDC69	2.06	3.82	-3.39	6.11E-03	-0.93	2.28	-9.27	2.26E-02
MYL12A	9.09	10.20	-2.15	6.21E-03	5.73	7.28	-2.93	9.16E-02
GPR161	7.67	6.58	2.13	6.58E-03	4.58	2.75	3.54	7.19E-02
STX3	5.14	6.44	-2.48	6.70E-03	1.32	3.47	-4.45	9.98E-02
RASGEF1A	4.47	6.07	-3.03	6.96E-03	-3.15	-0.43	-6.59	1.16E-01
CASP8	4.59	6.24	-3.13	7.17E-03	0.58	3.64	-8.34	5.22E-02
PTPN3	3.96	5.50	-2.90	7.19E-03	0.28	4.05	-13.60	5.13E-02
TMEM141	5.05	6.09	-2.06	7.33E-03	3.17	4.46	-2.43	9.48E-02
RDH10	7.06	8.71	-3.14	7.61E-03	2.02	6.20	-18.18	8.70E-02
PRDM16	7.84	6.12	3.28	7.87E-03	3.61	0.46	8.89	7.81E-02
ADAM22	6.74	5.60	2.20	7.91E-03	3.23	1.77	2.74	1.13E-01
BOK	4.37	5.77	-2.65	7.95E-03	1.80	4.48	-6.38	9.26E-02
DLL3	7.48	5.90	3.00	8.86E-03	6.20	1.21	31.80	6.96E-03
CD44	7.79	9.50	-3.26	9.33E-03	0.97	6.66	-51.48	1.16E-01
SYNE1	7.55	6.36	2.28	9.43E-03	5.80	2.90	7.48	9.93E-02
RASSF2	8.85	7.61	2.36	9.99E-03	5.39	1.48	15.04	5.54E-02
LIFR	9.34	7.93	2.66	1.03E-02	6.77	1.96	28.06	4.46E-02
PPARGC1B	3.82	5.13	-2.47	1.08E-02	-0.34	3.73	-16.82	5.41E-02
SRGAP1	8.90	7.56	2.52	1.10E-02	5.56	3.88	3.22	1.16E-01
PLEKHA7	7.59	6.54	2.07	1.10E-02	4.95	1.30	12.51	3.87E-02
PCDHGA8	5.98	4.72	2.40	1.26E-02	2.06	-0.50	5.89	6.95E-02
SRGAP3	8.57	7.28	2.44	1.30E-02	5.89	3.75	4.41	1.09E-01
TUBB2B	11.76	10.45	2.48	1.38E-02	9.08	4.64	21.73	6.51E-02

Probeset ID	Log2(expression)		Fold change	q-value	Log2(expression)		Fold change	q-value
	AT/RT-SHH	AT/RT-MYC	SHH/MYC	SHH vs MYC	AT/RT-SHH	AT/RT-MYC	SHH/MYC	SHH vs MYC
LMO4	8.94	7.71	2.35	1.40E-02	6.18	0.49	51.57	3.86E-02
KIAA0408	3.58	1.57	4.03	1.56E-02	4.09	-1.01	34.30	4.66E-02
SEPT3	7.74	6.61	2.19	1.66E-02	4.52	2.23	4.90	4.59E-02
ABAT	10.31	9.08	2.34	1.82E-02	5.19	2.44	6.70	5.41E-02
MSRB3	8.38	9.38	-2.01	1.86E-02	3.45	5.66	-4.62	1.05E-01
ITPR1	5.18	6.34	-2.25	1.93E-02	0.29	3.61	-9.99	1.06E-01
SDSL	2.21	3.77	-2.94	2.05E-02	-0.27	2.24	-5.71	5.74E-02
ADAP2	5.44	6.58	-2.20	2.44E-02	-1.96	1.18	-8.83	6.65E-02
IL27RA	4.05	5.53	-2.79	2.67E-02	1.91	4.58	-6.34	7.57E-02
ADAMTSL4	4.36	5.89	-2.89	2.79E-02	-0.95	2.39	-10.06	8.93E-02
APOC1	7.87	8.87	-2.00	3.00E-02	0.30	3.48	-9.08	1.94E-02
RGMB	8.73	7.72	2.01	3.12E-02	5.71	3.01	6.47	4.53E-02
UNC13A	3.38	4.64	-2.39	3.27E-02	4.56	6.65	-4.26	9.26E-02
GCHFR	5.27	6.30	-2.04	3.36E-02	-0.30	3.68	-15.82	5.55E-02
MSI1	3.79	2.78	2.01	3.70E-02	4.41	2.18	4.70	7.86E-02
CTSV	6.86	7.91	-2.08	3.73E-02	1.32	4.52	-9.19	1.05E-01
LFNG	6.33	5.05	2.44	3.96E-02	2.78	0.38	5.27	7.86E-02
FBLN2	4.02	5.34	-2.49	4.11E-02	-1.82	2.36	-18.16	1.12E-01
NTN1	8.08	6.89	2.29	4.78E-02	6.79	0.38	84.57	2.86E-02
SPECC1	6.81	5.23	2.99	5.21E-02	7.91	5.06	7.19	5.52E-02
WNT2B	4.88	6.15	-2.43	6.01E-02	0.02	1.44	-2.67	6.24E-02
TTYH1	7.78	5.84	3.85	6.23E-02	5.50	-0.49	63.90	9.34E-02
B4GALT1	4.90	6.03	-2.20	6.68E-02	2.09	4.16	-4.22	5.50E-02
TLE2	4.95	6.17	-2.33	6.78E-02	-0.66	3.35	-16.20	5.23E-02
ITGA7	5.01	7.07	-4.17	3.56E-03	5.09	1.16	15.33	1.54E-02
GLIPR2	6.40	7.48	-2.12	8.87E-03	4.01	1.67	5.05	1.14E-01
CDKN2B	4.52	5.82	-2.46	1.12E-02	2.82	-0.56	10.39	6.51E-02
STK17A	7.37	8.54	-2.25	1.79E-02	5.43	3.26	4.52	6.65E-02
COL6A2	4.40	6.30	-3.74	2.83E-02	5.08	2.22	7.27	9.28E-02
GREB1L	6.08	5.03	2.08	5.39E-02	0.48	3.45	-7.83	9.45E-02

7.2. List of Figures

7.3. List of Tables

8. Acknowledgements

First, I would like to thank Prof. Dr. Marc Remke for giving me the opportunity to work on this project. I still remember the day when I introduced myself and you explained your ideas to me. I just thought “This is exactly what I’m looking for”. Thank you for giving me room to express my developer spirit and thank you for encouraging, supporting and pushing me, especially among the presentation of scientific work on international conferences. Notably, thank you for pointing my way to Neuropathology.
Second, I would like to thank Prof. Dr. Guido Reifenberger for evaluating my thesis as a second supervisor and for teaching me in science and diagnostics.
I would like to thank Prof. Dr. Arndt Borkhardt for supporting this project.
Moreover, I would like to thank the Kind-Philipp-Stiftung für pädiatrisch-onkologische Forschung for granting me a scholarship for this project and the corresponding financial support.
Next, I would like to express my deepest gratitude to Jasmin for your invaluable scientific and personal advice and for always supporting my ideas and notions. Without you, I could not have developed so far. Moreover, thank you for always backing up my continuous employment, especially when I was about to sink into “post-exam” depressions. I really enjoyed sharing an office for half a year.
I would like to thank all other members of the AG Remke, especially Lena and Viktoria. I definitely miss our time together, especially numerous trips to scientific meetings in Dublin, Denver and San Francisco, that enriched my memory with unforgettable moments. Thank you for valuable input, sharing opinions and being good friends. It was an enormous pleasure to me.
Big thanks to Mara and Kübra for always giving me room to express my feelings about medicine, research, myself and everything else in a safe space referred to as the “Traurige Frühlingsrolle” meetings. Special thanks to Mara and Christian for so many laughs and crazy dedication.
I would like to thank Anna for guiding me through the start of my journey in life sciences and spending me words of confirmation. Thanks to Frauke for supporting me and this project with your incredible performance and focus. Thanks to Sarah for cushioning my work load when there was too much to take care of. Thank all of you three for taking so many urgent orders.

Moreover, I would like to thank Daniel and Nan for lots of scientific advice, help in evaluating data and fruitful discussions. Special thanks to Nan for sharing and supporting my interest in fancy scientific devices.

Thank you, Ulvi, for making me feel a lot less alone when I was working late in the lab. I probably will never ever work in a team with this kind of cohesion and benevolence again. And probably I will never ever experience such adventurous and legendary Christmas parties again. However, I will keep all these memories within my head and heart.

I would like to thank Dr. Ute Fischer and all current and former members of the KMT lab for supporting this project.

I would like to thank Johanna Theruvath and Siddhartha Mitra for supporting this project and working on the *in vivo* experiments. I hope we can intensify this collaboration in the future!

I would like to thank Eunice Paisana, Rita Cascão, Carlos Custódia and Cláudia Faria for productive cooperations and fruitful joint meetings in Lisbon and Düsseldorf.

I would like to thank Kristin for introducing and educating me in Neuropathology and covering me when I was working on science. I could not have imagined a better colleague to start my residency with!

I would like to thank Jörg, Christiane, Eva and Anna for educating me in Neuropathology and for backing me up when I was finalizing this project.

Finally, I would like to deeply thank my family and friends, especially my parents and my brothers, for all the love, for coping my emotional breakdowns and supporting me and my dedication on this project. Furthermore, I would like to express my profound gratitude to you, Philipp, not only for your stylistic advice, but for your patience and for making me laugh again, when things were not working out. Thank you for always standing by my side and caring for me.